THE UNIVERSITY
of ADELAIDE

Laminar Flow Control of a Flat Plate Boundary Layer Using Dielectric Barrier Discharge Plasma

Brad A. Gibson

School of Mechanical Engineering
The University of Adelaide
South Australia 5005
Australia

A thesis submitted in fulfillment of the requirements for the degree of Ph. D. in Engineering on the 31st of August 2012.

Ph. D. Thesis

Final version
31st of August 2012

Aerospace, Acoustics and Autonomous Systems Group
School of Mechanical Engineering
The University of Adelaide
South Australia 5005
Australia

Typeset by the author using LaTeX.
Printed in Australia.

Copyright © 2012, The University of Adelaide, South Australia.
All right reserved. No part of this report may be used or reproduced in any form or by any means, or stored in a database or retrieval system without prior written permission of the university except in the case of brief quotations embodied in critical articles and reviews.

To Thomas Alfred Gibson (dec.), Rodney Thomas Gibson, & Benjamin John Chartier;

my three favourite engineers.

Summary

The drag developed on an object as it moves through a fluid comprises of a number of components arising from various and differing fluid phenomena. For aerodynamic bodies such as aircraft, one of the most dominant components of the total drag force is that arising from shear interactions between the surface of the object and the fluid. In steady, cruise conditions this shear-induced skin friction drag can account for almost 50% of the total drag force on the body and hence this is the reason much interest surrounds the minimisation of this component.

Laminar Flow Control (LFC) is the field of aerodynamics focused on minimising skin friction, or viscous drag. The viscosity of a fluid, and the shear interactions between the layers of fluid and the aerodynamic body give rise to a boundary layer, a region of fluid with diminished fluid velocity and momentum. Laminar Flow Control aims to minimise the momentum deficit within the boundary layer by manipulating the flow within and encouraging favourable flow conditions to exist and be maintained. In essence, Laminar Flow Control attempts to maintain laminar flow within the boundary layer, improving the stability of the flow, delaying the onset of turbulence and the formation of a turbulent boundary layer that develops significantly more drag than an equivalent laminar structure.

A number of techniques exist for controlling and maintaining laminar flow within a boundary layer. Examples include compliant surfaces, acoustic arrays and suction, and all share the common trait of complexity, which to date has limited the application of such systems in the real world. In the search for simpler Laminar Flow Control technology, attention has been turned towards Dielectric Barrier Discharge (DBD) plasma actuators as a possible alternative. Through the formation of a small volume of plasma, these actuators are capable of producing an electrostatic body force that can couple with the surrounding air and bring about a jetting effect without the addition of mass. This jetting effect, if controlled effectively, can potentially favourably augment a boundary layer flow and lead to a delay in transition.

The work discussed in this thesis represents a contribution to the field of DBD-based Laminar Flow Control. The aim was to further investigate the potential of plasma actuators for improving the hydrodynamic stability of a boundary layer and hence contribute to the limited published data pertaining to this field. The research involved the development of a DBD-based LFC system in which plasma actuators were used to augment the most fundamental of boundary layer flows, the flat plate, Blasius-type. By measuring the augmentation to the velocity profile of the boundary layer brought about by the LFC system, the stability of the flow was able to be investigated and hence the feasibility of the technology determined.

The plasma actuators utilised in this research were designed such that control could be achieved over the shape of the induced jetting profile. To minimise adverse interactions with boundary layer flows, the plasma actuators were designed so that the magnitude and position of the maximal induced jetting velocity could be controlled. After consultation of the literature, novel actuators utilising orthogonally arranged electrodes were conceived and tested in a parametric study. Through variation of the distance to which the exposed electrode sat proud above the surface of the actuator, in addition to variation of the applied voltage, it was found that the desired control over the induced jet could be attained, leading to the identification of two mechanisms through which the DBD-based LFC system could be tuned. The details of the design and development of these orthogonal actuators and the effect of the electrode height on the jetting characteristics of the devices can be found in Gibson et al. (2009a) and Gibson et al. (2009b).

After identifying suitable and novel actuator arrangements, a tuning strategy was conceived to hasten the development of the LFC system. Rather than implementing the actuators and measuring the response of the boundary layer to the plasma first, Linear Stability Theory was instead used to identify desirable boundary layer augmentation objectives for the LFC system. Linear Stability Analyses (LSAs) were performed on a number of idealised boundary layer flows, obtained from curve fitting analytical functions to published DBD-augmented boundary layer data, as well as from boundary layer theory. The LSAs were conducted using an Orr-Sommerfeld Equation solver developed as part of this research, which utilises a finite differencing scheme. The outcome of this comparison process was that the developed DBD-based LFC system was used to attempt to augment the boundary layer such that the flow attained an asymptotic suction velocity profile, which would give the boundary layer a limit of stability almost two orders of magnitude greater than that of the base flow, and hence significant robustness to transition.

The conceived DBD-based LFC system was implemented into a Blasius-

type boundary layer which was formed over the Flat Plate Rig (FPR) designed and developed as part of this research. Initially a single actuator was utilised, positioned just upstream of the location of the critical Reynolds Number (limit of stability) of the flow. Due to the design of the FPR and the actuators utilised, it was possible to study the response of the layer to the plasma with and without a mild suction effect, introduced through a $5mm$ wide slot that was required for operation of the actuator. This mild suction effect was measured to be approximately $4Pa$, and by itself was found to be insufficiently strong enough to augment the flow such that it attained the characteristics of a boundary layer with uniform wall suction. With the FPR, measurements of the velocity profile of the boundary layer with and without flow control were made around the critical Reynolds Number location of the flow ($80000 < Re_x < 120000$), which allowed the changes to the stability of the flow to be studied.

As discussed in Gibson et al. (2012) the initial results of the DBD-based LFC system showed that the plasma was adversely affecting the stability of the flow. Subsequent tuning of the system was therefore performed through variation of the applied voltage of the actuator. From this tuning it was found that an actuator operated with an applied voltage of $19.0kV_{pp}$ (referred to as a *low-voltage* actuator) in conjunction with the mild suction effect, produced boundary layer characteristics akin to those of a flow exposed to uniform wall suction. In addition, an actuator operated with an applied voltage of $21.4kV_{pp}$ (referred to as a *high-voltage* actuator) was found to adversely affect the stability, even more so in the absence of the mild suction effect. The single low-voltage actuator was found to be able to maintain uniform wall suction-like characteristics for $50mm$ beyond the trailing edge of the encapsulated electrode. This finding pertaining to the use of the low-voltage actuator highlighted the potential of a single DBD device to develop uniform wall suction-like characteristics with only a mild suction effect through a single slot, and hence in a less complex fashion than conventional suction systems.

An attempt was made to maintain the favourable benefits of the single, low-voltage actuator by using two such actuators placed in series. However, the effect of this combined double-actuator/suction system differed only slightly from the suction-only system (with two slots instead of one), meaning that in this configuration, the use of the plasma was somewhat superfluous. Hence it could be concluded from the results of the research that a single low-voltage actuator operated in conjunction with a mild suction effect is more effective as a LFC system than a single mild-suction slot, but a combined double-low-voltage actuator/suction system is no better than a simpler and less energy consuming double-mild-suction slot system. It is,

however, anticipated that through the undertaking of future works, utilising additional actuators that have undergone further tuning, a LFC even more effective than the double suction slot system tested in this research will ultimately be developed.

Declarations

Originality

To the best of my knowledge and belief, the material contained within this work, except where due reference has been made, is original and contains no material previously published for the award of any other degree or diploma at another institution.

Permissions

I give consent to this copy of my thesis, when deposited in the University Library, being made available for loan and photocopying, subject to the provisions of the Copyright Act, 1968.

I also give permission for the digital version of my thesis to be made available on the web, via the University's digital research repository, the Library catalogue, the Australasian Digital Theses Program (ADTP) and also through web search engines, unless permission has been granted by the University to restrict access for a period of time.

Brad A. Gibson

Acknowledgements

The research documented in this thesis is the result of many individuals, who, with their care and support, have guided me through to its completion. To all of you I express my thanks.

To my supervisors, Dr. Maziar Arjomandi and A/Prof. Richard M. Kelso I reserve the first acknowledgements. Throughout my candidature the numerous discussions on history, politics, and life in addition to engineering have made my experience so much more enjoyable. You have also tolerated my numerous motorsport and bicycling fables that would have other lesser men dozing within moments. I thank you both sincerely.

Thanks to all of my friends, of whom there are many, who have supported me throughout my research endeavours. In particular sincere thanks to my office buddies Dorothy Missingham, Ben Chartier, Richie Jones and Mei Cheong. You have all been a constant source of fun, support, information and advice on everything from engineering to fine wine. Without our daily discussions around a hot cup of tea I would not have made it through.

The presentation of this thesis would never have attained any degree of professionalism without the help of Dr. Zebb Prime and Will Robertson. Thank you Zebb for responding to the daily calls to correct my misuse of LaTeX, and to Will, thanks for being a thorough and critical curator of the art of typesetting.

To all of the workshop staff at The School of Mechanical Engineering, thanks for the help, jokes, information and afternoon drinks. You have all been a source of knowledge fun and friendliness, and to you all I express my thanks.

During my research my family has always been by my side. Thanks to my parents Rodney and Sandra Gibson and to my sister Melissa Gibson for being patient with me, loving me and providing me with a warm and safe home.

Finally I save the biggest thanks to my partner Emma Lowe. You, above everyone else have endured the most. You have suffered the ups, the downs,

the enjoyment, the stress, the lack of sleep, the loss of hair, the anecdotes from the lab, the stories from the desk, and even participation in supervisor meetings. This journey has been as much hard work for you as it has been for me and through your love and support we have made it. Words cannot express my thanks and appreciation.

Contents

List of Figures

List of Tables

Nomenclature

Symbols

Greek

- α Velocity disturbance wavenumber, angle of attack
- Γ FDS variable
- Δ FDS variable, incremental change
- δ Boundary layer thickness, FDS variable, incremental change
- δ_w Streamline displacement due to presence of pressure tube close to a wall
- δ^* Boundary layer displacement thickness
- ϵ Apparent shift in probe position
- ε Dielectric coefficient
- η Non-dimensional distance normal to wall
- θ Boundary layer momentum thickness
- Λ Pohlhausen shape factor
- λ Velocity disturbance wavelength
- λ_D Debye length
- μ Dynamic viscosity
- ν Kinematic viscosity
- ξ Suction parameter, arbitrary variable
- ρ Fluid density

- ρ_c Charge number density
- σ Standard deviation
- Φ Discretised velocity disturbance amplitude
- ϕ Velocity disturbance amplitude
- φ Electric potential
- χ Ratio of electrode width to electrode length
- ψ Stream function
- ω Velocity disturbance circular frequency
- $\tilde{\omega}$ FDS variable

Roman

- A FDS variable
- a Plasma breakdown length perpendicular to actuator surface, arbitrary Falkner-Skan variable, arbitrary polynomial coefficient, super-ellipse major radius, local speed of sound
- B FDS variable
- b Plasma breakdown length parallel to actuator surface, arbitrary Falkner-Skan variable, arbitrary polynomial coefficient, electrode spanwise length, super-ellipse minor radius, cavity width
- C Capacitance, FDS variable
- C_p Pressure coefficient
- c Velocity disturbance propagation velocity, arbitrary polynomial coefficient
- $\tilde{c}$ FDS variable
- c_l Airfoil lift coefficient
- D Diode
- d Separation distance between electrodes, pressure tube outside diameter, cavity depth

- E Electric field strength
- E_0 Peak electric field strength, Output voltage of hot wire circuit
- E_b Breakdown electric field strength
- e exponential e
- e_c Electron charge
- err Error
- exp exponential e
- f Body force, applied frequency, measurement frequency, plasma body force, arbitrary Falkner-Skan variable, arbitrary Glauert wall jet variable
- G arbitrary variable
- g Arbitrary Falkner-Skan variable, arbitrary function, acceleration due to gravity
- H Boundary layer shape factor, Investigation height boundary
- h Discretisation distance (y-direction),
- I Length of electrical network (plasma actuator), Gain of current-boosting amplifier (hot wire circuit)
- I_0 Output current of hot wire circuit
- i Squareroot of negative one
- J Number of points in the y-direction
- K Gain of voltage-boosting amplifier (hot wire circuit)
- k_1 Electirc field gradient (x-direction)
- k_2 Electirc field gradient (y-direction)
- k Discretisation distance (x-direction), Trip wire diameter
- k Discretisation distance (x-direction), Trip wire diameter
- L Electrode chordwise length, left-hand side
- ln Natural logarithm

- M Momentum
- m Arbitrary Falkner-Skan variable
- N Maximum number, number of points in the x-direction
- n Number, amplification factor
- P Arbitrary point, static pressure
- q Dynamic pressure
- R Resistance, right-hand side
- Re Reynolds number
- r Variable set (matrix equation)
- $\tilde{r}$ FDS variable
- s Arbitrary variable
- t Time, thickness
- Tu Turbulence intensity
- U Arbitrary variable
- U_∞ Freestream velocity
- u Mean velocity, local x-direction velocity
- V Velocity vector, applied voltage
- v Local y-direction velocity
- v_0 Uniform suction velocity
- w Local z-direction velocity
- x x-direction (chordwise), boundary layer development length, parallel to wall
- y y-direction, normal to wall
- z z-direction (spanwise), height above the Earth's surface

Math

- ∞ Limit at infinity

Subscripts

Greek

- δ Based on boundary layer thickness
- δ^* Based on boundary layer displacement thickness

Roman

- a Pertaining to air, arbitrary resistance
- abs Absolute (error)
- app Applied to actuators
- b Body, pertaining to the backward-going discharge cycle, balance (hot wire bridge)
- $Blasius$ Pertaining to Blasius flow
- C Based on chord length
- c Pertaining to a charge, arbitrary resistance
- $Calculated$ Pertaining to calculated data
- $Cold$ At cold temperatures
- $Control$ Controlled
- $corrected$ Corrected mesurement value
- $crit$ Critical (point of stability)
- d Pertaining to the dielectric, based on pressure tube outside diameter
- e Edge
- $elec$ Pertaining to the electrodes
- $encapsulated$ Pertaining to the encapsulated electrode
- exp Distance to which exposed electrode sits proud above surface
- $exposed$ Pertaining to the exposed electrode
- f Pertaining to the forward-going discharge cycle

- fit Pertaining to a fitted curve
- h Horizontal (x) direction, voltage overshoot
- i Imaginary component, output of CTA bridge, ith element
- *instrument* Pertaining to the instrument
- j Due to plasma suction
- *jet* Jet
- k Based on trip wire diameter
- L Based on non-dimensional length item LE Pertaining to the leading edge
- max Maximal
- *measured* Pertaining to measured data
- N Pertaining to the maximum number N
- n Pertaining to the number n
- Op Operating (hot wire bridge)
- *Published* Pertaining to published data
- pp Peak-to-Peak
- qi Offset (voltage)
- r Real component
- rel Relative (error)
- S Arbitrary point of interest
- *scatter* Scatter (measurements)
- *spatial* Spatial
- t Eddy viscosity
- Tot Total
- tr Transition
- v Pertaining to the vertical (y) direction

- w Due to the wall, hot wire
- x Pertaining to the x-direction
- y Pertaining to the y-direction

Mathematical

- ∞ In the freestream
- 0 At the wall

Superscripts

- $\rightarrow$ Vector quantity
- $'$ Differentiation with respect to the normal direction
- $\acute{}$ Fluctuating quantity
- $\star$ Non-dimensional
- $\dot{}$ Derivative with respect to time

Acronyms

- AC Alternating Current
- CTA Constant Temperature Anemometry
- DBD Dielectric Barrier Discharge
- DC Direct Current
- DE Direct Equation
- DOC Direct Operating Costs
- FDS Finite Differencing Scheme
- FPR Flat Plate Rig
- ID Internal Diameter
- KBM Keller's Box Method
- LFC Laminar Flow Control

- LSA Linear Stability Analysis
- LST Linear Stability Theory
- NRMSD Normalised-Root-Mean-Square-Deviations
- OD Outside (External) Diameter
- OHR Over Heat Ratio
- OSE Orr-Sommerfeld Equation
- PDE Partial Differential Equation
- PDF Portable Document Format
- RSE Rayleigh Stability Equation
- TS Tollmien Schlichting
- ZPG Zero Pressure Gradient

1 Introduction

Environmental impact and service operating costs are of great concern to the global aviation industry. As of 2008 the aviation industry could no longer be considered an insignificant contributor of greenhouse gases, with approximately 2% of total CO_2 emissions being attributed to air transportation of tourists (Scott et al. 2008). Providing air tourism remains *business as usual* in the immediate future, then the greenhouse gas emissions will be "...in direct conflict with the efforts of the international community to achieve substantial emission reductions," (Pentelow and Scott 2010). Numerous world bodies committed to sustainable development recommend that by the Year 2050 the level of CO_2 in the atmosphere will need to decline to 50% of the level recorded in the Year 2000 if dangerous climatic changes are to be avoided (Pentelow and Scott 2010). Reducing aircraft fuel consumption is now more than ever of utmost importance to the global aviation industry and the community as a whole, particularly since aviation traffic is anticipated to rise in the future (Penner 1999). Reducing fuel consumption is also in the direct financial interest of the aviation sector. Fuel consumption, which is directly associated with vehicle drag, accounts for 22% of the Direct Operating Costs (DOC) of a commercial aircraft. According to Renneaux (2004) a reduction in drag of 1% can lead to a 0.2% reduction in the DOC of a large transport aircraft. Hence, minimising drag to reduce environmental impact and operating costs is currently the focus of much research.

The drag of an aircraft consists of a number of different components, of which viscous-derived skin friction drag is the most significant (Bertin 2002). As skin friction accounts for almost 50% of the total drag of a typical commercial aircraft (Figure 1.1) it is easy to understand why a large amount of research and development work is focused on reducing this source of viscous loss.

Viscous drag arises as a result of shear interactions between the surface of the body and the fluid through which it passes. The fluid essentially sticks to the surface, and thus creates a velocity gradient between the body and the freestream. This velocity gradient is indicative of a loss of freestream momentum, which is the result of viscous drag. The region in which the velocity gradient is prevalent is called the boundary layer and it is the behaviour of the flow within this region, which dictates the magnitude of the viscous drag force. The upstream regions of a boundary layer generally consist of laminar flow, which progressively manifests into a turbulent structure as the layer develops over the length of the body. The so-called *turbulent boundary layer* arising from the growth of disturbances within the flow field, is characterized by its increased thickness and developed skin friction. It is for this reason that aerodynamicists concerned with minimising viscous drag strive to maximise the extent of the laminar region using Laminar Flow Control (LFC) techniques.

Dielectric Barrier Discharge (DBD) plasma actuators have gained considerable interest in recent times as potential LFC devices. Through the generation of very small regions of surface plasma, DBD actuators are capable of imparting momentum to a fluid through electrostatic interactions between the moving charged particles of the plasma and the dipoles of the surrounding

NOTE:
This figure is included on page 2
of the print copy of the thesis held in
the University of Adelaide Library.

Figure 1.1: Components of drag affecting a typical aircraft in cruise, (adapted from Bertin 2002).

air molecules. The extent of the plasma force influence is limited to a region close to the actuator surface. This makes such devices ideal for redistributing momentum throughout a boundary layer, potentially in a way to improve hydrodynamic stability and thus delay transition from laminar to turbulence. This is why DBD actuators present as an attractive option for controlling the flow of a laminar boundary layer and hence the purpose of this research is to investigate how the DBD effect can be exploited for this task so as to contribute to the development of simple and more effective DBD-based LFC technology that will ultimately benefit the environment and global aviation industry.

1.1 Aims & objectives

Laminar Flow Control system design has a long and expansive history throughout which many diverse technologies have been proposed. The reluctance in adopting the currently available technologies has led to work into other potential flow control devices for LFC. The aim of this research is to investigate a novel approach to Laminar Flow Control design using Dielectric Barrier Discharge plasma. This technology as applied to LFC is in its infancy, with the potential of the system for LFC only being recognised in the past few years. The research presented in this thesis focusses on contributing to the limited amount of knowledge available that pertains to DBD-based LFC.

The research discussed herein is restricted in that the investigations have focused on the effects of DBD plasma on the hydrodynamic stability of a flat plate boundary layer flow in the absence of a pressure gradient. Mathematically, such a boundary layer is approximated by the *Blasius* solution, and is the most fundamental of external flows to which LFC strategies are studied analytically and numerically. Historically, assessing the changes to the stability characteristics for a Blasius flow has been the starting point for LFC system design (Schlichting 1955) and as such the effectiveness of DBD plasma in augmenting the stability of flat plate boundary in a Zero Pressure Gradient (ZPG) is of fundamental importance to the future development of the technology.

Blaisus flow can be described through suitable treatment of the governing equations of fluid mechanics. In addition, the hydrodynamic stability of Blasius flow is widely understood and can be calculated using potential flow techniques. This knowledge allows the stability of an augmented Blasius flow to be effectively benchmarked, whilst also providing assistance in formulating the required performance of the DBD-based LFC system. In the context of the research discussed here, the mathematical solution of the Blasius flow

and the hydrodynamic stability of said flow were used to formulate flow augmentation objectives for the DBD-based LFC system developed here.

After reviewing the theory and literature pertaining to DBD-based LFC, the resulting objectives of the research were defined as the following:

- to identify actuator configurations with potential to improve the hydrodyanmic stability of a flat plate laminar boundary layer in a ZPG based on the performance of these devices in quiescent air.
- to implement the actuators in a flat plate laminar boundary layer in a ZPG and assess the effect of the actuators on the stability of the flow.
- to attempt to tune the operation of the actuators so that the flow attains improvements to its stability.
- to strive to maximise the streamwise extent to which hydrodynamic stability improvements can be maintained.

In order to achieve the desired research objectives, a considerable amount of resources needed to be procured. Hence, in addition to the research objectives, a significant component of the research involved the following two tasks:

- the development of an *in-house* computational routine to solve the hydrodynamic stability equations pertaining to Blasius flow.
- the design, manufacture and development of a Flat Plate Rig (FPR) that was able to achieve experimental flows mimicking that of a Blasius boundary layer.

1.2 Thesis Outline

The thesis is presented in a number of chapters, the sequence of which highlight the chronology of the knowledge development and research undertakings. The early chapters introduce the principles of DBD-based LFC, from which the detailed objectives of the research can be identified. After discussing the design and development of the experimental apparatus, the results of the experimental investigations are presented in the later chapters.

An introduction and review of Laminar Flow Control is the topic of Chapter 2. In this review, the theory pertaining to boundary layer flows and their analysis is introduced. From the analytical description of boundary layer flows, the concept of hydrodynamic stability is introduced along with the theory and analytical techniques used to investigate the onset of boundary

layer transition. The theory of hydrodynamic stability provides the basis from which the objectives of LFC can be discussed, which consequently allows a critical review of LFC technologies to be presented. From the review it is revealed that significant scope exists to develop simpler techniques for augmenting hydrodynamic stability in boundary layer flows.

Chapter 3 contains a review of DBD plasma aerodynamics. As discussed in this chapter, DBD actuators are fundamentally simple devices that can produce a wall-jetting effect without the addtion of mass. It is this wall-jetting effect which has aroused interest in the use of DBD for LFC, but as is discussed, DBD-based LFC research is still in its infancy. Although much research has been undertaken investigating this jetting phenomenon, the complexities associated with actuator design mean that successful application of DBD actuators for boundary layer transition delay has been limited. The consequence of this is that scope exists to investigate the response of boundary layers to novel actuator configurations to further investigate ways to improve hydrodynamic stability in a boundary layer flow.

An important component of research into LFC is understanding the theory pertaining to hydrodynamic stability. This understanding includes possessing the capability to solve the equations of hydrodynamic stability in order that stability-improving mechanisms can be understood and this analytical information used to structure LFC system design. The equations of hydrodynamic stability possess no simple analytical solution, but through suitable mathematical treatment can be solved numerically. As part of this research, a numerical routine was scripted so as to provide this information to the research. The techniques that the routine calls upon in order to solve the equations are presented in Chapter 4 along with the validation of the method.

Chapter 5 presents the results of the work into developing novel and beneficial actuators for DBD-based LFC. Using the results of the literature review in conjunction with hydrodynamic stability analysis and an experimental parametric study, a novel actuator design was developed. These developed actuators, which are introduced as *orthogonal* actuators in the chapter, were the devices of choice for augmentation of the flat plate boundary layer flows investigated in this research.

The design and development of the Flat Plate Rig (FPR) used for investigating the DBD augmented boundary layer flows is the topic of Chapter 6. In addition to discussing the features of the FPR, Chapter 6 also presents details of the measurement equipment employed as well as the procedures of the undertaken experiments.

Preliminary experiments involving orthogonal actuators augmenting the

flat plate laminar boundary layer in a ZPG are presented in Chapter 7. These investigations revealed that the orthogonal actuators can be utilised with or without a very slight suction effect, and in doing so the flow of the fluid can be changed dramatically. An assessment of the performance of the actuators finds that the actuators in the tested configurations have an adverse effect on stability, but there exist opportunites to refeine the actuator operation for improved results.

Refinement of the actuator design and operation is presented in Chapter 8. Through variations of actuator applied voltage, actuator operation with most beneficial and most adverse stability effects are identified. The Chapter then compares the two actuator operations with and without suction, revealing that the lower applied actuator voltages provide improved perfromance, but the stability improvements dissipate downstream of the actuator.

In Chapter 9, experimental investigations are undertaken to maximise the stability improvements downstream of the actuator. This is attempted through the use of two identical actuators placed in series. The results reveal that the use of two actuators in this configuration seemingly destabilizes the flow, and that future work is required to identify possible combinations of actuators that can provide sustained improvements to flow stability.

The final chapter includes the conclusions and recommended future works pertaining to this research. As part of the dicussion on future works, the feasibility of the developed numerical codes and experimental equipment to undertake the future work are assessed.

1.3 Publications arising from this thesis

The research discussed in this thesis has led to the generation of a number of publications. These include international conference articles and journal manuscripts. The development of actuator designs for DBD-based LFC as discussed in Chapter 3 & 4 of this thesis was published in the following two conference articles:

- Gibson, B. A., R. M. Kelso, and M. Arjomandi (2009a). "Investigation of the Effect of Electrode Arrangement on Plasma Actuator Performance". In: *47th AIAA Aerospace Sciences Meeting and Exhibit*. 2009-1003. Orlando, FL.

- Gibson, B. A., R. M. Kelso, and M. Arjomandi (2009b). "Plasma Actuator Influence on Laminar Boundary Layer Flow". In: *2009 Asia-Pacific International Symposium on Aerospace Technology*. Nagaragawa, GIFU, Japan.

In addition to the conference articles, the results presented in Chapter 7 and are based on the following publication:

- Gibson, B. A., R. M. Kelso, and M. Arjomandi (2011b). "The Response of a Laminar Flat Plate Boundary to an Orthogonally Arranged Dielectric Barrier Discharge Actuator". In: *Journal of Physics D: Applied Physics* Vol. 45, No. 2, pp. 20502-20522.

1.4 Thesis format

In compliance with the formatting requirements of The University of Adelaide, the print and online versions of this thesis are identical. The exceptions exist for some images where Copyright approval for print in the online version was not obtained. In these instances the original images have been replaced with a black box.

The online version of the thesis is available as a PDF. It is known that the PDF version can be viewed in its correct fashion with the use of Adobe Reader 9.

2 Boundary Layers and Laminar Flow Control

The field of Laminar Flow Control research is concerned with minimising the skin friction over bodies moving through fluids. The work centres on the maintenance of laminar flow within the boundary layer that develops over the body as a result of viscous interactions between the fluid and the object. Understanding of the fundamental behaviour of a fluid within a boundary layer is paramount to the development of LFC strategies, and in this chapter the underlying fluid mechanics theory pertaining to LFC is presented.

The first section of this chapter defines a boundary layer, introduces the governing equations of motion applicable to a laminar layer and discusses the basic mechanisms that lead a boundary layer to transition from laminar to turbulent flow. Using this information the robustness of a laminar boundary layer to transition can be assessed using stability analysis techniques, which are introduced in the second part of this chapter. Improving the stability of a flow and its robustness to transition is the objective of plasma-based LFC technology and the final section of this chapter introduces some of the alternative LFC techniques researched to date.

2.1 The physics of boundary layers

As a body moves through a fluid, tangential forces develop between the layers of the fluid and the surfaces of the body upon which the fluid wets. These tangential (*frictional* or *shearing*) forces are associated with the viscosity of the fluid and work to oppose the motion of the object, creating a condition of *no-slip* at the fluid-wall interface. The consequence of the no-slip condition is that the velocity of the fluid at the wall is zero (i.e. the fluid is stationery) and a gradient in fluid velocity is established between the surface and the freestream. Representing a loss in freestream momentum, the velocity gradient results in the formation of viscous-induced or *skin friction* drag on the

body.

The condition of no slip exists for every fluid-surface interaction, meaning that even fluids of negligible viscosity will form a boundary layer over a wetted surface. Hence there is no escaping the development of skin friction drag. However by understanding the physics and motion of the fluid within a boundary layer it is possible to identify strategies to minimise the magnitude of the developed skin friction drag.

Beginning as a structure of negligible thickness at the leading edge of a surface, boundary layers thicken as they develop downstream, doing so in accordance with the geometry and pressure distribution associated with the body. Within the boundary layer many different flow structures varying in both space and time may exist, and encouraging some to exist and others to disappear can lead to a reduction in the developed drag. Typically, a boundary layer will have three types of gross flow structure (Figure 2.1). The initial upstream regions of the boundary layer generally contain laminar flow. The laminar region of the boundary layer contains essentially two-dimensional flow, which leads to a low local boundary layer thickness and minimal skin friction drag. As the boundary layer develops downstream of the leading edge, the laminar structure begins to become unsteady and during this phase, transitional flow exists, characterised by the inception of spanwise variations and increased vorticity, leading to the formation of small-scale vortices near the wall. Eventually these vortices breakdown and manifest into a turbulent flow and consequently a turbulent boundary layer. Turbulent boundary layers have the dubious trait of producing approximately ten-times the skin friction for a given Reynolds number than an equivalent laminar structure (Joslin 1998) and it is for this reason that LFC technology is focused on the maintenance of laminar flow within a developed boundary layer. It has been estimated that if laminar flow could be maintained on the wings of a large transport aircraft, fuel savings of up to 25% would be obtained (Thomas 1985).

Laminar Flow Control aims to maximise the extent of the laminar region of the boundary layer flow. For this reason, understanding the underlying physics of the flow and the motion of the fluid within the boundary layer is of paramount importance. The equations of motion for a boundary layer are obtained from the governing equation of fluid mechanics (the Navier-Stokes Equation, Equation 2.1) and continuity (Equation 2.2), with $\overrightarrow{f}$ representing the sum of the external body forces acting on the fluid. Restricting the research

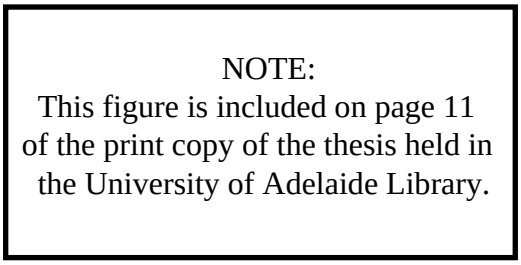

Figure 2.1: Schematic representation of different flow types in a typical boundary layer undergoing transition (White 1974).

from this point on to a two-dimensional boundary layer, the governing equations as applied to a boundary layer are simplified through an *order-of-magnitude-analysis* (Cebeci and Cousteix 1999, Schlichting 1955). The resulting equations of motion for the flow in the x and y directions are defined by Equation 2.3 & 2.4 respectively, with the simplified continuity expression defined by Equation 2.5.

$$\frac{D\overrightarrow{V}}{Dt} = -\frac{1}{\rho}\nabla p + \nu\nabla^2\overrightarrow{V} + \overrightarrow{f} \tag{2.1}$$

$$\frac{\partial u}{\partial x} + \frac{\partial v}{\partial y} + \frac{\partial w}{\partial z} = 0 \tag{2.2}$$

$$u\frac{\partial u}{\partial x} + v\frac{\partial u}{\partial y} = -\frac{1}{\rho}\frac{\partial p}{\partial x} + \nu\frac{\partial^2 u}{\partial y^2} - \frac{\partial}{\partial y}\left(\overline{u'v'}\right) \tag{2.3}$$

$$\frac{\partial p}{\partial y} = 0 \tag{2.4}$$

$$\frac{\partial u}{\partial x} + \frac{\partial v}{\partial y} = 0 \tag{2.5}$$

Solution of the governing equations is achieved with the aid of similarity concepts. Knowing that the velocity of the flow is zero at the wall-fluid

interface (the *no-slip* condition) and recognising that the velocity within the layer tends to the edge velocity (u_e) at the interface of the freestream and the boundary layer, then the velocity of the fluid inside the layer can be expressed as a function of the wall-normal spatial location within the layer (Equation 2.6). Using similarity techniques simplifies the velocity distribution within the layer such that it becomes a function of a single, non-dimensional variable, which is independent of the development length of the layer parallel to the wall, x. This variable (η, defined in Equation 2.7) is known as the *similarity variable* (Cebeci and Cousteix 1999, Schlichting 1955).

$$\frac{u}{u_e} = g\left(x, y\right) \tag{2.6}$$

$$\frac{u}{u_e} = g\left(\eta\right) \tag{2.7}$$

The similarity variable that appropriately describes the behaviour of the boundary layer is that employed by the Falkner-Skan technique for boundary layer flows (Equation 2.8). This variable, when used in conjunction with a dimensionless stream function (Equation 2.9), allows the boundary layer equations (Equations 2.3 & 2.4) to be reduced to a simpler differential equation referred to as the *Falkner-Skan Equation* (Equation 2.10), complete with transformed boundary conditions (Equations 2.11 & 2.12), and dimensionless pressure gradient parameter (Equation 2.13). The representation of the Falkner-Skan Equation presented here also includes terms to account for the term related to Reynolds shear stress found in the simplified Navier-Stokes Equation, $\overline{u'v'}$. These terms (Equations 2.14 & 2.15) are derived from the concept of eddy viscosity (see Cebeci and Cousteix 1999) and are included in this section for completeness. However, as will be shown in Section 2.1.1, these terms disappear when analysing a laminar boundary layer.

$$\eta = y\sqrt{\frac{u_e}{\nu x}} \tag{2.8}$$

$$f\left(\eta\right) = \frac{\psi\left(x, y\right)}{\sqrt{\frac{u_e}{\nu x}}} \tag{2.9}$$

$$\left(bf''\right)' + \frac{m+1}{2}ff'' + m\left[1 - \left(f'\right)^2\right] = x\left(f'\frac{\partial f'}{\partial x} - f''\frac{\partial f}{\partial x}\right) \tag{2.10}$$

$$\eta = 0, \quad f = f_w = -\frac{1}{\sqrt{u_e \nu x}}\int_0^x v_w dx, \quad f' = 0 \tag{2.11}$$

$$\eta = \eta_e, \quad f' = 1 \tag{2.12}$$

$$m = \frac{x}{u_e}\frac{du_e}{dx} \tag{2.13}$$

$$b = 1 + \frac{\nu_t}{\nu} \tag{2.14}$$

$$x\left(f'\frac{\partial f'}{\partial x} - f''\frac{\partial f}{\partial x}\right) \tag{2.15}$$

The Falkner-Skan representation of the boundary layer equations, although simpler than the Navier-Stokes Equation, still has no direct analytical solution. It can however be solved using numerical techniques and a solver capable of this (based on the scheme suggested by Cebeci and Cousteix 1999) has been developed as part of this research (as detailed in Chapter 4). By understanding the motion of the fluid within a boundary layer it is possible to develop strategies for encouraging the maintenance of laminar flow and reducing skin friction drag.

2.1.1 The Blasius boundary layer

The most fundamental of boundary layer flows is a laminar layer developed over a flat plate in the absence of a pressure gradient (or Zero Pressure Gradient, ZPG). This type of flow is more simply referred to as the *Blasius* boundary layer. For the Blasius boundary layer there is no Reynolds stress, since the flow is laminar, nor is there a pressure gradient (by definition). Hence the Falkner-Skan Equation for the Blasius layer can be reduced to an even simpler form (Equation 2.16, with boundary conditions defined by Equations 2.17 & 2.18).

$$f''' + \frac{1}{2}ff'' + = 0 \tag{2.16}$$

$$\eta = 0, \quad f = 0, \quad f' = 0 \tag{2.17}$$

$$\eta = \eta_e, \quad f' = 1 \tag{2.18}$$

The research into DBD-based LFC technology discussed in this thesis has focused on augmenting and controlling a Blasius-type boundary layer. Consequently, from this point onwards in the review of theory and literature, the discussion will be restricted in scope to pertain only to the Blasius layer, unless otherwise specified.

2.1.2 Boundary layer parameters of interest

A consequence of the study of the equations of motion pertaining to boundary layers is the identification of a number of useful and convenient parameters that aid in the development of Laminar Flow Control systems. Four of these parameters are introduced and discussed in this section. More detailed discussions of the four can also be found in numerous texts on fluid mechanics, including Cebeci and Cousteix (1999), Drazin (2002), Schlichting (1933), Bertin (2002), White (1974).

The boundary layer thickness (δ) is the distance from the wall of the body to the closest location where the velocity of the flow is equal to that of the freestream. In laminar boundary layer analysis, the boundary layer thickness is taken as the point where the local boundary layer velocity is equal to 99% of the value in the adjacent freestream velocity, u_e. The thickness of the boundary layer increases as the layer develops downstream. Laminar boundary layers are characteristically thinner than turbulent ones.

The thickness of a boundary layer can be difficult to discern experimentally and analytically. An alternative measurement which is more easily determined is the displacement thickness ($\delta^\star$) as defined in Equation 2.19. The displacement thickness represents the distance by which the external streamlines of the flow are displaced due to the presence and formation of the boundary layer. Similar to the boundary layer thickness, streamlines are displaced further by a turbulent layer and hence turbulent layers have higher displacement thickness values. In addition, the displacement thickness of a destabilised and transitional boundary layer is known to fluctuate, allowing displacement thickness to be used to assess the characteristics and stability of a boundary layer (Howe 1981).

$$\delta^\star = \int_0^\infty \left(1 - \frac{u}{u_e}\right) dy \tag{2.19}$$

The presence of the boundary layer also creates a momentum deficit in the flow. This deficit can be equated to an equivalent layer of fluid with a uniform flow velocity equal to the local freestream velocity. The height of this volume of fluid is called the momentum thickness, θ (defined in Equation 2.20). Again, like the boundary layer thickness and displacement thickness, laminar layers have smaller values of momentum thickness compared with turbulent boundary layers.

$$\theta = \int_0^\infty \frac{u}{u_e}\left(1 - \frac{u}{u_e}\right) dy \tag{2.20}$$

The ratio of displacement thickness to momentum thickness is called the shape factor (H) of the flow (Equation 2.21) and is of great significance in classifying boundary layer flows and predicting boundary layer transition. The value of the ratio differs for laminar and turbulent layers, flows experiencing adverse and favourable pressure gradients, and boundary layers controlled with suction. The shape factor for Blasius flow is constant and equal to 2.59. Laminar boundary layers typically have shape factor values between 2.0 and 4.0. The lower limit of this range corresponds to a boundary layer controlled with uniform suction, and the upper value corresponds to separated flow (White 1974). Study of the flat plate boundary layer in a favourable pressure gradient reveals that the shape factor of the flow will be between 2.0 and 2.59, and between 2.59 and 4.0 when exposed to an adverse pressure gradient (Cebeci and Cousteix 1999). Laminar boundary layers manipulated by some form of control can attain shape factor values between 1.6 and 2.0 (Ogata and Fujita 2009), but a sudden reduction in shape factor is suggestive of the development of a turbulent boundary layer, with fully developed turbulent boundary layers on flat plates having a nominal value of 1.4 (Schlichting 1955, Grundmann and Tropea 2007b), but typically varying between 1.4 and 1.6 (Grundmann and Tropea 2007b). Hence, assessment of the shape factor provides a convenient way to determine the effectiveness of LFC systems on delaying boundary layer transition.

$$H = \frac{\delta^\star}{\theta} \tag{2.21}$$

2.2 Hydrodynamic stability & transition

The evolution of a boundary layer flow from laminar to turbulent flow is known as *boundary layer transition*. Boundary layer transition is a complex process, consisting of numerous simultaneous events involving the growth and propagation of velocity disturbances throughout the layer. These disturbances are the result of external forces that perturb the flow, including surface irregularities and freestream turbulence. The process by which these disturbances enter the layer is known as *receptivity*. This is a separate area of boundary layer study to LFC and a comprehensive review of the subject is provided by Saric et al. (2002). In the context of the present research the process of receptivity is responsible for allowing disturbances to enter a boundary layer. If the conditions of the boundary layer are favourable to the disturbance, the associated velocity fluctuation will begin to amplify, leading to transition at some streamwise location along the surface of the body.

The growth of the disturbances depend on the type, the magnitude, the mechanism through which they enter the flow, and the conditions of the boundary layer itself. Consequently, as discussed by Morkovin (1988) and Saric et al. (2002), a boundary layer may follow one of many different paths on its way to becoming fully turbulent, as shown on the transition *road map* (Figure 2.2). In flows over aircraft wings and fuselages that are or are very nearly two-dimensional flows, the transition process often begins with the inception of primary modes (Thomas 1985, Saric et al. 2002). These primary mode instabilities are, in essence, two dimensional wave fronts that grow in an approximately linear fashion and the transition process involving these primary modes occurs over a comparatively large streamwise distance. The LFC technology pertaining to the undertaken research is focused on damping the growth of these linear primary mode disturbances. Consequently, the subsequent discussion of transition and LFC techniques in this thesis is in reference to natural transition involving the amplification of these linear, primary mode disturbances.

Transition involving linear disturbance amplification is often referred to as *natural transition* since it can occur with no external forcing (Schlichting 1955). This type of transition is the type of transition schematically represented in the previous section (Figure 2.1). Natural transition begins with the amplification of small disturbances at a near-linear rate. This growth results in the development of two dimensional wave fronts, the existence of which were first predicted by Tollmien (1929) and the nature of which mathematically identified by Schlichting (1933). It is for this reason that the two dimensional wave fronts are often referred to as *Tollmien-Schlichting* (T-S) waves, and primary mode transition results from the ultimate breakdown of these two dimensional flow structures into three dimensional turbulence.

The transition of a boundary layer due to the linear growth of disturbances within the flow is today widely accepted as a transition mechanism. However, historically this was not always the case. Schlichting (1933) had provided mathematical support to Tollmien's early work into boundary layer transition, but due to a lack of experimental evidence supporting the theory, the acceptance of the analytical results was limited (Schlichting 1955). The reason for this was a lack of suitable wind tunnels that possessed a sufficiently low level of turbulence and large enough test section required to observe the growth of the predicted disturbances. It was not until over two decades after the first prediction of these primary modes that experimental technology allowed the acquisition of results supporting the theory. The experiments were performed by Schubauer and Skramstad (1950) and are noteworthy, amongst other things, for the extremely low levels of turbulence

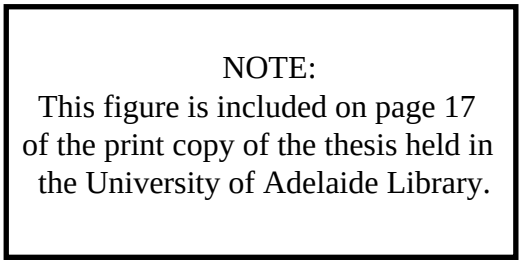

Figure 2.2: The *road map* from receptivity to transition (adapted from Saric et al. 2002).

that the researchers achieved in their investigations. Using a total of six flow screens in the settling chamber of a closed circuit wind tunnel at the National Bureau of Standards, turbulence levels of the order of 0.01% were attained by the researchers. This allowed the researchers to observe the natural transition process and observe the predicted linear growth of the primary mode disturbances.

Boundary layers transition from laminar to turbulent flow due to the growth of disturbances. It has been discussed how these disturbances can enter the flow, but the question of where these disturbances begin to grow and bring about transition still remains. The answer to this question is not trivial, and very difficult to ascertain due to the nature of the receptivity process and individual circumstances pertaining to each flow. To provide assistance in identifying the point of transition, the hydrodynamic stability of the flow can be studied. The hydrodynamic stability of the flow allows the spatial and temporal amplification of disturbances of different frequencies and wavelengths to be determined. This information can subsequently be used to provide approximate locations of transition, areas of concern for transition, as well as insights into ways to delay the transition process. The

details of the *hydrodynamic stability* (or simply *stability*) of the flow can be obtained by investigating the Navier-Stokes equation using Linear Stability Theory.

2.2.1 Linear Stability Theory & Analysis

By considering the governing equations of the flow within the boundary layer, the growth and behaviour of transition-inducing disturbances can be studied. This technique allows the prediction of the natural transition process and is referred to as Linear Stability Theory (LST). A detailed discussion of linear stability theory, its origins, attributes and predictions can be found in numerous texts, including Cebeci and Cousteix (1999), Drazin (2002), Schlichting (1955). Rather than repeat these discussions, the following section presents an introduction to the theory from which its usefulness to the research is subsequently derived. In line with the scope of the research, the theory and discussion presented are restricted to two-dimensional boundary layer flows.

Linear Stability Theory essentially involves the calculation of stability limits for the transition-inducing velocity fluctuations associated with primary mode disturbances. LST models each disturbance as periodic in both space and time and allows the onset of amplification for each disturbance (also referred to as *the point of marginal stability* for each disturbance) to be determined. By determining this point of marginal stability for a spectrum of disturbances it is thus possible to identify the disturbance frequencies and wavelengths to which the flow is susceptible, as well as the location within the boundary layer at which these disturbances become unstable. Furthermore, LST can be used to determine the spatial and amplification rates of the disturbances, which can subsequently be used to estimate the location of transition onset.

2.2.1.1 Derivation of the Theory

In LST the velocity disturbance is assumed to be two dimensional and periodic in both space and time. This assumption allows a single disturbance to be expressed as a stream function, $\psi(x, y, t)$ (Equation 2.22), derived from the complex variables $\omega = \omega_r + i\omega_i$ and $c = \frac{\omega}{\alpha} = c_r + ic_i$. ω_r represents the circular frequency of the oscillation, c_r the phase velocity of the disturbance, α the spatial wavenumber of the disturbance, and the imaginary components of the complex variables are the respective amplification factors. The function $\phi(y)$ describes the variation of the disturbance amplitude throughout the boundary layer.

$$\psi(x, y, t) = \phi(y)\, e^{i(\alpha x - \omega t)} \tag{2.22}$$

Consistent with potential flow theory, the components of the fluctuating velocity disturbance can be obtained through the differentiation of the stream function. Substitution of these derivatives into the governing Navier-Stokes Equations yields a fourth order eigenvalue problem, linearised about the velocity, u, of the base flow. This eigenvalue problem, commonly referred to as the *Orr-Sommerfeld Equation* or *OSE* (Equation 2.23), has boundary conditions related to the original governing equations of the boundary layer flow (Equation 2.24 & 2.25; note that the derivatives that feature in the OSE are with respect to y, i.e. the wall-normal direction).

$$(u - c)\left(\phi'' - \alpha^2\phi\right) - u''\phi = \frac{-i\nu}{\alpha}\left(\phi^{iv} - 2\alpha^2\phi'' + \alpha^4\phi\right) \tag{2.23}$$

$$y = 0,\ \phi = 0,\ \phi' = 0 \tag{2.24}$$

$$y = \delta,\ \phi = 0,\ \phi' = 0 \tag{2.25}$$

The consequence of the OSE is that the disturbances to which a flow is susceptible are dependent on the mean velocity characteristics of the flow. Although no analytical solution exists for the OSE, the eigenvalues of the equation can be determined through a number of techniques. In Chapter 4 the numerical method developed as part of this research in order to solve the OSE is presented and discussed. By using this numerical method to determine the frequencies and disturbances that the flow is susceptible to, it is possible to determine the Reynolds number at which each disturbance becomes unstable. Conversely it is possible to identify the disturbances that the flow is susceptible to at each Reynolds number. By finding these disturbances for every Reynolds number it is possible to construct a stability curve from which the stability of the flow can be understood. An example of such a curve is shown in Figure 2.3. For a given Reynolds number, any disturbance lying outside the circumscription of the locus will be damped and any lying within will be amplified. The consequence of this is that there exists a critical Reynolds number (and hence chordwise position) below which every disturbance will be damped, the so called *critical Reynolds number*, Re_{crit}. For the Blasius boundary layer, the critical Reynolds number based on displacement thickness, $Re_{\delta^*_{crit}}$ is approximately 575. In terms of chordwise position x, the critical Reynolds number is approximately 110000.

NOTE:
This figure is included on page 20
of the print copy of the thesis held in
the University of Adelaide Library.

Figure 2.3: Curve of neutral stability for a flat plate boundary layer (adapted from Schlichting 1933).

Amongst other things, LST provides some insight into strategies for LFC. A LFC system that can reduce the number of disturbances circumscribed by the stability locus and/or which increases the critical Reynolds number of the flow will improve the flow stability and a delay in the onset of natural transition.

General criterion for instability

The derivation of Linear Stability Theory is deeply grounded in the work of Reynolds and Lord Rayleigh undertaken in the 19th century (Schlichting 1955). Although neither was able to mathematically describe stability phenomena sufficiently accurately, some general insights were able to be gleaned from their undertakings. One of the most important is the general criterion for instability that stems from the *Rayleigh Stability Equation* (the RSE, Equation 2.26), itself an inviscid form of the OSE and one based on the same assumptions.

$$(u-c)\left(\frac{\partial^2\phi}{\partial y^2}-\alpha^2\phi\right)-\frac{\partial^2 u}{\partial y^2}\phi=0 \tag{2.26}$$

If the RSE is multiplied by its complex conjugate and integrated from y_1 to y_2, the resulting homogeneous equation (Equation 2.27) contains an imaginary component of vital importance (Equation 2.28). Through study of the

imaginary component it can be inferred that if the quantity $\frac{\partial^2 u}{\partial y^2}$ changes sign on the interval from y_1 to y_2, then the flow will become unstable (Rayleigh 1880). This postulation was supported and reinforced by Fjørtoft (1950) who proved, through modification of the original theory, that $\frac{\partial^2 u}{\partial y^2}(u - u_S) < 0$, (where y_S is a point corresponding to $\left.\frac{\partial^2 u}{\partial y^2}\right|_{y_S} = 0$ and $u_S = u(y_S)$) is a necessary condition required for a disturbance to become amplified. Hence the presence of an inflection point in the velocity profile of a boundary layer is a necessary and often sufficient requirement for boundary layer transition (Drazin 2002). The consequence of these mathematical analyses is that any augmentation to a boundary layer flow occurring through the use of a LFC system must avoid the introduction of inflection points into the mean velocity profile of the flow, or if it does introduce an inflection, this needs to decay in space and time rather than amplify.

$$\int_{y_1}^{y_2} \left[\left| \frac{\partial \phi}{\partial y} \right|^2 + \alpha^2 |\phi|^2 \right] dy + \int_{y_1}^{y_2} \left[\left(\frac{1}{u - c} \right) \left(\frac{\partial^2 u}{\partial y^2} \right) |\phi|^2 \right] dy = 0 \tag{2.27}$$

$$c_i \int_{y_1}^{y_2} \left[\left(\frac{1}{u - c} \right) \left(\frac{\partial^2 u}{\partial y^2} \right) |\phi|^2 \right] dy = 0 \tag{2.28}$$

2.2.1.2 Predicting transition from LST results

The results of linear stability theory have been shown by some researchers to be useful in locating the streamwise position of transition. The methods attempt to locate the spatial distance between the point of neutral stability and turbulent breakdown, and subsequently allows the streamwise location from some reference point to be located. Liepmann (1945) suggested that the turbulent breakdown occurs when the ratio of instability shear stress to the viscous shear stress of the base flow exceeds some critical value. Using this idea Smith and Gamberoni (1956) and Ingen (1956) proposed that breakdown would occur when a disturbance introduced at a point of the curve on neutral stability is amplified by a factor of $e^{n_{cr}}$. Smith and Gamberoni (1956), using results of measurements from low turbulence intensity experiments, suggest that $n_{cr} \approx 9$. This value corresponds to an amplitude amplification of approximately 8000.

To accommodate for the effects of freestream turbulence, a correction to the e^n method has been formulated by Mack (1977), who suggested that the amplification ratio required for complete turbulent breakdown should decrease with increasing freestream turbulence, T_u. Thus a corrected form of the critical amplification factor is given by Equation 2.29.

$$n_{cr} = -8.43 - 2.4ln\left(T_u\right) \tag{2.29}$$

An alternative to the e^n method is to use shape factor correlations to locate the transition point. The method is described by Wazzen et al. (1981) and is a shortcut based on LST and the e^n methodology. For a boundary layer with a shape factor value between 2.1 and 2.8 the chordwise position of transition (x_{tr}) is found using Equation 2.30. This method is both computationally efficient, requiring only mean velocity profile data, and sufficiently accurate for quick estimates of the location of transition.

$$log\left(\frac{u_e x_{tr} e^9}{\nu}\right) = -40.4557 + 64.8066H - 26.7538H^2 + 3.3819H^3 \tag{2.30}$$

As shown in the transition road map (Figure 2.2) the process is lengthy and can take a number of different paths, with or without primary transition modes. Thus, more formally, transition can be thought of as the space and time over which the flow goes from featuring disturbances beginning to amplify, to the time when the flow is fully turbulent (Cebeci and Cousteix 1999), and hence the actual location needs to be inferred from experimental study. However, the two prediction techniques discussed here provide a convenient shortcut for obtaining a useful estimate of the extent of laminar and turbulent flow within a given boundary layer.

2.2.1.3 Laminar Flow Control and augmentation of stability

There are two ways in which the stability of a fluid can be augmented. Understanding of both stems from the physics described by the OSE. The first is to change the mean flow characteristics of the boundary layer through thinning and profile shaping. The second is to use wave superposition to attenuate the linear disturbances, and impede their growth. Of the two, the former results in augmentation of the curve of neutral stability, and thus provides a more broadband, and potentially more robust approach to LFC. For this reason the research discussed in this thesis developed a LFC technique based on augmentation of the mean flow characteristics of a boundary layer.

In this section, the effect of two common LFC techniques that augment the mean flow characteristic are theoretically introduced. This allows an insight into how pressure gradient augmentation and boundary layer suction can be used to improve the stability of a flow and delay transition. In addition, it highlights the requirements that a plasma-based LFC system will have to meet.

Effects of pressure gradient

Through clever consideration and design of an aerodynamic surface it is possible to achieve improvements in boundary layer stability. Passive laminar flow control can be realised by altering the pressure distribution over a body through shape optimisation. The effect of the pressure gradient is related to the Pohlhausen shape factor (Λ) associated with the boundary layer velocity profile (Equation 2.31). A positive value of Λ corresponds to an accelerating flow, with a favourable pressure gradient, and the converse is true for a negative value of Λ. A favourable pressure gradient is found to increase the critical Reynolds number of the flow and reduce the range of frequencies to which the boundary layer is sensitive (Figure 2.4).

$$\Lambda = \frac{\delta^2}{\nu}\frac{dU}{dx} \tag{2.31}$$

Variations in the shape of a body augments the pressure distribution and can thus provide improvements to flow stability and transition delay. An experimental study conducted by Cousteix and Pailhas (1979) studied the evolution of transition over an airfoil. Consistent with the theory, the researchers found that an adverse pressure gradient over the upper surface promoted boundary layer transition. The areas with greatest pressure gradients differed slightly from the theory due to the formation of separation bubbles and

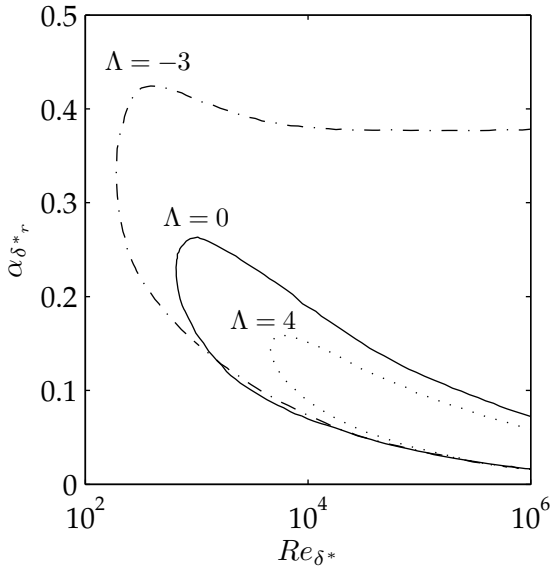

Figure 2.4: Curves of neutral stability for a flat plate boundary layer with pressure gradient augmentation (adapted from Schlichting 1955).

separation of the boundary layer, however the regions of moderate pressure gradient agreed well with the theoretical predictions.

Pressure gradient augmentation has found much use in the design of low Reynolds number airfoils. In the design of these airfoils, controlling the location of transition is critical in reducing the size of the separation bubbles, ensuring flow reattachment, minimising drag and maximising performance (Lissaman 1983). Pressure augmentation for positioning transition has led to many low Reynolds number designs including those developed by Selig et al. (1989) that offer improved performance in low Reynolds number flows without the high drag associated with high Reynolds number airfoils operated at low speeds (Lissaman 1983). Although pressure shaping is not being used to delay transition and minimise skin friction drag in low Reynolds number airfoil design, the results of such designs do demonstrate how variation of the pressure gradient over a body might be used in a LFC system.

Varying the pressure gradient over a boundary layer requires alteration of the geometry of the body over which the flow is formed. Therefore, it may not be practical to do this if certain geometrical design features take precedence over drag minimisation. Hence it is feasible to suggest that this may be the reason why pressure gradient augmentation for reducing skin friction drag is yet to find extensive commercial application.

Effects of suction

The use of suction for Laminar Flow Control involves the use of a permeable wall surface that is able to remove fluid from the boundary layer through a wall-normal suction effect. Suction has a two-fold benefit to the maintenance of a laminar boundary layer and subsequent reduction in drag. Firstly, suction serves to thin a boundary layer and hence make it less likely to become turbulent. Secondly, suction augments the velocity profile of the boundary layer and compels it to remain laminar in regions that would otherwise be turbulent. The result is that a boundary layer with suction possesses a higher limit of stability and critical Reynolds number than one without (Schlichting 1955).

Boundary layer suction is conceptually interpreted as a boundary layer in which there is a vertical component of velocity towards and through the wall. As discussed by Schlichting (1955), if a uniform suction velocity (v_0) is applied to a flat plate boundary layer with a zero pressure gradient, it is found that the velocity profile within the layer asymptotes towards a profile, which is independent of location, and of constant displacement thickness (Equation 2.32). In addition, the shape factor of the flow asymptotes to a

constant value of 2.

$$u(y) = u_e \left[1 - exp\left(\frac{v_0 y}{\nu}\right)\right] \tag{2.32}$$

The consequence of suction on the stability of the boundary layer is highly beneficial. As shown by Bussmann and Münz (1942) (as cited by Schlichting 1955) a boundary layer in which the velocity profile is that of the asymptotic suction profile has a critical Reynolds number (based on displacement thickness) two orders of magnitude greater than that of the base Blasius flow. In addition, Bussmann and Münz (1942) (as cited by Schlichting 1955) approximated the velocity profiles of the boundary layer during the development towards asymptotic suction. For various suction parameters (Equation 2.33) the authors observed that an increasing value of the suction parameter leads to an increase in the critical Reynolds number, and a reduction in the range of unstable disturbances and frequencies circumscribed by the curve of neutral stability.

$$\xi = \left(\frac{-v_0}{u}\right)^2 \frac{ux}{\nu} \tag{2.33}$$

The use of suction hence improves flow stability and delays transition. The effect of suction is similar to the use of a favourable pressure gradient in as much as the boundary layer becomes thinner, with a more favourable velocity profile. Unlike shape optimisation however, suction can be applied to existing geometries and it can be controlled. These facets of suction improve its usefulness and potential for LFC.

2.2.1.4 Transition delay with wave superposition

Given the linear behaviour of the two-dimensional waves, it is possible to exploit the principle of wave superposition to delay the onset of transition. Whilst this strictly does not augment the stability of the fluid by invoking gross changes to the mean flow characteristics, the technique is based on LST and for completeness is introduced here. Through LST it is possible to identify the particular frequencies and wavelengths to which a flow is susceptible. This information can then be used as a guide for identifying the presence of potentially unstable disturbances in a flow. If found, the growth can be attenuated by introducing a counter-disturbance out of phase with that already present. This counter-disturbance will subsequently destructively interfere with the present disturbance, thus reducing its amplitude and hence delaying its contribution to the breakdown of laminar flow in the layer. Using

wave superposition on appropriate disturbances throughout the entire layer can theoretically delay transition indefinitely.

Early verification of the use of wave superposition for transition delay was provided by Wehrmann (1965). Using a flexible wall on which a boundary layer was formed, the velocity fluctuations associated with an artificially introduced perturbation of fixed frequency were able to be damped or amplified depending on the relative phase and amplitudes of the oscillations applied to the wall. Later studies conducted in the 1980s and beyond have supported this work (Milling 1981, Thomas 1983) and alternative control devices such as heating and cooling elements (Liepmann and Nosenchuck 1982, Liepmann et al. 1982) and acoustic arrays (Li and Gaster 2006, Opfer 2002, Sturzebecher and Nitsche 2002, Sturzebecher and Nitsche 2003a, Sturzebecher and Nitsche 2003b, Baumann et al. 2000) have been shown to be effective in delaying boundary layer transition.

2.3 Brief review of Laminar Flow Control systems

Research into Laminar Flow Control can be traced back to the late 1920s and early 1930s with the work of Tollmien (1929) and Schlichting (1933) predicting the existence of primary mode transition. A detailed review of the subsequent research into LFC that followed is given by Joslin (1998) and in this it becomes clear that the history of LFC research has been heavily dependent upon the global price of oil. This is seen by the documented resurgence in interest in LFC research that occurred during the 1970s. During the 1970s, the aviation industry, faced with rising oil costs, searched for ways to improve aerodynamic efficiency and reduce fuel consumption; LFC was an obvious area of interest.

To date, LFC systems that have made it to flight trials have used suction, shape optimisation, or a combination of both, to augment the mean velocity characteristics and hence limits of stability of a boundary layer flow (Joslin 1998). There is a lack of discussion of flight tests using active wave cancellation techniques and this can be attributed to the complex sensing requirements and reliability concerns required to make them effective in real-world scenarios. Suction systems have been found to be effective, but complex, with the need to incorporate a reliable pumping source in the system, as well as difficulties in manufacturing surfaces with the required slots. Shape optimisation is less complex, but has been shown to be vulnerable to the formation of three dimensional instabilities that cause the systems to be ineffective without the use of some active flow control, such as suction (Joslin 1998). Hybrid Laminar Flow Control uses suction over the leading edge of a

surface and shape optimisation over the remainder to offer a less complex system, but one with similar performance that attained solely with suction (Joslin 1998).

Both the Lockheed and the Douglas aircraft companies demonstrated the potential of a suction-based LFC system during the 1980s (Fischer et al. 1983). The two companies developed leading edge suction systems for a Lockheed C-140 aircraft. One was placed on each side of the wing, ahead of the front spar and both companies reported that laminar flow could be maintained for up to 12% of the chord length of the wing (Hefner and Sabo 1987). Subsequent simulated airline services were operated with this aircraft, and the results were positive for the development of LFC technology. According to Maddalon and Braslow (1990) the use of the LFC systems required no input from the crew other than the activation of the system on board. In addition the systems were found to be reliable, a point of utmost importance for any innovative aviation technology.

Over the past three decades, other aircraft have been tested with suction and hybrid LFC systems, showing the potential and effectiveness of the technology. A recent example is the hybrid system applied to the tail fin of an Airbus A320. According to Schrauf and Horstmann (2004), a 15% reduction in the total drag of an A320 can be realised if the system used on the tail fin was applied to all lifting surfaces of the aircraft. However, in its initial form, the technology was found to be too heavy and complex to be considered feasible for commercial application (Schrauf and Horstmann 2004). Subsequent design refinement has lead to reductions in complexity and system weight, to levels possibly viable for commercial use (Schrauf and Horstmann 2004), yet still to date no LFC technology is utilised commercially in the global aviation industry. Hence further work into the development of LFC technology is clearly required, warranted and justified.

According to Joslin (1998), LFC technology is yet to find wide acceptance in the aviation sector as it is unclear as to what the long term technical and economical viability of conventional LFC technology is. The future of LFC, claims Joslin (1998), resides in novel and innovative technologies, including synthetic jet actuators like DBD devices. It is anticipated by Joslin (1998) that these alternative actuators may provide significant improvements over existing technology, with less expense and complexity. As discussed in greater detail in Chapter 3, just recently wind tunnel experiments have shown DBD plasma devices as being capable of delaying boundary layer transition (Grundmann and Tropea 2007a, Grundmann and Tropea 2007b, Grundmann and Tropea 2009). With no moving parts and proven capability, DBD actuators may prove to be the future LFC system foretold by Joslin

(1998), providing of course enough resources are allocated to thoroughly research the capabilities of this innovative technology.

2.4 Summary

In this chapter the fundamentals of boundary layer theory have been introduced, allowing an understanding of Laminar Flow Control and its objectives to be attained. All LFC systems aim to improve the hydrodynamic stability of a flow, thus attenuating the growth of transition-inducing disturbances and hence delaying the onset of turbulent flow.

By studying the equations of motion that describe the behaviour and hydrodynamic stability of the fluid within a boundary layer, the discussion within this chapter has shown how the robustness of a boundary layer to transition can be augmented through shape optimisation, suction and wave superposition techniques. However, as demonstrated in the literature, the weight and complexity of current LFC systems, particularly those incorporating wave superposition techniques, has meant that LFC technology is yet to be widely utilised in the aviation industry. Consequently, there exists significant room for the development of simpler, more robust and cost-effective systems incorporating DBD plasma, and the research discussed in this thesis aims to do this by contributing to the development of DBD-based technology to control the flow within a laminar boundary layer.

3 Literature Review

Having introduced the concept of Dielectric Barrier Discharge plasma-based Laminar Flow Control in the preceding chapter, a review of DBD plasma flow control is presented in this chapter. The review includes a discussion of the fundamental performance of DBD actuators, the parameters that affect the jetting characteristics that such devices produce, and how DBD actuators have to date been used for augmenting and controlling boundary layer flows. Particular attention is given to identification of mechanisms through which the jetting characteristics of DBD actuators can be controlled so as to allow the formulation of feasible tuning strategies for the DBD-based LFC system that was to be developed. The chapter concludes with a summary of the research objectives of this work, and the identified novel actuator designs and tuning strategies discussed in detail in Gibson et al. (2009b).

3.1 DBD plasma: an alternative flow control device

Dielectric Barrier Discharge (DBD) actuators have gained significant interest amongst researchers in recent years for use as flow augmentation devices. Unlike flow control techniques such as suction, which were being experimentally trialled in the 1950s (Joslin 1998), the first experimental demonstrations of a DBD actuator augmenting a boundary layer flow at low speeds occurred only 13 years ago (Roth et al. 1998). Through the production of a small, self-sustaining volume of surface plasma, using electrodes operated at high voltages, DBD devices are able to couple with and contribute to the momentum of a surrounding fluid. The momentum addition arises from the development of an electrostatic force, associated with the movement of charged particles within the developed plasma, which interacts with the dipoles of the surrounding fluid molecules and results in a localised jetting phenomenon (Roth and Dai 2006, Corke et al. 2010).

A typical DBD actuator features two electrodes, connected to a high voltage Alternating Current (AC) power source, and separated by a dielectric

surface, which together are capable of inducing a fluid flow in the vicinity of the plasma (Figure 3.1). Providing that the amplitude of the electric field established between the electrodes is greater than the plasma breakdown field strength (E_b, defined as the value that allows electron-ion pairs to be established in the isolated gas) then a self sustaining plasma will be formed between the electrodes (Corke et al. 2010). Once established, the electric field strength required to sustain the discharge diminishes to E_s, which, like the breakdown field strength, is a function of the operating conditions of the plasma (Corke et al. 2010). In environments at or near atmospheric pressure, DBD plasma formation requires lower peak field strengths than equivalent Direct Current (DC) plasma formation techniques such as corona discharge. Consequently DBD plasma technology can potentially be more reliable and more energy efficient than DC systems, making them more ideal for real-world usage (Corke et al. 2010).

Associated with the electric field developed by the plasma discharge is a net electrostatic body force. This body force can be used to couple with the molecular structure of weakly ionized and weakly polarised gases such as air, and it is this body force which can be utilised for flow control. At the same time, the technique of plasma formation is limited in its usefulness for controlling conducting fluids such as water. The developed body force gives rise to a jetting effect without the addition of mass. For this reason, DBD actuators can be referred as *synthetic wall-jets* (Santhanakrishan and Jacob 2006, Santhanakrishan and Jacob 2007, Mello et al. 2007) and when the performance of DBD wall-jets is studied, similarities with Glauert-type wall-jets can be clearly seen, (Figure 3.2).

The plasma produced by a DBD actuator results from collisional activity

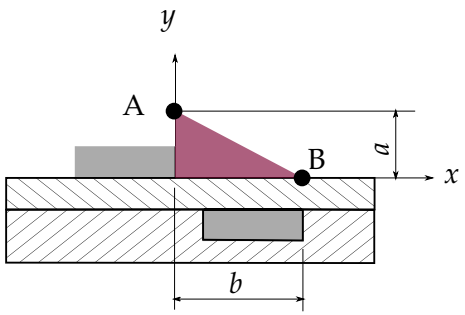

Figure 3.1: Schematic representation of a DBD actuator and the induced flow developed by the device.

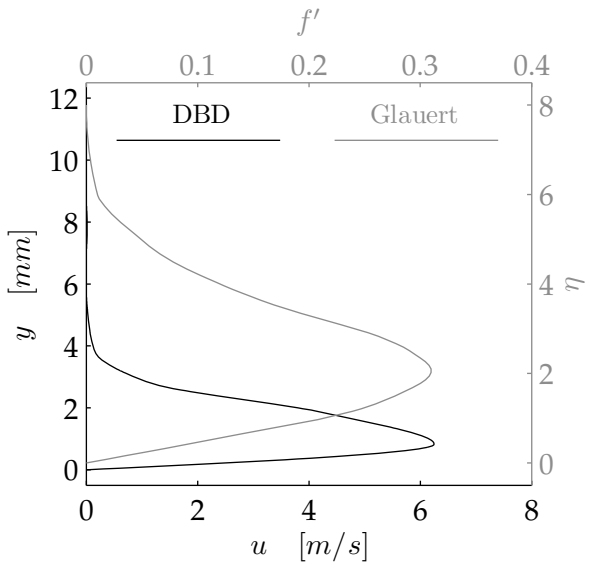

Figure 3.2: Comparison of DBD actuator with a Glauert wall-jet. DBD results from the author. For the Glauert results the velocity and height are plotted in an equivalent non-dimensional form as discussed by Glauert (1956).

involving charged particles. As discussed by many authors, during one half of the AC cycle, electrons leave the exposed electrode and move towards the encapsulated one, accelerated by the strong electric field between the two. During the movement the electrons collide with the surrounding air molecules, leading to localised ionisation and plasma formation (Roth 2001, Font 2004, Van Dyken et al. 2004, Roth and Dai 2006, Abe et al. 2007, Forte et al. 2007, Cho et al. 2008, Corke et al. 2010). On reaching the dielectric surface the electrons accumulate, creating a pseudo-cathode, whilst also making themselves available for collisional activity in the second half-cycle (Kogelschatz et al. 1997, Enloe et al. 2004b). Once the polarity of the current source reverses, the accumulated electrons on the dielectric discharge and move back towards the exposed electrode, creating further ionisation. The time scale of the process depends on the actuator and the ambient conditions, but in air is reported to be approximately $10ns$ (Falkenstein and Coogan 1997). The ionisation process is asymmetrical, with differing densities of charged particles per half-cycle, a direct consequence of the electron accumulation on the dielectric (Kogelschatz et al. 1997, Enloe et al. 2004b). Consequently the body force produced by the plasma differs between each half-cycle. For many years this asymmetric ionisation cycle created much debate amongst researchers as to the direction of the body force during each half-cycle. Some

researchers who attempted to model the developed plasma suggested that the direction of the body force changed between half-cycles, but when averaged over a complete cycle was directed towards the encapsulated electrode (Font 2004, Font and Morgan 2005). This gave rise to the so called *PUSH-pull* force production mechanism, where the capitalisation indicates the relative magnitudes of the forces (Corke et al. 2010). Experimental evidence, however, does not support this, with numerous experiments conducted in quiescent air suggesting a *PUSH-push* force production mechanism in which a force directed towards the encapsulated electrode is developed in each half cycle (Forte et al. 2006, Enloe et al. 2009). This is supported by the numerical modelling of the plasma conducted by Orlov (2006) and Orlov et al. (2006), and hence it is now accepted that DBD actuators contribute to the momentum of a fluid in both half-cycles of the discharge (Corke et al. 2010).

An important property of the plasma is the temperature at which it is formed. In a DBD actuator the plasma is developed in non-thermal equilibrium and the associated electrical energy couples into the surrounding gas to form energetic particles. This consequently allows the gas temperature to essentially remain unchanged (Corke et al. 2010). According to Falkenstein and Coogan (1997) this phenomena is attributed to the ability of electrons to accumulate on the surface of the dielectric, which inhibits thermal arcing from occurring. Consequently the flow control effects of DBD actuators can be attributed solely to the developed body force and not localised heating of the fluid.

3.2 Laminar Flow Control with DBD actuators

The magnitude of the force developed by a DBD actuator is far from large. Even though DBD actuators produce very little in the way of *brute force*, the fact that the actuator is capable of having a dramatic influence on a surrounding region of fluid makes these devices suitable candidates for laminar flow control systems.

Present DBD technology is limited to providing actuation forces of the order of $0.020^{N}/_{m}$ (Baughn et al. 2006, Thomas et al. 2009), which is by no means large. It is for this reason that much attention has been given to utilising these devices for low Reynolds number and laminar flow applications where the magnitude of the force becomes relatively more significant and effective. An example of the effectiveness was observed in the work of Corke et al. (2002). Using a single DBD actuator placed at a normalised chordwise position ($\frac{x}{C}$) equal to 0.72, these authors were able to achieve an increase in the lift coefficient of a NACA 0009 airfoil of approximately 0.050 , at a

Reynolds number based on chord length of 18000, for all angles of attack measured (Figure 3.3). These results corroborate well with other reported improvements in low Reynolds number airfoil performance brought about by the use of DBD actuators (Post and Corke 2003, Gaitonde et al. 2006, Munska and McLaughlin 2006, Rizzetta and Visbal 2011).

For use as a Laminar Flow Control device, the DBD actuators need to be capable of favourably augmenting the laminar component of a boundary layer. One of the first experiments that measured the effect of a DBD device on a boundary layer flow was that performed by Roth et al. (2000), who used an array of 26 DBD actuators placed in series and measured the response of the layer to these actuators at a chordwise Reynolds number of 40000. Two tests were performed, one with the electrodes arranged in a streamwise fashion, the other with the electrodes placed in a spanwise fashion. These experiment were some of the first physical demonstrations of DBD flow augmentation and as such the actuators were not designed to favourably augment the flow. The results showed that significant augmentation of the flow occurred with operation of the streamwise arranged array, with severe inflections in the measured velocity profile (Figure 3.4). In addition smoke visualisation revealed the development of longitudinal vortices, consistent with the promotion of transition. For the spanwise case, less dramatic flow augmentation was observed, but inflections were still introduced into the

NOTE:
This figure is included on page 33
of the print copy of the thesis held in
the University of Adelaide Library.

Figure 3.3: Effect of DBD plasma on the lift coefficient of a NACA 0009 airfoil, $Re_C = 18000$, (adapted from Corke et al. 2002).

velocity profile and both sets of results suggested that the DBD actuators were useful for promoting boundary layer transition, irrespective of the arrangement of the electrodes.

The response of a flat plate boundary layer to the presence of a single Dielectric Barrier Discharge actuator was the focus of a study undertaken by Jacob et al. (2004). With the actuator electrodes arranged in a spanwise fashion, the velocity profile at a streamwise Reynolds number of 30000 was recorded using Particle Image Velocimetry. The plasma actuator was found to significantly accelerate the flow in the boundary layer, but in doing so introduced a very large inflection in the flow. From this it was concluded that DBD actuators have a noticeable effect on boundary layers, including the ability to make the layer become unstable through the introduction of inflections in the velocity profile, corroborating the earlier observations of Roth et al. (2000).

Newcamp (2005) utilised a single DBD actuator with spanwise electrodes in experimental investigations to delay boundary layer separation on the suction side of a Pak-B-type low pressure turbine blade. Velocity profile measurements were taken 7.1mm downstream of the exposed electrode at

NOTE:
This figure is included on page 34
of the print copy of the thesis held in
the University of Adelaide Library.

Figure 3.4: Effect of actuator electrode orientation on boundary layer velocity profiles, $Re_x = 40000$ (adapted from Roth et al. 2000). Note that the profiles are plotted using dimensionless coordinates.

various Reynolds numbers, with the actuator operated at various power levels. The actuators were found to significantly augment the boundary layer profile at all Reynolds numbers investigated. For the low Reynolds number case ($Re_x = 40000$) the augmentation was found to introduce vortex structures leading to boundary layer destabilisation for all actuator powers tested (Figure 3.5). Whilst this may be beneficial for delaying boundary layer separation, it is not so useful for LFC system design. However the augmentation was found to be dependent on the power of the actuator and this suggests that varying actuator power can be used as a tuning mechanism for a DBD-based LFC system.

In addition to actuator power, Baughn et al. (2006) showed that the response of a flat plate boundary layer to a DBD actuator is dependent on the frequency at which the actuator is operated. Measuring the velocity profiles of the boundary layer at chordwise Reynolds numbers between 95000 and 140000, it was found that the response of the boundary layer was more dramatic for higher applied actuator frequencies. Of interest to LFC-system design was that an actuator operated at a fixed applied voltage was able to augment the boundary layer in a seemingly stable fashion when operated with a lower frequency for both flow speeds measured (Figure 3.6). However, the investigation of Baughn et al. (2006) was conducted at a Reynolds number

NOTE:
This figure is included on page 35
of the print copy of the thesis held in
the University of Adelaide Library.

Figure 3.5: DBD actuator influence on a low Reynolds number boundary layer developed over the suction side of a Pak-B-type low pressure turbine blade, $Re_x = 40000$ (adapted from Newcamp 2005).

close to the critical value for Blasius flow, and analysis of the published velocity data suggests that the flow was not completely laminar throughout the investigation region. Hence the results of Baughn et al. (2006) suggest a mechanism through which tuning of a DBD-based LFC system could potentially be achieved, but future work focused on comparing the results of Baughn et al. (2006) with a similar study conducted on a completely laminar flow would be beneficial to LFC system design.

Although the literature discussed so far was not pertaining specifically to DBD-based LFC design, it does highlight why minimal details of such technology exist in the literature. The destabilising effects of DBD actuators on the velocity profiles of the flows observed in most experimental investigations discussed explain why Johnson and Scott (2001) reported that the use of DBD actuators led to disturbance amplification in boundary layer flows, concluding, like Porter et al. (2007), that DBD actuators can be used as effective boundary layer tripping devices. A subsequent experimental study undertaken by Magnier et al. (2009) corroborated these reports. The investigation measured the response of a flat plate boundary layer to DBD devices placed at four different chordwise locations, at freestream speeds between $15^{m}/_{s}$ and $22^{m}/_{s}$. Magnier et al. (2009) reported that the synthetic

NOTE:
This figure is included on page 36
of the print copy of the thesis held in
the University of Adelaide Library.

Figure 3.6: DBD actuator influence on a flat plate boundary layer with different applied frequencies, at a constant applied voltage $V_{app} = 15.5kV_{pp}$ (adapted from Baughn et al. 2006).

jets of the DBD actuators promoted transition in the boundary layer, moving the point of transition to a position just aft of the actuator being operated. Interestingly however is that Magnier et al. (2009) showed that by increasing the voltage of the actuators augmentation of the resultant turbulent layer could be achieved, and this may be useful for delaying the onset of fully turbulent flow if and when transition does occur.

The adverse effects on flow stability discussed in the three reports of Johnson and Scott (2001), Porter et al. (2007), and Magnier et al. (2009) suggest why comparatively more and diverse research has been undertaken into boundary layer separation control. An example of such work is that of Balcer et al. (2006) in which the authors showed how DBD actuators could successfully couple with boundary layer flows so as the effect could be used to re-attach a separated boundary layer on a flat plate. Balcer et al. (2006) reported that the success of the re-attachment was dependent upon the power of the actuators used, suggesting that tuning of the system was required so as to achieve desired results. A subsequent numerical study conducted by Mello et al. (2007) investigated the effect of a zero-net mass flux synthetic jet actuators on a flat plate boundary layer and the flow over a hypothetical airfoil. The results corroborated with those obtained by Balcer et al. (2006), revealing that the use of these synthetic jets, of which DBD actuators are a type, lead to dramatic increases in shear near the surface of the wall. In some cases studied, the shear was found to increase by up 100%. As discussed in the results the dramatic increases in shear at the wall lead to the introduction of destabilising velocity profile inflections, directing the authors to conclude that the jets were adverse for controlling transition, but potentially beneficial for controlling boundary layer separation, as was demonstrated by Post and Corke (2003), Newcamp (2005), and Balcer et al. (2006).

It is only in rather recent times that favourable benefits to the stability of a boundary layer have been attained through the use of DBD actuators. The first such study in which DBD actuators were used to successfully improve the stability of a flat plate boundary layer to an artificially introduced disturbance was conducted by Grundmann and Tropea (2007b). The authors utilised a single DBD actuator, operated in a pulsed fashion, to perturb a flat plate boundary layer by introducing a Tollmien-Schlichting instability into the flow. A curved wall above the flat plate was used to generate an adverse pressure gradient over the plate, which amplified the instability, leading to transition occurring within the confines of the experimental test section. Downstream of the disturbance actuator, two more DBD actuators, placed in series and operated in a steady mode, were used to damp the growth of the disturbance and achieve a 15% increase in the extent of the laminar region.

The reported increased delay in transition was supported by measurements of the boundary layer velocity profile throughout the experiment region in addition to measurements of the turbulence intensity within the layer downstream of the third actuator. For a location 130mm downstream of the third actuator, the velocity profile after disturbance attenuation was shown to reduce in thickness, and return to a profile very similar to the theoretical (and desirable) Blasius solution. In addition, the turbulence intensity was also significantly reduced throughout the layer and both of these observations support the notion of laminar boundary layer maintenance. Further support was revealed through comparison of the boundary layer shape factors before and after attenuation. As was seen in the evolution of the shape factor with and without plasma control (Figure 3.7, the sharp drop in shape factor (indicative of the onset of a turbulent boundary layer i.e. transition) occurred at $x = 800mm$ for the controlled flow, occurring approximately 150mm later than that reported for the uncontrolled case.

The positive experimental results obtained by Grundmann and Tropea (2007b) themselves did not manifest without significant work, trial and error. As discussed by Kriegseis et al. (2009) successful DBD-based transition delay is strongly dependent on shape and size of the electrode of the actuator. Using Proper-Orthogonal-Decomposition Particle Image Velocimetry Kriegseis et al. (2009) investigated the response of a boundary layer to actuators with

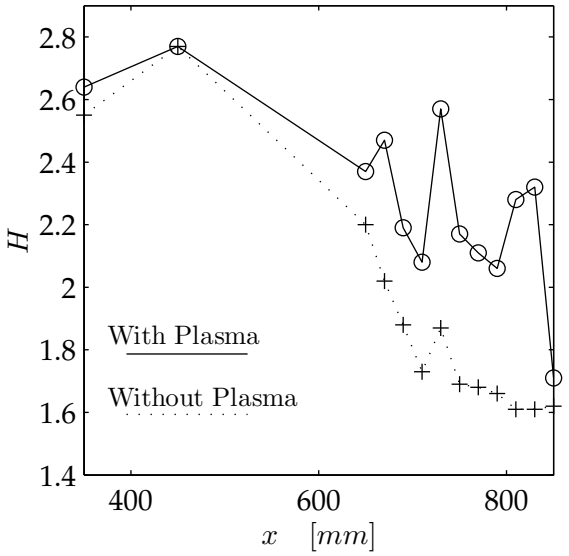

Figure 3.7: Evolution of shape factor with and without plasma (adapted from Grundmann and Tropea 2007b).

various values of electrode size ratio (Equation 3.1). The results showed that the position of maximum induced velocity and the topology of the augmented boundary layer could be controlled through variation of the electrode size ratio. Based on the results of the study, the authors suggest that an electrode size ratio of 0.25 should be used for the design of a LFC with conventional actuators, as other ratio values tend to destabilise the flow. In the context of DBD-based LFC design, these conclusions are significant as they represent the first attempts made by researchers to identify and design actuators specifically for LFC purposes.

$$\chi^{\star} = \frac{L_{exposed}}{L_{encapsulated}} \tag{3.1}$$

In light of the positive results of Grundmann and Tropea (2007b) a significant amount of numerical and analytical work has been done in regards to DBD-based LFC system design. Since the vertical component of the induced velocity developed by a DBD actuator is small, with a magnitude less than 1% of the boundary layer edge velocity, the underlying assumptions of laminar boundary layer flow still pertain to DBD-augmented flows (Duchmann et al. 2010). Using this knowledge and numerical investigations undertaken by Quadros (2009), and Quadros et al. (2009) (as cited by Duchmann et al. 2010) into a DBD-augmented boundary layer flow, Duchmann et al. (2010) conducted a Linear Stability Analysis on a flat plate boundary layer within the vicinity of the experimental investigations of Grundmann and Tropea (2007b). The combined results of Quadros (2009), Quadros et al. (2009), and Duchmann et al. (2010) corroborated with the measurements of Grundmann and Tropea (2007b), showing that the use of the DBD actuators slightly reduces the displacement thickness of the boundary layer in the region of marginal stability of the base flow, which, in conjunction with the velocity profile augmentation, results in a increased limit of stability for the controlled boundary layer.

A subsequent study performed by Grundmann and Tropea (2007a) utilised a DBD actuator to attenuate Tollmien-Schlichting instabilities of a particular frequency. Using a very similar experimental setup as that used for the other study conducted by Grundmann and Tropea (2007b), a single downstream control actuator was used in a pulsed fashion to attenuate an instability of known frequency introduced upstream by a vibrating ribbon. Using the principle of wave superposition, the control actuator was operated out of phase with the disturbance and was shown to be successful in attenuating the growth of the disturbance as determined by measuring the Power Spectral Density of the flow before and after control. The attenuation of the distur-

bance (along with its harmonics and sub-harmonics) downstream of the control device indicated that DBD actuators can be utilised for LFC based on wave superposition, without the need to augment the mean characteristics and hence gross stability characteristics of the flow. However, given the complex feedback control required to utilise such systems in the real-world, a simpler, passive technique using mean flow augmentation is arguably more desirable and suggests why passive systems have historically been the subject of more flight test programs (Joslin 1998).

A final note on the results of DBD-based LFC research to date is that the actuators used have all been of the type with electrodes laid in the spanwise direction. As discussed by Roth et al. (2000), spanwise electrodes have a less dramatic augmentation effect on a boundary layer than equivalent streamwise devices, indicating that the positive DBD-based LFC arises from finesse, rather than brute force.

The collective efforts of Grundmann and Tropea (2007a), Grundmann and Tropea (2007b), Quadros (2009), and Duchmann et al. (2010) have shown the potential for DBD actuators to be used for LFC. With a subsequent publication reviewing and confirming the positive experimental results of DBD-based LFC (see Grundmann and Tropea 2009) it is now possible to conceive a future that includes plasma-based Laminar Flow Control technology. However, as is evident in the literature, the lack of numerous and diverse results of successful DBD-based LFC highlights the need for further work in the area. A large amount of failure in the realisation of favourable boundary layer augmentation can be attributed to poor actuator operation and design. The jetting characteristics of a typical actuator dramatically increase the velocity of the layer close to the wall. This velocity increase and the associated rise in fluid shearing at the surface brings about inflections in the velocity profile that manifest into flow destabilisation. Possessing the ability to augment the jetting characteristics of the plasma so as to mitigate this is highly desirable, and techniques discussed thus far include using electrode size ratio, actuator power and applied frequency. Identifying additional tuning techniques will be most beneficial for developing DBD-based LFC and this should include searching for alternative and novel plasma actuators in addition to the conventional type (schematically represented in Figure 3.1) that have been used exclusively in such research to date.

3.3 Actuator tuning mechanisms for LFC

To implement DBD actuators into a LFC system and successfully achieve an improvement to the stability of a flow, the device must do so whilst

avoiding satisfying the general criterion for instability. As discussed in the literature, DBD devices are very capable of coupling with and augmenting the momentum of a boundary layer, but generally do so in a way that destabilises the flow. There have been very few demonstrations of successful DBD-based LFC, and this can be attributed to the induced wall-jetting effect introducing destabilising inflections in the velocity profile of the flow. Therefore, the ability to control the magnitude and position of the maximum jetting velocity of the synthetic jet is desirable for it would provide a mechanism through which the DBD system can be tuned so as to manipulate the flow in a stable fashion. It has been shown in this discussion of the literature that electrode size ratio, applied frequency and actuator power can be used to tune the response of a boundary layer. In this section, other possible tuning mechanisms are discussed.

Numerous geometric and electrical parameters dictate the jetting performance of a DBD device. These parameters include, applied voltage, applied frequency, electrode material, electrode width, electrode size ratio, dielectric material, dielectric thickness and application. Numerous studies have sought to optimise DBD actuators by measuring the jetting performance obtained from variations in various parameters (Abe et al. 2007, Cho et al. 2008, Forte et al. 2007, Roth and Dai 2006, Van Dyken et al. 2004). However, the large number of variables influencing actuator performance, the coupled nature between the geometrical and electrical parameters of the device, as well as the intended application for the plasma actuator, make it difficult to identify the optimal arrangement a device should posses. An example of the complicated parameter coupling can be seen by comparing maximum jetting velocity (u_{max}) measurements recorded for similar actuators operated with varied applied voltages and frequencies obtained from the work of Forte et al. (2007) (Figure 3.8). Using maximum jetting velocity as the optimisation objective the results show that no unique solution exists. These results are consistent with trends shown in an earlier parametric investigation conducted by Roth and Dai (2006). Of interest, however, is the increase in maximum jetting velocity with increasing applied frequency (Figure 3.8b). As described by Orlov (2006), the extent of the plasma region does not change with variations in applied voltage, hence meaning that the plasma propagation velocity must increase as a result of the diminished half-cycle times. This has a direct consequence on the thrust produced by the actuator (Thomas et al. 2009) and the maximum induced jetting velocity, u_{max}. As discussed by Corke et al. (2010), the result of this frequency dependency is that there exists an optimal applied frequency for each actuator (although this is non-trivial to find and is beyond the scope of this research), which manifests into a maximum value of u_{max},

as a function of applied frequency, for a given applied voltage (Figure 3.9, Roth and Dai 2006).

The study of Baughn et al. (2006) reinforced the notion of frequency-based actuator tuning. In this study, the authors showed that, at a given applied power, both the magnitude and location of the maximum induced jetting velocity of an actuator could be controlled through variation of the applied frequency (Figure 3.10). These results reinforced what was found in the subsequent investigation performed by Baughn et al. (2006) in which the influence of the same actuator on a boundary layer flow was found to vary with applied frequency, with the lower applied frequency seemingly better for LFC (see Section 3.2, Figure 3.6). Ostensibly, variation of the magnitude and position of the maximum induced jetting velocity augments the growth and development characteristics of the boundary layer flow, through changes in the local rates of shear throughout the layer (akin to the changes in boundary layer growth arising from variations in freestream velocity). Hence it can be concluded from the work of Baughn et al. (2006) that the applied frequency can be used to tune the jetting profile of a DBD actuator, with a lower applied frequency more favourable for LFC (Figure 3.6).

Other parameters that are known to affect the maximum jetting velocity

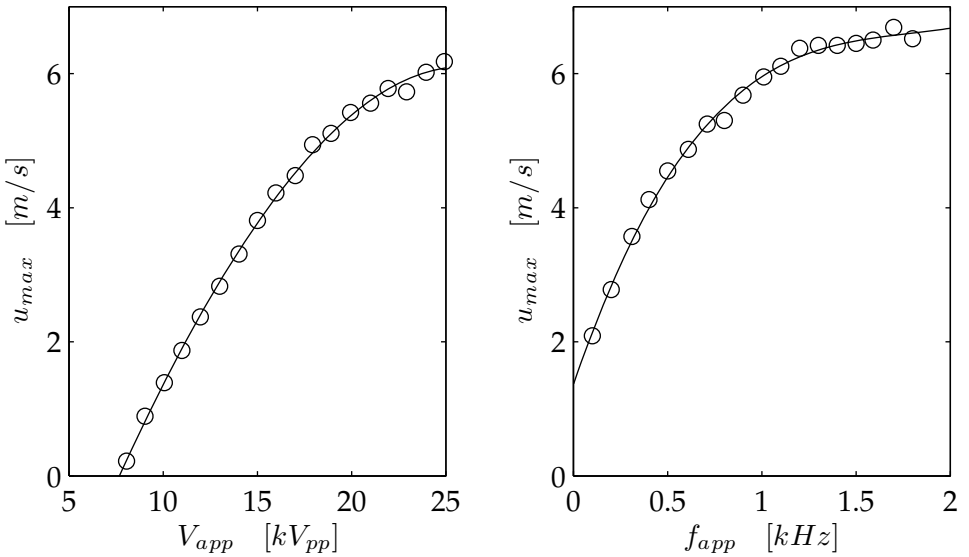

(a) Evolution with applied voltage for a fixed applied frequency of $1kHz$.

(b) Evolution with applied frequency for a fixed applied voltage of $20kV_{pp}$.

Figure 3.8: Effect of electrical operating parameters on maximum induced velocity (adapted from Forte et al. 2007).

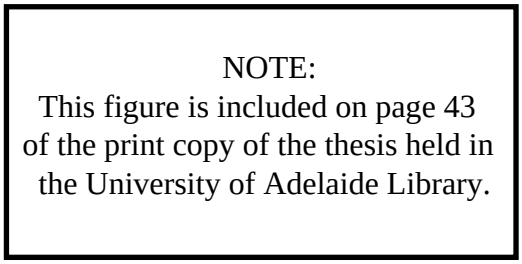

Figure 3.9: Effect of applied frequency on maximum induced velocity (adapted from Roth and Dai 2006).

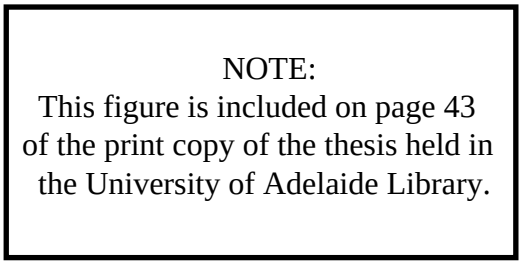

Figure 3.10: Velocity profiles for a DBD actuator operated at a constant power (37.5*W*), at various applied frequencies (adapted from Baughn et al. 2006).

include the chordwise separation between electrodes, electrode arrangement, and the dielectric material used (Abe et al. 2007, Cho et al. 2008, Forte et al. 2007, Hoskinson 2009b, Roth and Dai 2006, Van Dyken et al. 2004, Corke et al. 2010). In addition, Hoskinson et al. (2008), Hoskinson (2009a), and Hoskinson (2009b) showed experimentally and analytically that the exposed electrode diameter has a significant effect on the body force produced by an actuator. Using circular electrodes, the authors showed that the net force increases as the diameter of the wire decreases, independent of actuator applied voltage and electrode material. Analytically, they also showed a similar trend with material thickness of rectangular electrodes (Hoskinson 2009b). Whilst it is valuable to know how to control the maximum jetting velocity (and body force), in the context of the present LFC research work, it is more useful to understand how to control the profile of the wall jet and the location of the maximum jetting velocity so as to ensure the general criterion for instability is not satisfied (something not discussed by Hoskinson et al. 2008, Hoskinson 2009a, Hoskinson 2009b). Moreover, this control should be easily implemented to allow for easy LFC system tuning. Thus a more useful observation from the literature is that observed in the measurements of (Roth and Dai 2006). Through variation of applied voltage, the authors of this study found that both the magnitude and location of the maximum jetting velocity could be controlled, through the same mechanism exploited by applied frequency. For both an actuator with a Teflon^{TM} dielectric surface (Figure 3.11a) and a quartz dielectric (Figure 3.11b) an increase in applied voltage led to an induced jetting velocity that had an increased maximum jetting velocity at a location closer to the surface of the devices. In the interest of reducing the developed shear stress at the wall, so as to minimise the risk of inducing inflections in the velocity profile, the results of Roth and Dai (2006) suggest that an actuator operated at a lower applied voltage may be better suited for a LFC system.

Thus far it has been identified that the electrode size ratio, applied voltage, frequency and power of the actuator can be used as tuning mechanisms for DBD actuators. A further tuning parameter is identified by considering the properties of the electrical field established within the actuator. A simple linear model of the electric field established between the electrodes of a DBD actuator is described by Shyy et al. (2002). It assumes that the electric field decreases linearly downstream of the exposed electrode. Although this linear behaviour is inconsistent with the experimental results that show that the electric field decays exponentially (Enloe et al. 2004a, Orlov 2006, Orlov et al. 2006), the model is sufficient for giving a conceptual understanding about how the geometry of a DBD actuator can be used to augment the developed

NOTE:
This figure is included on page 45
of the print copy of the thesis held in
the University of Adelaide Library.

Figure 3.11: Velocity profiles of a DBD actuator for various applied voltages (adapted from Roth and Dai 2006).

plasma region. It is this conceptual understanding that is of value to the tuning of a DBD-based LFC system.

Shyy et al. (2002) assumed that the developed plasma region can be considered as a simplified, two dimensional region varying linearly in strength in both the direction parallel to the surface (the x-direction) and in the y-direction normal to the wall (Figure 3.12). The plasma extends from the point of maximum electric field strength (E_0), assumed to be on the surface of the dielectric at the trailing edge of the exposed electrode, to the point where the field strength diminishes to the plasma breakdown value E_b. The extent of the plasma in both the x and y directions is defined by dimensions a and b respectively, with the rates of electric field decay in these directions given by Equation 3.2 & 3.3 respectively. By assuming that the peak electric field strength is a function of the applied voltage and separation between the electrodes (Equation 3.4), then the electric field can be approximated by Equation 3.5. In this expression, E represents the magnitude of the electric field strength, which varies linearly according to Equation 3.6.

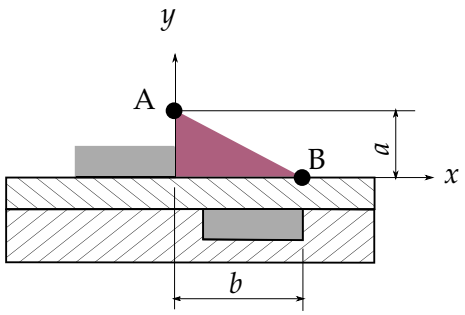

Figure 3.12: The linear approximation of the electric field within a DBD actuator adapted from the work of Shyy et al. (2002).

$$k_1 = \frac{E_0 - E_b}{b} \tag{3.2}$$

$$k_2 = \frac{E_0 - E_b}{a} \tag{3.3}$$

$$E_0 = \frac{V_{app}}{d} \tag{3.4}$$

$$\vec{E} = \left(\vec{E_x}, \vec{E_y}\right) = \left(\frac{Ek_2}{\sqrt{k_1^2 + k_2^2}}, \frac{Ek_1}{\sqrt{k_1^2 + k_2^2}}\right) \tag{3.5}$$

$$|E_0| = E_0 - k_1 x - k_2 y \tag{3.6}$$

The model of Shyy et al. (2002) highlights the dependency of the developed plasma region and electrostatic body force on the geometry and positioning of the actuator electrodes. Similarly, the model developed by Orlov (2006) and Orlov et al. (2006) highlights the dependency of the plasma region on the geometry and arrangement of the electrodes. The method of Orlov (2006) and Orlov et al. (2006) divides the region over the covered electrode into N parallel sub-circuits (Figure 3.13a). Each sub-circuit consists of an air capacitor (C_{a_n}), dielectric capacitor (C_{d_n}), and a resistive element for both the forward-going and backward-going discharge cycles (R_{f_n} & R_{b_n} respectively). In addition, two Zener diodes for each discharge cycle (D_{f_n} & D_{b_n} respectively) are included to represent the threshold voltage values for plasma initiation (Figure 3.13b). According to the model, the electrical properties of each sub-circuit are dependent upon the distance of each from

the exposed electrode. Assuming that the network paths are parallel, and that the length of each (I_n) scales with the position number (n), then the air capacitance of each sub-circuit scales with $1/n$, and the resistance of each scales with n (Orlov 2006, Orlov et al. 2006, Corke et al. 2010). These assumptions then allow the time-varying voltage of each circuit to be found. These voltage values provide the boundary conditions for the calculation of the electric potential (φ) throughout the field, which is subsequently achieved by solving the Poisson equation (Equation 3.7, where ε is the dielectric coefficient, and λ_D is the Debye length). Finding the potential throughout the field can subsequently be used to find the time dependent electrostatic body force, however this is a non-trivial task, requiring numerical techniques to solve (Orlov 2006, Orlov et al. 2006).

$$\nabla \left(\varepsilon \nabla \varphi \right) = \frac{1}{\lambda_D^2} \varphi \tag{3.7}$$

Although finding the developed body force is difficult, the technique of Orlov (2006) and Orlov et al. (2006) highlights the dependency of the developed body force on the geometry and arrangement of the electrodes. This is consistent with the much simpler model of Shyy et al. (2002), in which the geometry and positioning of the electrodes affects the developed plasma region and body force. However, unlike the model of Shyy et al. (2002), the method of Orlov (2006) and Orlov et al. (2006) predicts the correct scaling of body force with actuator voltage, and it is also capable of finding the correct direction of the resultant body force vector.

As previously discussed, the body force associated with DBD devices arises from the developed electric field between the electrodes. Thus if the geometry of the electric field can be augmented then the behaviour of the plasma synthetic jet will also be altered. This is evident from the results of Forte et al. (2007) where the maximal jetting velocity of an actuator was found to be dependent on the horizontal separation between the electrodes (d_h), and is consistent with the body force models of Shyy et al. (2002), Orlov (2006) and Orlov et al. (2006). But what effect would variation in the vertical extent of the plasma have on the synthetic jet? The destabilisation of boundary layer flows observed in the literature were attributed to the dramatic increases in fluid velocity and shear close to the surface brought about by the use of typical actuators. If the extent of the field in the wall-normal direction could be altered, manipulated and controlled, then it is hypothesised that the magnitude and position of the maximum jetting velocity could be controlled and tuned to provide favourable flow augmentation. This could be achieved by varying the extent to which the exposed electrode sits proud

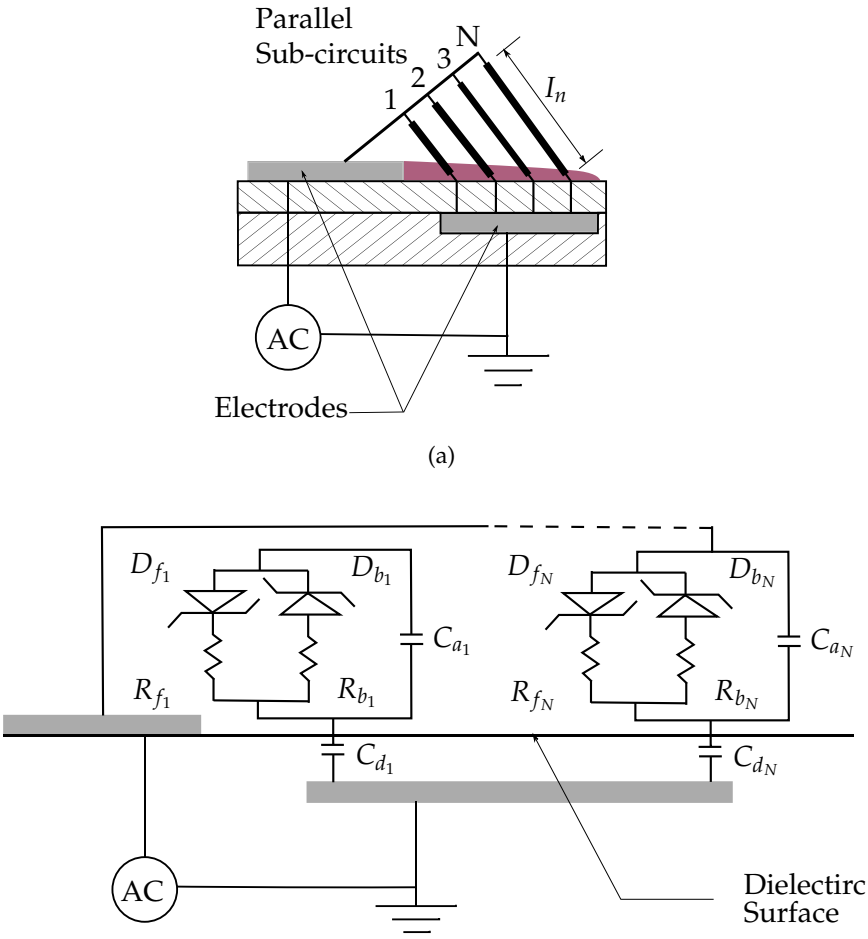

Figure 3.13: Space-time lumped-element circuit model for a single-dielectric barrier discharge plasma actuator as discussed by Orlov (2006) and Orlov et al. (2006). The concept is schematically represented in (a) and the equivalent circuit diagram is shown in (b).

above the surface of the dielectric. However no discussion directly pertaining to this variation in electrode exposure height was found in the literature, suggesting that experimental works looking into DBD actuator tuning through variation of this geometric parameter should be undertaken. In addition to the electrode size ratio (Equation 3.1) and previously discussed electrical operation parameters, an additional geometric tuning mechanism based on variations in electrode exposure height would be of tremendous benefit to the development of plasma-based LFC technology.

3.4 Consolidation of literature & research objectives

The field of Dielectric Barrier Discharge flow control is a relatively recent area of aerodynamic research. Unlike techniques such as suction that have been researched for over 50 years, it is only in the last decade that significant research has been undertaken into developing DBD technology for flow control purposes. It is for this reason that the development of DBD-based LFC has only just begun, with demonstration of successful DBD-based LFC occurring in only the latter half of the past decade.

As discussed, DBD actuators can be successfully used to augment the behaviour of a boundary layer. However achieving the augmentation in such a way as to avoid destabilisation of the flow has been achieved in only a few experimental works. Even in these experimental works, much trial and error was required to obtain a delay in boundary layer transition. Couple this fact with the lack of global research specifically focusing on the development of DBD-based LFC, and it becomes clear as to why DBD-based LFC technology is not currently being utilised in real-world flight trials. For this reason, investigating methodologies and technology utilising DBD actuators is warranted, justified and recommended. This is the fundamental reason for undertaking the research discussed in this thesis; to provide additional resources and information pertaining to the development and furthering of DBD-based LFC technology, through the development and testing of alternative LFC systems.

The developed DBD technology utilised for LFC has to date utilised actuators with a conventional geometric arrangement. Restricting research to these arrangements could easily result in an oversight of more beneficial designs. Hence it was decided that novel actuator designs would be conceived, developed and investigated as part of this research. This novel actuator was to be such that it could provide the opportunities for performance tuning based on changes to the geometry of the electrodes. As highlighted in the literature review, being able to manipulate the vertical extent of the plasma

region would provide a mechanism to control the position of the maximum velocity of the synthetic jet. Without previous results on which to base this tuning on, it was identified that augmentation could be achieved through variation of the height to which the exposed electrode sits proud above the dielectric surface. Consequently, as part of this research, these novel actuators needed to be studied and developed in a quiescent environment before implementation in the LFC system, and this investigation is discussed in Chapter 5.

DBD actuators were found, from the literature, to be capable of augmenting the mean flow characteristics of a boundary layer so as to delay the onset of transition. In addition, DBD devices were found to be capable of attenuating disturbances of particular frequencies using the principle of wave superposition. However, as discussed, the use of this principle for LFC requires complex sensing and feedback control, which makes such systems difficult to realise in the real-world. Hence, from the review of the literature, it was concluded that the research described in this thesis would be focused on LFC through mean flow augmentation only.

In the review of the literature it was noted that the development of the LFC technology had used a significant amount of trial and error, which is both timely and labour intensive. With the large amount of literature regarding ways in which DBD actuators can augment flows it was possible to identify combinations of actuator parameters that would be more favourable for a LFC system. These include actuators operated with lower voltages and lower frequencies. In addition it was noted that an electrode size ratio of 0.25 provided the best LFC performance for conventional style actuators, a value as used by Grundmann and Tropea (2007a), Grundmann and Tropea (2007b), Grundmann and Tropea (2009), and Kriegseis et al. (2009). It was also discussed how these parameters, in addition to actuator power, could be used to tune output of the actuator based on the response of the fluid. The development of a tuning technique was therefore conceived as part of this research, in which the performance of the LFC system to be developed would be based on desired velocity characteristics. As Linear Stability Theory was found to be applicable to flows augmented by plasma, LST was to be used for identifying augmentation objectives. As discussed in Chapter 5, the favourable characteristics were based on conceivable flow augmentation possibilities arising from plasma actuators as found in published results of low Reynolds number boundary layer augmentation.

The research objectives discussed here were conceived so as to contribute to the fundamental development of DBD-based LFC technology. For this reason the research was formulated so as to focus on the control of a laminar

boundary layer formed over a flat plate in a Zero Pressure Gradient. Not only had such research not been performed before, it would also provide the most fundamental point of reference for the boundary layer augmentation. As discussed in the proceeding chapters (Chapters 7, 8, & 9), novel DBD-based LFC technologies have been developed and tested in the region of marginal stability of a Blasius-type layer. The effectiveness of the technology has been evaluated using similar techniques to those utilised in other published works, namely measurement and study of the augmented boundary layer velocity profiles and the evolution of the displacement thickness and shape factor within the flow.

4 Solving the Orr-Sommerfeld Equation

The Orr-Sommerfeld Equation (OSE) is a fourth order eigenvalue problem describing the growth of flow disturbances in space and time. The equation was introduced in Chapter 2 (Equation 2.23) with boundary conditions represented by Equation 2.24 & 2.25. As discussed earlier, the OSE relates properties of the mean boundary layer flow to the periodic behaviour of the possible disturbances to identify those that will destabilize the flow and subsequently to locate the onset of flow instability. Being able to solve the OSE for this research was necessary so that strategies for improving the stability of the studied boundary layers could be determined. No analytical solution exists for the OSE, and hence solving the equation requires specialised mathematical techniques and/or sufficient computing power to handle the iterative processes that are employed. As a result few software packages are capable of such analysis and if they are available, then the lack of detailed documentation requires that the user understands the underlying mathematics to obtain useful results. Consequently an OSE solver was developed as part of this research to address these issues and hence allow the hydrodynamic stability of the investigated flows to be analysed.

The purpose of solving the OSE is to determine the properties of the velocity disturbances to which the flow is susceptible at all Reynolds numbers. By determining these properties, namely the frequency and wavelength of the disturbance, it is possible to construct a curve of neutral stability for the flow and use this to discuss the stability of the flow and predict the onset of boundary layer transition.

As mentioned, the complexity of the Orr-Sommerfeld Equation means that specialised mathematical techniques are required in order to extract useful information regarding the stability of a flow and its robustness to transition. Such techniques not only need to be numerically stable and precise, but also must be able to cope with the mathematical stiffness of the equation.

As the Reynolds number of a flow analysed by the OSE increases and tends to infinity, the upper and lower branches of the curves of neutral stability tend to zero. This makes the equation challenging to solve within the limits of computational precision. In the past, three types of solution technique have been successfully used to directly solve the equation. Chronologically the first is perturbation theory combined with heuristic techniques. These were employed by Tollmien (1929) to provide the first approximate solutions of the OSE for a Blasius boundary layer. With the advent of effective computer technology, matrix-based finite differencing schemes were developed and employed that could provide faster and more accurate results, as used by Jordinson (1970), and Cebeci and Cousteix (1999). Being an eigenvalue problem it is also possible to utilise spectral theory to solve the problem directly, as used by Danabasoglu and Biringen (1990), and Reeh (2008). As the OSE solver utilised in this work is a tool for investigating improvements to flow stability brought about by DBD plasma, selection of the appropriate technique was based on familiarity with the mathematical techniques employed in the solver. For this reason a finite differencing scheme technique was selected and developed.

4.1 Formulating the OSE solver

The solver developed for solving the Orr-Sommerfeld Equation is based on the numerical technique discussed by Cebeci and Cousteix (1999) and Cebeci (1999). The technique employs Keller's Box method to discretise the OSE and solve for the eigenvalues of the equation numerically. Essentially a trial and error method, for a known Reynolds number and corresponding mean boundary layer velocity profile, the method uses educated guesses of appropriate values for the eigenvalues of the equation. The technique then uses these guesses in conjunction with a Newtonian step to determine the eigenvalues at each location in the boundary layer. Beginning at the wall then moving to the freestream and back to wall, the method checks for convergence to the correct boundary condition at the wall. If the boundary condition is not met, variational techniques are employed to provide an improved guess. This iterative procedure repeats itself until the eigenvalues are determined at the particular Reynolds number. The technique is then repeated at all Reynolds numbers of interest until the curve of neutral stability is sufficiently complete.

Three key components feature in the OSE solver. The first is the discretization of the OSE and the establishment of the Finite Differencing Scheme (FDS). The second is the implementation of the FDS, and the final component

is iteration of the FDS until a solution is found. Only successful development and implementation of all three components allows the OSE to be solved accurately.

4.1.1 Keller's Box Method

Keller's Box Method (KBM) is an implicit finite differencing scheme developed for solving the thin shear-layer equations (with boundary conditions) that apply to a wide variety of flow problems (Keller 1978, Cebeci and Cousteix 1999). Two strong points of the KBM are that it is unconditionally stable and it retains second-order accuracy, even when the mesh is non-uniform (Cebeci and Cousteix 1999). Given the previous application of this method for solving boundary layer equations and the OSE, it was deemed most appropriate to utilise the KBM and implement it in solving the OSE for the research present.

To understand the formulation of the KBM, it is convenient to consider the application of the method to the solution of a simple Partial Differential Equation (PDE) and its respective boundary conditions (Equation 4.1 & 4.2). The KBM is implemented such that the PDE is first reduced to an equivalent system of two first-order equations (Equation 4.3 & 4.5). The computational region of the PDE is next discretised into arbitrary rectangles (Figure 4.1) with $(N+1) \times (J+1)$ points. The values at some of these points are provided by the boundary conditions of the original problem, which can be expressed in finite differencing notation as Equation 4.5. These values are then used to derive estimates for the unknown points using a centred differencing approach, taking estimates at the midpoints of the finite differencing rectangles.

$$\frac{\partial U}{\partial x} = \frac{\partial^2 U}{\partial y^2} \equiv U'' \tag{4.1}$$

$$y = 0,\ U = a;\ y = L,\ U = b. \tag{4.2}$$

$$U' = G \tag{4.3}$$

$$G' = \frac{\partial U}{\partial x} \tag{4.4}$$

$$U_0 = a,\ U_J = b \tag{4.5}$$

The KBM technique relies on the recognition that the value at the midpoint of the differencing rectangle in the x and y directions (as defined in

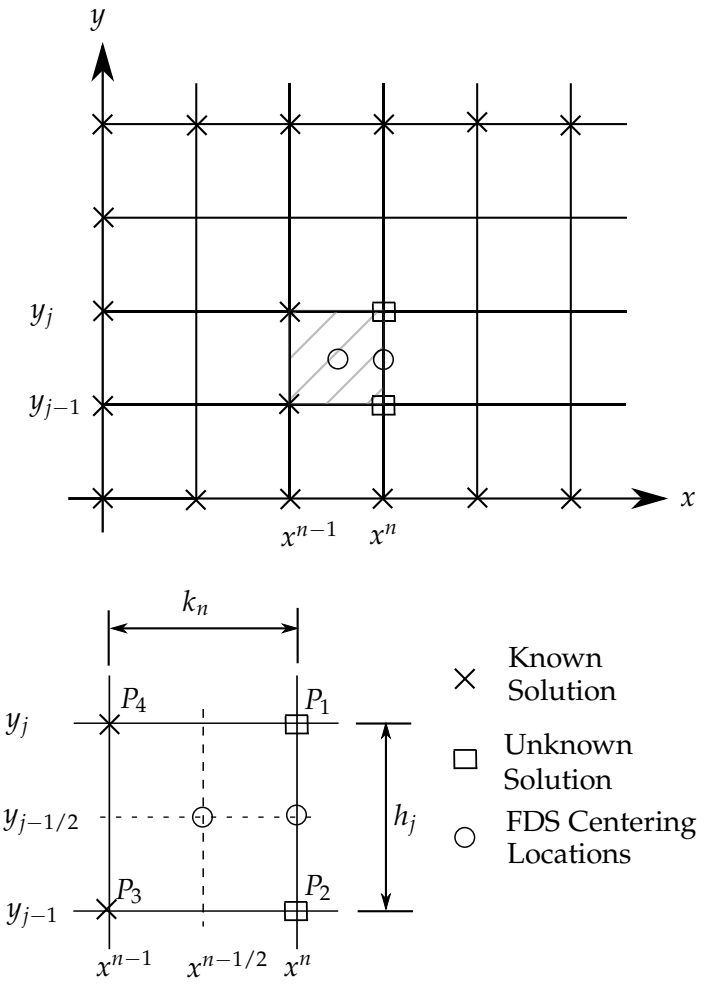

Figure 4.1: Discretisation of the computational region for solution via the box method (adapted from Bradshaw et al. 1981).

Figure 4.1) can be expressed as Equation 4.6 & 4.7 respectively. In addition the derivative of the quantity in the y direction can be approximated as Equation 4.8. Recognising this allows the first order equations of the PDE (Equation 4.3 & 4.5) to be expressed as two difference equations (Equation 4.9 & 4.10), which subsequently allow the estimates of the PDE to be found at all points of the computational region.

$$g_j^{n-1/2} = \frac{1}{2}\left(g_j^n + g_j^{n-1}\right) \tag{4.6}$$

$$g_{j-1/2}^n = \frac{1}{2}\left(g_j^n + g_{j-1}^n\right) \tag{4.7}$$

$$\left(g'\right)_{j-1/2}^n = \frac{g_j^n - g_{j-1}^n}{h_{j-1}} \tag{4.8}$$

$$\frac{U_j^n - U_{j-1}^n}{h_{j-1}} = G_{j-1/2}^n \rightarrow U_j^n - U_{j-1}^n - \frac{h_{j-1}}{2}\left(G_j^n + G_{j-1}^n\right) = 0 \tag{4.9}$$

$$G_j^n - G_{j-1}^n - \frac{h_{j-1}}{k^n}\left(U_j^n + U_{j-1}^n\right) = h_{j-1}\left(\left(G'\right)_{j-1/2}^{n-1} - \frac{2}{k^n}U_{j-1/2}^{n-1}\right) \tag{4.10}$$

The difference equations derived are linear and as such the system of equations formed for all points of the computational region can be expressed in matrix-vector form (Equation 4.11). In expanded matrix form (Equation 4.12), the right-hand sides of the difference equations are replaced by $(r_1)_j$ & $(r_2)_j$ (defined in Equation 4.13 & 4.14) and the term $R_{j-1/2}^{n-1}$ is also introduced (as defined in Equation 4.15).

$$A\vec{\delta} = \vec{r} \tag{4.11}$$

$$\begin{bmatrix} \begin{matrix} U_0 & G_0 \end{matrix} & & \begin{matrix} U_j & G_j \end{matrix} & & \begin{matrix} U_J & G_J \end{matrix} \\ \begin{Bmatrix} 1 & 0 \\ -1 & -\frac{h_0}{2} \end{Bmatrix} & & \begin{Bmatrix} 0 & 0 \\ 1 & -\frac{h_0}{2} \end{Bmatrix} & & \\ \begin{Bmatrix} -\frac{h_{j-1}}{k^n} & -1 \\ 0 & 0 \end{Bmatrix} & \begin{Bmatrix} -\frac{h_{j-1}}{k^n} & 1 \\ -1 & -\frac{h_{j-1}}{2} \end{Bmatrix} & \begin{Bmatrix} 0 & 0 \\ 1 & -\frac{h_{j-1}}{2} \end{Bmatrix} & 0 & \\ 0 & \begin{Bmatrix} -\frac{h_{J-1}}{k^n} & -1 \\ 0 & 0 \end{Bmatrix} & \begin{Bmatrix} -\frac{h_{J-1}}{k^n} & 1 \\ 1 & 0 \end{Bmatrix} \\ \rightarrow & & & & \end{bmatrix} \begin{bmatrix} \begin{pmatrix} U_0 \\ G_0 \end{pmatrix} \\ \begin{pmatrix} U_j \\ G_j \end{pmatrix} \\ \begin{pmatrix} U_J \\ G_J \end{pmatrix} \end{bmatrix}$$

$$= \begin{bmatrix} \begin{pmatrix} (r_1)_0 \\ (r_2)_0 \end{pmatrix} \\ \begin{pmatrix} (r_1)_j \\ (r_2)_j \end{pmatrix} \\ \begin{pmatrix} (r_1)_J \\ (r_2)_J \end{pmatrix} \end{bmatrix} \tag{4.12}$$

$$(r_1)_0 = a, \quad (r_1)_j = h_{j-1} R^{n-1}_{j-1/2}, \quad (1 \leq j \leq J) \tag{4.13}$$

$$(r_2)_j = 0, \quad (0 \leq j \leq J-1)\,(r_2)_J = b \tag{4.14}$$

$$R^{n-1}_{j-1/2} = \left(G'\right)^{n-1}_{j-1/2} - \frac{2}{k^n} U^{n-1}_{j-1/2} \tag{4.15}$$

The matrix vector representation of the system of first order equations (Equation 4.11) can be expressed in a compact expanded fashion that allows for greater ease when developing a computer-based solution routine (Equation 4.16, 4.17, & 4.18). For the PDE under consideration the A_0, A_j, A_J, B_j & C_j terms are 2×2 matrices (defined in Equation 4.19, 4.20, 4.21, 4.22, & 4.23), and the $\overrightarrow{\delta}_j$ & $\overrightarrow{r}_j$ terms are 2×1 vectors (defined in Equation 4.24 & 4.25).

$$A = \begin{vmatrix} A_0 & C_0 & & & & & & \\ B_1 & A_1 & C_1 & & & & & \\ & \cdot & \cdot & \cdot & & & & \\ & & & \cdot & \cdot & & & \\ & & & B_j & A_j & C_j & & \\ & & & & \cdot & \cdot & \cdot & \\ & & & & & B_{J-1} & A_{J-1} & C_{J-1} \\ & & & & & & B_J & A_J \end{vmatrix} \tag{4.16}$$

$$\overrightarrow{\overrightarrow{\delta}} = \begin{vmatrix} \overrightarrow{\delta}_0 \\ \overrightarrow{\delta}_1 \\ \cdot \\ \cdot \\ \overrightarrow{\delta}_j \\ \cdot \\ \overrightarrow{\delta}_{J-1} \\ \overrightarrow{\delta}_J \end{vmatrix} \tag{4.17}$$

$$\overrightarrow{\overrightarrow{r}} = \begin{vmatrix} \overrightarrow{r}_0 \\ \overrightarrow{r}_1 \\ . \\ . \\ \overrightarrow{r}_j \\ . \\ \overrightarrow{r}_{J-1} \\ \overrightarrow{r}_J \end{vmatrix} \tag{4.18}$$

$$A_0 \equiv \begin{vmatrix} 1 & 0 \\ -1 & \frac{-h_0}{2} \end{vmatrix} \tag{4.19}$$

$$A_j \equiv \begin{vmatrix} \frac{-h_{j-1}}{k^n} & 1 \\ -1 & \frac{-h_j}{2} \end{vmatrix}, 1 \leq j \leq J-1 \tag{4.20}$$

$$A_J = \begin{vmatrix} \frac{-h_J}{k^n} & 1 \\ 1 & 0 \end{vmatrix} \tag{4.21}$$

$$B_j = \begin{vmatrix} \frac{-h_{j-1}}{k^n} & -1 \\ 0 & 0 \end{vmatrix}, 1 \leq j \leq J \tag{4.22}$$

$$C_j = \begin{vmatrix} 0 & 0 \\ 1 & \frac{-h_j}{2} \end{vmatrix}, 0 \leq j \leq J-1 \tag{4.23}$$

$$\overrightarrow{\delta}_j = \begin{bmatrix} U_j \\ G_j \end{bmatrix} \tag{4.24}$$

$$\overrightarrow{r}_j = \begin{bmatrix} (r_1)_j \\ (r_2)_j \end{bmatrix} \tag{4.25}$$

To solve the matrix-vector equation, determine $\overrightarrow{\delta}_j$ and hence solve the original PDE, a block elimination method is utilised, as discussed by Bradshaw et al. (1981), and Cebeci and Cousteix (1999). This method employs two sweeps through the computational domain. The first sweep is to solve a number of recursion equations (Equation 4.26, 4.27, 4.28, 4.29, & 4.30) with new variables Γ_j, $\tilde{\omega}_j$, & Δ_j. The second sweep then determines estimates for $\overrightarrow{\delta}_j$ using two more recursion formulae (Equation 4.31 & 4.32).

$$\Delta_0 = A_0 \tag{4.26}$$

$$\Gamma_j \triangle_{j-1} = B_j, \quad j = 1, 2, ..., J \tag{4.27}$$

$$\Delta_j = A_j - \Gamma_j C_{j-1}, \quad j = 1, 2, ..., J \tag{4.28}$$

$$\tilde{\omega}_0 = \tilde{r}_0 \tag{4.29}$$

$$\tilde{\omega}_j = \tilde{r}_j - \Gamma_j \tilde{\omega}_{j-1}, \qquad 1 \leq j \leq J \tag{4.30}$$

$$\Delta_J \overrightarrow{\delta}_J = \overrightarrow{\omega}_J \tag{4.31}$$

$$\Delta_j \overrightarrow{\delta}_j = \overrightarrow{\omega}_j - C_j \overrightarrow{\delta}_{j+1}, \qquad j = J-1, J-2, ..., 0 \tag{4.32}$$

Solution of the recursion formulae ultimately leads to estimates of the solution to the original PDE (Equation 4.1 & 4.2), and since the technique is general in nature, it can readily be used to find the eigenvalues of the OSE.

4.1.2 Implementation of the KBM to the OSE

To implement the KBM to determine the eigenvalues of the OSE, the PDE needs to be manipulated into an appropriate form. The form suggested by Cebeci and Cousteix (1999) is a non-dimensional, homogeneous type, and to arrive at it, a number of steps are required.

The first step suggested by Cebeci and Cousteix (1999) is to define new non-dimensional length and velocity variables (Equation 4.33, 4.34, & 4.36) along with three additional variables that are formed from the terms in the original OSE, ξ_1, ξ_2, & ξ_3 (Equation 4.37, 4.38, & 4.39 respectively). The result of this step is the development of non-dimensional forms of the disturbance amplitude, wavenumber and frequency (Equation 4.40, 4.41, & 4.42), a modified version of Reynolds number (Equation 4.36), and the re-formulation of the OSE into a non-dimensional, homogeneous equation (Equation 4.43). Note that the $\star$ superscripts have been dropped from Equation 4.43 for clarity and from this point onwards in the discussion and formulation of the OSE solver all terms discussed will be non-dimensional unless otherwise stated. In addition the superscript $\prime$ represents differentiation with respect to the dimensionless form of y, (which is η).

$$x^\star = \frac{x}{\sqrt{\frac{\nu x}{u_e}}} = \frac{x}{L} \tag{4.33}$$

$$y^\star = \frac{y}{L} = \eta \tag{4.34}$$

$$u^\star = \frac{u}{u_e} \tag{4.35}$$

$$Re^\star = \frac{u_e L}{\nu} \tag{4.36}$$

$$\xi_1^2 = (\alpha^\star)^2 \tag{4.37}$$

$$\xi_2^2 = \xi_1^2 + iRe^\star \left(\alpha^\star u^\star - \omega^\star\right) \tag{4.38}$$

$$\xi_3 = iRe^\star \alpha^\star \left(u^\star\right)'' \tag{4.39}$$

$$\phi^\star = \frac{\phi}{L} \tag{4.40}$$

$$\alpha^\star = \frac{2\pi L}{\lambda_x} \tag{4.41}$$

$$\omega^\star = \frac{\omega L}{u_e} \tag{4.42}$$

$$\phi^{iv} - \xi_1^2 \phi'' - \xi_2^2 \left(\phi'' - \xi_1^2 \phi\right) + \xi_3 \phi = 0 \tag{4.43}$$

Having written the OSE in a non-dimensional, homogeneous format, it is next reduced to an equivalent system of first-order differential equations (Equation 4.50, 4.51, 4.52 & 4.62) with corresponding boundary conditions (Equation 4.57 & 4.3).

$$\phi' = f \tag{4.44}$$

$$f' = s + \xi_1^2 \phi \tag{4.45}$$

$$s' = g \tag{4.46}$$

$$g' = \xi_2^2 s - \xi_3 \phi. \tag{4.47}$$

$$y = 0,\ \phi = 0,\ f = 0 \tag{4.48}$$

$$y = \delta,\ g + \xi_2 s = 0,\ s + \left(\xi_1 + \xi_2|_{y=\delta}\right) f + \xi_1 \left(\xi_1 + \xi_2|_{y=\delta}\right) = 0. \tag{4.49}$$

The system of first order differential equations is then discretised into a mesh of $J+1$ points, with $y = 0$ represented by y_0 and $y = \frac{\delta}{L}$ by y_J. The values of the quantities (f, s, g, ϕ) at each point are approximated as (f_j, s_j, g_j, ϕ_j) and to these the central differencing scheme of the KBM is applied (Equation 4.50, 4.51, 4.52, & 4.53). For convenience a number of additional variables are introduced and these are defined in Equation 4.54, 4.55, 4.56, 4.57, & 4.58.

$$\phi_j - \phi_{j-1} - c_3 \left(f_j + f_{j+1}\right) = (r_1)_j = 0 \tag{4.50}$$

$$f_j - f_{j-1} - c_3 \left(s_j + s_{j+1}\right) - c_1 \left(\phi_j + \phi_{j-1}\right) = (r_3)_{j-1} = 0 \tag{4.51}$$

$$s_j - s_{j-1} - c_3 \left(g_j + s_{j+1}\right) = (r_2)_j = 0 \tag{4.52}$$

$$g_j - g_{j-1} - c_4 \left(s_j + s_{j+1}\right) - c_2 \left(\phi_j + \phi_{j-1}\right) = (r_3)_{j-1} = 0. \tag{4.53}$$

$$c_3 = \frac{h_{j-1}}{2} \tag{4.54}$$

$$c_1 = \xi_1^2 c_3 \tag{4.55}$$

$$c_2 = -\left(\xi_3\right)_{j-1/2} c_3 \tag{4.56}$$

$$c_4 = \left(\xi_2^2\right)_{j-1/2} c_3 \tag{4.57}$$

$$h_{j-1} = y_j - y_{j-1} \tag{4.58}$$

At the limits of the computational domain ($j = 0$ and $j = J$), the conditions for the FDS are obtained from the original boundary conditions of the OSE and rewritten as Equation 4.59, 4.60, 4.61, & 4.62. Again, for convenience, new variables are defined and expressed in Equation 4.63, 4.64, & 4.65.

$$\phi_0 = (r_1)_0 = 0 \tag{4.59}$$

$$f_0 = (r_2)_0 = 0 \tag{4.60}$$

$$f_J + \tilde{c}_3 s_J + \tilde{c}_1 \phi_J = (r_3)_J = 0 \tag{4.61}$$

$$g_J + \tilde{c}_4 s_J = (r_4)_J = 0 \tag{4.62}$$

$$\tilde{c}_3 = \frac{1}{\xi_1 + \xi_2} \tag{4.63}$$

$$\tilde{c}_1 = \xi_1 \tag{4.64}$$

$$\tilde{c}_4 = \xi_2 \tag{4.65}$$

The system of difference equations derived for the OSE is homogeneous and hence has trivial solutions $f_j = s_j = g_j = \phi_j = 0$ for all j. This creates a problem when trying to solve for the eigenvalues of the OSE, particularly when using matrix methods such as the block elimination method employed in this research. Overcoming this is achieved by setting one of the boundary conditions to be non-zero and then iterating until a non-trivial solution is found that satisfies the original value of the modified boundary condition. In the context of the present work the boundary condition $\phi_0' = f_0 = 0$ is replaced by $\phi_0'' = s_0 = 1$ and an iterative scheme is used to find $f_0(\alpha, \omega, Re) = 0$, i.e. the original value of the boundary condition.

Application of the KBM results in an equivalent matrix-vector representation of the dimensionless, homogeneous OSE (Equation 4.126, 4.127, & 4.128). As the equivalent first order system of the OSE contains four equations, the A_j, B_j & C_j terms of the matrix-vector format represent 4×4 matrices (defined in Equation 4.69, 4.70, 4.71, 4.72, & 4.73), and the $\overrightarrow{\delta}_j$ & $\overrightarrow{r}_j$ terms represent 4×1 vectors (defined in Equation 4.74 & 4.75).

$$A = \begin{vmatrix} A_0 & C_0 & & & & & & \\ B_1 & A_1 & C_1 & & & & & \\ & \cdot & \cdot & \cdot & & & & \\ & & & \cdot & \cdot & & & \\ & & & B_j & A_j & C_j & & \\ & & & & \cdot & \cdot & \cdot & \\ & & & & & B_{J-1} & A_{J-1} & C_{J-1} \\ & & & & & & B_J & A_J \end{vmatrix} \tag{4.66}$$

$$\vec{\vec{\delta}} = \begin{vmatrix} \vec{\delta}_0 \\ \vec{\delta}_1 \\ . \\ . \\ \vec{\delta}_j \\ . \\ \vec{\delta}_{J-1} \\ \vec{\delta}_J \end{vmatrix} \tag{4.67}$$

$$\vec{\vec{r}} = \begin{vmatrix} \vec{r}_0 \\ \vec{r}_1 \\ . \\ . \\ \vec{r}_j \\ . \\ \vec{r}_{J-1} \\ \vec{r}_J \end{vmatrix} \tag{4.68}$$

$$A_0 \equiv \begin{vmatrix} 1 & 0 & 0 & 0 \\ 0 & 1 & 0 & 0 \\ (c_1)_1 & (c_3)_1 & 1 & 0 \\ (c_2)_1 & (c_4)_1 & 0 & 1 \end{vmatrix} \tag{4.69}$$

$$A_j \equiv \begin{vmatrix} 1 & 0 & -(c_3)_j & 0 \\ 0 & 1 & 0 & -(c_3)_j \\ (c_1)_{j+1} & (c_3)_{j+1} & 1 & 0 \\ (c_2)_{j+1} & (c_4)_{j+1} & 0 & 1 \end{vmatrix}, \; 1 \le j \le J-1 \tag{4.70}$$

$$A_J = \begin{vmatrix} 1 & 0 & -(c_3)_J & 0 \\ 0 & 1 & 0 & -(c_3)_J \\ (\tilde{c}_1) & (\tilde{c}_3) & 1 & 0 \\ 0 & (\tilde{c}_4) & 0 & 1 \end{vmatrix} \tag{4.71}$$

$$B_j = \begin{vmatrix} -1 & 0 & -(c_3)_j & 0 \\ 0 & -1 & 0 & -(c_3)_j \\ 0 & 0 & 0 & 0 \\ 0 & 0 & 0 & 0 \end{vmatrix}, \; 1 \le j \le J \tag{4.72}$$

$$C_j = \begin{vmatrix} 0 & 0 & 0 & 0 \\ 0 & 0 & 0 & 0 \\ (c_1)_{j+1} & (c_3)_{j+1} & -1 & 0 \\ (c_2)_{j+1} & (c_4)_{j+1} & 0 & -1 \end{vmatrix}, \; 0 \leq j \leq J-1 \tag{4.73}$$

$$\overrightarrow{\delta}_j = \begin{bmatrix} \phi_j \\ s_j \\ f_j \\ g_j \end{bmatrix} \tag{4.74}$$

$$\overrightarrow{r}_j = \begin{bmatrix} (r_1)_j \\ (r_2)_j \\ (r_3)_j \\ (r_4)_j \end{bmatrix} \tag{4.75}$$

Having discretised the OSE and established an equivalent matrix vector form of the equation, what remains is calculation of the eigenvalues of the equation. The solution of the two-dimensional OSE is dependent on the disturbance wavenumber and frequency, as well as the local Reynolds number of the flow. As both wavenumber and frequency are complex, there are essentially five eigenvalues that need to be determined. Solving for five unknown eigenvalues is challenging, but consideration of the physics of the problem simplifies the analysis. Disturbances may grow in both space and time, but generally the source of the disturbance, particularly in laboratory conditions, is controlled and fixed. This consequently means that the disturbance, as it propagates downstream, will grow or decay only in space, as was the case for in the experiments of Schubauer and Skramstad (1950). Thus it is convenient to solve the OSE using what is referred to as *Spatial Amplification Theory* (Cebeci and Cousteix 1999), as it provides solutions that can be verified experimentally.

In Spatial Amplification Theory, the growth rate of the frequency is zero (i.e. $\omega_i = 0$), and hence only four unknown eigenvalues need to be considered and solved. This is still a challenging task to undertake, so it is convenient to identify what information is sought from the OSE before beginning any numerical analyses. For the purpose of the research presented in this document, it is of interest to know at what chordwise location disturbances within the boundary layer will begin to grow when the boundary layer is augmented by DBD plasma. This involves determining the Reynolds numbers at which the spatial amplification rates (α_i) of a spectrum of disturbances are equal to

zero. By finding these Reynolds numbers it is possible to construct a curve of neutral stability for various boundary layer flow cases manipulated by a LFC system. Consequently, to construct the curves of neutral stability, the wavenumbers and frequencies of disturbances with zero spatial amplification rate need to be determined at each Reynolds number of interest. Thus the matrix equation can be solved by selecting a Reynolds number, setting the spatial amplification rate to zero, and finding only the two unknown eigenvalues, α_r & ω_r.

To find the two remaining eigenvalues, the original boundary condition of the OSE needs to be met (Equation 4.76). Meeting this original boundary condition essentially involves solving a system of two equations with two unknowns (α_r & ω_r) and these can be solved by using an iterative scheme based on Newton's Method. For a fixed value of Reynolds number and zero spatial amplification rate, initial guesses of α_r & ω are made. The matrix-vector equation is then solved using the block elimination method and if the initial boundary condition (Equation 4.76) is satisfied, then the eigenvalues will have been found and these can then be used as the guesses at the next Reynolds number of interest. If the eigenvalue guesses are not correct, then the iterative scheme is used to provide a better guess. If α_r^ν & $\omega^\nu$are the ν^{th} iterates, then the $(\nu+1)^{th}$ iterates can be found using Equation 4.77 & 4.78.

$$f_0\left(\alpha, \omega, Re\right) = 0 \tag{4.76}$$

$$\alpha_r^{\nu+1} = \alpha_r^\nu + \delta\alpha_r^\nu \tag{4.77}$$

$$\omega^{\nu+1} = \omega^\nu + \delta\omega^\nu \tag{4.78}$$

Determination of appropriate incremental changes to the iterates ($\delta\alpha_r^\nu$ & $\delta\omega^\nu$) is achieved by linearly expanding α_r^ν & ω^ν about f_0. Dropping the subscript 0, introducing a new variable Δ_0 (Equation 4.79), and taking $f_r^{\nu+1} = f_i^{\nu+1} = 0$, the incremental changes can be found (Equation 4.80 & 4.81).

$$\Delta_0 = \left(\frac{\partial f_r}{\partial \alpha_r}\right)^\nu \left(\frac{\partial f_i}{\partial \omega}\right)^\nu - \left(\frac{\partial f_i}{\partial \alpha_r}\right)^\nu \left(\frac{\partial f_r}{\partial \omega}\right)^\nu \tag{4.79}$$

$$\delta\alpha_r^\nu = \frac{1}{\Delta_0}\left[f_i^\nu \left(\frac{\partial f_r}{\partial \omega}\right)^\nu - f_r^\nu \left(\frac{\partial f_i}{\partial \omega}\right)^\nu\right] \tag{4.80}$$

$$\delta\omega^\nu = \frac{1}{\Delta_0}\left[f_r^\nu \left(\frac{\partial f_i}{\partial \alpha_r}\right)^\nu - f_i^\nu \left(\frac{\partial f_r}{\partial \alpha_r}\right)^\nu\right] \tag{4.81}$$

The derivatives of f_r& f_i can be found by differentiating the matrix vector representation of the OSE (Equation 4.126, 4.127, & 4.128). This leads to two variational equations (4.82 & 4.83) and two further systems of linear equations, both with the same coefficient matrix A as determined for the OSE.

$$A\left(\frac{\partial \overrightarrow{\overrightarrow{\delta}}}{\partial \alpha_r}\right)^{\nu} = -\left(\frac{\partial A}{\partial \alpha_r}\right)^{\nu} \overrightarrow{\overrightarrow{\delta}}^{\nu} = \overrightarrow{\overrightarrow{r}} \tag{4.82}$$

$$A\left(\frac{\partial \overrightarrow{\overrightarrow{\delta}}}{\partial \omega}\right)^{\nu} = -\left(\frac{\partial A}{\partial \omega}\right)^{\nu} \overrightarrow{\overrightarrow{\delta}}^{\nu} = \overrightarrow{\overrightarrow{r}} \tag{4.83}$$

The vectors on the right-hand side of the variational equations differ from that of the OSE, and also differ for each case. The elements of the vectors $\overrightarrow{r}_j$ when applied to the case of variation in α_r,are given by Equation 4.84, 4.85, 4.86, 4.87, & 4.88.

$$(r_1)_j = (r_1)_j = 0 \tag{4.84}$$

$$(r_3)_{j-1} = 2\left(\frac{\partial c_1}{\partial \alpha_r}\right)\phi_{j-1/2} \tag{4.85}$$

$$(r_4)_{j-1} = 2\left(\frac{\partial c_4}{\partial \alpha_r}\right)s_{j-1/2} + 2\left(\frac{\partial c_2}{\partial \alpha_r}\right)\phi_{j-1/2} \tag{4.86}$$

$$(r_3)_J = -\left(\frac{\partial \tilde{c}_3}{\partial \alpha_r}\right)_J s_J - \left(\frac{\partial \tilde{c}_1}{\partial \alpha_r}\right)_J \phi_J \tag{4.87}$$

$$(r_4)_J = -\left(\frac{\partial \tilde{c}_4}{\partial \alpha_r}\right)_J s_J \tag{4.88}$$

For the case of variation in ω the elements of the vectors $\overrightarrow{r}_j$ are given by Equation 4.89, 4.90, 4.91, 4.92, & 4.93.

$$(r_1)_j = (r_1)_j = 0 \tag{4.89}$$

$$(r_3)_{j-1} = 0 \tag{4.90}$$

$$(r_4)_{j-1} = 2\left(\frac{\partial c_4}{\partial \omega}\right)s_{j-1/2} \tag{4.91}$$

$$(r_3)_J = -\left(\frac{\partial \tilde{c}_3}{\partial \omega}\right)_J s_J \tag{4.92}$$

$$(r_4)_J = -\left(\frac{\partial \tilde{c}_4}{\partial \omega}\right)_J s_J \tag{4.93}$$

Using the techniques outlined thus far in this chapter it is possible to find the eigenvalues of the OSE at a given Reynolds number and for a particular spatial amplification rate. Once the eigenvalues at one particular Reynolds number are found, the eigenvalues at a nearby Reynolds number can be found efficiently by using the previously calculated eigenvalues as the initial guess. According to Cebeci and Cousteix (1999) this technique works well when the derivative $\frac{\partial \alpha_r}{\partial Re}$ is small, and this can be ensured by using a very fine discretisation of the flow field in the chordwise (x) direction.

4.2 OSE validation - Curve of neutral stability of the Blasius flow

The numerical method formulated to solve the OSE was realised through the development of a computer routine written in the Matlab™ scripting language. The resulting computer application (based on the technique described by Cebeci 1999) capable of solving the OSE required validation before it could be used to investigate the affects on hydrodynamic stability brought about by DBD plasma flow augmentation. The validation procedure involved using the discussed technique to calculate the eigenvalues for a flow with known and published solutions to the OSE. The most appropriate flow for the validation purpose was the Blasius boundary layer that was introduced in Chapter 2. To reiterate the fundamental characteristics of such a flow, the Blasius boundary layer describes the behaviour of fluid within a laminar boundary layer developed over a flat plate in a Zero Pressure Gradient (ZPG). Not only is this the most fundamental external flow for which an experimentally verified, analytical description exists, it is also the most fundamental external flow historically studied in hydrodynamic stability analyses (Tollmien 1929, Schlichting 1933, Schlichting 1955, Cebeci and Cousteix 1999, Drazin 2002). Hence validation of the OSE solver was performed through calculation of the eigenvalues for Blasius flow.

Although published results for the Blasius boundary layer exist (see Schlichting 1955), it was deemed necessary, for two reasons, to develop a method to solve the equations as part of this research. The first was the increased solution fidelity available through a developed solution strategy. The second was the ability to assist in handling and passing data directly to the OSE solver through a correctly designed computer routine that shared common variables with those required for the OSE solver.

4.2.1 Implementation of the box method to solve the Blasius flow equations

The numerical technique developed was used to solve the Falkner-Skan representation of the Blasius boundary layer (see Chapter 2, Equation 2.16, with boundary conditions described by Equation 2.17 & 2.18). The procedure for solving this equation using the KBM is similar to that previously discussed for the OSE solver, and is commenced by first rewriting the Falkner-Skan Equation as an equivalent system of two, first-order Differential Equations (DEs, Equation 4.94 & 4.95), in terms of new variables $u(x,\eta)$ & $v(x,\eta)$.

$$f' = u(x,\eta) = \frac{u}{u_e} \tag{4.94}$$

$$u' = v(x,\eta) = \frac{1}{u_e}\frac{du}{d\eta} \tag{4.95}$$

When solving the Falkner-Skan Equation for Blasius flow using a finite differencing scheme, it is just as convenient to derive a solution to the Falkner-Skan Equation (and its boundary conditions), which includes the terms associated with Reynolds shear stress (expressed in terms of the new variables $u(x,\eta)$, and $v(x,\eta)$, Equation 4.96, 4.97, & 4.98). Then, to solve for Blasius flow, all that is required is that the parameters b and m be set to unity and zero respectively.

$$\left(bf''\right)' + \frac{m+1}{2}ff'' + m\left[1-\left(f'\right)^2\right] = x\left(f'\frac{\partial f'}{\partial x} - f''\frac{\partial f}{\partial x}\right) \tag{4.96}$$

$$\eta = 0, \quad f = f_w(x), \quad f' = 0 \tag{4.97}$$

$$\eta = \eta_e, \quad f' = 1 \tag{4.98}$$

The next step in the formulation of the solution scheme is to rewrite the DEs as centred finite differencing approximations using the meshing technique of the KBM (Equation 4.99 & 4.100). Following this step, new variables are introduced (Equation 4.101, 4.102, 4.103, 4.104, & 4.105) and then the PDE expression of the Falkner-Skan Equation (Equation 4.96) is approximated by a centred differencing scheme, centred at the centre of the rectangular elements of the computational region (Equation 4.106, with modified boundary conditions given by Equation 4.107 & 4.108). In the reformulation of the Falkner-Skan equation, the terms L & R have been

introduced for convenience, and these represent the left and right sides of the original PDE respectively.

$$\frac{f_j^n - f_{j-1}^n}{h_j} = \frac{u_j^n + u_{j-1}^n}{2} v \equiv u_{j-1/2}^n \tag{4.99}$$

$$\frac{u_j^n - u_{j-1}^n}{h_j} = \frac{v_j^n + v_{j-1}^n}{2} v \equiv v_{j-1/2}^n \tag{4.100}$$

$$a^n = \frac{x^{n-1/2}}{k_n} \tag{4.101}$$

$$a_1 = \frac{m^n + 1}{2} + a^n \tag{4.102}$$

$$a_2 = m^n + a^n \tag{4.103}$$

$$R_{j-1/2}^{n-1} = -L_{j-1/2}^{n-1} + a^n \left[(fv)_{j-1/2}^{n-1} - \left(u^2\right)_{j-1/2}^{n-1} \right] - m^n \tag{4.104}$$

$$L_{j-1/2}^{n-1} = \left\{ \left(\tfrac{1}{h_j} \right) \left(b_j v_j - b_{j-1} v_{j-1} \right) + \tfrac{m+1}{2} \left(fv \right)_{j-1/2} + \ldots \right\}^{n-1} \left\{ \ldots m \left[1 - \left(u^2 \right)_{j-1/2} \right] \right\}^{n-1} \tag{4.105}$$

$$\left(\tfrac{1}{h_j} \right) \left(b_j^{n1} v_j^n - b_{j-1}^n v_{j-1}^n \right) + a_1 \left(fv \right)_{j-1/2}^n - a_2 \left(u^2 \right)_{j-1/2}^n + a^n \left(v_{j-1/2}^{n-1} f_{j-1/2}^n - f_{j-1/2}^{n-1} v_{j-1/2}^n \right) = R_{j-1/2}^{n-1} \tag{4.106}$$

$$f_0^n = f_w, \quad u_0^n, \tag{4.107}$$

$$u_J^n = 1 \tag{4.108}$$

Having formulated the finite differencing scheme, and re-written the boundary layer equations in terms of this scheme, an iterative technique is required to calculate the properties of the boundary layer. Given the boundary conditions of the equation, along with a systematic approach to solving the problem, it can be assumed that f_j^{n-1}, u_j^{n-1}, & v_j^{n-1} will be known at each location in the η direction. This means that the FDS approximated PDE of the boundary layer equations forms a system of $3\,(J+1)$ equations with an equal number of unknown quantities. Newton's Method can then be utilised to solve this system by introducing the following iterates, $f_j^{(\nu)}$, $u_j^{(\nu)}$, & $v_j^{(\nu)}$.

The initial guesses for the iterates ($\nu = 0$) can be known for all locations within the computational domain by using the value of the three variables at the previous x-station, in conjunction with the boundary conditions of the governing equation. Subsequent iterates are then obtained from Newton's Method and can be represented by the following three equations, Equation 4.109, 4.110, & 4.111.

$$f_j^{(\nu+1)} = f_j^{(\nu)} + \delta f_j^{(\nu)} \tag{4.109}$$

$$u_j^{(\nu+1)} = u_j^{(\nu)} + \delta u_j^{(\nu)} \tag{4.110}$$

$$v_j^{(\nu+1)} = v_j^{(\nu)} + \delta v_j^{(\nu)} \tag{4.111}$$

Substituting the iterates into the boundary layer PDE and dropping the quadratic terms, along with the introduction of nine new variables (Equation 4.112, 4.113, 4.114, 4.115, 4.116, 4.117, 4.118, 4.119, & 4.120), results in an equivalent system of linear equations (Equation 4.121, 4.122, & 4.123) with boundary conditions (Equation 4.124) that can be expressed in a matrix vector form (Equation 4.125).

$$(s_1)_j = \left(\frac{1}{h_j}\right) b_j^{(\nu)} + \frac{a_1}{2} f_j^{(\nu)} - \frac{a^n}{2} f_{j-1/2}^{n-1} \tag{4.112}$$

$$(s_2)_j = -\left(\frac{1}{h_j}\right) b_{j-1}^{(\nu)} + \frac{a_1}{2} f_{j-1}^{(\nu)} - \frac{a^n}{2} f_{j-1/2}^{n-1} \tag{4.113}$$

$$(s_3)_j = \frac{a_1}{2} v_j^{(\nu)} + \frac{a^n}{2} v_{j-1/2}^{n-1} \tag{4.114}$$

$$(s_4)_j = \frac{a_1}{2} v_{j-1}^{(\nu)} + \frac{a^n}{2} v_{j-1/2}^{n-1} \tag{4.115}$$

$$(s_5)_j = -a_2 u_j^{(\nu)} \tag{4.116}$$

$$(s_6)_j = -a_2 u_{j-1}^{(\nu)} \tag{4.117}$$

$$(r_1)_j = f_{j-1}^{(\nu)} - f_j^{(\nu)} + h_j u_{j-1/2}^{\nu} \tag{4.118}$$

$$(r_3)_{j-1} = u_{j-1}^{(\nu)} - u_j^{(\nu)} + h_j v_{j-1/2}^{\nu} \tag{4.119}$$

$$(r_2)_{j1} = R^{n-1}_{j-1/2} - \left[\left(\frac{1}{h_j}\right)\left(b^{(\nu)}_j v^{(\nu)}_j - b^{(\nu)}_{j-1} v^{(\nu)}_{j-1}\right)\right] + \left[a_1 (fv)^{(\nu)}_{j-1/2} - a_2 \left(u^2\right)^{(\nu)}_{j-1/2}\right] + \left[a^n \left(v^{n-1}_{j-1/2} f^{(\nu)}_{j-1/2} - f^{n-1}_{j-1/2} v^{(\nu)}_{j-1/2}\right)\right] \tag{4.120}$$

$$\delta f_j - \delta f_{j-1} - \frac{h_j}{2}\left(\delta u_j + \delta u_{j-1}\right) = (r_1)_j \tag{4.121}$$

$$\delta u_j - \delta u_{j-1} - \frac{h_j}{2}\left(\delta v_j + \delta v_{j-1}\right) = (r_3)_{j-1} \tag{4.122}$$

$$(s_1)_j \delta v_j + (s_2)_j \delta v_{j-1} + (s_3)_j \delta f_j + (s_4)_j \delta f_{j-1} + (s_5)_j \delta u_j + (s_6)_j \delta u_{j-1} = (r_2)_j \tag{4.123}$$

$$\delta f_0 = 0, \quad \delta u_0 = 0, \quad \delta u_J = 0 \tag{4.124}$$

$$A \overrightarrow{\overrightarrow{\delta}} = \overrightarrow{\overrightarrow{r}} \tag{4.125}$$

Again, the matrix vector representation of the system of first order equations (4.125) can be expressed in a compact expanded fashion that allows for greater ease when developing a computer-based solution routine (Equation 4.126, 4.127, & 4.128). The A_0, A_j, A_J, B_j & C_j terms are 3×3 matrices (defined in Equation 4.129, 4.130, 4.131, 4.132, & 4.133 respectively), and the $\overrightarrow{\delta}_j$ & $\overrightarrow{r}_j$ terms are 3×1 vectors (defined by Equation 4.134 & 4.135).

$$A = \begin{vmatrix} A_0 & C_0 & & & & & & \\ B_1 & A_1 & C_1 & & & & & \\ & \cdot & \cdot & \cdot & & & & \\ & & & \cdot & \cdot & & & \\ & & & B_j & A_j & C_j & & \\ & & & & \cdot & \cdot & \cdot & \\ & & & & & B_{J-1} & A_{J-1} & C_{J-1} \\ & & & & & & B_J & A_J \end{vmatrix} \tag{4.126}$$

$$\overrightarrow{\overrightarrow{\delta}} = \begin{vmatrix} \overrightarrow{\delta}_0 \\ \overrightarrow{\delta}_1 \\ . \\ . \\ \overrightarrow{\delta}_j \\ . \\ \overrightarrow{\delta}_{J-1} \\ \overrightarrow{\delta}_J \end{vmatrix} \tag{4.127}$$

$$\overrightarrow{\overrightarrow{r}} = \begin{vmatrix} \overrightarrow{r}_0 \\ \overrightarrow{r}_1 \\ . \\ . \\ \overrightarrow{r}_j \\ . \\ \overrightarrow{r}_{J-1} \\ \overrightarrow{r}_J \end{vmatrix} \tag{4.128}$$

$$A_0 \equiv \begin{vmatrix} 1 & 0 & 0 \\ 0 & 1 & 0 \\ 0 & -1 & -h_1/2 \end{vmatrix} \tag{4.129}$$

$$A_j \equiv \begin{vmatrix} 1 & -h_j/2 & 0 \\ (s_3)_j & (s_5)_j & (s_1)_j \\ 0 & -1 & -h_1/2 \end{vmatrix}, 1 \leq j \leq J-1 \tag{4.130}$$

$$A_J = \begin{vmatrix} 1 & -h_J/2 & 0 \\ (s_3)_J & (s_5)_J & (s_1)_J \\ 0 & 1 & 0 \end{vmatrix} \tag{4.131}$$

$$B_j = \begin{vmatrix} -1 & -h_j/2 & 0 \\ (s_4)_j & (s_6)_j & (s_2)_j \\ 0 & 0 & 0 \end{vmatrix}, 1 \leq j \leq J \tag{4.132}$$

$$C_j = \begin{vmatrix} 0 & 0 & 0 \\ 0 & 0 & 0 \\ 0 & 1 & -h_{j+1}/2 \end{vmatrix}, 0 \leq j \leq J-1 \tag{4.133}$$

$$\overrightarrow{\delta}_j = \begin{bmatrix} \delta f_j \\ \delta u_j \\ \delta v_j \end{bmatrix}, \qquad 0 \leq j \leq J \tag{4.134}$$

$$\overrightarrow{r}_j = \begin{bmatrix} (r_1)_j \\ (r_2)_j \\ (r_3)_j \end{bmatrix}, \qquad 0 \leq j \leq J \tag{4.135}$$

The same block elimination method used to solve the OSE is subsequently employed to solve the matrix equation, and from this the characteristics of the Blasius boundary layer can be determined.

4.2.2 Validation of the solution of the Blasius flow

The usefulness of the Falkner-Skan equation for analysing boundary layer flows is that it is an ordinary differential equation in terms of the non-dimensional variable η. By definition this can only occur if η is independent of the boundary layer development length x, which is the case when considering Blasius flow (Cebeci and Cousteix 1999). Consequently, physical concepts typically associated with computational fluid mechanics, such as Reynolds number, have no direct impact on the solution of the Falkner-Skan equation. However, these terms can be related to the solution of the Falkner-Skan equation (if necessary) by considering the original transformations used to derive the equation. Since the purpose of this section is to validate the solution of the Falkner-Skan equation only, conversion of the results to physical concepts, such as Reynolds number, are not presented.

The solution of the Falkner-Skan equation for Blasius flow has unique characteristics which help to simplify the numerical solution. These characteristics provided an efficient means to check the validity of the numerical technique developed to solve the Falkner-Skan equation, and hence also the validity of the OSE solver, with simple computational grid designs. The Blasius boundary layer, by definition, is formed on a flat plate in the absence of a pressure gradient. Thus the edge velocity is constant along the entire development length of the layer, and equal to the freestream velocity. Hence, $u(x, \eta_e) = u(\eta_e) = u_\infty$ for all streamwise positions, hence making the solution essentially invariant with respect to streamwise position. Consequently, a regular, rectangular grid in terms of η and Re_L was used to discretise the computational domain and solve the boundary layer equations. One hundred grid points were used in the η-direction. The grid spacing in the η-direction

was recommended by Cebeci (1999) to be set at 0.2, however, given the available computing resource this value was decreased to 0.1. The grid spacing on the Re_L-axis was not as critical due to the independence of the solution with respect to streamwise location. However, for completeness, the details of the Re_L grid used are thus: 60 data points with a spacing of 37.1425, with the values at these points subsequently manipulated by the solver so as to generate a grid distribution in terms of non-dimensional length $x^\star$ (as per Equation 4.33).

To solve the Falkner-Skan equation for Blasius flow, an initial guess for the velocity distribution (f') at the first streamwise station was required. This initial guess was derived by assuming that the velocity distribution at the first streamwise location approximates a third-order polynomial (Equation 4.136) as recommended by Cebeci (1999). Using the original boundary conditions of the flow (Equations 4.97 & 4.98), Equation 4.136 can be solved to obtain a finite-differencing approximation for the initial estimates of $f' = u$, f, and v (Equations 4.137, 4.138, & 4.139 respectively), and these approximations were those used to initiate the solution for Blasius flow (using the technique described by Cebeci 1999).

$$f' = a + b\eta + c\eta^3 \tag{4.136}$$

$$u_j = \frac{3}{2}\frac{\eta_j}{\eta_e} - \frac{1}{2}\left(\frac{\eta_j}{\eta_e}\right)^3 \tag{4.137}$$

$$f_j = \frac{\eta_e}{4}\left(\frac{\eta_j}{\eta_e}\right)^2\left[3 - \frac{1}{2}\left(\frac{\eta_j}{\eta_e}\right)^2\right] \tag{4.138}$$

$$v_j = \frac{3}{2}\frac{1}{\eta_e}\left[1 - \left(\frac{\eta_j}{\eta_e}\right)^2\right] \tag{4.139}$$

Solution convergence was checked by investigating the value of the incremental iterate for v beyond the edge of the boundary layer (in the η-direction). As the solution of the Blasius boundary layer is well known, it was understood that the edge of the boundary layer (as calculated by the routine) should correspond to $\eta = \eta_e \sim 5.3$ Hence, beyond this location, it was known that v should be constant and equal to 0. Thus, by investigating the value of $\delta v_{\eta=8.0}$, the degree of convergence could be ascertained. For the analyses performed using the solver described in this section, the system of equations was deemed to have converged when the value of $\delta v_{\eta=8.0}$ was less than $1.0E-04$, as recommended by Cebeci (1999). If convergence was not achieved after 5 iterations, then revision of the solution inputs was called for.

Having implemented the Keller Box Method to solve the boundary layer equations for Blasius flow, the solution protocol was verified against the published results of Schlichting (1955). The value of the non-dimensional stream function ($f(\eta)$) at various values of η (Table 4.1), along with corresponding values of the first derivative (Table 4.2) and second derivative (Table 4.3) of the function were compared with the published data. For all values compared, the difference between the two sets of data (Equation 4.140) were found to be less than 0.20%, hence validating the accuracy of the results obtained throughout this research using the KBM finite differencing scheme.

$$err(Data) = \frac{abs(Data_{Published} - Data_{Calculated})}{Data_{Published}} \times 100\% \tag{4.140}$$

In addition to the calculation of the non-dimensional stream function and its derivatives, the numerical solver developed as part of this research was also used to calculate the shape factor for Blasius flow. The shape factor value was found to be 2.59, which again is consistent with published data (Schlichting 1955, White 1974, Cebeci and Cousteix 1999, Drazin 2002). For validation completeness, the plot of f' versus η was also constructed (Figure 4.2) and was found to exhibit the traits of the Blasius Layer, including a value of η at the boundary layer edge of 5.3, which again agrees with published

Table 4.1: Comparison of calculated values of f with published data from Schlichting (1955).

η	$f_{Published}$	$f_{Calculated}$	$err(f)[\%]$
0.0	0.0000	0.0000	0.00
0.8	0.1061	0.1061	0.00
1.6	0.4203	0.4202	0.02
2.4	0.9223	0.9220	0.03
3.2	1.5691	1.5686	0.03
4.0	2.3058	2.3051	0.03
4.8	3.0853	3.0846	0.02
5.6	3.8803	3.8795	0.02

Table 4.2: Comparison of calculated values of $f'$with published data from Schlichting (1955).

η	$f'_{Published}$	$f'_{Calculated}$	$err(f')[\%]$
0.0	0.0000	0.0000	0.00
0.8	0.2647	0.2647	0.00
1.6	0.5168	0.5166	0.04
2.4	0.7281	0.7288	0.10
3.2	0.8761	0.8759	0.02
4.0	0.9555	0.9554	0.01
4.8	0.9878	0.9878	0.00
5.6	0.9975	0.9975	0.00

Table 4.3: Comparison of calculated values of $f''$with published data from Schlichting (1955).

η	$f''_{Published}$	$f''_{Calculated}$	$err(f'')[\%]$
0.0	0.3321	0.3320	0.03
0.8	0.3274	0.3273	0.03
1.6	0.2967	0.2966	0.03
2.4	0.2281	0.2281	0.00
3.2	0.1391	0.1392	0.07
4.0	0.0642	0.0643	0.16
4.8	0.0219	0.0219	0.00
5.6	0.0054	0.0054	0.00

data (Schlichting 1955, White 1974, Cebeci and Cousteix 1999, Drazin 2002). Consequently it was concluded that a successful routine for solving the boundary layer equations had been developed, and hence the output could be used to calculate the stability characteristics of the Blasius boundary layer for validation of the OSE solver.

4.2.3 Solution of the OSE for Blasius flow

To validate the OSE solver, curves of neutral stability were constructed for the Blasius boundary layer. As discussed above, a numerical scheme was used to obtain the characteristics of the Blasius flow required to undertake a Linear Stability Analysis on the boundary layer. The validation was performed by

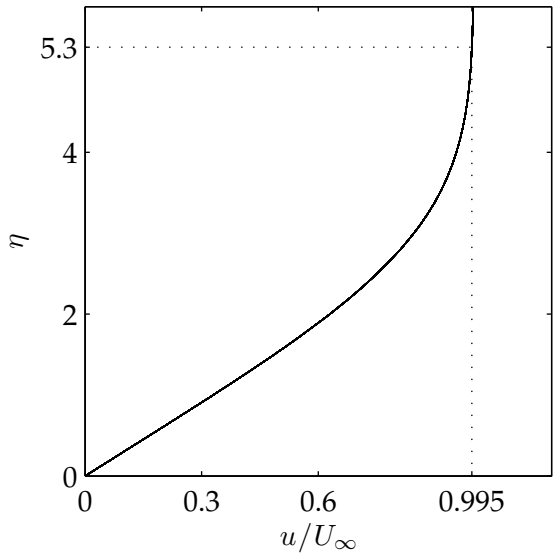

Figure 4.2: Dimensionless velocity profile plot of the Blasius Layer as calculated using the KBM.

calculating the curves of neutral stability of the flow, corresponding to zero spatial amplification rate ($\alpha_i = 0$).

The solution methodology, as described in Section 4.1.2, was based on an initial guess of the two unknown eigenvalues (α_r & ω_r), solving the recursion formulae of the routine, and checking the differences between the calculated eigenvalues and the original guess. For the analyses performed using the solver described in this section, the system of equations were deemed to have converged when the incremental changes to the iterates of α_r & ω (Equations 4.80 & 4.81) were less than $1.0E-04$, as per the recommendations of Cebeci (1999). If convergence was not achieved after 10 iterations, then an improved guess was called by the routine. A limit was also placed on the variable Δ_0 (Equation 4.79) to eliminate singularities in the calculation of the incremental changes to the iterates. A minimum value of $1.0E-06$ was placed on this variable as per the recommendations of Cebeci (1999), with further calculations ceasing at the respective Reynolds number if this condition was not met.

Both the curve for the wavenumber (Figure 4.3) and frequency (Figure 4.4) were computed, using a Re_L step of 27, and η step of 0.1 (with points extending from the wall to the edge of the boundary layer). This step size was sufficient to obtain curves exhibiting the characteristics of published curve data (Schlichting 1955, Cebeci and Cousteix 1999).

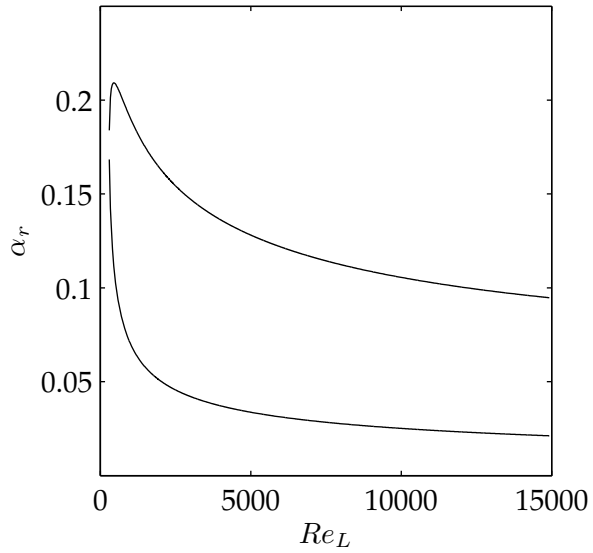

Figure 4.3: Curve of neutral stability (wavenumber) for Blasius Flow

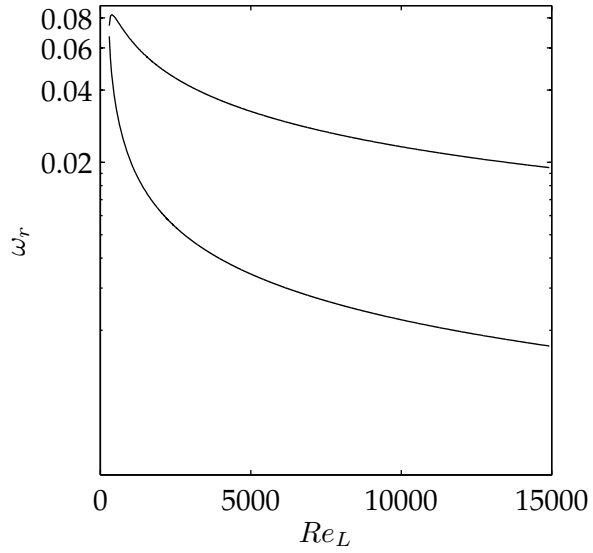

Figure 4.4: Curve of neutral stability (frequency) for Blasius Flow

A closer comparison of the wavenumber curve with data points published by Cebeci and Cousteix (1999) show excellent agreement (Figure 4.5). The slight discrepancies between points arises from the way in which the published data were obtained by measuring points from the curves published by Cebeci and Cousteix (1999). The important outcome from this comparison is that the predicted critical Reynolds number for the flow, $Re_{L_{crit}}$ calculated by the solver is 300 (equivalent to $Re_{\delta^*_{crit}} = 520$), again consistent with the results of Cebeci and Cousteix (1999). Consequently, it can be concluded that the developed OSE solver is accurate and capable of finding the eigenvalues of the OSE for external flows such as those that were studied in this research.

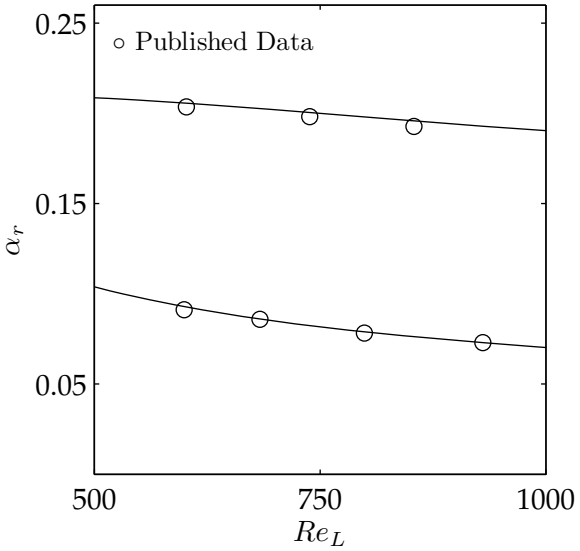

Figure 4.5: Validation of OSE solver with published results from Cebeci and Cousteix (1999).

4.3 Summary

In this chapter the methodology used to develop a solver for the Orr-Sommerfeld Equation (OSE) has been discussed. The lack of analytical solutions for the OSE has led to the use of a finite differencing scheme based on the Keller Box Method to rewrite the OSE as an equivalent system of linear equations, which can be solved numerically to find the hydrodynamic stability characteristics of boundary layer flows.

The solver developed as part of this research is based on the mathematical methodologies of Cebeci and Cousteix (1999). This solver has been verified using the characteristics of a Blasius boundary layer and has shown excellent agreement with published results. Consequently the OSE solver is capable of providing useful information regarding the hydrodynamic stability of external flows, which allows it to be subsequently used to investigate the stability of plasma-augmented flows and hence determine strategies and objectives for the DBD-based Laminar Flow Control systems studied in this research.

5 Tuning Guidelines for the Plasma-based Laminar Flow Control System

Controlling the stability of a laminar boundary layer, as discussed in Chapter 2, is a challenging task due to the complicated physical phenomena needed to be controlled. Knowing the way in which a Laminar Flow Control actuator can augment a flow is hugely beneficial to designing such systems, but as discussed in Chapter 3, predicting the behaviour of DBD devices is challenging, due to the numerous parameters dictating their performance. In addition, the difficulties associated with measuring the flow induced about a plasma actuator further complicates the design of a DBD-based LFC system. It is for these reasons that there has been limited success in the development of DBD-based LFC systems to date. Therefore, to address these issues in this research, prior to undertaking experimental investigations involving the augmentation of a laminar flat plate boundary layer with DBD plasma, preliminary experimental and numerical work was undertaken. The aim of this preliminary work was to identify suitable actuators to be incorporated into the DBD-based LFC system to be used for the Blasius layer experiments and to also determine the performance objectives that this LFC system would strive to meet.

The review of the literature (Chapter 3) suggested that a novel actuator design with the capability to vary the height to which the exposed electrode sits proud above the dielectric surface may allow for improved control over the induced jetting profile and maximum jetting velocity. If such control could be attained, it was postulated that it would be an ideal tuning parameter for DBD-based LFC systems. The first section of this chapter contains the results of an undertaken experimental investigation looking at the performance of the novel actuator design that was conceived during the research, as it is operated in quiescent conditions. The results discussed here are essentially a

reformulation of those published by Gibson et al. (2009a), and these results led to a decision being made as to what actuator design to be used for the subsequent boundary layer experiments.

The second section of this chapter discusses numerical investigations undertaken to assist in specifying the velocity augmentation objectives of the DBD-based LFC system. Using a number of published experimental and theoretical velocity profiles, the Orr-Sommerfeld Equation solver developed as part of this research (discussed in Chapter 4) was used to calculate curves of neutral stability for augmented Blasius boundary layer flows. From these numerical analyses, desired augmentation effects were determined for the DBD-based LFC system to be developed. The intention was to use these desired augmentation effects as a benchmark to tune the DBD system against during the subsequent experimental investigations that were undertaken as part of this research (see Chapter 7, 8, & 9).

5.1 Orthogonal actuator performance in quiescent air

During the literature review (Chapter 3), the performance of the plasma actuator was discussed in terms of the electric field developed between the electrodes of the device. This discussion was based on the simplified linear analysis described by Shyy et al. (2002), as well as the electric field description given by Orlov (2006) and Orlov et al. (2006). From this discussion it was identified that attaining control over the profile of the synthetic jet through geometry variations would be beneficial to the development of a DBD-based LFC system because of the simple system tuning such control would provide. As discussed in the literature review, it was decided to achieve this variation during this research by augmenting the wall-normal extent of the plasma region through variations in actuator geometry. However, prior to this research, no studies had specifically attempted to achieve this objective and hence this parametric study was formulated.

To vary the vertical extent of the plasma region the formulated parametric study sought to investigate what effect the extent to which the exposed electrode sat proud above the dielectric surface (exposure height, y_{exp}) had on the jetting performance of a DBD actuator. In order to achieve the desired variation in exposure height, actuators with electrodes arranged in an orthogonal arrangement were designed and utilised. Prior to this research, experiments involving orthogonal actuators had not been conducted and hence this parametric study marked the first investigations into novel, orthogonally arranged actuators.

Throughout the investigation, a number of geometrically similar orthogonal actuators were tested and operated at the same electrical conditions. The only variation between the actuators was the value of the electrode exposure height (y_{exp}). By measuring the induced jetting profile, the effectiveness of these devices as LFC devices were able to be investigated, and compared with more conventional actuator configurations with parallel electrodes.

5.1.1 Parametric investigation set up

The parametric investigation had two aims. The first was to assess the capability of orthogonal actuators as flow control devices, and for this reason the performance of each orthogonal actuator was compared with a more conventional design incorporating parallel electrodes. The second objective was to examine whether the jetting could be controlled by varying the exposure height of the orthogonal actuators. Therefore, the orthogonal actuators tested differed in the value of electrode exposure height.

5.1.1.1 Actuator design

Being a parametric investigation (focused on the variation of the y_{exp} parameter only), all actuators tested were manufactured of the same materials, with the same geometry and same electrical operating conditions. The orthogonal actuators were manufactured from a $500mm \times 500mm \times 25mm$ block of acrylic, from which a $20mm$ wide groove was milled. The exposed electrode was placed on the leading surface of the block, and the encapsulated electrode was placed in the groove, such that the critical dimensions pertaining to the operation of the actuator were achieved (Figure 5.1). The wall formed by the leading surface was found to be most effective in preventing detrimental arcing between the two electrodes, which would have otherwise destroyed the actuator and prevented useful plasma from being formed. During the investigation the exposed electrode exposure height, y_{exp} was varied in $0.5mm$ increments from $-1.0mm$ to $2.0mm$. A summary of the other critical dimensions of the actuators used is as follows:

- electrode material: tinned copper,
- electrode thickness: $t_{elec} = 0.1mm$,
- electrode chordwise length: $L = 12.5mm$,
- electrode spanwise length: $b = 100mm$,
- dielectric thickness: $d_v = 2mm$,

- encapsulated electrode buried in Kapton^{TM},
- horizontal gap between the electrodes $d_h = 2.5mm$ (selected as an appropriate average value based on the results of Forte et al. 2007).

The parallel actuator used as a comparison for the orthogonal actuators (Figure 5.2) had similar critical dimensions, with some minor modifications to account for the unique design of the actuator. For ease of manufacture, the parallel actuator was manufactured from a $200mm \times 60mm \times 2mm$ block of acrylic, with the exposed electrode buried in Kapton^{TM} to prevent possible arcing between the electrodes. This actuator represented a typical DBD actuator, and was found to have similar performance to devices used in other studies (as discussed in Section 5.1.2).

The electrodes of each actuator were connected to an ElectroFluids Systems Mini-Puls 2 proprietary plasma generator system. For all investigations, a sinusoidal input to the electrodes, with a fixed applied frequency of $13kHz$ and fixed applied voltage of $16kV_{pp}$, was used. These parameters were chosen as they were found to produce uniform discharges for all actuators tested, whilst also being similar to the electrical inputs used in other published works (Enloe et al. 2004a, Van Dyken et al. 2004, Enloe et al. 2004b, Enloe et al. 2003).

The voltage was checked for each actuator by connecting a PicoScope 5203 PC-based oscilloscope to the output of the MiniPuls2 via the 1 : 1000 voltage divider integrated into the plasma generator system.

5.1.1.2 Velocity measurements

Time-averaged dynamic pressure measurements for each actuator were obtained $5mm$ downstream of the trailing edge of the encapsulated electrode,

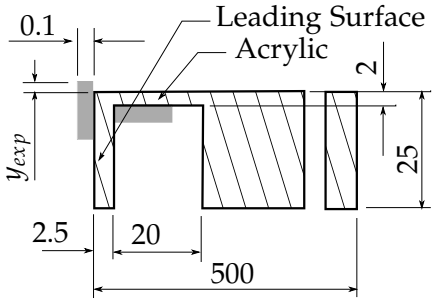

Figure 5.1: Critical dimensions of the orthogonal actuators used in the parametric investigation.

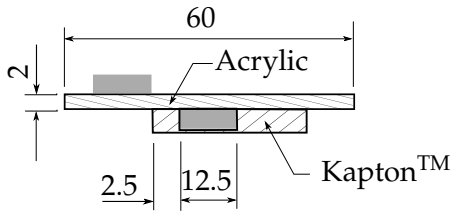

Figure 5.2: Critical dimensions of the parallel actuator used in the parametric investigation.

using a total pressure tube with an internal diameter of 1.2mm (and an external diameter of 1.65mm) connected to an MKS *398* differential Baratron with a frequency response of 40Hz, and pressure range of 0 to 1$Torr$. The momentum comparison undertaken in this study was modified to minimise the effect of absolute uncertainties in the measurements. Since the Baratron provided a linear response to pressure, it was decided in the interest of minimising uncertainties, that comparisons between the performance of each actuator would be based on the amount of chordwise momentum flux imparted on the air per unit span length (Equation 5.1), which was derived from measurements of the downstream dynamic pressure obtained from the baratron (q) and the maximum measured value of the dynamic pressure throughout the investigations (q_{max}).

$$\frac{\dot{\overrightarrow{M_x}}}{b} = \int_0^H \rho U^2 dy = 2\int_0^H q dy = 2q_{max}\int_0^H \left(\frac{q}{2q_{max}}\right) dy \tag{5.1}$$

A total of 120000 measurements, made at a sampling frequency of 4000Hz, were taken at 1.0mm height increments above the surface of each actuator. The measurements were made to a height of $y = H = 10.825mm$, which corresponded to a value at which no actuators produced a discernible change in the measured pressure. It is acknowledged that the sampling rate selected for the pressure tube measurements was far greater than the frequency response of the Baratron itself. However, since the increased number of samples did not cause a noticeable increase in computation time during post-processing, such a high sampling was considered not to have a detrimental effect on the research.

5.1.2 Investigation results

5.1.2.1 Plasma development

The first results obtained from the parametric investigation were qualitative in nature, based on comparisons between the plasma formed by the parallel actuator and an orthogonal actuator with an electrode exposure value of $0.0mm$. It was found that an orthogonal actuator was capable of producing a synthetic jet effect and hence the first objective of the investigation had been achieved. Comparisons between the plasma volume produced by an orthogonal-type actuator and the more conventional parallel-type showed that the orientation and vertical arrangement of the exposed electrode has a significant effect on the performance of the device. The plasma volume produced by the parallel-type (Figure 5.3a) was found to be denser, and less filamentary than that produced by the orthogonal device (Figure 5.3b). In addition, the vertical extent of the plasma region developed by the parallel actuator was observed to be less than that for the orthogonal-type.

The more filamentary plasma associated with the orthogonal actuator has been attributed to a denser electrostatic field being present within the vicinity of the electrodes, as compared with a parallel device, due to the relative proximity of the two electrodes. Since $y_{exp} = 0$ for this actuator, the strongest regions of the electric field were contained exclusively along the surface of the dielectric with less free space than that for the parallel device. The observed consequence of this was more micro-discharges along the surface, and hence a more filamentary plasma. In terms of the jetting characteristics of the actuators, the results suggested that the transferred chordwise momentum was distributed over a smaller height for the parallel

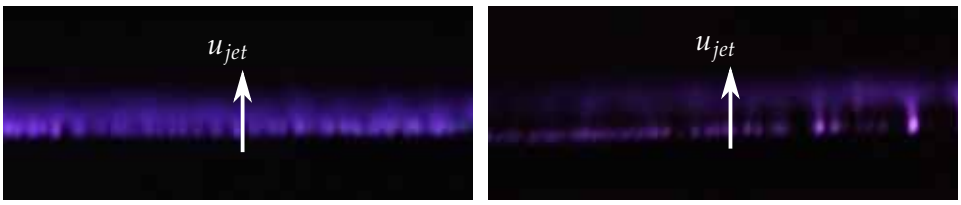

(a) Parallel actuator (b) Orthogonal actuator, ($y_{exp} = 0$)

Figure 5.3: Plasma produced in quiescent air. Images were taken directly above the respective encapsulated electrodes. Net induced wall-jet velocity u_{jet} is parallel to the page and directed from page bottom to page top.

actuator and that the orthogonal device produced a fuller jetting profile potentially more suited for use in an LFC system. It is postulated that the increased vertical extent of the induced jet for the orthogonal actuator is caused by a stronger pseudo-cathode effect along the dielectric surface, arising from the stronger electrostatic field, as discussed by Kogelschatz et al. (1997), and Enloe et al. (2004b). The nature of the electrostatic field produced by the actuator dictates that the ejection of electrons from the exposed electrode is most likely to occur along the chordwise direction. The strong electrostatic field allows particles to accumulate on the dielectric surface sooner during the first discharge half-cycle, forcing subsequently-developed plasma particles to travel in longer, less direct trajectories. Hence, for an orthogonal actuator, the charged particles are required to travel a greater vertical distance, thus increasing the vertical extent of the generated plasma region (Figure 5.4).

With reference to the electric field, it is hypothesized that the the strong electric field strength at the surface of the actuator creates a more uniform distribution of charge at the surface, which then forc

The observations obtained from the study of the developed plasma were supported by the pressure measurements made downstream of each actuator. The plotting of dynamic pressure at various heights above the dielectric surface (Figure 5.5) revealed that the pressure profiles for the orthogonal actuators were fuller than that for the parallel device, with a shallower velocity

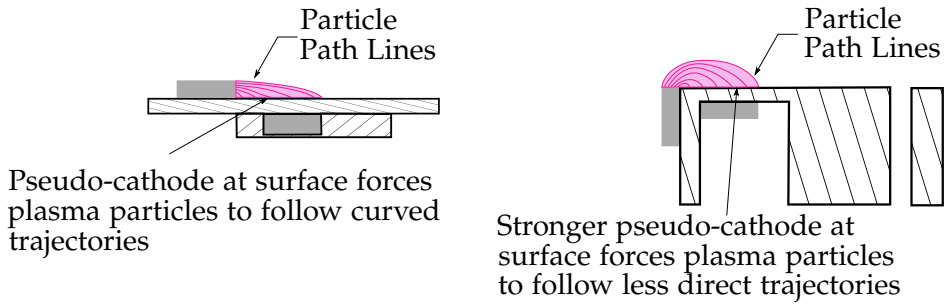

(a) Parallel actuator

(b) Orthogonal actuator, ($y_{exp} = 0$)

Figure 5.4: Suggested plasma particle paths for parallel and orthogonal actuators. It is hypothesised that a stronger electrostatic field produced by the orthogonal actuator creates a more effective pseudo-cathode that forces plasma particles to travel in longer, less direct trajectories.

gradient and hence diminished shear stress close to the wall. In addition, a relationship was found to exist between exposure height and the profile fullness, with the fullest distribution being observed for the case corresponding to $y_{exp} = -0.5mm$. The fullness of the profiles was seen to diminish as the value of y_{exp} departed from $-0.5mm$, and it was noticed that for positive values of y_{exp}, the value of the pressure at the measurement location downstream of the actuator was zero for all vertical positions measured. Furthermore, it was observed that the position of maximal jetting velocity (u_{max}) varied between the actuators, and hence was dependent on the value of the exposure height. In addition, it was noticed that for $0.5mm \leq yexp \leq 2.0mm$, the chordwise extent of the plasma region was significantly reduced, with the plasma confined to a region very near the exposed edge of the uncovered electrode. This effect was attributed to a drastic change in the electric field arrangement for positive values of y_{exp}, which caused a containment of the developed plasma, which thus prevented the plasma region from extending far along in the chordwise direction, which would have allowed for discernible pressure measurements to have been obtained.

5.1.2.2 Velocity measurements

The maximum induced chordwise velocity (u_{max}) for each actuator was calculated to assist in placing the results in context with other published studies. This measure also allowed the experimental method to be validated against similar investigations. Although no values of maximum induced chordwise velocity were found in the literature for the same set of electrical and geometric parameters utilised in this work, Forte et al. (2007) reported a maximum induced jetting velocity of approximately $4.75m/s$ for a parallel-type actuator with the following parameters (that were found to be the most similar to those used in the present study).

For the parallel actuator studied in this parametric study, a maximum velocity of $3.30m/s$ was measured. Although less than the value obtained by Forte et al. (2007), it is of similar magnitude, and as discussed in Forte et al. (2007) the difference can be attributed to the higher applied voltage used by Forte et al. (2007). Hence the result of maximal measured induced velocity for the conventional actuator supported the accuracy and validity of the experimental measurements obtained from this parametric study.

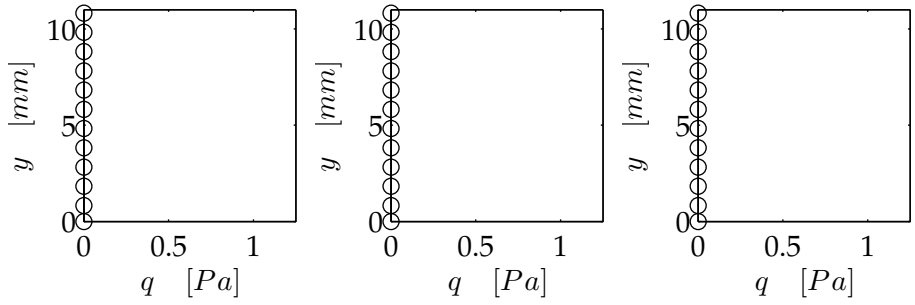

(a) Orth., $y_{exp} = 2.0mm$

(b) Orth., $y_{exp} = 1.5mm$

(c) Orth., $y_{exp} = 1.0mm$

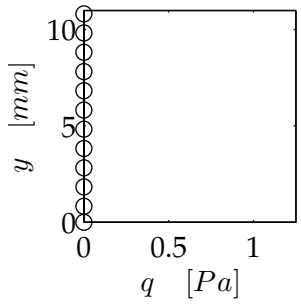

(d) Orth., $y_{exp} = 0.5mm$

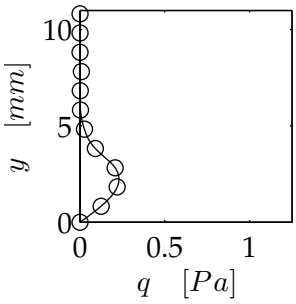

(e) Orth., $y_{exp} = 0.0mm$

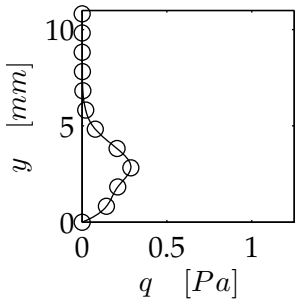

(f) Orth., $y_{exp} = -0.5mm$

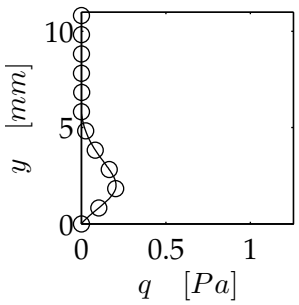

(g) Orth., $y_{exp} = -1.0mm$

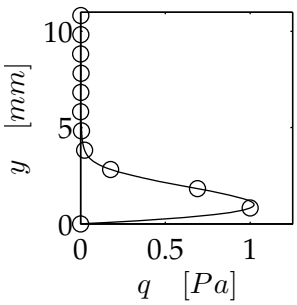

(h) Parallel type

Figure 5.5: Dynamic pressure plots obtained from the parametric investigation. (Cubic-spline interpolation used between data points for clarity).

Table 5.1: Comparison of actuator parameters used in the parametric study and the work of Forte et al. (2007).

Parameter	Parametric Study	Study of Forte et al. (2007)
Electrode material	Tinned copper	Aluminium
Electrode thickness	$0.1mm$	$0.1mm$
Electrode chordwise length	$12.5mm$	$12.5mm$
Electrode spanwise length	$100mm$	$200mm$
Dielectric material	Acrylic	Acrylic
Dielectric thickness (vertical direction)	$2mm$	$2mm$
Dielectric thickness (horizontal direction)	$0mm$	$2.5mm$
Applied voltage	$16kV_{pp}$	$20kV_{pp}$
Applied frequency	$13kHz$	$13kHz$

Forte et al. (2007) demonstrated in their work the existence of an optimum chordwise gap for developing maximal induced chordwise velocity. For an applied voltage of $20kV_{pp}$ and applied frequency of $700Hz$, a given actuator produced a quadratic relationship between the induced maximum chordwise velocity and chordwise separation distance (d_h) with a maximum velocity value occurring for a separation of $5.0mm$. The results of the conducted experimental study discussed here also revealed a similar relationship existing between the maximum induced chordwise velocity and the extent to which the exposed electrode lay above the actuator surface, (Figure 5.6). For an orthogonal actuator, the highest maximum induced velocity ($u_{max} = 1.75m/s$) was found for an exposure height of $-0.5mm$, which also corresponded with the value of y_{exp} that produced the fullest pressure profile.

Another intersting result from the study pertains to the maximum induced jetting velocity produced the conventional actuator. The results show that for a fixed set of electrical and geometric parameters, the parallel actuator produces approximately twice the maximum velocity of the optimum orthogonal device. This suggests that parallel actuators can provide a greater velocity increase in the chordwise (x) direction, albeit with an increased velocity gradient, and hence fluid shearing at the wall.

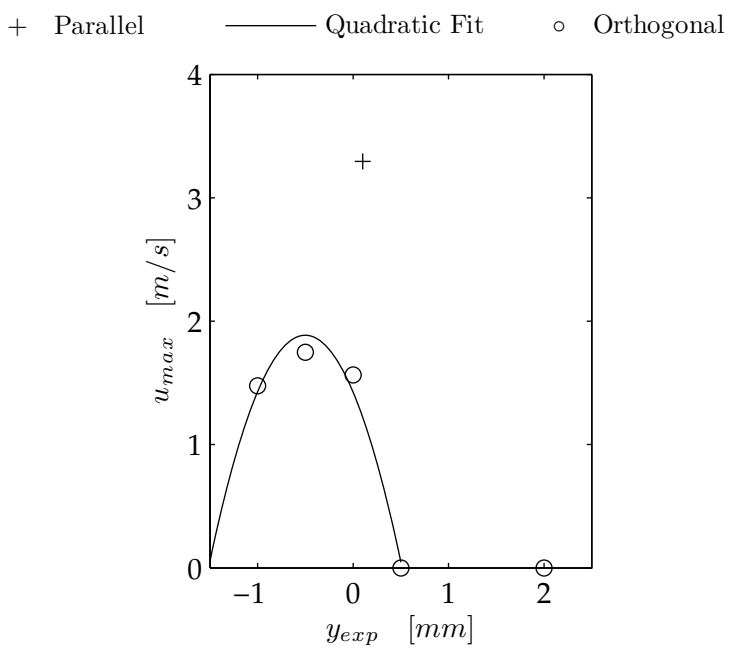

Figure 5.6: Maximum chordwise velocity results for tested actuators

5.1.2.3 Momentum analysis

The momentum analysis was conducted using data of normalised pressure plotted against vertical position. Cubic-spline fitting was used between the data values obtained experimentally, to generate continuous velocity profiles, which were then numerically integrated using Simpson's Rule to yield the magnitude of chordwise (x-direction) momentum per unit span length imparted by each actuator.

The results of the momentum analysis revealed a dependence of actuator-induced momentum on y_{exp} similar to the maximum induced chordwise velocity (Figure 5.7). Even though the orthogonal actuators were effective over a larger wall-normal distance, the parallel device still produced approximately twice the momentum as the optimum orthogonal device. In addition, the momentum was imparted closer to the wall.

5.1.3 Conclusions of the parametric investigation

The jetting characteristics of a single DBD plasma actuator were found to be affected by the arrangement and geometry of the electrodes used to generate the plasma. For a given operating voltage and frequency, this investigation found that an orthogonal actuator produces a plasma region that is more

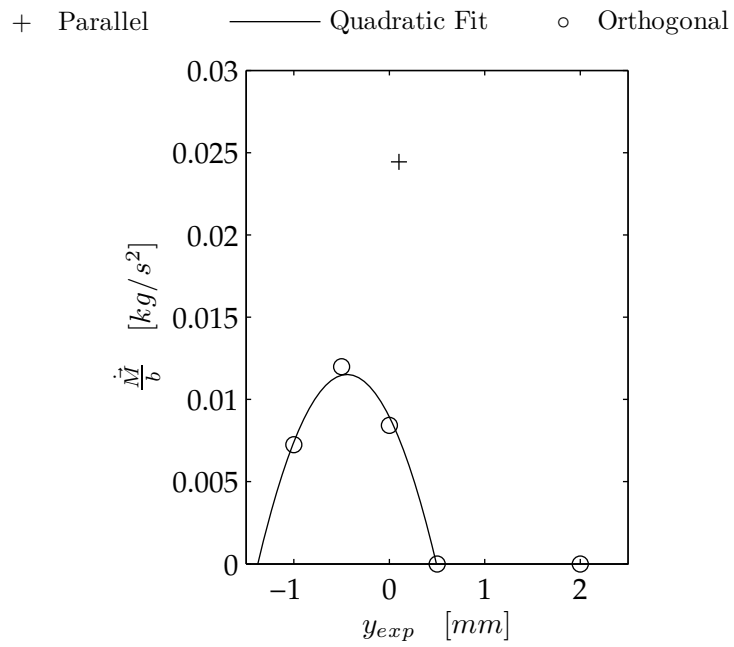

Figure 5.7: Chordwise momentum results for studied actuators

filamentary and more voluminous than that produced by a parallel device. These observations have been attributed to an increased density in the electric field and an increase in the distance normal to the actuator surface that the charged particles of the plasma discharge are required to travel.

The study also revealed that the momentum and velocity produced by an orthogonal actuator is affected by the value to which the exposed electrode of the device lies above the surface of the dielectric (y_{exp}). Through variation of this parameter in a number of orthogonal actuators, analysis of obtained pressure measurements show that an optimum value of y_{exp} exists, corresponding to the greatest actuator-induced chordwise maximal velocity and actuator-imparted chordwise momentum (per unit span length) in quiescent surroundings. More important however, was the discovery of an alternative means of augmenting the jetting distribution of a DBD actuator, through variations of the y_{exp} value. Orthogonal actuators produced more voluminous plasma regions with peak velocity values further away from the actuator surface compared with the more conventional parallel-type. This value could also be altered through changes to y_{exp}. This result is significant to DBD-based LFC as it demonstrates another mechanism through which the synthetic jetting effect can be altered. Thus varying y_{exp}, so as to change the position and value of the maximum jetting velocity, provides a mechanism

through which a DBD-based LFC system can be tuned so as to maximise the performance of the system without satisfying the general criteria for instability.

A final point of interest surrounding orthogonal actuators is the lower maximum jetting velocities associated with such devices. The lower maximum jetting velocities of orthogonal devices (as compared with parallel-type actuators) suggests that orthogonal actuators will be less likely to introduce large inflections in the velocity profile of a boundary layer, and hence suggest that such actuators will be well suited for use in a LFC system.

5.2 Solving the OSE for LFC design guidelines

The parametric study revealed that orthogonal actuators produce fuller velocity profiles, with diminished fluid shearing close to the wall, as well as a mechanism through which the magnitude and position of the maximum jetting velocity can be controlled. For these reasons it was suggested that orthogonal actuators would be favourable Laminar Flow Control devices. This suggestion, however, is limited in its usefulness, as the effect of the actuator on the boundary layer cannot be assessed through a simple parametric study in quiescent conditions. In the absence of a suitable analytical description of the flow field around a DBD actuator that could be utilised the simulate the effect of the orthogonal actuators on a flat plate boundary layer in a ZPG in a timely fashion, it was decided to use Linear Stability Theory to identify favourable velocity augmentation characteristics for improving the stability of an approximately equivalent Blasius flow. From the resulting Linear Stability Analyses, it was then possible to identify what the velocity characteristics of the augmented boundary layer should look like, and thus provide a benchmark flow response that the actuators in the DBD LFC system can be tuned to achieve.

Using the Orr-Sommerfeld Equation solver developed as part of this research, (as discussed in Chapter 4) the effect of idealised Laminar Flow Control was investigated by determining the curves of neutral stability for modified Blasius boundary layers. The idealised flow augmentation from the LFC, represented by modified boundary layer velocity profiles, was derived through application of approximated analytical functions to published results of DBD-augmented boundary layer flows, as well as the case for the Blasius flow exposed to uniform wall suction. With the assistance of suitable assumptions pertaining to the development of these augmented boundary layers, these velocity profiles were used to obtain the critical Reynolds number for different velocity profile augmentations, and thus provide insight into how

the operation of the orthogonal actuators to be used in the subsequent experimental investigations should be tuned so as to provide favourable benefits to the stability of the Blasius layer.

5.2.1 Stability analyses of augmented boundary layers

Four stability analyses were conducted to provide insights into how the orthogonal actuators should augment the Blasius layer to improve hydrodynamic stability. As these were conducted prior to experimental results being available from this research, the first three utilising velocity profiles derived from published experiments. These velocity profiles were sourced from the work of Newcamp (2005), who published results for a boundary layer augmented by a single actuator operated at different applied power levels. These results consequently allowed three stability analyses to be conducted on a boundary layer augmented by three different DBD flow control systems.

The fourth analysis investigated a widely studied and fundamental LFC scenario. In this analysis the stability characteristics of a boundary layer exposed to uniform wall suction were determined for comparison, and further system benchmarking suggestions.

On completion of all four analyses, the improvement in the critical Reynolds number for the varied flow strategies was able to be determined. The improvements were expressed as a ratio between the controlled critical Reynolds number and the original critical Reynolds number of the flow ($\frac{Re_{crit_{Control}}}{Re_{crit_{Blasius}}}$), and from this ratio, recommendations were made in regard to how the orthogonal actuators used in the subsequent experimental investigations of this research were to augment the boundary layer flow.

5.2.1.1 Controlled boundary layer based on published DBD results

Newcamp (2005) published measurements of a boundary layer augmented by conventional parallel actuators operated at three different power levels. These experiments were conducted at a chordwise Reynolds number of 40000, and they were most detailed in terms of measurement resolution available to the research at the time of the preliminary work. In addition to being obtained at a Reynolds number beneath the critical value of Blasius flow, the results showed how variations in an electrical parameter alters the velocity profile augmentation observed in the boundary layer; of relevance to the scope of the research.

What was observed from the results of Newcamp (2005) was that for all power levels, the boundary layer, as compared with the Blasius layer at

the equivalent position, became thinner, with increased local velocity values close to the wall. In addition, the shape of the velocity profile was found to be dependent on the power level at which the actuator was operated. Using these results, it was concluded that DBD actuators have the potential to significantly thin a boundary layer, augment the velocity profile, and that this augmentation was a function of the electrical operation of the plasma actuator, which suggested a mechanism through which a DBD LFC system could be tuned and henced galvanised the discussion in Section 3.3.

Closer inspection of the velocity profiles showed that the plasma actuators introduced prominent inflections in the flow (Figure 5.8, 5.9, & 5.10), which were having a local destabilising effect on the boundary layer. However, this was not considered to be of great concern in the context of the numerical investigations that were undertaken. As discussed in Section 3.3 various electrical parameters are capable of *tuning* the induced jetting profile and maximum induced jetting velocity. Naturally, if these parameters are not tuned correctly, inflections in the velocity profiles will occur, and thus this is the likely reason for the inflections in the results of Newcamp (2005). Using the data of Newcamp (2005) as an indication of how a DBD actuator may augment a boundary layer flow, and coupling this with the knowledge of how an actuator can be tuned (Section 3.3), it was hypothesised that a DBD actuator could augment a boundary layer in such a way so as to show characteristics of the results of Newcamp (2005), albeit in a stable fashion. Consequently the data of Newcamp (2005) were used as a guide to conceive and generate a family of velocity profiles that could potentially could be obtained through the use of DBD actuators.

Using the same non-dimensional length ($y^\star = \eta = \frac{y}{L} = y\sqrt{\frac{u_e}{\nu x}}$) and velocity ($u^\star = u(\eta) = \frac{u}{u_e}$) variables as used in the Falkner-Skan Equation, a family of velocity profiles described by Equation 5.2 (with second derivative defined by Equation 5.3), were found to roughly approximate the gross characteristics of the DBD-augmented flows of Newcamp (2005). Through approximation of the results of Newcamp (2005) it was assumed that the value of η at the edge of the boundary layer (η_e) was the same as that of Blasius flow (approximately 5.3).

$$u(\eta) = \frac{1 - a^{(-k\eta)}}{1 - a^{(-k\eta_e)}} \tag{5.2}$$

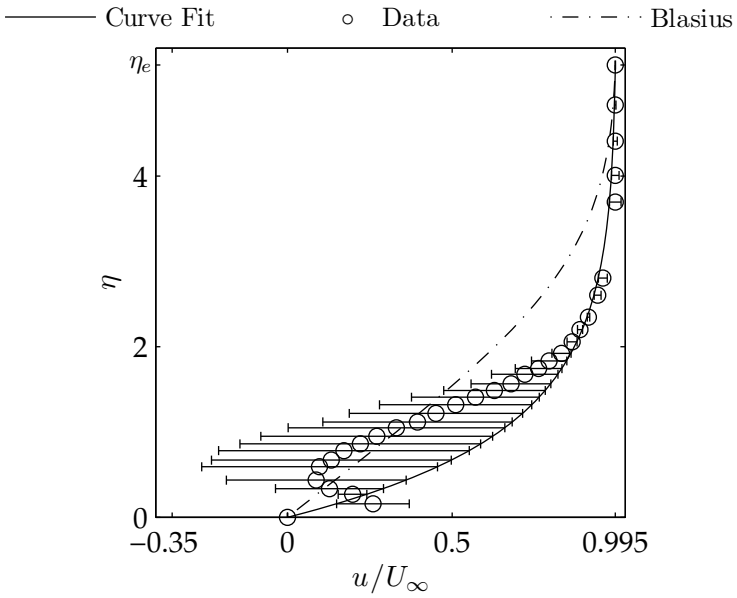

Figure 5.8: Result of analytical curve fitting between assumed DBD-augmented flow and the results of Newcamp (2005) for an actuator operated at $P = 15W$. Error bars show differences between the experimental data and approximated curve fit.

$$u''(\eta) = \frac{-k^2 a^{(-k\eta)} ln^2(a)}{1 - a^{(-k\eta_e)}} \tag{5.3}$$

The selection of the variables a and k was made by simultaneously attempting to minimise the Normalised-Root-Mean-square-Deviations between the fitted velocity profile and the measured experimental data (Equation 5.4) and the error between the measured and fitted momentum thickness values (Equation 5.5). The momentum thickness values for the experimental results were obtained through integration of the published data using Simpson's rule. The values of the variables for each velocity profile can be found in Table 5.2.

$$NRMSD = \frac{\left[\sum_{i=1}^{n} = \left(u/U_\infty|_{measured} - u/U_\infty|_{fit}\right)^2\right]^{1/2}}{n} \Big/ u(\eta_e) - u(0) \tag{5.4}$$

$$err(\theta) = \frac{abs(\theta_{measured} - \theta_{fit})}{\theta_{measured}} \times 100\% \tag{5.5}$$

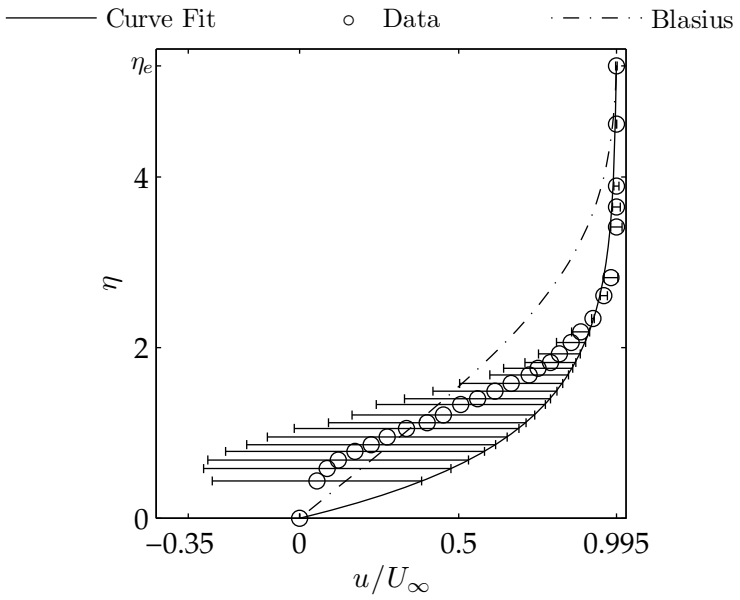

Figure 5.9: Result of analytical curve fitting between assumed DBD-augmented flow and the results of Newcamp (2005) for an actuator operated at $P = 20W$. Error bars show differences between the experimental data and approximated curve fit.

Table 5.2: Curve fitting coefficients used to approximate the DBD-augmented velocity profiles.

Actuator Power $[W]$	a	k	$NMRSD[\%]$	$err\,(\theta)$ $[\%]$
15	1.90	1.60	19.6	16.3
20	1.48	2.83	22.6	22.9
25	2.00	1.68	13.4	13.5

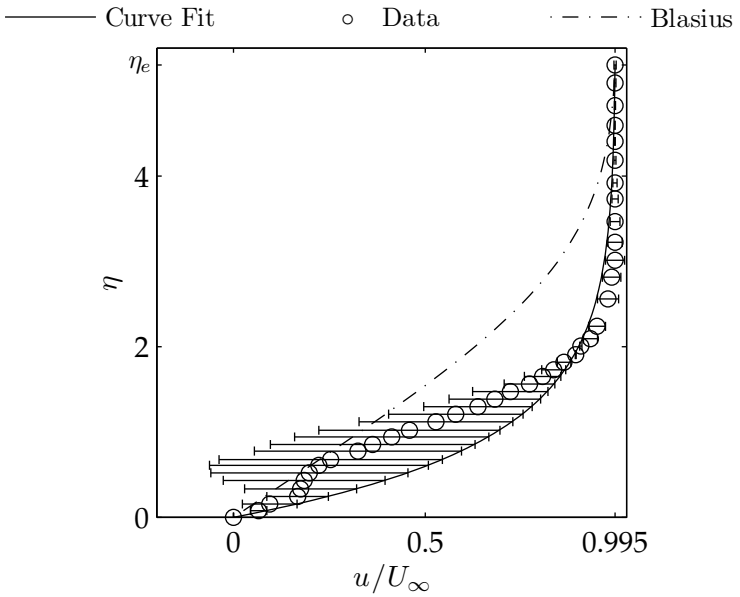

Figure 5.10: Result of analytical curve fitting between assumed DBD-augmented flow and the results of Newcamp (2005) for an actuator operated at $P = 25W$. Error bars show differences between the experimental data and approximated curve fit.

Even after attempting to approximate the data with as much accuracy as possible, it is conceded that the results of the curve fitting (Figure 5.8, Figure 5.9, and Figure 5.10) are poor for all actuators. With the exception of the data points between $\eta = 2$ and $\eta = \eta_e$, the quality of fit is very poor. However, this attempt at fitting a family of profiles to the data of Newcamp (2005) is not a wasted exercise. To reiterate, the purpose of the curve fitting was to identify feasible boundary layer velocity profiles that can be produced using DBD actuators, and as is subsequently discussed in Section 8.2, experimental results pertaining to this research will reveal an actuator that could augment a boundary layer to produce a velocity profile with a very good level of fit to the conceived family of functions. Moreover, the LSAs performed on the velocity profiles described here provide necessary information to identify the eigenvalues obtained in Section 8.2.

The subsequent Linear Stability Analyses conducted on the assumed velocity profiles assumed that the DBD plasma was formed by a sufficient number of actuators so as to produce similar velocity profiles (defined by Equation 5.2) throughout the entire layer. The resulting spatial and temporal curves of neutral stability (Figures 5.11 & 5.12 respectively) showed that the

assumed DBD-augmented velocity profiles have a significant effect on the stability of the flow. These were created using regular rectangular computational grids, (10000 points in the Re_x-direction with spacing of $5.0E+05$, 100 points in the η-direction with spacing of 0.54)The critical Reynolds number for the augmented flows is seen to be related to the individual velocity profiles, themselves related to the electrical operation of the DBD device. Based on the assumptions of the investigation, the lowest power actuator ($P = 15W$) was found to attain the highest critical Reynolds number, 46 times greater than that of the base Blasius flow (Table 5.3). Hence any DBD-based LFC system that can produce boundary layer characteristics described by the velocity profiles studied here would have significant benefits to flow stability, with the best being characteristics associated with the low power actuator.

A point worth mentioning about the results for the idealised DBD-augmented flows is that the boundary layers in the presence of such flow control become susceptible to smaller wavelength (higher wavenumber) and higher frequency disturbances, as compared with Blasius flow. In the real-world, preventing such disturbances from entering the layer may prove very challenging. This is because of the small physical dimensions required by

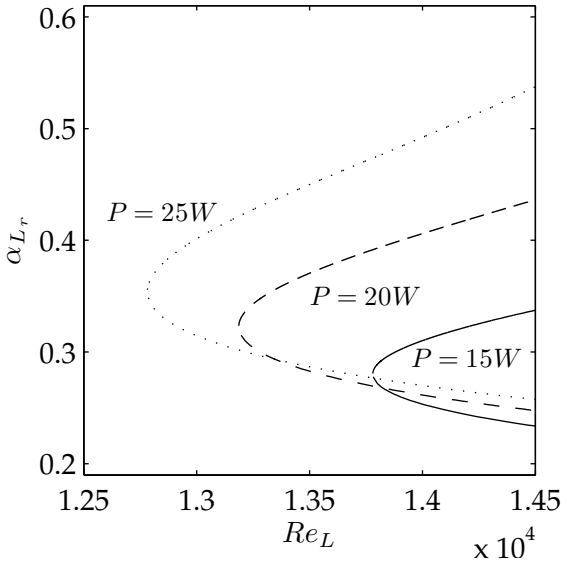

Figure 5.11: Curves of neutral stability (wavenumber) for the assumed DBD-controlled boundary layers.

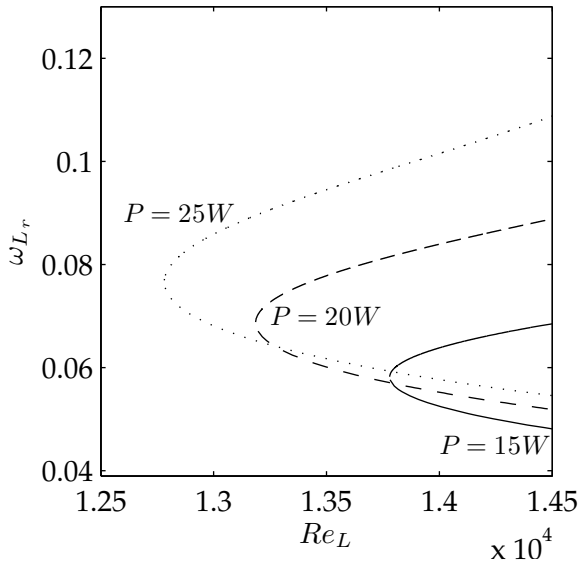

Figure 5.12: Curves of neutral stability (frequency) for the assumed DBD-controlled boundary layers.

Table 5.3: Comparison of critical Reynolds number for different, idealised controlled flows.

Actuator Power $[W]$	$Re_{L_{crit}}$	$\frac{Re_{crit_{Control}}}{Re_{crit_{Blasius}}}$
Blasius	300	1
15	13800	46
20	13200	44
25	12800	42.5

such sources for these disturbances, meaning that numerous small protuberances on the surface could readily destabilise the flow within the boundary layer.

5.2.1.2 Boundary layer controlled with uniform suction

The final Linear Stability Analysis conducted was that for the boundary layer augmented by uniform wall suction. As described in Chapter 2, the velocity profile of the boundary layer with uniform suction is described by an exponential function (Equation 2.32). The velocity profile can be simplified by recognising that the displacement thickness of the boundary layer with uniform suction asymptotes to a constant value (Equation 5.6). For the

purpose of investigating the hydrodynamic stability of a flow augmented by uniform wall suction it is sufficient to assume that this displacement thickness is constant throughout the entire length of the layer. This consequently allows the velocity profile to be redefined in terms of the displacement thickness (Equation 5.7), as discussed by Schlichting (1955), Cebeci and Cousteix (1999) and Drazin (2002).

$$\delta^{\star} = \frac{\nu}{-v_0} \tag{5.6}$$

$$u\left(y\right) = u_e \left[1 - exp\left(\frac{-y}{\delta^{\star}}\right)\right] \tag{5.7}$$

When calculating the curves of neutral stability for a flow with the asymptotic suction profile it is more appropriate to normalise lengths by the displacement thickness of the boundary layer, as the similarity variable used to describe Blasius flow does not adequately describe the characteristics of such a flow. Hence, to calculate the curves of neutral stability for a flow with the asymptotic suction profile, the OSE solver was modified such that the Reynolds number, wavenumber and frequency normalised against the boundary layer displacement thickness.

To validate the capability of the OSE solver to handle differing normalised variables, the spatial (Figure 5.13) and temporal (Figure 5.14) curves of neutral stability for Blasius flow based on displacement thickness were calculated. A regular rectangular computational domain was used with 100 points in the non-dimensional height direction (0.1 grid spacing) and 2000 points in the Reynolds number direction (156.7 spacing for $0 \leq Re_{\delta^*} < 4900$, 495.6 spacing for $4900 < Re_{\delta^*} \leq 500000$). The curves agree well with those published by Schlichting (1955), Reeh (2008), and the critical Reynolds number based on displacement thickness ($Re_{\delta^{\star}_{crit}}$) was determined to be 520, which again agreed with published data Schlichting (1955), Cebeci and Cousteix (1999), and Reeh (2008).

Using the OSE solver, the spatial (Figure 5.15) and temporal (Figure 5.16) curves of neutral stability for the boundary layer with the asymptotic suction profile were calculated. As for the Blasius calculations, a rectangular computational domain was used with 1000 points in the non-dimensional height direction (0.06 grid spacing) and 2000 points in the Reynolds number direction (3.5 spacing for $46500 \leq Re_{\delta^*} < 50000$, 450 spacing for $50000 < Re_{\delta^*} \leq 500000$). In addition to the loci circumscribing a smaller number of unstable eigenvalues with reduced magnitudes, the critical Reynolds number was found to be approximately 47000. The results, which agree with those published by Reeh (2008), imply that the limit of stability for the flow with

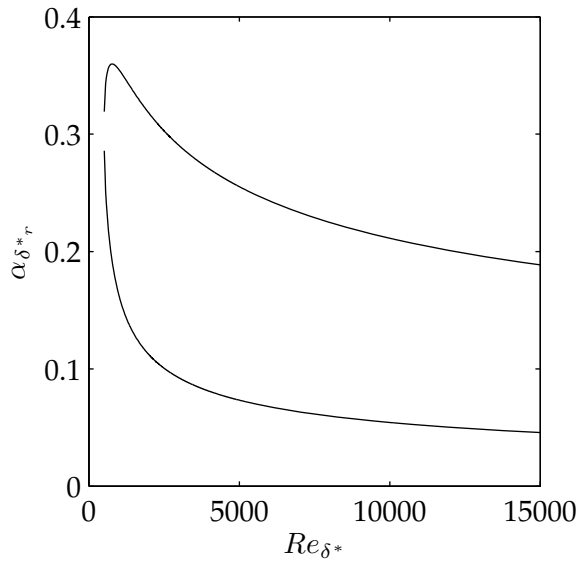

Figure 5.13: Curve of neutral stability based on displacement thickness (wavenumber) for Blasius flow.

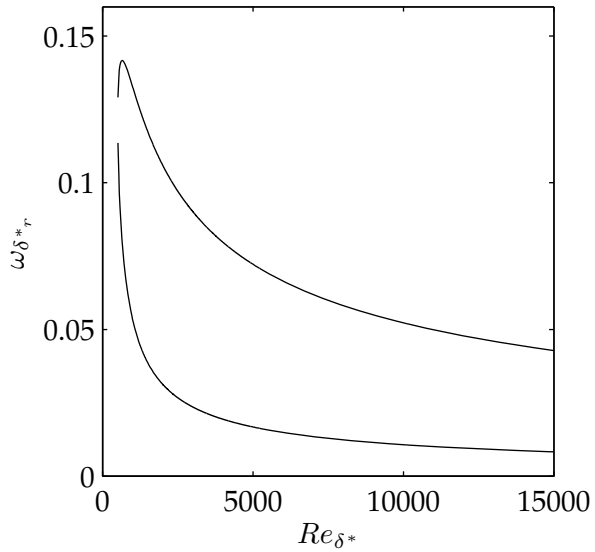

Figure 5.14: Curve of neutral stability based on displacement thickness (frequency) for Blasius flow.

uniform wall suction is almost 90 times that of the base Blasius flow (Table 5.4). In addition, the flow with uniform wall suction becomes susceptible to larger wavelength, lower frequency disturbances that potentially could be easily prevented from entering the layer, given the large dimensions of the sources required to produce them.

5.2.2 Conclusions of the Linear Stability Analyses

Based on the results of the stability analysis for the boundary layer with the asymptotic suction profile it was suggested that the DBD-based LFC system incorporating the orthogonal actuators should attempt to augment a boundary layer so as to mimic the behaviour of the asymptotic suction profile. Of the four idealised, augmented boundary layer flows for which Linear Stability Analyses were conducted during this research, the boundary layer with an asymptotic suction profile achieved the best improvement to the limit of stability. The stability of a boundary layer with an asymptotic suction profile is significantly greater than that of Blasius flow, with the critical Reynolds number associated with it being approximately two orders of magnitude greater than that for Blasius flow. Also, such a profile is

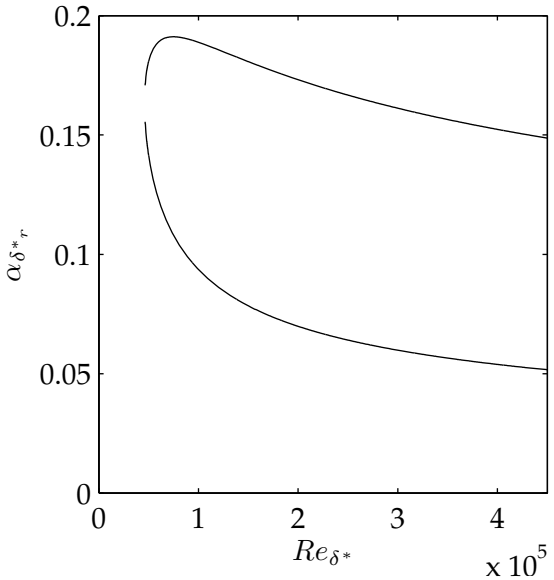

Figure 5.15: Curve of neutral stability based on displacement thickness (wavenumber) for uniform suction.

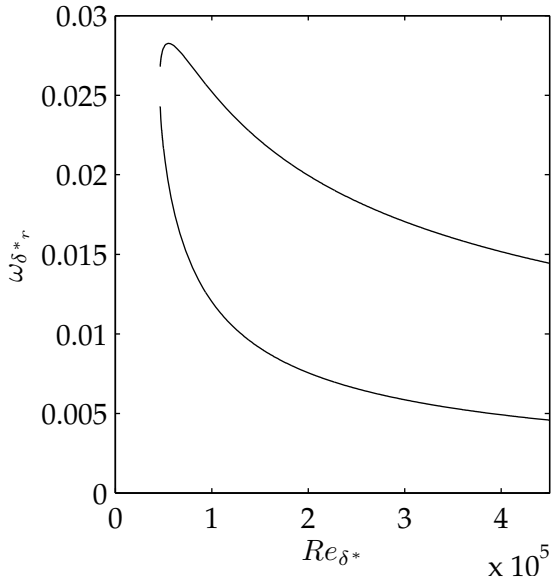

Figure 5.16: Curve of neutral stability based on displacement thickness (frequency) for uniform suction.

Table 5.4: Comparison of critical Reynolds number between Blasius flow and a boundary layer with uniform suction.

Actuator Power $[W]$	$Re_{\delta^*_{crit}}$	$\frac{Re_{crit_{Control}}}{Re_{crit_{Blasius}}}$
Blasius	520	1
Uniform Suction	47000	90

susceptible to longer wavelength, lower frequency disturbances, which in the real-world are potentially easier to detect and control in the boundary layer because of the large dimensions of the sources required to generate them.

Consequently, during the experimental development of a DBD-based LFC system as part of this research, it was decided that the DBD-based LFC would be tuned so as to attempt to augment the boundary layer in a fashion mimicking uniform wall suction. This meant that the system would attempt to cause the velocity profile of the flow to attain the exponential profile defined by Equation 5.7, as well as a constant shape factor of 2 throughout the controlled region.

Tuning of the actuator was to be made such that the measured velocity profiles and shape factor values attained the correct values, using the knowledge of tuning techniques derived from the literature review and orthogonal

actuator parametric study. Using this tuning, it was anticipated that a DBD-based system would be able to emulate a system involving suction in a much simpler fashion, without the need to remove fluid from the boundary layer with complicated and high power pumping devices.

5.3 Summary & conclusions

An objective of this research was to identify novel Dielectric Barrier Discharge actuator configurations with the potential to provide favourable benefits to the stability of a Blasius boundary layer. As discussed in this chapter, orthogonal actuators were identified as satisfying this objective.

Orthogonal actuators are defined as those having the exposed electrode placed at a right angle to the encapsulated electrode. Prior to this research, no work into the development of orthogonal actuators had been undertaken. Through an experimental, parametric investigation it was found that orthogonal actuators produce less 'aggressive' jetting profiles, that are fuller, with less fluid shearing close to the wall. In addition the magnitude and position of the maximum jetting velocity of the actuator can be controlled through variation of the height to which the exposed electrode sits proud above the surface of the device. For these reasons, orthogonal actuators were identified and recommended for implementation into a LFC system when trying to improve the stability of a flat plate boundary layer in a ZPG.

In addition to recognising the gross differences between orthogonal and conventional (parallel) DBD actuators, the parametric study highlighted some interesting jetting characteristics of orthogonal devices. In particular it was found that no discernible jetting effect can be developed with a value of y_{exp} greater than $0mm$, and that the most forceful orthogonal actuator was the one that had a y_{exp} value of $-0.5mm$.

As a final note on the results of the parametric investigation, it was found that both the force and maximum jetting velocity of an equivalent, conventional parallel actuator were significantly greater than the most forceful orthogonal device. However, these two performance attributes may be detrimental to the performance of the device in a LFC system due to the thinness of the induced jet, and the high fluid shearing developed near the wall as a result of the jet. Hence, the orthogonal actuators studied in this chapter were still recommended for the subsequently developed DBD-based LFC system.

To assist in the development of a DBD-based LFC system using orthogonal actuators, Linear Stability Analyses were performed on a number of idealised and assumed velocity profiles. The profiles used were derived from published

experimental results for DBD-augmented boundary layer flows as well as boundary layer theory. Although the assumed velocity profiles were not perfect fits to the data, the assumptions captured the gross characteristics of the augmentation, and allowed for trends to be identified as to how a DBD actuator may augment a boundary layer flow in a stable fashion. Of the three DBD-augmented flows studied, the one associated with a lower power actuator produced the most favourable results. However, stability improvements associated with the assumed velocity profiles were found to be smaller than those that can be attained through the use of uniform wall suction. For this reason it was concluded that the DBD-based LFC system that was to be developed during this research was to aim to emulate the performance of a suction-based LFC system.

In summary, the discussion presented in this chapter led to two significant outcomes and specifications for the DBD-based LFC system that was developed as a part of this research. The results suggested that orthogonal actuators were to be used and tuned in an attempt to emulate the performance of uniform suction. The results of the development of such an LFC system are presented in the proceeding chapters.

6 Experimental Apparatus

The performance of the novel, orthogonal actuators as LFC devices has been assessed experimentally using the KC Wind Tunnel facility at The University of Adelaide, Australia. All experiments were conducted on a rig specially developed for this project, the so-called *Flat Plate Rig* (FPR). The FPR was used in conjunction with numerous measurement devices to assess the effectiveness of the orthogonal actuator in augmenting a laminar boundary layer and improving its hydrodynamic stability.

Throughout the research project a number of flow conditions and actuator configurations were tested. However, many parameters pertaining to the rig, as well as experimental procedures were consistent for all experimental investigations. This chapter discusses the similar conditions under which all experimental investigations were conducted, as well as detailing the features of the instrumentation used.

6.1 Wind tunnel

The experimental investigations undertaken in this work were conducted in the KC Wind Tunnel at the University of Adelaide (Figure 6.1). The KC Wind Tunnel is a closed-return-type tunnel with a removable test section. Into this test section was placed the FPR developed to undertake the experiments associated with this project.

The working cross-section of the KC Wind Tunnel is $0.5m \times 0.5m$ with a test section length of $2.5m$. The FPR (Figure 6.2) was designed to optimise the use of this test section, achieving this by utilising the full length available and mounting directly to the outlet of the contraction, (which has ratio of $6:1$).

The KC Wind Tunnel can be operated at speeds of up to $30^{m}/_{s}$ with a low level of turbulence. During the experimental investigations the turbulence intensity of the wind tunnel was measured using a single-wire hot wire probe (technical details of its operation are subsequently discussed in Section

Figure 6.1: The KC Wind Tunnel at the University of Adelaide.

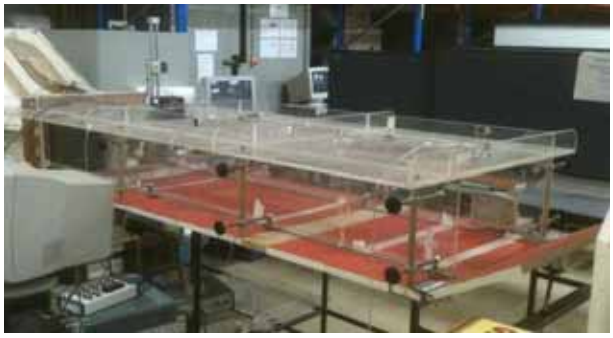

Figure 6.2: Flat Plate Rig (FPR) as installed in the KC Wind Tunnel.

4 of this chapter). The turbulence intensity, as measured by the probe, was found to range between 0.8% and 0.4% of the freestream velocity for flow speeds between $2^m/_s$ and $14^m/_s$ (Figure 6.3a). Assuming isotropic turbulence conditions within the tunnel, then the turbulence intensity in the x-direction, (chordwise and parallel to the plate, defined more formally in Figure 6.8) reduces to an approximate value between 0.6% and 0.3% (Figure 6.3b).

Although the freestream turbulence level of the KC wind tunnel is quite low at less than 0.6% for the freestream velocities of interest, it is around 10 times higher than what has been traditionally used for LFC investigations (Schubauer and Skramstad 1950, Wang and Gaster 2005, Watmuff 2006, Grundmann and Tropea 2007b, Grundmann and Tropea 2007a, Grundmann and Tropea 2009). However, unlike previous studies where the focus has been to acquire actual transition locations and disturbance amplification rates, the intent of the research for which the KC Wind Tunnel was being

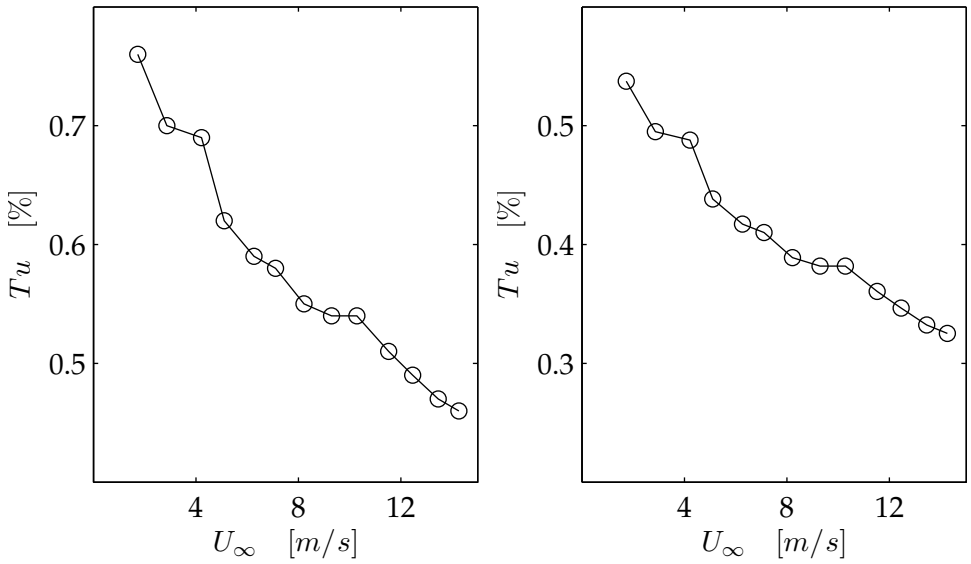

(a) Resultant level of turbulence intensity. (b) Isotropic x-direction turbulence intensity.

Figure 6.3: Turbulence intensity measurements for the KC Wind Tunnel.

used was different. Instead of attempting to ascertain actual disturbance growth and transition location brought about by the inception of freestream turbulence (through the process of *receptivity*; see Section 2.2), the research was focused upon the mechanisms through which the mean velocity profiles of the boundary layer could be augmented in such a way so as to delay the development of instabilities in the flow. The only requirement for this was that the turbulence level be less than 1% so as to prevent bypass transition from occurring freely and rapidly in the layer (Brandt et al. 2004), thus preventing any study of a laminar boundary layer. As mentioned, this was not the case, and laminar boundary layers were developed readily in the KC Wind Tunnel throughout this work (see Section 6.5). Consequently, the objectives of the research were able to be achieved in KC Wind Tunnel, as any improvement (or detriment) to the stability of the studied boundary layers would be discernible via comparison of instability development for all of the studied augmented boundary layers.

The working cross-section of the KC Wind Tunnel is $0.5m \times 0.5m$ with a test section length of $2.5m$. The FPR (Figure 6.2) was designed to optimise the use of this test section, achieving this by utilising the full length available and mounting directly to the outlet of the contraction, (which has ratio of $6:1$).

Although the freestream turbulence level of the KC wind tunnel is quite low at less than 0.6% for the freestream velocities of interest, it is around 10 times higher than what has been traditionally used for LFC investigations (Schubauer and Skramstad 1950, Wang and Gaster 2005, Watmuff 2006, Grundmann and Tropea 2007b, Grundmann and Tropea 2007a, Grundmann and Tropea 2009). However, unlike previous studies where the focus has been to acquire actual transition locations and disturbance amplification rates, the intent of the research for which the KC Wind Tunnel was being used was different. Instead of attempting to ascertain actual disturbance growth and transition location brought about by the inception of freestream turbulence (through the process of *receptivity*; see Section 2.2), the research was investigating mechanisms through which the mean velocity profiles of the boundary layer could be augmented in such a way so as to delay the development of instabilities in the flow. The only requirement for this was that the turbulence level be less than 1% so as to prevent bypass transition from occurring freely and rapidly in the layer (Brandt et al. 2004), thus preventing any study of a laminar boundary layer. As mentioned, this was not the case, and laminar boundary layers were developed readily in the KC Wind Tunnel throughout this work (se Section 6.5). Consequently, the objectives of the research were able to be achieved in the comparatively *noisy* KC Wind Tunnel, as any improvement (or detriment) to the stability of the studied boundary layers would be discernible via comparison of instability development for all of the studied augmented boundary layers.

6.2 Flat Plate Rig (FPR)

To achieve the desired boundary layer characteristics in the investigations, special consideration was required in the design of the flat plate. These included a definable origin for the boundary layer, control of the pressure gradient over the plate, the capability for DBD devices to be inserted into the rig at desired locations, as well as provisions for measurement instruments to be inserted. The result was the development of the Flat Plate Rig (FPR), which was used for all experimental boundary layer investigations pertaining to this research (Figure 6.2).

A flat plate boundary layer with an identifiable location of the origin cannot be achieved simply by placing a flat plate into a flow. The finite thickness and blunt leading edge of the flat plate lead to bluff body separation effects that distort the origin of the formed boundary layer (Narasimha and Prasad 1994). To address this issue, two techniques are widely employed. The first is the use of a knife-edged leading edge as employed on the rigs used in

a number of LFC investigations (Thomas 1983, Grundmann and Tropea 2007a, Grundmann and Tropea 2007b, Grundmann and Tropea 2009). This ensures that the flat plate is infinitesimally thin at the leading edge, minimising any flow separation. However, such a leading edge cannot guarantee the absence of separation and is intolerant of small angles of the impinging flow. It also challenging to manufacture an infinitesimally thin leading edge. An alternative is the use of a super-elliptical leading edge as discussed by Narasimha and Prasad (1994) and as used throughout this research project. Narasimha and Prasad (1994) suggest that a super-ellipse with an index of 3 (Equation 6.1) produces a leading edge of minimal development length for a given thickness, without undesirable flow separation at the leading edge. In this equation (Equation 6.1) x_{LE} & y_{LE} represent the Cartesian coordinates of the leading edge, b the minor radius of the ellipse, and a the major radius of the ellipse. Not only does such a leading edge satisfy the no-separation criterion with some tolerance of minor flow misalignment, but the symmetry of the leading edge allows for a robust method for locating the stagnation point, through measurement of the pressure differential eitherside of the centreline. Since the leading edge is curved, some discrepancy between the *virtual* origin of the Blasius Layer and the origin of the real layer will exist, but this was deemed to have only a minor impact on the quality of the results.

$$\left(\frac{(a-x_{LE})}{a}\right)^3+\left(\frac{y_{LE}}{b}\right)^3=\left(\frac{(6b-x_{LE})}{6b}\right)^3+\left(\frac{y_{LE}}{b}\right)^3=1 \qquad (6.1)$$

The leading edge (Figure 6.4) was designed and manufactured from *6061* aluminium with a nominal major radius of $114mm$. Two $0.5mm$ diameter pressure tappings drilled on adjacent sides of the centreline, $80mm$ downstream of the leading edge, were incorporated into design for location of the stagnation point. The outer diameter of these tappings was increased to $1/8''$ via the use of brass tubing, before being connected to an MKS 398 differential Baratron 0 to $1Torr$ pressure transducer via $1/8''$ internal diameter silicone tubing. By equating the static pressure at both tapping locations, the location of the stagnation point at the tip of the leading edge could be assured. Positioning of the stagnation point on the tip of the leading edge could subsequently be achieved by varying the angle of the trailing edge circulation flap of the FPR.

The FPR (Figure 6.5) was designed with a nominal cross-section of $500mm \times 300mm$, $2000mm$ in length and manufactured from medium density fibreboard. The rig was designed with removable panels that allow the addition of plasma actuators at desired locations. To control the location of the stagnation point and eliminate any developed circulation over the FPR a

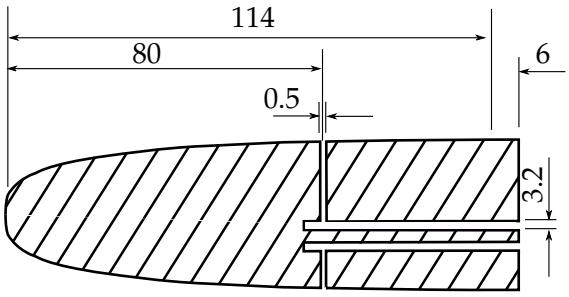

Figure 6.4: Dimensions (in *mm*) of leading edge of experimental flat plate.

downstream circulation flap was incorporated into the design. The length of the flap was selected to be 12.5% of the chord length of the flat plate (250*mm*) consistent with the dimensions used in a similar experiment (Thomas 1983). Through the use of a screw thread, the flap could be raised and lowered as appropriate to balance the flow and pressure eitherside of the super-elliptical leading edge.

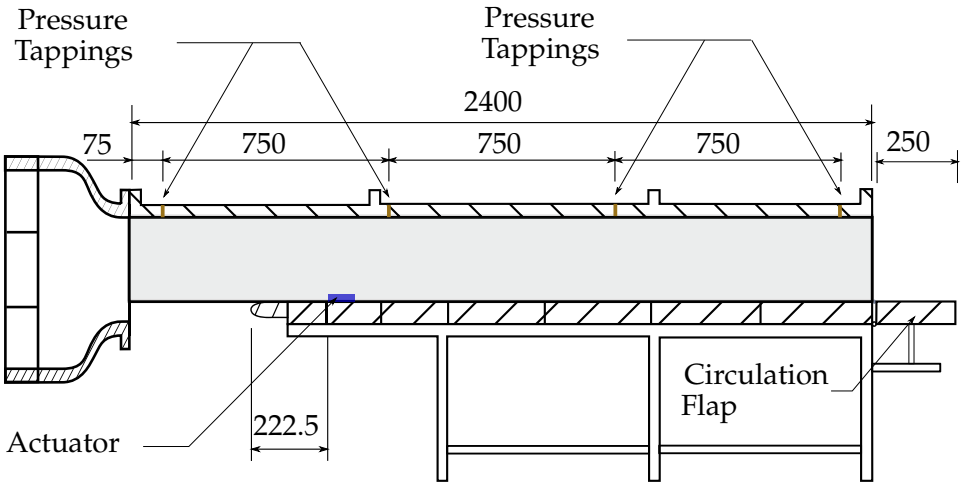

Figure 6.5: Side view of the FPR showing significant dimensions (in *mm*) of rig.

The flat plate section of the rig was encapsulated in an acrylic enclosure. The walls of this enclosure were fixed at the leading edge only, allowing the sides to move laterally downstream of the contraction of the wind tunnel. Attached to these walls were threaded rods located at three equidistant positions. Through appropriate winding of the rods, the cross-sectional area

and hence static pressure along the length of the rig could be adjusted, allowing for fine control of the pressure gradient over the rig (Figure 6.6). Four 0.5mm diameter pressure tappings spaced 750mm apart were positioned in the roof of the enclosure (Figure 6.5) and used to measure the pressure gradient along the FPR. Throughout the investigations the gradient along the rig was measured to be approximately $0^{Pa}/_{m}$ as required, ranging between $-0.50^{Pa}/_{m}$ and $0.02^{Pa}/_{m}$ (Figure 6.7).

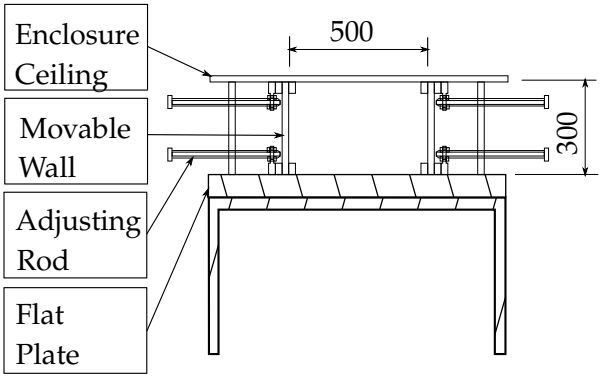

Figure 6.6: End view of FPR showing method of pressure gradient adjustment (dimensions in mm).

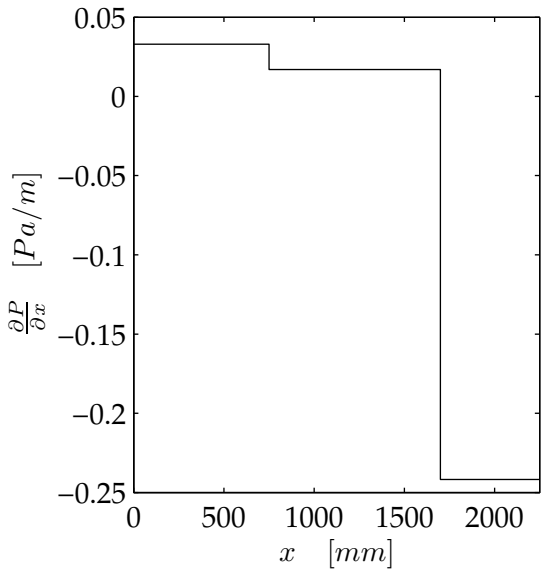

Figure 6.7: Pressure gradient over length of FPR.

The FPR was designed to allow experimental investigations to be made in the region of the boundary layer containing the location of the critical Reynolds number of the flow (approximately 110000 based on chord length). For a nominal freestream velocity of $5^{m}/_{s}$), this meant that the boundary layer investigations were made between chordwise positions of $x = 243mm$ to $x = 323mm$, (as defined in Figure 6.8).

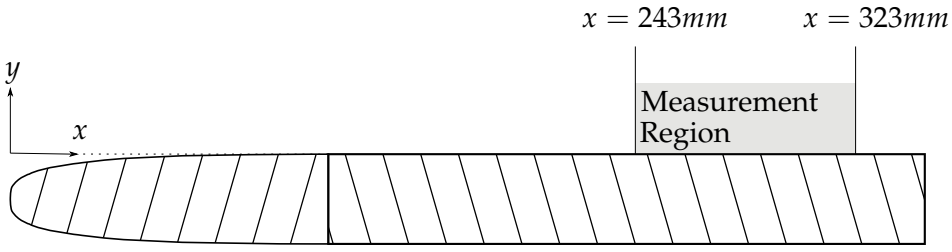

Figure 6.8: Formal definition of the origin pertaining to the experimental investigations and region (shaded grey) over which measurements were made (dimensions in mm). The origin is defined as the point parallel to the leading edge and surface of the flat plate.

6.3 Plasma actuators

The purpose of the experimental investigations involving boundary layer flow was to assess the response of the fluid to the presence of orthogonal actuators. To minimise the variations in parameters for the investigations, the geometry and materials of the devices were fixed. These parameters were derived from experience obtained during the preliminary experiments in quiescent air, which were discussed in Chapter 5, with slight modifications to dimensions so as to form plasma over the entire spanwise length of the FPR test section and hence restrict the plasma augmentation to a two-dimensional boundary layer. Although according to Kriegseis et al. (2009) a ratio of electrode width to length of 0.25 produces favourable benefits to boundary layer stability, the fact that this ratio was applicable to conventional (parallel) actuators meant that this ratio was not applied to the actuators used in this research. Instead, precedence was given to establishing two-dimensional flow conditions and uniformity of plasma production over the entire span of the test section. In addition, the height to which the exposed electrodes sat proud above the dielectric surface (y_{exp}) was selected to be $0mm$. Although

the most voluminous actuator, which produced the greatest force for a given set of parameters, was found to correspond with a y_{exp} value of $-0.5mm$ (as discussed in Chapter 5), $0mm$ was selected for its ease of manufacture. In addition the fundamental nature of the work allowed a somewhat arbitrary selection of the y_{exp} value. Consequently the geometric parameters of the actuators utilised for all investigations were as follows:

- electrode material: tinned Copper,
- electrode thickness: $t_{elec} = 0.1mm$,
- electrode chordwise length: $L = 12.5mm$,
- exposed electrode spanwise length: $b_{exposed} = 500mm$,
- encapsulated electrode spanwise length: $b_{encapsulated} = 700mm$,
- height to which exposed electrode sat proud above dielectric: $y_{exp} = 0mm$,
- dielectric material: acrylic,
- dielectric thickness: $3mm$ (in both the horizontal, d_h, and vertical, d_v, directions).

Energy for the actuators was supplied by an ElectroFluidSystems Mini-Puls 2 proprietary plasma generator system. This device is capable of producing a high voltage sinusoidal output with frequencies between $5kHz$ and $30kHz$. The actuators studied in this investigation were found to be highly sensitive to the applied frequency. Very poor plasma formation was observed for applied frequencies above $13kHz$ and below $10kHz$, with qualitatively best plasma formation occurring for an applied frequency of $12kHz$, as observed during preliminary tests. This observation is consistent with the suggestion of Orlov (2006) of the existence of an optimal applied frequency value for an actuator (see Section 3.3). For the actuators described here, the optimal applied frequency value existed within a (relatively) narrow band of $3kHz$. Since it was not the objective of this research to fully optimise the applied frequency for the actuators used, but rather to tune the actuators so as to improve the stability characteristics of a flat plate boundary layer flow, the applied frequency was set at a constant value for all experiments. Hence, for all investigations, a pure sinusoidal input with an applied frequency, f_{app}, of $12kHz$ was used. Not only did this result in useful plasma formation, which was observed to influence the flow, but the electrical parameters were found

to be similar to those used in other works (Enloe et al. 2003, Enloe et al. 2004a, Enloe et al. 2004b, Van Dyken et al. 2004, Gibson et al. 2009a). With this arrangement the voltage across the actuator electrodes, V_{app} was varied between $18kV_{pp}$ and $24.2kV_{pp}$.

The actuators were manufactured from two machined pieces of acrylic. The dimensions of the devices (Figure 6.9) were such that they could be easily integrated into the FPR through replacement of one of the removable panels in the rig with the actuator. Beginning with a block of acrylic with dimensions of $800mm \times 125mm \times 25mm$, a $60mm$ wide slot was machined along the spanwise length of the actuator so as to leave a $3mm$ material thickness along the leading and top surfaces. On the leading surface of this piece of acrylic was placed the exposed electrode. Into the machined slot a second piece of acrylic of size $800mm \times 60mm \times 10mm$, was placed. This second piece of acrylic had attached to its top surface the second electrode, which when positioned inside the slot became encapsulated. A brass bolt (M8) threaded through the second piece provided a connection to the encapsulated electrode.

6.4 Experimental anemometry

Measuring the dynamic conditions within a boundary layer is challenging, particularly since dramatic changes to the mean flow occur within very small spatial regions. Because of these spatial constraints, hot wire anemometry is often employed. However, attempting to utilise hot wire anemometry in and

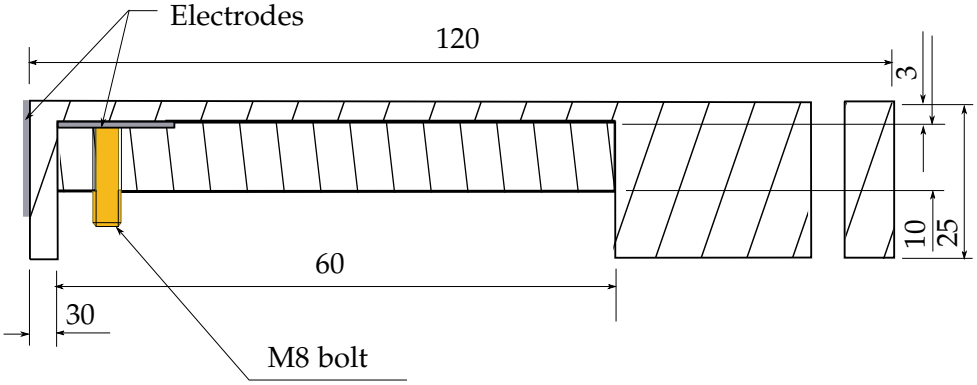

Figure 6.9: Schematic of orthogonal actuators used throughout research. Electrodes are shaded in purple, electrical connection bolt is in gold (dimensions in *mm*).

around the region of a plasma actuator presents many problems.

First and foremost, hot-wire anemometry faces the challenge of arcing occurring between the probe and the plasma. As discussed by Johnson and Scott (2001) & Wilkinson (2003), arcing quickly destroys probes placed too close to the plasma. Consequently, Johnson and Scott (2001) could not investigate any region closer than 3.5*mm* (lateral separation) from the plasma, and at least 1.0*mm* above the dielectric. In addition, for reliability Wilkinson (2003) also used pressure tube anemometry to substantiate their results.

Electrical interactions between the charged plasma and the hot-wire probe can also introduce measurement uncertainties. As discussed by Wilkinson (2003) significant measurement errors occur when the probes are near the direct vicinity of the plasma, with glow discharge developing on the probes and interfering with the electrical signal of the probe. Electrical isolation of the probe can help minimise this, but there is no guarantee (Wilkinson 2003). A solution is to use a specially developed constant-current anemometer system featuring an electrical control unit that places a small differential voltage across the body of the probe, which decouples the electrical-grounds of the wire and the probe (Huang 2005). However, these systems are not widely available (Huang 2005 developed their own), and are a complex derivative of current hot-wire technology. Moreover, the additional circuitry does not guarantee probe accuracy and reliability, as evident by Huang (2005) who also used pressure tube anemometry to galvanise their results.

Whilst work has been published on DBD-based LFC, which includes hot-wire anemometry measurements, there have been substantial limitations on the region of investigation. Highlighting this is the work of Grundmann and Tropea (2007b). The hot-wire anemometry results published by the authors were obtained at least 90*mm* downstream of the DBD-actuators. Whilst this eliminated the risk of damage to the probes, it also meant a large *shadow region* existed in the measurement data.

The review of the literature suggests that hot-wire techniques are not the most suitable for investigating plasma-augmented flows where high frequency measurements are not required. As changes to the mean behaviour of flows was the focus of the undertaken research, small-scale total pressure tubes were instead selected for investigating the studied boundary layers. Whilst it is widely known that pressure tubes suffer from proximity effects close to surfaces, this is not a unique trait, but one that is also shared with hot-wire probes (Hultgren and Ashpis 2003). Moreover, there exists a long history of research into pressure tube calibration focused on minimising this effect (and others) as discussed in Section 6.4.2.1. Hence, pressure tubes were a very suitable instrument for measuring the velocity profiles pertaining to

this research. In addition, the use of pressure tubes allowed measurements to be obtained close to the plasma actuator, well inside the distances described in the literature (e.g. Grundmann and Tropea 2007b). As described in Section 6.6.2), pressure tubes allowed velocity data to be obtained 20mm downstream of the actuator (beginning at the trailing edge of the encapsulated electrode); data that (as described in the literature) would otherwise have been difficult to reliably obtain using a hot-wire probe.

In addition to the pressure tubes, hot wire anemometry still found use in the experimental work. The high frequency response required to measure turbulence intensity meant that hot-wire probes were used to characterise the turbulence intensity of the KC Wind Tunnel.

To ensure adequate precision and accuracy when using the anemometry equipment, specialised considerations had to be made with regard to the way data was measured and processed. Although both the hot wire and pressure tube anemometry systems converted fluid velocity data to voltage measurements, each system required differing and specialised manipulation of measurement data.

6.4.1 Hot-wire anemometry

Constant Temperature hot wire anemometry (CTA) was utilised during this project to obtain turbulence information relating to mean flow of the KC Wind Tunnel. CTA technology is widely understood and available, featuring excellent spatial and temporal resolution (Perry 1982, Bruun 1995). For these reasons, CTA was ideal for assessing the turbulence of the freestream.

The CTA system used was an TSI Inc. IFA 100 Constant Temperature Anemometry system, which, like all CTA systems, makes use of heat transfer principles from a small, heated hot wire probe. Placement of the probe into a fluid flow brings about a transfer of heat from the probe to the fluid, the magnitude of which is dependent upon the velocity of the flow crossing it. By using an electronic feedback circuit, the CTA system maintains the temperature of the probe by modulating the current through the sensor. The output of the circuit is calibrated against known flow speeds. Hence by measuring the change in output voltage of the CTA circuit it is possible to monitor and deduce the speed of the fluid flow at a particular instance.

As is the case for all CTA systems, the feedback electronics for the TSI Inc. IFA 100 is based on a Wheatstone bridge, of which the hot wire probe forms a resistive element, R_w (Figure 6.11). The variable resistive element, R_b is selected with consideration to the intended operating resistance of the probe, R_{Op}. During operation, the feedback circuit balances the bridge

Figure 6.10: TSI Inc. IFA 100 CTA system as used throughout this project.

voltages, E_a and E_b by varying the feedback current, I_0. By measuring the voltage difference brought about by the feedback current, E_0, it is possible to obtain a measurement for the instantaneous velocity of the fluid crossing the probe.

To improve the performance of the CTA circuit, a gain amplifier (with a gain value of K) is used to enhance the system sensitivity in conjunction with a current-boosting amplifier (I). The use of the amplifier introduces a small offset voltage (E_{qi}) that contributes to the output of the circuit (Equation 6.2) and needs to be considered in the setup of the bridge. In a proprietary circuit such as the TSI Inc. IFA *100* the effects of the offset voltage are mitigated by following the recommended setup procedures for the system (*Operating Manual for TSI IFA-100 Constant-Temperature Anemometer* 2000).

$$E_0 = K\left(E_i + E_{qi}\right) \tag{6.2}$$

The actual voltage output of the CTA bridge is related to the values of the resistive elements and the feedback current (Equation 6.3). Whilst two of these resistive elements have a fixed resistance value, the nominal resistance of the probe (R_w) and the balance resistance (R_b) vary with the selected probe and its intended operating temperature. During this research, the probe resistance was nominated by selecting an appropriate overheat ratio, OHR (Equation 6.4), for the sensors. The probes used in this work were commercially sourced TSI Inc. $1210 - T1.5$ units, manufactured of platinum-coated tungsten, with a diameter of $3.8\mu m$. As recommended by TSI Inc. (*Operating Manual for TSI IFA-100 Constant-Temperature Anemometer* 2000), an OHR value of 1.8 was used for these probes, and the cold resistance (R_{cold}) of

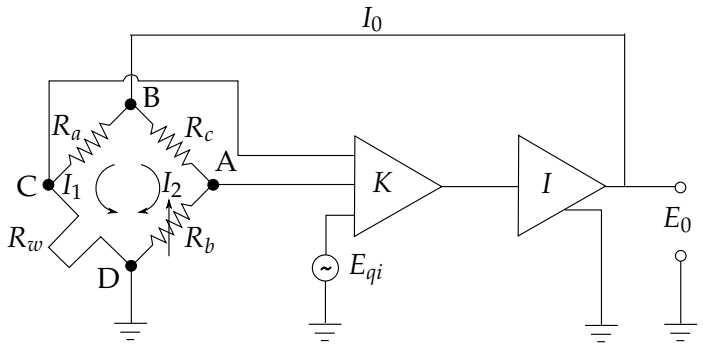

Figure 6.11: Electronic schematic of CTA bridge. The hot wire probe lies between points C & D.

the sensors was obtained by measuring their resistances at room temperature.

$$E_i = \frac{-I_0(R_w R_c - R_a R_b)}{R_w + R_a + R_b + R_c} \tag{6.3}$$

$$OHR = \frac{R_{Op}}{R_{Cold}} = \frac{R_w}{R_{Cold}} \tag{6.4}$$

Optimisation of the frequency response of the CTA circuit is dependent upon the characteristics of individual hot wire probes. According to Freymuth (1977) a convenient way to optimise the circuit for a given probe is to measure the response of the CTA circuit to a square wave input superimposed upon the offset voltage (E_{qi}). Freymuth (1977) suggests that optimum temporal behaviour is achieved when the voltage response (V) of the circuit to the square wave demonstrates an undershoot of approximately 15% of the amplitude of the signal, h (Figure 6.12). To achieve this suitable adjustments to the offset voltage and balance inductance of the variable resistive element (R_b) are made until the response of the bridge images that of the ideal response.

Using the recommended set up procedures of the TSI Inc. IFA 100, optimum probe frequency response was easily realised during the experimental investigations. The process involved setting the bridge offset voltage (E_{qi}) to the recommended value for the probe (as according to *Operating Manual for TSI IFA-100 Constant-Temperature Anemometer* 2000), before superimposing the square wave signal. Measuring the output using a Tektronix $TDS1000B$ Oscilloscope, the balance inductance was slowly varied until the output of the bridge suitably represented that of the ideal response.

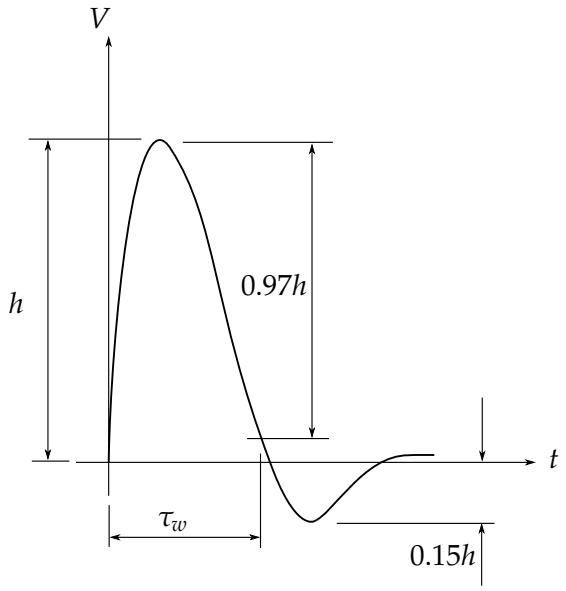

Figure 6.12: Ideal frequency response of the CTA hot wire probe.

6.4.1.1 Velocity calibration of probes

Velocity calibration of the hot wire probes was performed using an *in-situ* technique. A Pitot-static probe was placed in the freestream of the FPR test section and used to first measure the mean velocity of the flow. Once the mean velocity measurements were obtained, the hot-wire probe was placed in the same location, and the CTA circuit output voltage measured and recorded. Repeating this process for a number of velocities resulted in the construction of a calibration *look-up* table. Cubic spline interpolation between the points of the table subsequently provided the means for converting experimental flow measurements into fluid velocities.

6.4.2 Pressure tube anemometry

Pressure tubes were used throughout the experimental work to measure and record total pressure values within the studied boundary layers. The use of these tubes provided a robust velocimetry method that gave adequate spatial and temporal resolution, whilst being cost effective. The operational principle of the tubes is fundamentally simple, making use of Bernoulli's equation as applied to the flow along a streamline (Equation 6.5). A streamline enters the tube and is stagnated, upon which the static pressure caused by the stagnation is resolved by a pressure transducer. By subtracting the ambient

static pressure of the flow from the pressure measurement, and noting that insignificant changes in height occur along the stagnating streamline, then a measure of the dynamic pressure is obtained. From the dynamic pressure measurement, a straightforward calculation yields the local value of the fluid velocity (Equation 6.6).

$$P_{Tot} = P + 1/2\rho u^2 + gz = constant \tag{6.5}$$

$$u = \sqrt{\frac{2\left(P_{Tot} - P\right)}{\rho}} \tag{6.6}$$

The tubes utilised in this experimental work were manufactured to present as small as possible cross-sectional area when positioned in the flow. Given the small dimensions of the boundary layer thicknesses that were to be investigated (of the order of $5mm$), utilising small tubes was paramount to ensure suitable spatial resolution. The tubes were consequently manufactured from $25G \times 1''$ medical-grade stainless steel tubing, the type employed in hypodermic needles. The outside diameter (OD) of the tube was $500\mu m$, with a corresponding internal value of $250\mu m$. To provide suitable access to the boundary layer, and connectivity to the pressure sensing device, the small diameter tubes were attached to a length of $1/8''$ OD brass tubing, which was itself attached to the pressure sensor by means of $1/8''$ internal diameter silicone tubing. To eliminate buffeting of the brass tubing by the flow, a second length of brass tubing was soldered to the downstream side of the pressure tube to provide additional support (Figure 6.13).

An MKS 398 differential Baratron pressure transducer was used to measure the pressure obtained from the total pressure tubes. The baratron, which featured a frequency response of $40Hz$, was calibrated with a sensitivity of $10^V/_{Torr}$ over a range spanning from $0V$ to $10V$. The pressure tubes were connected to the total pressure side of the baratron, and the static pressure side was connected to the pressure tapping immediately above the investigation region.

6.4.2.1 Pressure tube calibration

Robust as they are, pressure tubes do suffer from a number of calibration issues. These issues arise as a result of two fluid phenomena. The first is the deflection of the fluid streamlines around the tube due to its presence. The second arises from viscosity, which creates errors in pressure tubes of small diameters. Since the work carried out in this research utilised tubes of small diameters, both of these phenomena needed to be taken into account.

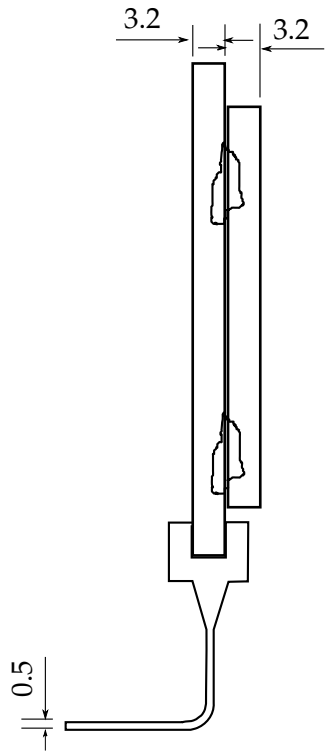

Figure 6.13: Schematic design of total pressure tubes employed in this work (dimensions in *mm*).

The presence of the pressure tube within a sheared flow brings about a displacement error. The displacement error arises due to the flow obstruction that the tube creates, which causes the fluid streamlines to deflect around the tube (Figure 6.14). The result is that the fluid is displaced towards the regions of greater shear, meaning that the pressure measurement recorded at a particular location is incorrect. A convenient way to consider the phenomenon is to think of the measurement suffering from an apparent shift in probe position. This form of correction, known as the *displacement correction* (McKeon et al. 2003), has been discussed by many authors and is accounted for by changing the relative position of the probe measurement by a value dependent on the outer diameter of the pressure tube, d (Equation 6.7). The apparent shift in probe position, ϵ, typically attains a value between $0.08 < \epsilon < 0.16$ (MacMillan 1954, MacMillan 1957, Patel 1965, Tavoularis and Szymczak 1989, McKeon et al. 2003).

$$\frac{\Delta y}{d} = \epsilon \tag{6.7}$$

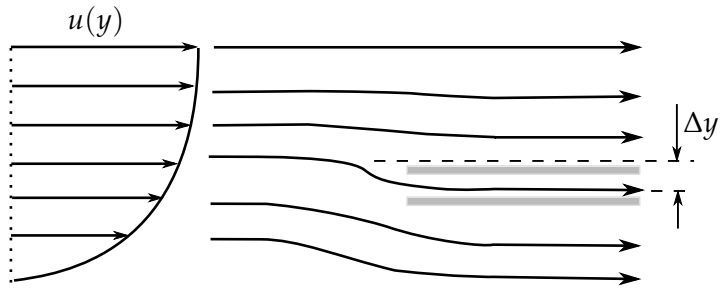

Figure 6.14: Error due to displacement. The walls of the tube are shown in grey.

For the purpose of this investigation, the displacement correction was made using the recommendations of MacMillan (1957) and the so-called *MacMillan correction*. According to McKeon et al. (2003), the Macmillan correction is the most widely used and benefits from suitable accuracy and straightforward implementation. For this theory, the apparent shift in probe position, ϵ, is assumed to be a constant value of 0.15.

The flows studied as part of the experimental work also suffered from an additional mechanism that displaces the streamlines. When a probe is placed near to a wall, the pressure tube resembles a forward facing step. The result is that the streamlines of the flow are displaced away from the wall and over the tube by a distance of δ_w (Fig 6.15) and an error in the measured velocity is obtained. The error due to the wall was discussed by MacMillan (1957) and the author suggested when the ratio $y/d < 2$, a correction for the wall should be used (Equation 6.8) in conjunction with that already given by the displacement correction (Equation 6.7).

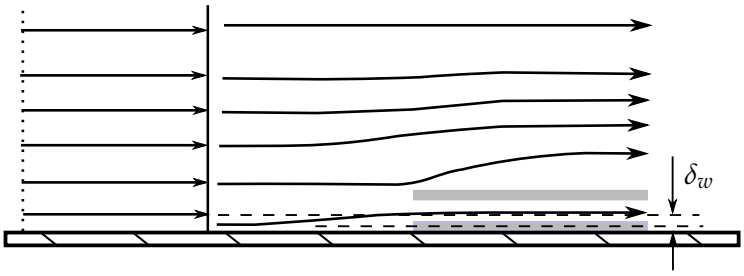

Figure 6.15: Error due to the presence of the wall. The walls of the tube are shown in grey.

$$\frac{\Delta u}{u_{measured}} = 0.015exp\left[-3.5\left(\frac{y}{d} - 0.5\right)\right] \tag{6.8}$$

The final correction applied to the measured data was that associated with viscous effects within the tube. According to Zagarola and Smits (1998) fluid viscosity has an effect on the measured pressure coefficient for Reynolds numbers based on the pressure tube diameter, Re_d, between 30 and 1000 (as described by Equation 6.9). Since Re_d was less than 200 for the investigations undertaken, this correction was implemented, and was done so through the expansion of Equation 6.9 to find the polynomial relationship between the measured velocity value, $u_{measured}$, and the corrected value, $u_{corrected}$ (Equation 6.10). For each measurement value, Equation 6.10 was solved using the polynomial root-finding algorithms of Matlab^{TM}.

$$C_P = 1 + \frac{10}{Re_d^{1.5}} \tag{6.9}$$

$$\left(\frac{d}{\nu}\right)^{1.5} u_{corrected}^{3.5} + 10u_{corrected}^2 - u_{measured}^2 \left(\frac{d}{\nu}\right)^{1.5} u_{corrected}^{1.5} = 0 \tag{6.10}$$

For the cases without plasma, some measurements near the wall had a value of Re_d less than 30, with the smallest value being 10. However, given the lack of information pertaining to viscous corrections for small pressure tubes, and the scope of this investigation focusing on the overall response of the boundary layer, it was assumed that the viscous correction (Equation 6.9) was applicable to all measurements made.

The corrections were implemented in a sequential fashion as per the recommendations of McKeon et al. (2003). The first correction made on each measurement value was that for viscous effects, followed by streamline displacement, and then finally the influence of the wall (where applicable).

6.4.2.2 Spatial positioning of pressure tubes

Accurate positioning of the pressure tubes was of paramount importance given the dependency of flow stability indicators on velocity gradients. Inaccurate positioning can lead to poor curvature in derived velocity profiles, hence suggesting apparent instabilities in the results that are nothing more than an artefact of poor measurement. Every effort was made to measure pressure tube position as accurately as possible with the equipment available.

Positioning of the pressure tube was achieved via the use of a Mitotoyo^{TM} manual height gauge (spatial resolution: $\pm 5\mu m$), manually aligned to position

guides on the enclosure of the FPR. The pressure tubes themselves were clamped to the height gauge, and were fed down between slots in the enclosure, cut parallel to the centreline of the FPR.

The position guides were installed parallel to the centre-line of the FPR. The arrangement was such that the pressure tubes were always located parallel to the centreline of the FPR, (i.e. in a fixed spanwise position), and collinear when at the surface of the FPR, when the height gauge was butted against the position guide. Datum markings and *mm* graduations on the position guide (referenced from the leading edge of the FPR) were used to locate and measure the position of the ends of the pressure tubes in the x-direction.

Limit stops in the design of the clamp ensured that the pressure tubes were always clamped to the height gauge in the same vertical position relative to the reference frame of the height gauge. A steel square was used to align the pressure tubes, parallel to the height gauge base, such that the tube ends were perpendicular to the freestream velocity.

Location of the pressure tubes in the y-direction was achieved by careful visual positioning of the tube to the FPR surface, and inspection of witness marks in the surface of the FPR. When setting up the equipment, the tubes were lowered to the surface until just touching, raised and then lowered further until the tubes were observed/witnessed to just touch. The measured positions at these touch conditions then became the reference datums for the wall, from which all subsequent, respective measurements were made.

The thoroughness implemented in positioning the pressure tubes ensured that any artefacts in the measured data arising from errors in positioning were minimised as best as possible within the limitations of the equipment. A further discussion of the effect of potential positioning errors is presented in Section 6.4.2.3.

6.4.2.3 Uncertainty in pressure tube measurements

Every effort was made to minimise error in the experimental velocity measurements. However, both systematic and random errors occurred. In this section an analysis of the sources of error is presented.

The Baratron used to obtain the pressure measurements represents a source of systematic error. The inherent limitations of the instrument meant that a systematic, absolute error of 0.08% of the measured pressure value affected all measurements.

A prevalent source of error in the measurements was pressure tube misalignment. Although every effort was made to minimise spatial positioning

errors of the tube (see Section 6.4.2.2), some uncertainty did exist. However, according to Chue (1975), a misalignment of less than 10° for a tube of dimensions similar to those used for the experiments produces an error in the measured pressure of less than 1%. It has been ascertained that, through the use of squares (i.e. simple alignment tools), this alignment condition was never breached. Thus, an absolute error in pressure due to probe misalignment was taken as being 1% for each measurement.

The inherent accuracy of the Baratron and the probe misalignment error were taken as as constant absolute instrument errors affecting all measurements. By finding the square root of the sum of the squares of theses two errors (Equation 6.11), an estimate in the absolute error in pressure of the instrument was calculated as being 1.00%.

$$err_{abs_{instrument}} = \sqrt{\sum_{i=1}^{N} Err_i^2} \tag{6.11}$$

Due to the absolute error of the height gauge used to position the pressure tube, error exists in the measured data due to the velocity gradients in the boundary layer. Quantification of this error has been made by considering the absolute error in the height gauge. Since the resolution of the height gauge is known ($\pm 5\mu m$), the relative error in velocity associated with tube displacement can be estimated by considering the local velocity gradient at a measurement location, and calculating the error in velocity arising from a positioning error equal to the absolute error in the height gauge (Equation 6.12). For example, the maximum determined velocity gradient at any measurement location was found to be the value at $y = 0.25mm$ for the case of a single actuator operated at $V_{app} = 24.2kV_{pp}$, with mild suction (see Figure 8.1). At this location, the normalised local velocity gradient $\left(\frac{\partial\left(u/U_{infty}\right)}{\partial y}\right)$ was found to be $1821^1/_m$, which accounted for an absolute error in velocity due to tube displacement (local velocity gradient) of 1.21%.

$$err_{rel_{spatial}} = \frac{5\mu m \left.\frac{\partial u}{\partial y}\right|_y}{u} \tag{6.12}$$

Scatter was present in all of the measurements taken throughout the experimental program, and this scatter constitutes another source of error. Like the error due to tube displacement, the scatter is best described in terms of a relative error. Consistent with best practice, the scatter in the measurement data is shown on the graphed measurement results as $\pm 2\sigma$ (where σ is the standard deviation in the measurement data). Although the scatter varied

between measurement data (the result of random errors that are difficult to quantify, for example movement of people in the laboratory), it was found to be generally consistent, with an approximate value of $\pm 0.03 U_\infty$. Thus, as a sidenote, the relative velocity error due to scatter can be approximated as 3% of the freestream velocity for all measurements (Equation 6.13). For the example discussed above (an actuator operated at $V_{app} = 24.2 kV_{pp}$, with mild suction; see Figure 8.1), the actual scatter was found to be 2.24% of the freestream velocity, hence meaning that the absolute error in velocity due to scatter was 2.96%.

$$err_{rel_{scatter}} = \frac{2\sigma_u}{u} \approx \frac{0.03 U_\infty}{u} \tag{6.13}$$

The analysis discussed in this section allows the errors in the measured data to be quantified. By considering the four sources of absolute and relative errors highlighted, the total error for any velocity measurement ($err\,(u)$) can be estimated by finding the square root of the sum of the squares of all the errors (Equation 6.14). Using the example already analysed in this discussion, the error to be found in a typical measurement is $u_{measured} = u \pm 3.25\%$, (actual values $u = 3.98 \pm 0.130^{m}/_{s}$, with a calculated instrument velocity error of 0.499%). It is, however, reiterated that the error for each measurement is not necessarily constant, but dependent upon the local velocity, velocity gradient and scatter for that measurement; information that can be discerned from the graphed results.

$$err\,(u) = \sqrt{\sum_{i=1}^{4} Err_i^2} \tag{6.14}$$

The error analysis shows that the greatest source of error is scatter in the data. Thus, a first order estimate of the error for any measurement can be quickly ascertained simply by studying the scatter in the graphed value, which, as mentioned, is shown as ± 2 standard deviations.

6.4.3 Data acquisition

The anemometry measurements from both the hot-wire and pressure tube anemometry techniques were recorded digitally throughout the research. Using a National Instruments PCI-6229 A/D card, voltage outputs from both the IFA 100 CTA system and MKS 398 differential Baratron were logged, and then retrieved for appropriate post-processing.

The sampling rates and sampling times differed between the two anemometry techniques. The values of sampling rate and record time for the CTA

measurements were $10kHz$ and $10s$ respectively (based on the recommendations of Bruun 1995). These values were found to be sufficient for measurement of the turbulence intensity of the wind tunnel. For the pressure tube anemometry, the sampling rate used was $4000Hz$. The sampling time was derived from a convergence study, conducted at two measurement points, one inside the layer (Table 6.1) and one just beyond the edge (Table 6.2). Mean velocity data were found to converge to within 0.5% after 3 seconds at both locations. An explanation for this short required sampling time is the manual positioning of the pressure tubes. The manual positioning took in excess of 10 seconds per data point, hence allowing the flow sufficient time to stabilise between measurement points (as supported in the results of the convergence study). Consequently, to allow boundary layer investigations to be performed in a timely manner, a record time of $3s$ was used for pressure tube measurements. It is acknowledged that the sampling rate selected for the pressure tube measurements was far greater than the frequency response of the Baratron itself. However, since the increased number of samples did not cause a noticeable increase in computation time during post-processing, such a high sampling rate was considered not to have a detrimental effect on the results.

The electrical parameter measurements for the experiments were obtained through the use of the internal voltage scope of the Mini-Puls 2 plasma generator. The internal scope is a voltage divider with a nominal ratio of 1 : 1000, which allowed a measurement of the voltage applied to the

Table 6.1: Results of pressure measurement convergence study for measurements inside boundary layer ($x = 120mm$, $y = 0.700mm$).

Sample Time $[s]$	u $[^m/_s]$	Difference to previous record time
1	3.84	N/A
2	3.92	2.1%
3	3.94	0.5%
4	3.94	0.0%
5	3.92	0.3%

Table 6.2: Results of pressure measurement convergence study for measurements just beyond boundary layer edge ($x = 120mm$, $y = 5.725mm$).

Sample Time $[s]$	u $[m/s]$	Difference to previous record time
1	6.94	N/A
2	6.95	$2.7E-02\%$
3	6.95	$0.7E-02\%$
4	6.95	$0.3E-02\%$
5	6.94	$1.2E-02\%$

electrodes to be obtained. The scope was connected to a PicoScope 5203 PC-based oscilloscope. The oscilloscope had a sample rate of $1^{GS}/_{s}$, and a maximum record length of $0.128s$, with $8-bit$ resolution and a bandwidth of $250MHz$. Such a high sampling rate was necessary to resolve features of the plasma discharge, such as the filamentary micro discharges that have lifespans of the order of $100ns$ (Corke et al. 2010).

6.4.4 Presentation of anemometry results

For investigations pertaining to the research discussed in this thesis, the anemometry results have been processed and presented as x-station-specific velocity profiles. These velocity profile plots have been constructed using cubic splines fitted between the measured data. Using these cubic splines, it was possible to estimate the value of the derivative of velocity with respect to wall-normal direction $\left(\frac{\partial u}{\partial y}\right)$ and this data, in conjunction with the velocity profiles, has been used to determine the effect of the plasma-based LFC system on the studied flows, by studying the characteristics of the local maxima and minima in this profile.

In addition, when discussing the results for the plasma augmented flows, contours of the entire flow field (for each investigation) have been plotted using the total pressure measurements.

The spacing between points on the velocity contours was determined by the position at which pressure measurements were obtained. Hence, the spacing in the x and y directions of the contour plots is $\Delta x = 10mm$ and $\Delta y \sim 0.5mm$ respectively. (Note that due to slight changes in spacing resulting from application of the displacement correction, the spacing in the y direction on the contour plots is only approximately constant. In addition, $\Delta x = 40mm$ between $x = 263mm$ and $x = 303mm$ for the double actuator results (Chapter

9) due to an inability to obtain measurements at $x = 273mm$, $x = 283mm$ and $x = 293mm$ when two actuators were operating).

The velocity contours have been constructed using 20 equally spaced levels corresponding to different values of normalised local boundary layer chordwise velocity, beginning at ${}^{u}/_{U_\infty=0}$. The resolution between levels is 0.05 units, and linear interpolation has been used between the measured velocity data to obtain the contour level values.

6.5 Performance of the FPR

Prior to commencing experimental investigations involving DBD actuators, the ability of the FPR to produce a boundary layer mimicking a Blasius flow was investigated. The preliminary experiments involved operating the wind tunnel at the intended freestream speed of the LFC investigations (approximately $5 \pm 0.6{}^{m}/_{s}$) and mapping the boundary layer in the region of interest. For this project the region corresponded to that where the Reynolds number of the layer becomes critical, which based on chord length is approximately 110000. Consequently the boundary layer was mapped from $x = 243mm$ to $x = 313mm$ (Figure 6.16), for a freestream velocity of $U_\infty = 5.62{}^{m}/_{s}$, and Reynolds number per unit length of $\frac{Re_x}{x} = 370000{}^{1}/_{m}$ for all x except $x = 263mm$. Note that for $x = 263mm$, drift in the wind tunnel motor speed resulted in slightly different (but still satisfactory) values of freestream velocity and Reynolds number per unit length $5.32{}^{m}/_{s}$ and $350000{}^{1}/_{m}$ respectively).

The measured boundary layer profiles showed good agreement with Blasius flow (Figure 6.16) and laminar behaviour as demonstrated by the contour plot of the measurements (Figure 6.17). There are some small inflections present in the profiles, as evident by the local maxima/minima in the plots of $\frac{\partial u}{\partial y}$, but these are seen to attenuate slightly downstream, suggesting that the flow is both laminar and stable. The Normalised-Root-Mean-Square Deviations (NRMSD) between the measured velocity profiles and Blasius theory (Equation 6.15) were less than or equal to 7.50% for all x-locations studied (Table 6.3) and the errors in shape factor between the Blasius profile and the measurements (defined by Equation 6.16) were found to be satisfactorily low (Table 6.4). It was thus concluded that the FPR was successful at producing a flat plate boundary layer that exhibited Blasius-type characteristics, and that the experiments using DBD actuators to augment the stability of the flow would provide meaningful insights into DBD-based LFC design.

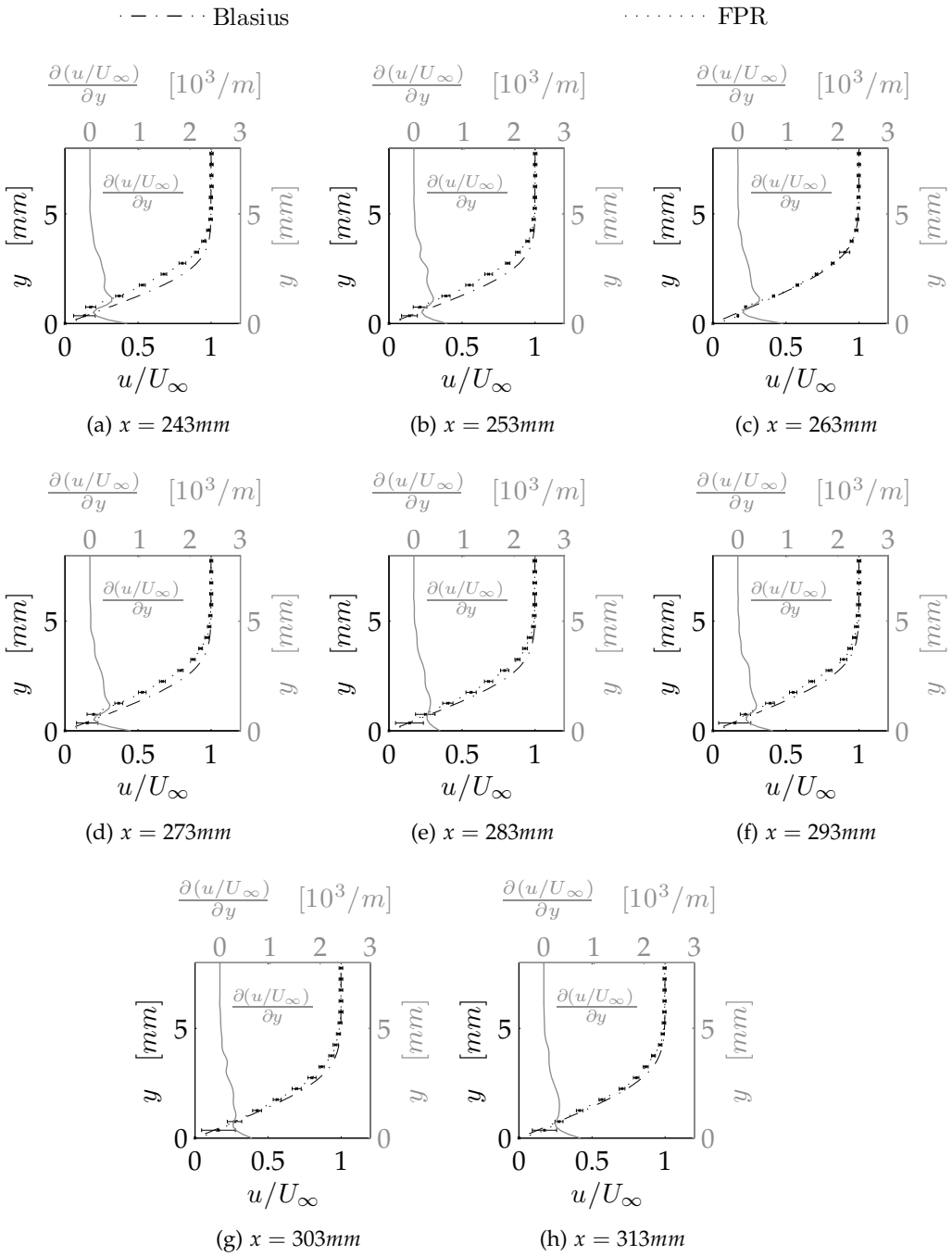

(a) $x = 243mm$ (b) $x = 253mm$ (c) $x = 263mm$

(d) $x = 273mm$ (e) $x = 283mm$ (f) $x = 293mm$

(g) $x = 303mm$ (h) $x = 313mm$

Figure 6.16: Velocity profile measurements obtained from the FPR, $U_\infty = 5.62^m/_s$, $\frac{Re_x}{x} = 370000^1/_m$ for all x except $x = 263mm$. For $x = 263mm$, $U_\infty = 5.32^m/_s$, $\frac{Re_x}{x} = 350000^1/_m$. Derivative information for measured data only.

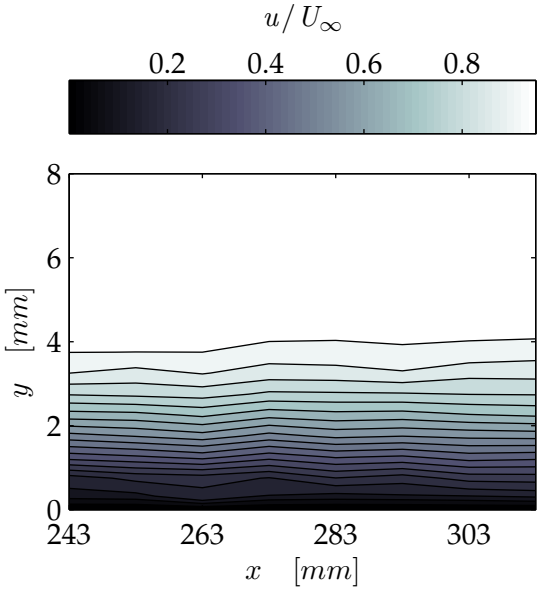

Figure 6.17: Contour plot of measurements obtained from the FPR, $U_\infty = 5.62^{m}/_{s}$, $\frac{Re_x}{x} = 370000^{1}/_{m}$ for all x except $x = 263mm$. For $x = 263mm$, $U_\infty = 5.32^{m}/_{s}$, $\frac{Re_x}{x} = 350000^{1}/_{m}$.

$$NRMSD = \frac{\left[\sum_{i=1}^{n=}\left({}^{u}/_{U_\infty}|_{measured} - {}^{u}/_{U_\infty}|_{Blasius}\right)^2\right]^{1/2}}{\frac{n}{u(\delta) - u(0)}} \tag{6.15}$$

$$err(H) = \frac{abs(H_{Blasius} - H_{measured})}{H_{Blasius}} \times 100\% \tag{6.16}$$

6.6 Experimental investigations involving DBD

The experimental investigations involving the FPR were focused on mapping and measuring the response of a flat plate boundary layer with a zero pressure gradient to a variety of actuator configurations, positioned near to the location of the Critical Reynolds number for the flow. In this chapter, details of the experimental set up used in all have been presented. Specific details for particular investigations are discussed in the relevant chapters where results are presented.

Table 6.3: Normalised-Root-mean-square-Deviations between measurements from FPR and Blasius theory.

$x[mm]$	$NRMSD[\%]$
243	7.47%
253	5.91%
263	7.50%
273	6.09%
283	4.06%
293	3.99%
303	2.83%
313	2.50%

Table 6.4: Shape factor values obtained from FPR.

$x[mm]$	H	$err(H)[\%]$
243	2.7921	7.80%
253	2.6594	2.68%
263	2.5037	3.33%
273	2.6253	1.36%
283	2.5401	1.93%
293	2.5947	0.18%
303	2.4368	5.92%
313	2.4224	6.47%

6.6.1 Preliminary experiments

Preliminary investigations incorporating a single DBD actuator were undertaken for the purpose of identifying particular experimental issues associated with the rig that would need to be taken into consideration for the subsequent detailed LFC studies. The results of these investigations revealed a number of such issues. The first of these pertained to the formation of plasma on the large acrylic actuators used for the boundary layer investigations. When the exposed electrode was sandwiched between the acrylic and FPR, no plasma was observed to form. The lack of surrounding air seemingly *choked* the actuator, and inhibited it from producing any discernible wall-jetting effect. It was found to be necessary to separate the actuator by a distance of $5mm$ from the trailing edge of the upstream flat plate section, in order to create a wall

jetting effect that augmented the boundary layer. Seemingly, the volume of air that could surround the electrode in the gap was necessary for producing useful plasma.

The second phenomenon associated with the large actuators in the FPR was that in *quiescent* air, even the actuators separated by a gap from the FPR did not produce a jetting effect that could be measured at the trailing edge of the encapsulated electrode. However, as the experimental results testify when a boundary layer was present, a plasma jetting effect was formed that had a profound effect. Moreover the effect was found to be dependent on the applied voltage of the DBD device. The reason for the inconsistencies lay in the dimensions of the actuators used in the boundary layer investigations. As these were over five times the size than the actuators studied in the quiescent-air parametric study (Chapter 5), the energy of the plasma generator was dispersed over a greater area, and thus it would be expected that a reduction in the quiescent-air jetting effect would occur. However, as mentioned, the large plasma actuators were observed to significantly augment the boundary layer of the FPR, and since the development of the DBD-based LFC technology is based on the augmentation capabilities of the system, it was not deemed necessary to measure the quiescent-air performance of the various large actuators tested. Instead, emphasis was placed on measuring the response of the FPR boundary layer to the various actuator configurations, and relating these back to the parameters of the actuators.

The consequence of the two phenomena discussed here is that two interesting configurations could be tested for each actuator. The first was a sealed case, where the bottom and spanwise ends of the gap were sealed to prevent a strong suction effect from dominating the control of the boundary layer (Figure 6.18). The second case was one with the plasma working in conjunction with a mild suction force. By opening the ends of the gap in the spanwise direction (150mm away from the ends of the electrode), the boundary layer could be exposed to the pressure difference between the test section and the ambient environment. This pressure difference amounted to a mild suction effect of 4Pa, and allowed the transfer of fluid from the boundary layer (Figure 6.19). It was anticipated that through the use of the plasma actuator with the mild suction (Figure 6.20) the effect of the suction could be enhanced, and thus potentially create a LFC system of great benefit.

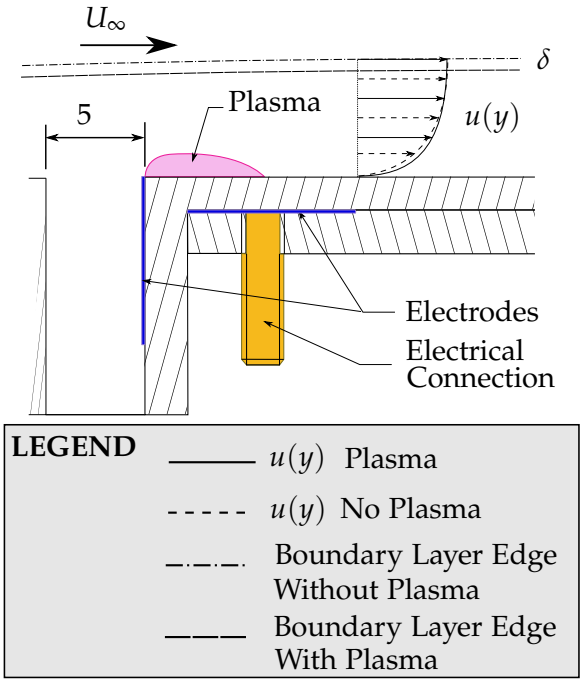

Figure 6.18: Schematic arrangement of plasma actuator and corresponding fluid flow for the case without mild suction. The plasma is shown in purple (dimensions in *mm*).

6.6.2 Focused investigations

Based on the observations during the preliminary investigations, three focused studies were performed as part of this research. In all three studies, configurations with and without the mild suction effect were tested. The first investigation looked at the response of the laminar boundary layer to the presence of a single orthogonal DBD actuator. Little consideration was given to the operation of the actuator in this study, with the plasma generator operated in the middle of its operational range so as to produce plasma that noticeably augmented the boundary layer. Refinement of the operation of the single actuator was the focus of the second investigation. A parametric study examining the effect of actuator applied voltage was performed, leading to investigations regarding the response of the layer to the seemingly most beneficial and most adverse actuator operations. The final study sought to maximise the effect of the single actuator by using a second actuator placed downstream of the first. Again, the response of the layer to the most beneficial and most adverse actuator operation were measured.

In line with the scope of the research, all investigations were restricted

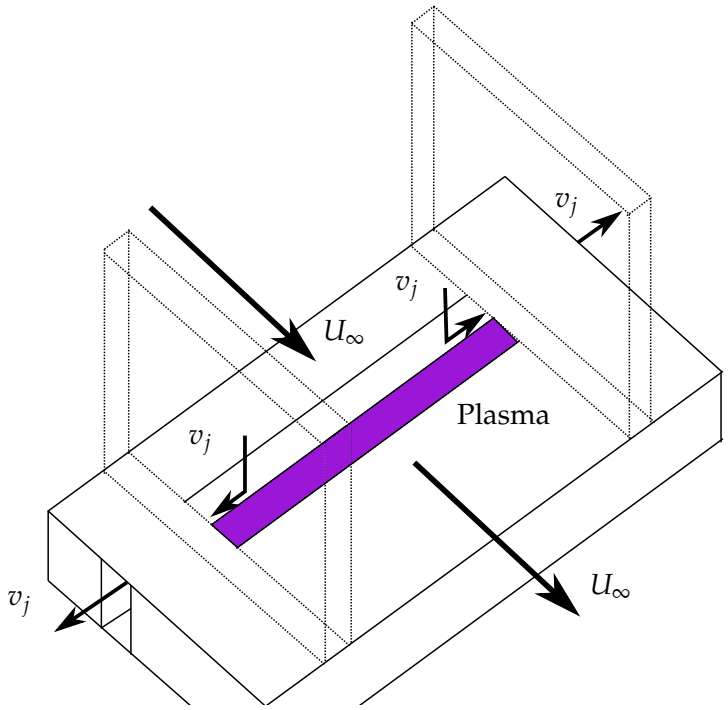

Figure 6.19: Schematic of the establishment of the mild suction effect used in conjunction with the DBD actuators. The plasma is shown in purple.

to two dimensions only. This meant that measurements of the boundary layer were taken along the centreline of the FPR. The upstream actuator used for each investigation was positioned such that its trailing edge was $243mm$ downstream of the leading edge in the x direction. This placed the trailing edge of the actuator at a chordwise Reynolds number (Re_x) of 80000, which allowed the plasma to augment the flow near to its critical Reynolds number value, through a Reynolds number range (based on chord length) from 80000 to 120000. The response of the boundary layer near to the critical Reynolds number was measured by recording the velocity profile at a number of stations downstream of the actuator. Each station was nominally spaced a distance of $10mm$ apart and for all investigations, measurements were obtained to a position of $x = 313mm$. For some configurations it was possible to obtain measurements up to $x = 323mm$ through slight modifications of the rig, and this is noted in the relevant chapters.

At each chordwise station, velocity measurements were recorded at a number of locations normal to the surface (also referred to as the *wall*) of the FPR. Beginning at the surface ($y = 0$), measurements were taken at a

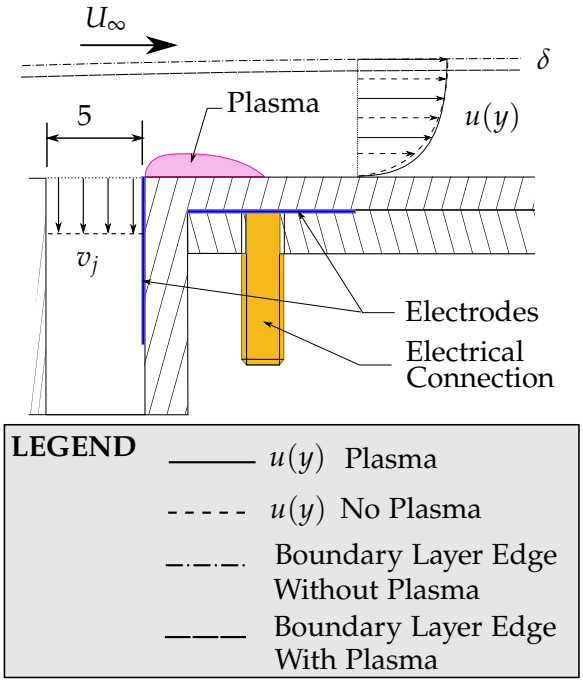

Figure 6.20: Schematic arrangement of plasma actuator and corresponding fluid flow for the case with mild suction. The plasma is shown in purple (dimensions in mm).

pitch of $500\mu m$, concluding at $y = 8mm$, which was in the freestream for all chordwise stations. This pitch value, equivalent to the OD of the pressure tube, provided an efficient way to capture the velocity characteristics of the boundary layer (the intention was that fluid at all heights within the layer would have been sensed by the probe), whilst minimising the position error to a value of 0.01% (see Section 6.4.2.2).

6.6.3 Comments on the effect of the presence of the actuator slot

Laminar boundary layers are highly sensitive to the presence of surface steps, both forward-facing and backward-facing. Therefore it is pertinent to consider the underlying effect of the actuator slot on the stability of the boundary layer flows investigated.

When the cavity is sealed (i.e. the *no-suction* case), the slot in the surface represents a dimensionally significant perturbation to the flow. Although the leading and trailing edges of the slot are essentially co-planar, local separation of the flow within the slot region means that the two edges represent backward-facing and forward-facing steps respectively. Wang and

Gaster (2005) showed that the transition point of a boundary layer can be brought upstream through the use of forward-facing and backward-facing steps. Using hot-wire anemometry, Wang and Gaster (2005) showed that the transition point of a flat plate boundary layer moves forward with increasing step height (for both forward-facing and backward-facing), independent of freestream velocity. However, since such transition was not observed in any of the focused investigations conducted, the experimental results indicate that the slot was not perturbing the flow in a fashion generally associated with surface steps.

Although not a surface step, the localised flow separation created by the slot cavity means that it will produce both acoustic and shear resonant frequencies (East 1966). Using the data in (East 1966), the first modes of each can be approximated by Equations 6.17 & 6.18 respectively, for a cavity that has a length, $d = 25mm$, and a depth, $d = 5mm$, placed in the nominal freestream velocity for the experiments of $U_\infty = 5.5^m/_s$, with an assumed local speed of sound, $a = 344^m/_s$. Using these equations, a value of $13kHz$ for the first acoustic mode, and $600Hz$ for the first shear mode can be determined. Converting these to non-dimensional circular frequency yields 370.0 for the acoustic mode, and 17.1 for the shear mode, both far too large to cause transitionin the boundary layer at the location of the cavity. Consequently, it is suggested that the cavity (for the no-suction case) has very little direct influence on the stability of the boundary layer, and that the driving force of the flow augmentation is the DBD actuators.

$$\frac{fd}{a} = 0.2 \tag{6.17}$$

$$\frac{fb}{U_\infty} = 0.5 \tag{6.18}$$

When the cavity is opened (i.e. the *mild suction* case), the cavity becomes a suction slot. This slot acts to draw boundary layer fluid from near the wall, resulting in an increased stability of the flow. In this case, the mild suction produced by the slot forms a component of the LFC system, in line with such systems discussed in the literature (see Joslin 1998). On a systems level, the direct influence of the cavity, good or bad, is not as important as the ultimate effectiveness of the LFC system. Thus, the ultimate effect of the slot on the studied boundary layers is discussed in the chapters pertaining to the results of the focused investigations (Chapters 7, 8, & 9).

6.6.4 Comments on the value and certainty of single plane measurements

The history of boundary layer investigations reveals that the first step in developing new boundary layer control techniques is to restrict studies to two dimensions. The research discussed here is of the same category; new research in an emerging field of Laminar Flow Control. Hence the focused flat plate boundary layer investigations performed as part of this research were restricted to measurements on a single plane, consistent with other, typical work in the field of both Laminar Flow Control (eg Wang and Gaster 2005) and DBD-based LFC (eg Grundmann and Tropea 2009). As per the methodologies in the literature, the plane of measurement was along the spanwise-centreline of the flow. In addition the measurement region was approximately 40 boundary layer thicknesses away from the ceiling of the cavity, and approximately 100 boundary layer thicknesses away from the sidewalls, hence minimising the wall-proximity effects of the FPR enclosure. Consequently, through the use of such a large experimental enclosure, and by following the techniques described in the literature, measures were implemented to minimise any spanwise variation in the developed boundary layers, which proved to be effective, based on the performance of the FPR (see Section 6.5).

By extension, spanwise variation in the developed boundary layers for the purely plasma-augmented flows was also kept to a minimum. However, with the introduction of the mild suction effect, it is expected that increased spanwise variation developed. It can be deduced from the literature that the suction velocity along the cavity would not have been uniform (Humphrey and Whitelaw 1977, Sotiropoulos and Patel 1992). However, assuming that the flow was symmetrical through the cavity (a good assumption considering the symmetry of the FPR), then the cavity can be treated as two, mirrored, right-angled ducts, of variable cross-section. Through these ducts, fluid is removed from the boundary layer (under the mild pressure difference), resulting in the augmented boundary layer, albeit with spanwise variations resulting from introduced streamwise vorticity. However, since the cavity is (approximately) symmetrical, this vorticity would have been mirrored either side of the measurement plane, hence producing a small, symmetrical variation between the centreline and the side walls. Thus the experimental data provide a good indication of the effectiveness of the DBD-based LFC system with suction; results that form an excellent basis from which future work can be undertaken (see Section 10.2).

6.6.5 Calculation of boundary layer parameters

Calculation of the displacement and momentum thickness values for all investigations was achieved through numerical integration. The technique used cubic spline integration, that fitted cubic splines between data points and then integrated the resultant piecewise polynomials.

6.7 Summary

In this chapter the experimental equipment developed and utilised for the research has been introduced and discussed. The resulting rig that was developed, the Flat Plate Rig (FPR), aimed to achieve flow characteristics mimicking those of the Blasius boundary layer. Through careful design, the FPR was developed such that the pressure gradient over the test section could be controlled, and this resulted in suitable flow conditions for the research program.

In addition to introducing the experimental equipment, the chapter also discussed the procedures and methodologies employed in the experimental investigations. This discussion highlighted the operation and positioning of the orthogonal DBD actuators and the region of experimental investigation. As mentioned, the results of the focused experimental investigations to which these details pertain are the presented in the following chapters.

7 Response of the Laminar Layer to a Single Orthogonal Actuator

In quiescent air, orthogonal DBD actuators were observed to produce wall jetting characteristics potentially suitable for a Laminar Flow Control of a flat plate boundary layer in a Zero Pressure Gradient. To determine just how effective these actuators would be, the response of a Blasius boundary layer to the actuators needed to be observed. The experimental investigation discussed in this chapter was formulated to investigate this response, and determine whether or not the developed DBD-based LFC would produce an effect similar to that of an LFC system utilising uniform wall suction.

The investigation used a single orthogonal actuator positioned in accordance with the experimental set up discussed in Chapter 6 and results were obtained for cases with and without subtle suction. Due to the preliminary nature of this investigation the plasma generator was driven in the middle of its operating range, which corresponded to an applied voltage of $22.2kV_{pp}$.

The results discussed in this chapter are those presented in Gibson et al. (2012). The results show the evolution of the augmented boundary layer velocity profile downstream of the actuator. From these results, information regarding the effect of the actuator on the stability of the flow was gleaned, which led to recommendations for subsequent, refined experimental investigations.

7.1 Flow response to a single orthogonal actuator

Prior to the use of the plasma, the response of the boundary layer to only the mild suction effect was investigated. The measured velocity profiles (Figure 7.1) showed that the mild suction effect was capable of augmenting the velocity profile, but with some degree of destabilisation. The velocity profiles showed similarities along the length of the investigation region, but inflections in the profiles were immediately introduced in the upstream locations by

the presence of the slot. However, these instabilities were observed to damp downstream until $x = 293mm$, accompanied by a reduction in the shear at the wall. Beyond $x = 293mm$ some additional instability growth was seen in the measurements, possibly arising from some downstream disruption to the flow, rather than as a result of the slot.

Under the presence of the mild suction effect the layer was also observed to become thinner over the entire investigation region, but this effect did abate downstream of the suction slot, as evidenced by the increasing similarity between the controlled and uncontrolled boundary layer profiles in the downstream locations.

The velocity contours for the boundary layer exposed to the mild suction (Figure 7.2) showed that the development of the boundary layer was fairly regular. The contours showed approximately monotonic growth of the boundary layer, with reduced thickness over the length of the investigation region, which ultimately suggested that the mild suction slot was having a favourable effect on the stability of the flow.

When the plasma actuator was switched on, the stable flow control provided by the mild suction effect was seen to disappear (Figure 7.3). Whilst the layer became thinner with the plasma, the flow became less stable, with significant increases in shear at the wall, and instabilities that became amplified downstream of the actuator. At a distance of $30mm$ downstream of the actuator, a very noticeable inflection in the velocity profile was observed, and this instability arising from this inflection was not seen to attenuate downstream, but rather slightly grow and become accompanied by additional instabilities, higher up in the boundayr layer (as was observed in the gowth of local maxima/minima in the plot of $\frac{\partial u}{\partial y}$). In addition, the boundary layer became thicker, which meant that all observations from the velocity measurements were consistent with reduced hydrodynamic stability.

The destabilisation of the flow was noticeable in the contour plot of the boundary layer velocity (Figure 7.4). The increased thinning brought about by the plasma was seen to be limited to only $30mm$ downstream of the actuator. Beyond this location, rapid thickening was noticed. Thus, the velocity measurements suggested that the orthogonal actuator operated at an applied voltage of $22.2kV_{pp}$ had an adverse affect on the stability of the laminar boundary layer.

Removal of the mild suction effect was seen to produce an even greater adverse affect on the stability of the boundary layer (Figure 7.5). In the absence of the mild suction effect, the velocity profile was observed to become unsteady immediately downstream of the actuator at $x = 243mm$, as was evident by the significant and large inflection introduced into the velocity

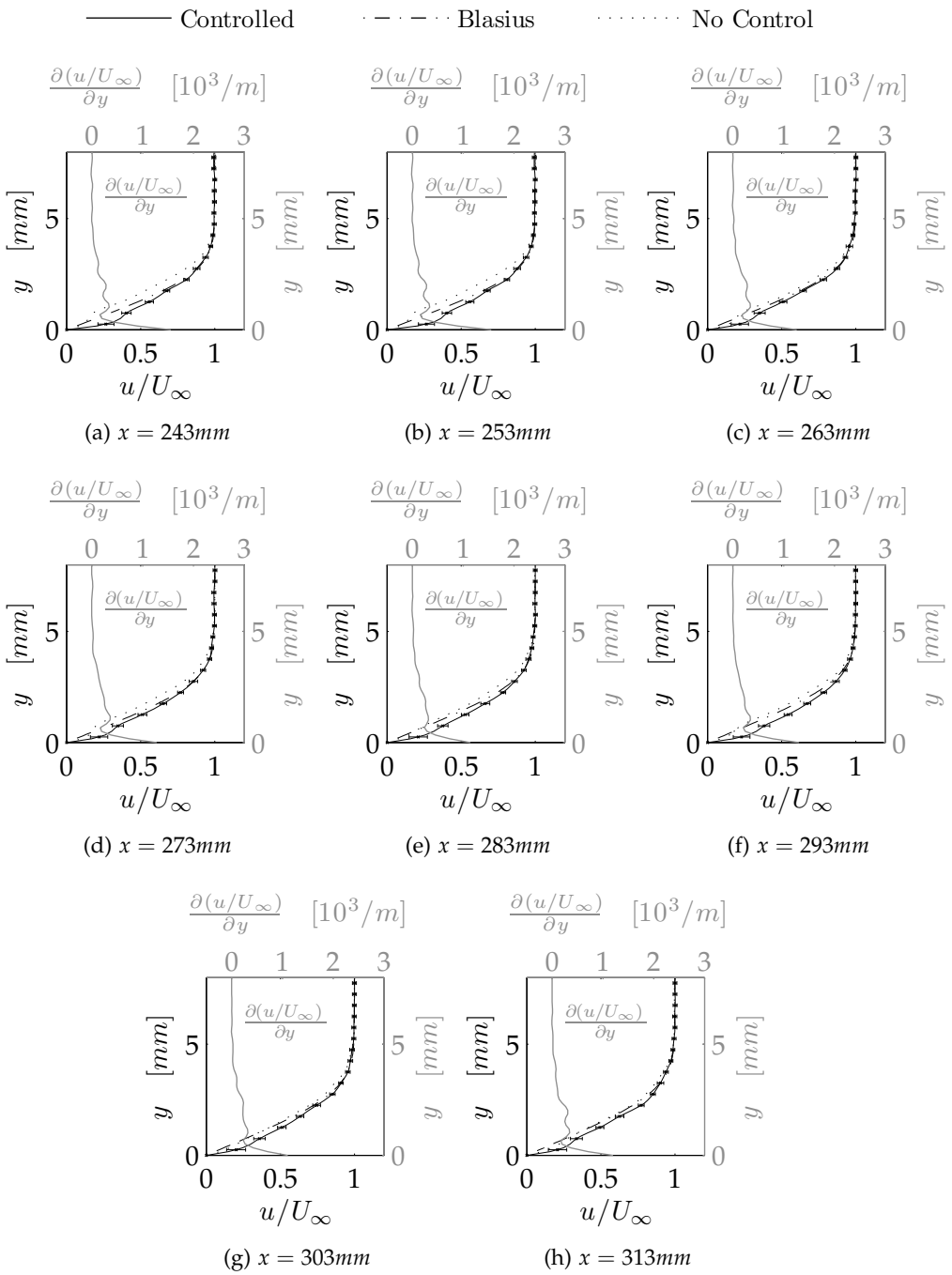

(a) $x = 243mm$ (b) $x = 253mm$ (c) $x = 263mm$

(d) $x = 273mm$ (e) $x = 283mm$ (f) $x = 293mm$

(g) $x = 303mm$ (h) $x = 313mm$

Figure 7.1: Velocity profiles for the boundary layer exposed to the mild suction only, $U_\infty = 4.88^m/_s$, $\frac{Re_x}{x} = 340000^1/_m$. Derivative data for controlled case only. 'No Control' case from FPR test shown for indicative reference only.

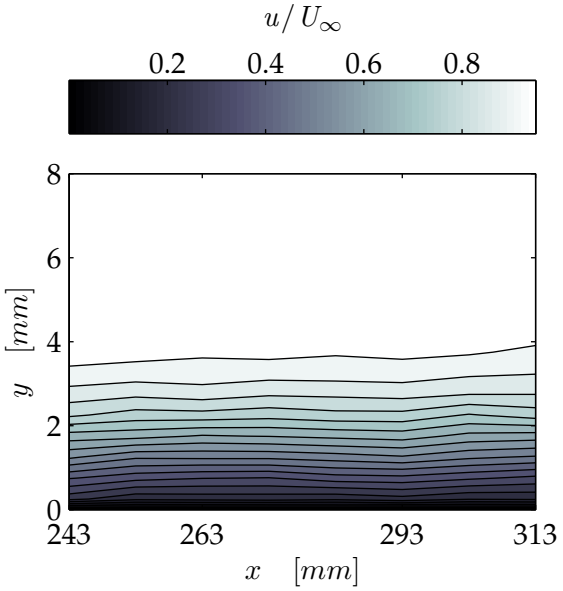

Figure 7.2: Velocity contours for the boundary layer exposed to the mild suction only, $U_\infty = 4.88^m/_s$, $\frac{Re_x}{x} = 340000^1/_m$.

profile. As such, the layer was satisfying the general criterion of instability (as discussed in Chapter 2). Although the inflection was accompanied by some initial thinning, (down to approximately 75% of the thickness of the original layer at $x = 253mm$), this thinning was seen to be negated rather quickly, only $20mm$ further downstream. Furthermore, beyond $x = 263mm$, the velocity profiles were observed to become increasingly unstable in nature, with additional instabilities entering the upper regions of the boundary layer and becoming amplified (as was observed in the gowth of local maxima/minima in the plot of $\frac{\partial u}{\partial y}$).

A large amount of flow irregularity was observed in the velocity contours for the case without suction (Figure 7.6). Without the suction effect, the layer was seen to become thicker, and in the most downstream locations the thickness exceeded that for the base flow as detailed in Chapter 6. Thus the velocity contours indicated that the plasma actuator was adversely affecting the stability of the flow, with the case without suction proving to be the most adverse.

To assess the influence of the orthogonal plasma actuators on the flow in more detail, it was useful to study the evolution of both the displacement thickness and shape factor of the flow with and without control. As discussed in Chapter 2, fluctuations in the displacement thickness indicate instabilities

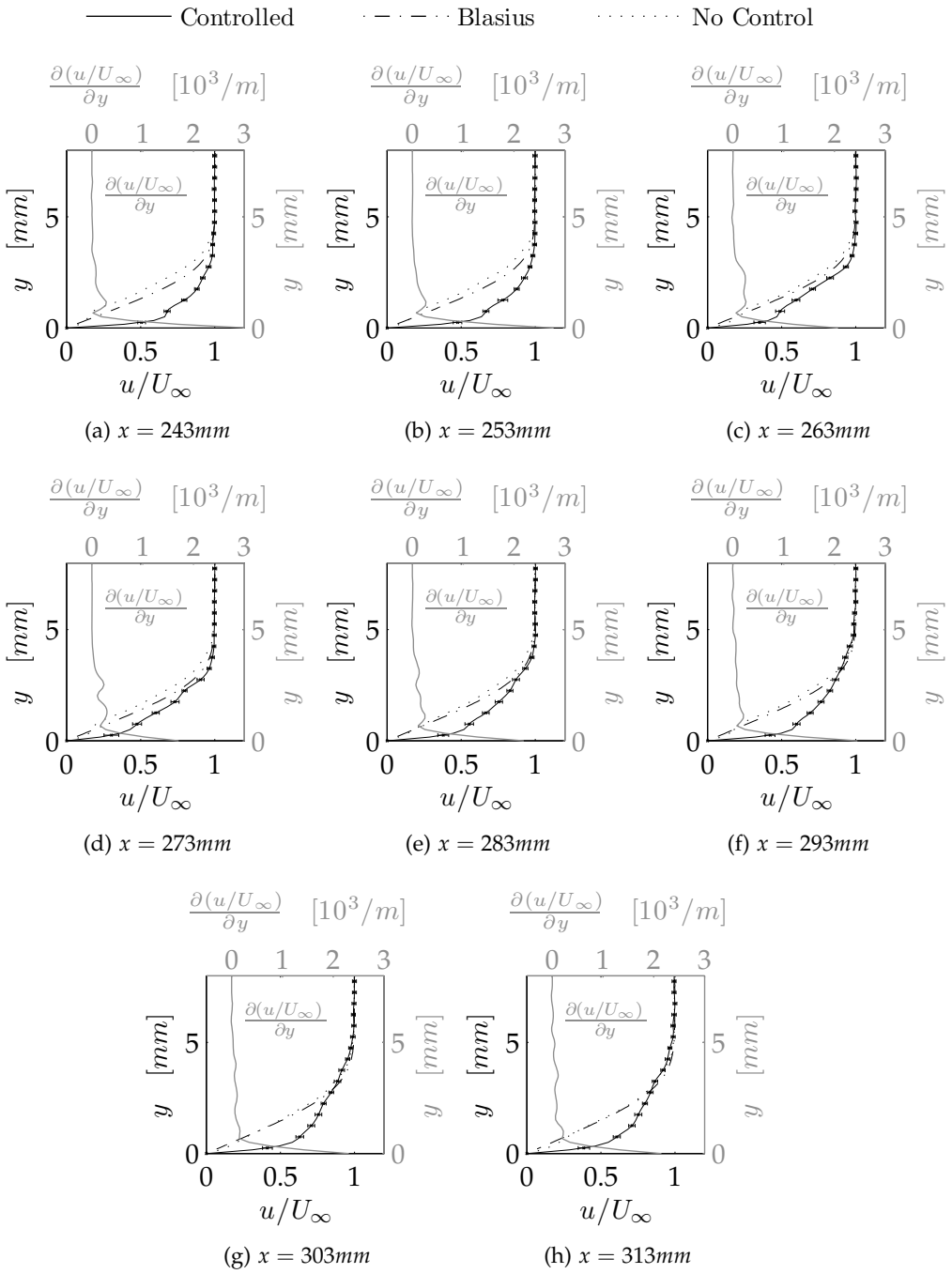

(a) $x = 243mm$ (b) $x = 253mm$ (c) $x = 263mm$

(d) $x = 273mm$ (e) $x = 283mm$ (f) $x = 293mm$

(g) $x = 303mm$ (h) $x = 313mm$

Figure 7.3: Velocity profiles with suction, $V_{app} = 22.2kV_{pp}$, $U_\infty = 4.86^m/_s$, $\frac{Re_x}{x} = 340000^1/_m$. Derivative data for controlled case only. 'No Control' case from FPR test shown for indicative reference only.

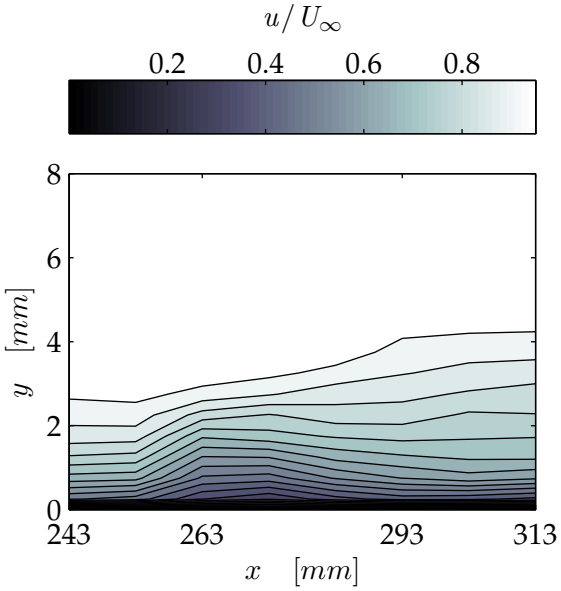

Figure 7.4: Velocity contours with suction, $V_{app} = 22.2kV_{pp}$, $U_\infty = 4.86^{m}/_{s}$, $\frac{Re_x}{x} = 340000^{1}/_{m}$.

and destabilisation in the flow, meaning that the value of the shape factor was able to be used to classify the type of flow (i.e. laminar or turbulent).

The evolution of the displacement thickness for both the case with mild suction (Figure 7.7) and without (Figure 7.8) indicated some unsteadiness being introduced to the flow by means of the plasma actuator. Whilst the plasma with and without the suction was seen to be capable of reducing the displacement thickness below that achieved by just the suction alone, the fluctuations suggested that the thinning was done in an destabilising fashion, creating instabilities that developed and propagated in space. In addition, the measurements for the case without plasma did not show a monotonic increase in the value, suggesting that even with the mild suction effect only, some destabilising of the flow and instability introduction may also have been occurring.

Study of the shape factor evolution graphs with suction (Figure 7.9) and without (Figure 7.10) supported the observations gleaned from the analysis of the velocity and displacement thickness data. Without the plasma, the shape factor was reduced to a value close to the desirable value of 2 over the entire length, as discussed in Section 5.2.2. This suggested that the mild suction was providing some benefit to the stability of the flow, without the layer becoming turbulent. Conversely the experimental results revealed that the orthogonal

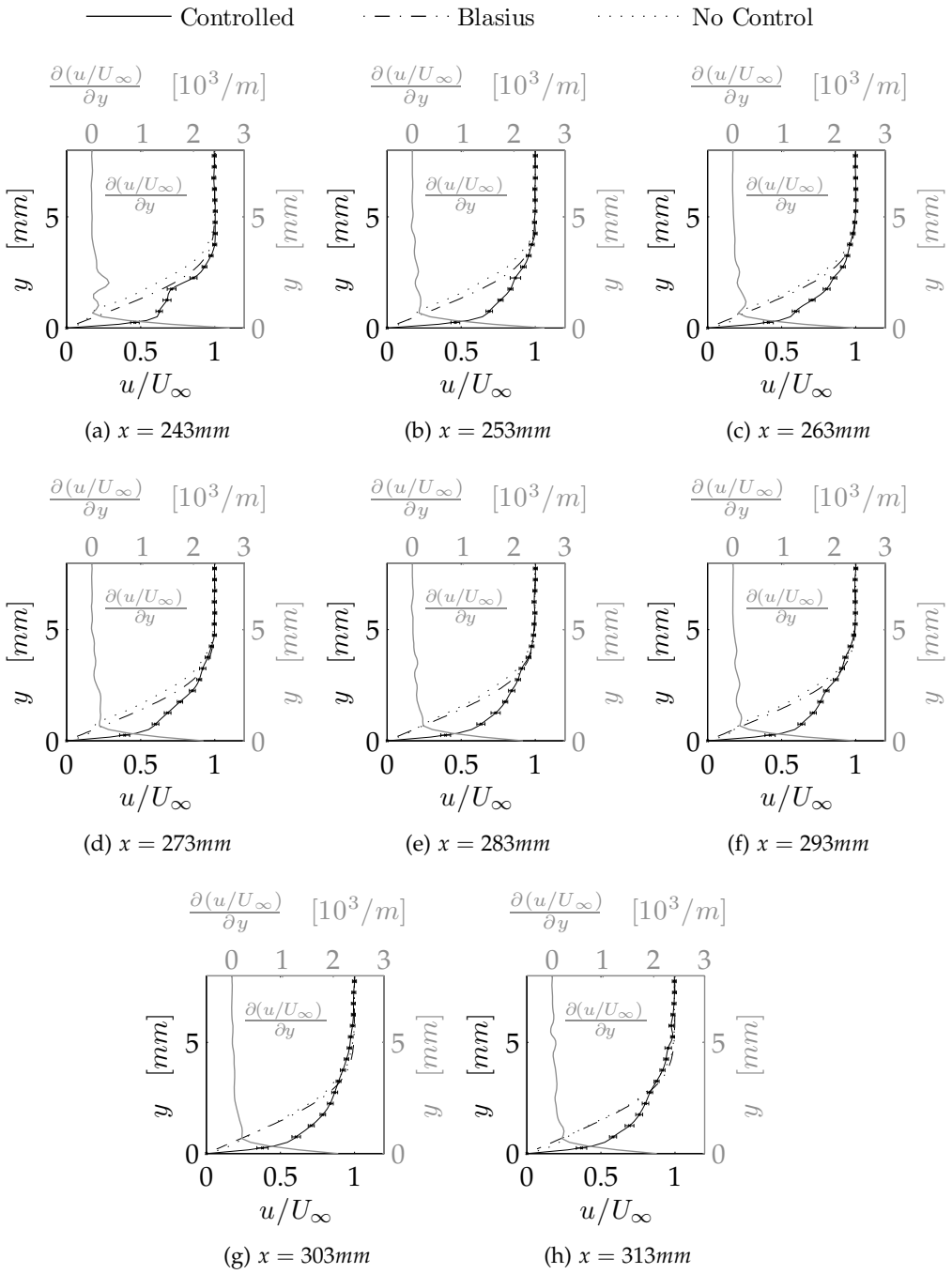

(a) $x = 243mm$ (b) $x = 253mm$ (c) $x = 263mm$

(d) $x = 273mm$ (e) $x = 283mm$ (f) $x = 293mm$

(g) $x = 303mm$ (h) $x = 313mm$

Figure 7.5: Velocity profiles without suction, $V_{app} = 22.2kV_{pp}$, $U_\infty = 4.86^m/_s$, $\frac{Re_x}{x} = 340000^1/_m$. Derivative data for controlled case only. 'No Control' case from FPR test shown for indicative reference only.

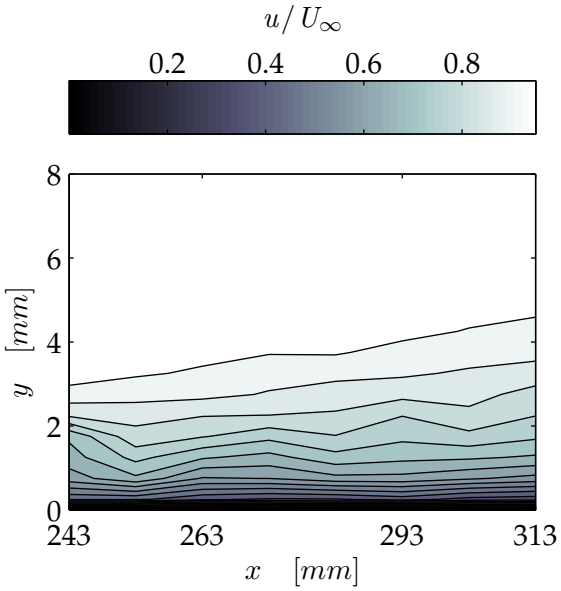

Figure 7.6: Velocity contours without suction, $V_{app} = 22.2kV_{pp}$, $U_\infty = 4.86^{m}/_{s}$, $\frac{Re_x}{x} = 340000^{1}/_{m}$.

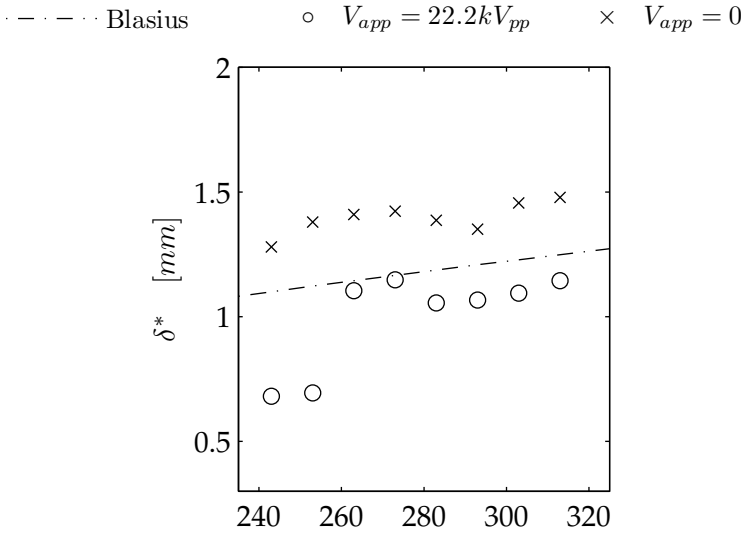

Figure 7.7: Evolution of displacement thickness for control with mild suction.

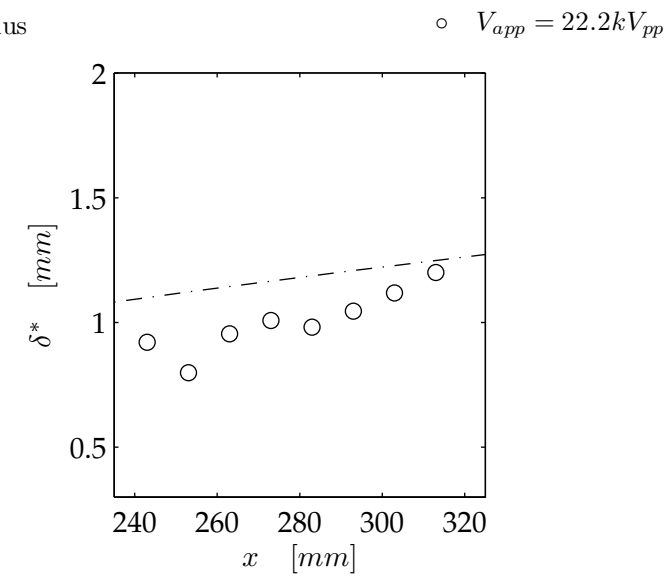

Figure 7.8: Evolution of displacement thickness for control without suction.

plasma actuator significantly reduced the value over the entire region of interest for both the case with suction and the case without. Without the combined use of suction, the shape factor remained consistent over the entire length at approximately 1.6, suggesting that turbulent flow was present. This result supported the previous conclusions that the plasma actuator operated by itself adversely affected the stability of the flow. When used in conjunction with the mild suction, the evolution of the shape factor of the flow suggested that there could be some potential to use a DBD-based LFC system like that studied. Immediately downstream of the actuator the value reduced to 1.6 before it increased towards a value of 2 between $x = 253mm$ and $x = 273mm$. This peak was of interest, as the value was consistent with positive stability improvement results observed in other published investigations for DBD-based LFC (Grundmann and Tropea 2007a, Grundmann and Tropea 2007b, Grundmann and Tropea 2009) and corresponded with the desired value for the DBD-based LFC system under development in this work. However, at $x = 283mm$, a sharp drop in the value was observed, which suggested that the flow was becoming unstable beyond this location. Consequently the use of the actuator combined with the mild suction effect appeared to be capable of improving stability slightly for a very short distance downstream.

Overall the results of the experimental investigation suggested that orthogonally-arranged DBD actuators of the design discussed had an adverse impact on the stability of the flow when operated with an applied voltage of

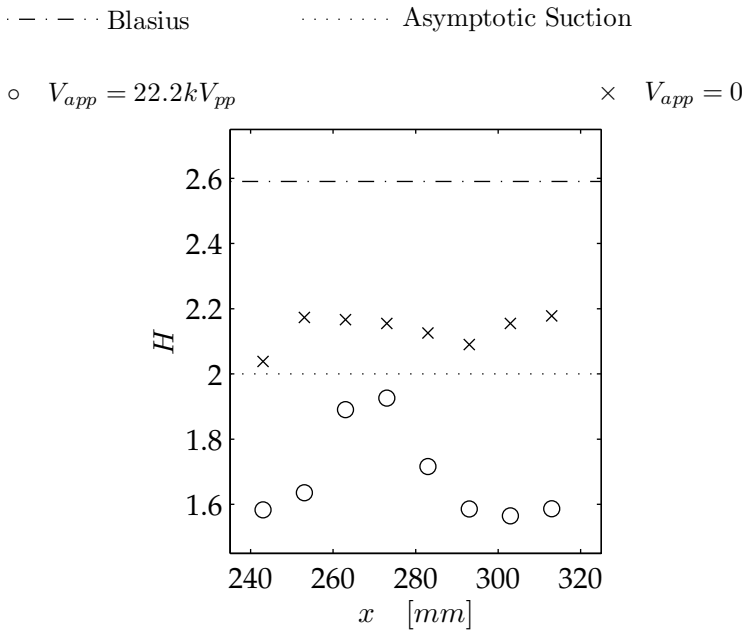

Figure 7.9: Evolution of shape factor for control with mild suction.

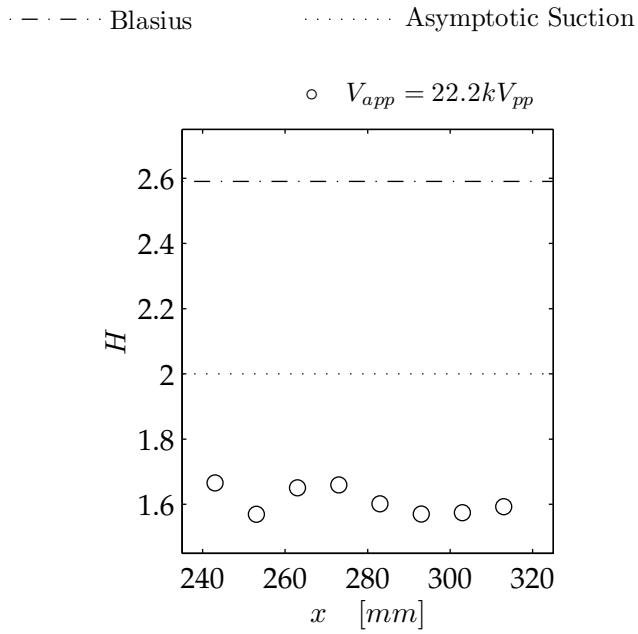

Figure 7.10: Evolution of shape factor for control without suction.

22.2kV_{pp}. Whilst the devices clearly thin the layer initially by approximately 25%, the rapid redistribution of momentum within the layer seemingly promoted conditions of instability that led to a rapid thickening of the layer further downstream of the device and, subsequently, transition into more chaotic, turbulent flow behaviour. Such phenomena suggest that these devices would be more useful for promoting boundary layer transition rather than delaying it, like other published observations noted for the conventional parallel actuator arrangements (Johnson and Scott 2001, Porter et al. 2007).

The dramatic thinning of the boundary layer that was able to be realised through the use of orthogonal actuators is, however, of significant interest. With no moving parts, the orthogonal actuators essentially acted as solid state suction devices, and thus with further development could provide for an improved suction-based LFC system. As observed in this work, the thinning of the boundary layer brought about by the actuator ultimately resulted in a detrimental effect on flow stability, but by encouraging a small amount of suction around the actuator, the dramatic thinning was able to be achieved in a stable fashion for some distance downstream of the device.

The difficulty with which successful transition delay is achieved with DBD devices is evident in the lack of published positive results. It is therefore unreasonable to expect orthogonally arranged DBD actuators to achieve this without considerable, concentrated work on the design and implementation of such devices. Thus, it is reasonable to ask; what actuator designs, if any should be studied and developed? In this work, an orthogonal actuator was implemented because of the seemingly favourable jetting characteristics for LFC produced by such a device. As noted, this hypothesis was not strictly supported, with the most favourable benefits to boundary layer control observed for the case where a small suction force was applied to the actuator. The resultant improvements with the suction effect suggest that the DBD actuator would benefit from producing a jetting profile characteristic of the combined plasma and suction system studied in this work. In addition to providing potential, favourable improvements to hydrodynamic stability, the dramatic boundary layer thinning able to be achieved with such an actuator could find use in other areas of flow control. Unlike the results obtained with conventional actuators by Grundmann and Tropea (2007a), Grundmann and Tropea (2007b) and Grundmann and Tropea (2009) where the thinning effect was barely noticeable nor discussed, orthogonal actuators may prove to be very useful in inhibiting flow separation due to the fact that the layer is thinned and the magnitude of the velocity near the wall is increased, an effect that can be exploited for delaying separation (Chang 1976). Consequently orthogonal actuators may become more versatile and ultimately more useful

flow control devices.

7.2 Summary & conclusions

The investigation discussed in this chapter attempted to assess the effects of orthogonally-arranged DBD actuators on the hydrodynamic stability of a flat plate boundary layer in a zero pressure gradient. The jetting characteristics of an orthogonal device differ significantly from those of a conventional, parallel actuator, most notably featuring a fuller jetting profile (Gibson et al. 2009a). The results suggest that orthogonally-arranged actuators are able to interact with a boundary layer, significantly thin it, and ultimately affect the stability characteristics of the flow. When operated independently, the DBD actuator investigated was found to reduce the thickness of the layer by approximately 25% immediately downstream of the device. However, the dramatic redistribution of the momentum within the layer brought about by the plasma ultimately resulted in destabilisation of the flow, suggesting that the arrangement studied was more beneficial as a flow tripping device.

By operating the actuator in conjunction with a mild suction effect at the wall immediately upstream of the actuator, the thinning effect of the plasma was able to be increased. In addition, a favourable reduction in the shape factor to a value close to 2 and maintenance of stable flow characteristics were observed immediately downstream of the plasma for a distance of $40mm$. Further downstream, a rapid thickening of the layer was evident, suggesting that the flow improvements able to be attained with a single actuator are limited.

The results of the experimental work suggest that through refined actuator design, Laminar Flow Control may be achievable using a combination of conventional techniques and orthogonally arranged DBD actuators. In Chapter 3 it was suggested that actuators operated with a comparatively lower applied voltage may be more beneficial to LFC given the 'less aggressive' jetting characteristics associated with such devices. Such lower applied voltage actuators may not introduce such large inflections in the velocity profile immediately downstream of the plasma like those observed during this investigation. Thus, by refining the operation of the orthogonal actuators, and using them in conjunction with the mild suction effect, it seems feasible that the stability of the Blasius flow can be augmented favourably. The investigation undertaken to test this hypothesis is the subject of the next chapter.

8 Refinement of Actuator Operation for Improved Control

The operation of a single orthogonal actuator in a flat plate boundary layer flow was observed to strongly augment the behaviour of the fluid downstream of the device, at Reynolds numbers near to the critical value. For an actuator operated with an applied voltage of $22.2kV_{pp}$, significant re-distribution of momentum within the layer was observed, combined with noticeable thinning of the boundary layer. The consequence of this momentum re-distribution was destabilisation of the flow beyond the DBD actuator, evident by the observed inflections in the boundary layer velocity profiles (and local maxima/minima in the derivative data), which failed to attenuate downstream and hence resulted in a satisfaction of the general criterion for instability. These inflections were accompanied by a rapid drop in the shape factor of the flow to values of approximately 1.6, which suggested the onset and presence of turbulent flow. Even with the assistance of a mild suction effect of $4Pa$ at the location of the actuator, destabilisation of the flow was observed. Thus it can be concluded that in order to harness the effects of DBD plasma for Laminar Flow Control, refinement of the actuator operation is required.

In the previously discussed experimental investigations, the destabilising effect on the flow was seen to be reduced with the use of the mild suction effect. Using this result, an improved actuator design and operation strategy were formulated. The strategy involved measuring the augmentation in the velocity profile of the boundary layer brought about by changes in the applied voltage of the DBD device, used in conjunction with the mild suction. This refinement strategy was based on the results of the literature review, which revealed that actuators operated at lower voltages produce fuller velocity profiles with diminished maximum jetting velocities, which potentially would not destabilise the flow through strong momentum re-distribution. Although the parametric study performed as part of this research also showed how

variation of the exposed electrode exposure height could be used to control the magnitude and position of the maximum jetting velocity, variation of the applied voltage was easier to implement in a more timely and (as observed) equally effective fashion. In this chapter the results of the refinement study are presented. Firstly the parametric investigation looking at the variation of the velocity profile with applied voltage immediately downstream of the actuator is presented. In the later sections of the chapter, the focus of the discussion shifts to analysis of the results pertaining to the response of the boundary layer to the refined operation of the actuator.

8.1 Parametric investigation for operation refinement

A parametric investigation was formulated to study the effects of actuator applied voltage on the control attained by the DBD system. The aim was to tune the DBD system through variation of the actuator applied voltage so as to identify what actuator applied voltage would result in the most favourable velocity profile augmentation for LFC.

The investigation involved measuring the velocity profile of the boundary layer immediately downstream of the trailing edge of the encapsulated electrode of the actuator (at $x = 243mm$), for various applied voltage values. The location was selected as the closest proximity to the plasma region (for the defined investigation region, see Chapter 6) and thus the most likely spot for instabilities to initiate. The actuator was operated at 8 different applied voltages ranging from $0kV_{pp}$ to $24.2kV_{pp}$, and the freestream velocity of the flow was fixed at $U_\infty = 5.30^{m}/_{s}$, $Re_x = 89000$. The measured velocity profiles (Figure 8.1) showed a strong dependence on the applied voltage.

At large applied voltages, the velocity profile was observed to bulge and inflect close to the wall. The size of the bulge increased with the applied voltage. In addition, at voltages above $19.0kV_{pp}$, this bulge was observed to lead to localised boundary layer velocities exceeding the freestream value. Even though the displacement thickness was observed to diminish as the voltage increased (Figure 8.2) the velocity profile inflections introduced by the high-voltages, accompanied with localised velocities within the boundary layer exceeding the freestream value, suggest that the actuators operated at applied voltages greater that $19.0kV_{pp}$ were adversely affecting the stability of the flow by easily satisfying the general criterion for instability. This conclusion was supported by the values of the shape factor for these configurations (Figure 8.3). With increasing applied voltage, the value of the shape factor was seen to drop towards 1.6, which in conjunction with the large inflections

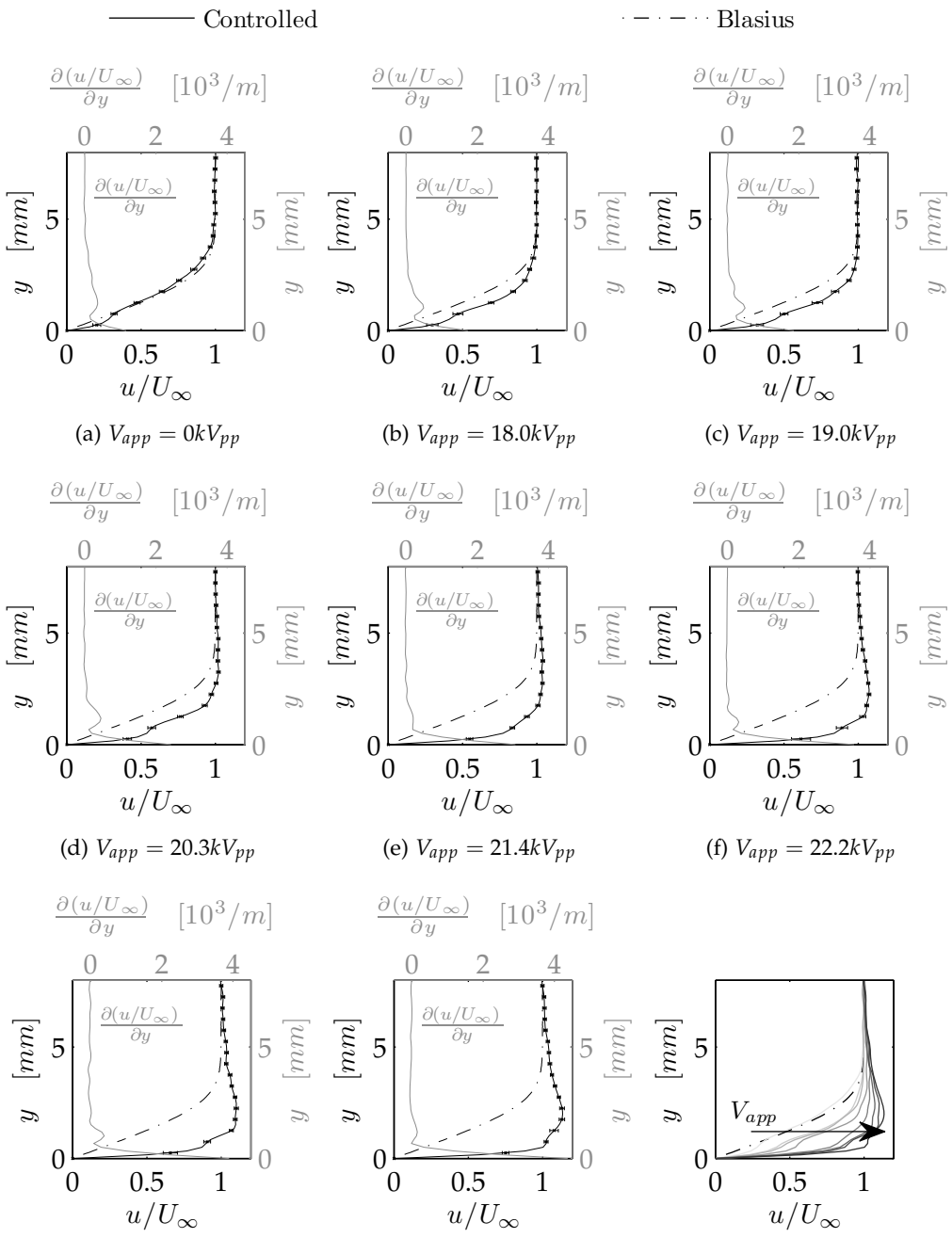

(a) $V_{app} = 0kV_{pp}$ (b) $V_{app} = 18.0kV_{pp}$ (c) $V_{app} = 19.0kV_{pp}$

(d) $V_{app} = 20.3kV_{pp}$ (e) $V_{app} = 21.4kV_{pp}$ (f) $V_{app} = 22.2kV_{pp}$

(g) $V_{app} = 23.4kV_{pp}$ (h) $V_{app} = 24.2kV_{pp}$ (i) Comparison of all

Figure 8.1: Variation in velocity profiles at $x = 243mm$ due to changes in applied voltage of the DBD actuator, $U_\infty = 5.30^m/_s$, $\frac{Re_x}{x} = 340000^1/_m$. Derivative data for controlled cases only. 'No Control' case from FPR test shown for indicative reference only.

in the respective velocity profiles, is indicative of transition to turbulent flow (Grundmann and Tropea 2007a, Grundmann and Tropea 2009).

The results of this parametric investigation supported what was observed by the mapping of the boundary layer response to the actuator operated $22.2kV_{pp}$. Most notably the results confirmed the sharp reduction in shape factor and displacement thickness that were observed in the previously discussed study, which led to the development of turbulent flow. Whilst operating the actuator at an applied voltage of $22.2kV_{pp}$ was deemed unsuitable for improving the stability of a laminar flow, the results of this parametric investigation revealed that a device operated at a lower voltage may provide stability improvements.

For applied voltages of $18.0kV_{pp}$ and $19.0kV_{pp}$, the inflections in the velocity profiles were smaller than those observed for the higher voltages, whilst there were also no instances of localised boundary layer velocities exceeding the freestream value. Whilst inflections can be an indicator of flow instability (as discussed in Chapter 2), it is more useful to assess the growth of these instabilities to asess the stability characteristics of the flow. As will be described in Section 8.2, the inflections introduced by the actuator operated at $V_{app} = 19.0kV_{pp}$ were seen to decay downstream of the actuator. Hence, it is argued that lower applied voltage values are able to augment the boundary layer in a stable fashion.

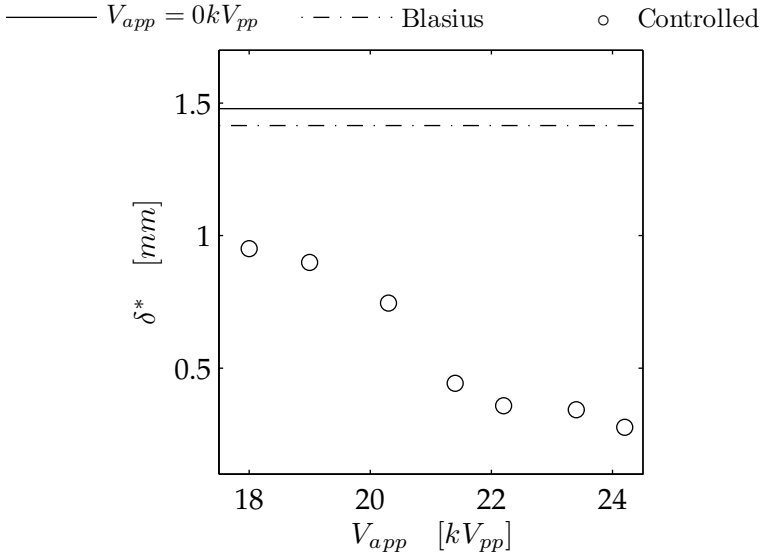

Figure 8.2: Effect of applied voltage on displacement thickness (with mild suction).

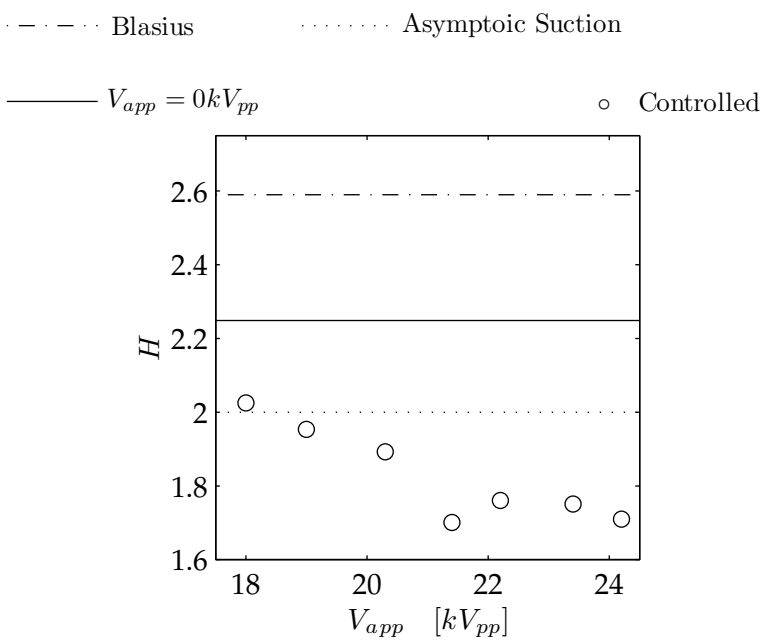

Figure 8.3: Effect of applied voltage on shape factor (with mild suction).

The shape factor of the flow augmented by the lower applied voltage actuators was found to be approximately 2 for both configurations. In addition, the augmented velocity profiles showed excellent agreement with the asymptotic suction velocity profile, with the $NRMSD$ between the measurements and theory for the two configurations being 7.1% (Figure 8.4). As discussed in Chapter 5, the objective of the research was to develop a DBD-based LFC system capable of mimicking the performance of uniform wall suction. This corresponds with a system that augments a boundary layer so as it attains a shape factor value of 2 (see Section 5.2.2). Thus the parametric investigation suggests that the actuators in such a system should be operated at lower voltages, either $18.0kV_{pp}$ or $19.0kV_{pp}$, to provide such a response, and hence support the conclusions of Chapter 3, which suggested that actuators operated at comparatively lower applied voltages (for a given set of electrical and geometric parameters) would be more beneficial to improving flow stability than comparatively higher voltage devices.

Based on the results of the parametric investigations, the response of the boundary layer to the low-voltage actuator needed to be studied and compared to the results for an actuator operated with a high applied voltage.

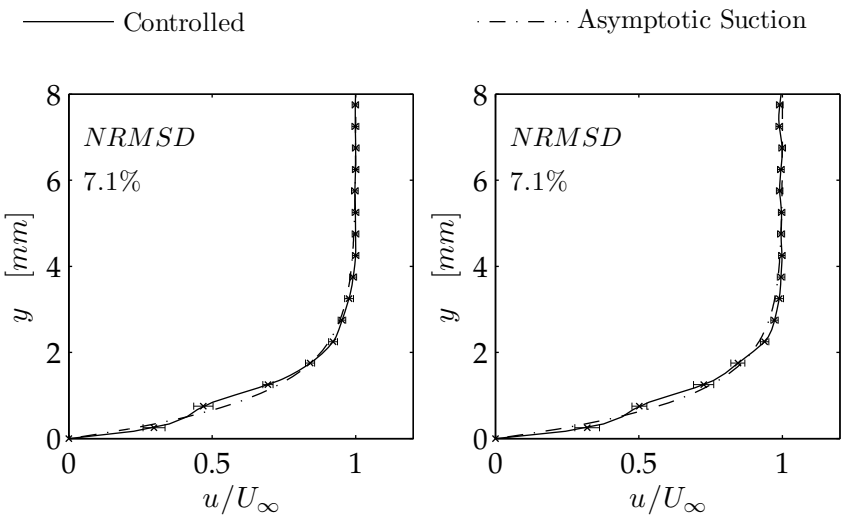

(a) $V_{app} = 18.0kV_{pp}$ (b) $V_{app} = 19.0kV_{pp}$

Figure 8.4: Comparison between asymptotic suction profile and measured velocity profiles from low-voltage augmentation and mild suction.

Of the two low-voltage values ($18.0kV_{pp}$ and $19.0kV_{pp}$) that caused the layer to attain a shape factor value of approximately 2, the subsequent mapping study investigated the response to an applied voltage of $19.0kV_{pp}$, due to the slightly thinner displacement thickness that its operation provided, which is more beneficial to improving hydrodynamic stability (Schlichting 1955).

In addition to studying the response of the layer to the low-voltage actuator operated with mild suction, a subsequent, converse study was undertaken focusing on the response of the flow to an applied voltage of $21.4kV_{pp}$. The actuator, when operated at this voltage produced the lowest shape factor value, which implied that this voltage produced the greatest degree of destabilisation within the flow. Thus, by looking at the response of the layer to this seemingly adverse actuator an investigation into a most effective DBD-based boundary layer trip could be made. More importantly, however, the results would provide further support for the hypothesis that stability improvements are dependent (amongst other factors) on the applied voltage of the actuator.

8.2 Application of OSE solver to parametric study results

To reinforce the experimental results of the parametric investigation, a Linear Stability Analysis was undertaken on an idealised flow resulting from the use of a single DBD actuator operated at an applied voltage of $19.0kV_{pp}$. The analysis used the same methodology and approach as discussed in Section 5.2.

8.2.1 Velocity profile fit

The first stage was to describe the velocity proficle in terms of the non-dimensional length and velocity variables η & $u\,(\eta)$, and the velocity function described by Equation 5.2 (with second derivative defined by Equation 5.3). Based on the experimental results, the variables a & k were selected to mimic the asymptotic suction profile. Consequently a was set to e^1 and k set to 1.113. Moreover, from the experimental results, η_e was calculated to be 2.76, and hence this value was used, as opposed to 5.3, which was used in the preliminary analyses discussed in Chapter 5.

The availability of actual experimental data obtained with the intention of use in LFC design meant that the analytical velocity profile developed for the experimental data showed much better agreement than those used in the preliminary analyses described in Section 5.2 (Figure 8.5). The $NRMSD$ was calculated to be 7.0% (as defined by Equation 5.4), comparable to the direct asymptotic suction profile value of 7.1% (Figure 8.4b). In addition, the fit agreed much better in the lower regions of the velocity profile close to the wall. Consequently, greater confidence could be placed in the results of the LSA discussed in this section.

8.2.2 LSA for experimental data

As per the analyses described in Section 5.2, the analysis using the experimental data assumed that the DBD plasma was formed by a sufficient number of actuators so as to produce similar velocity profiles (defined by Equation 5.2) throughout the entire layer.

The computational domain for the analysis was constructed in a regular, rectangular grid. The discretisation in the Re_x-direction was $1.59E+05$ (found to be necessary for a stable solution), and a spacing of 0.0278 was used in the η direction (corresponding to 100 data points in this direction).

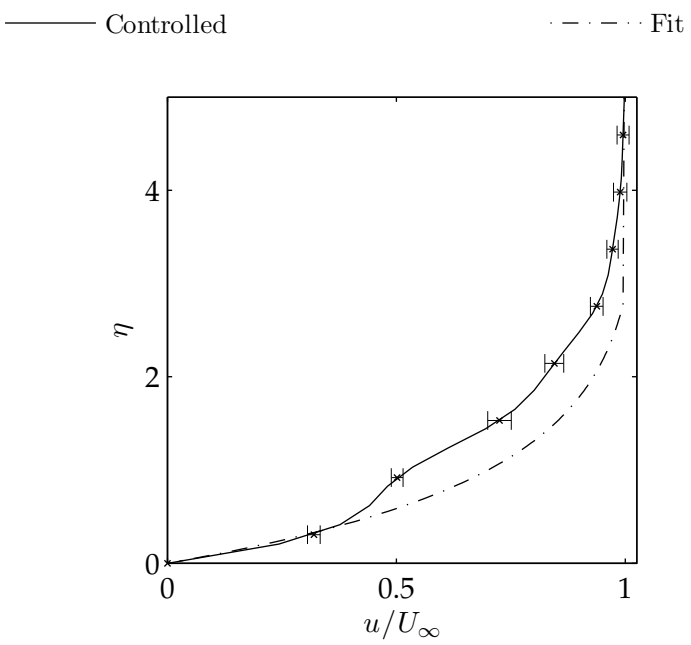

Figure 8.5: Analytical velocity profile fit to experimental data for use in the Linear Stability Analysis.

The resulting spatial and temporal curves of neutral stability (Figures 8.6 & 8.7 respectively) showed that a boundary layer flow exhibiting the assumed velocity characteristics is significantly more stable than a Blasius flow (as is to be expected). The critical Reynolds number $Re_{L_{crit}}$ was found to be 312000, two orders of magnitude higher than that for Blasius Flow ($Re_{L_{crit}} = 300$), a result consistent with the effects of uniform suction for which the critical Reynolds number is approximately 90 times greater than for Blasius flow (see Section 5.2).

Similar to the hypothesised boundary layer flows described in Section 5.2, the augmented flow analysed was seen to become susceptible to slightly smaller wavelength (higher wavenumber) and higher frequency disturbances at the critical Reynolds number (as compared with Blasius flow). However, given the significant improvement in critical Reynolds number achieved, the potential location of transition onset (related to $Re_{L_{crit}}$) is moved so far downstream that this drawback is mitigated.

The results of the Linear Stability Analysis presented here provide significant support for the use of a low-voltage actuator (as defined in this research) with mild suction. Of all the hypothesised flows studied throughout this research, the one that can mimic the response of a flat plate boundary layer

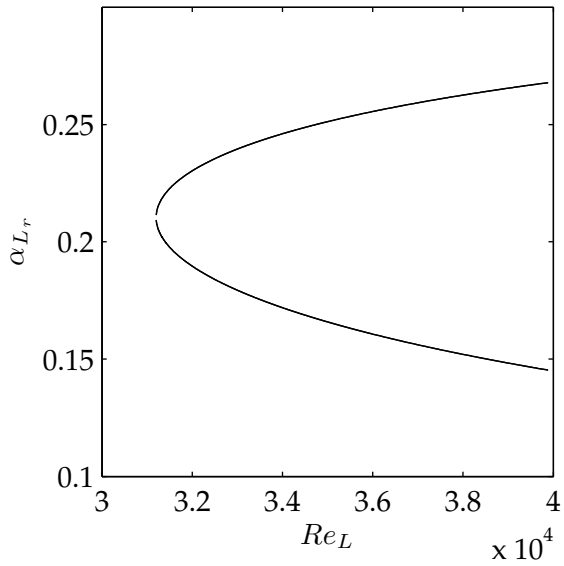

Figure 8.6: Curve of neutral stability (frequency) for the low-voltage actuator ($V_{app} = 19.0kV_{pp}$).

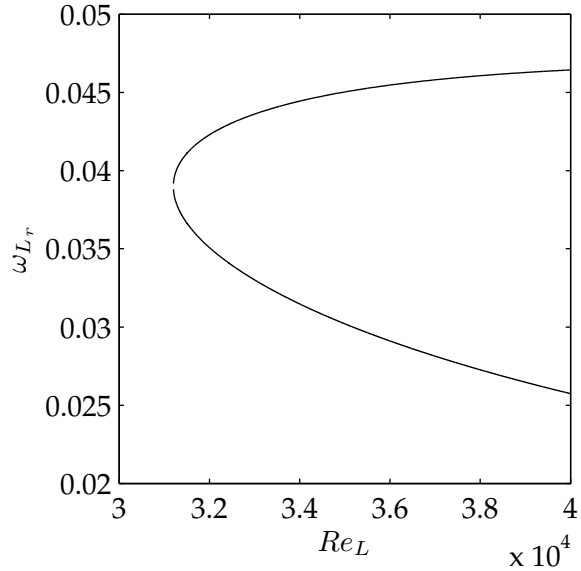

Figure 8.7: Curve of neutral stability (frequency) for the low-voltage actuator ($V_{app} = 19.0kV_{pp}$).

to this experimentally studied actuator is, based on the stability analyses conducted, the most beneficial for improving the stability of a flat plate boundary layer. Consequently, the results of the LSA presented here provide theoretical support for experimentally investigating the response of the flat plate boundary layer to the low-voltage actuator (with mild suction) system.

8.3 Flow response to refined actuator operation

8.3.1 Plasma control in conjunction with mild suction

The preliminary experimental investigations discussed in Chapter 7 suggested that orthogonal actuators would work more favourably as LFC devices if used in conjunction with a mild $4Pa$ suction effect. For this reason, the response of the flat plate boundary layer to the refined actuator applied voltages in conjunction with the mild suction effect was investigated first.

From the parametric study it was identified that an actuator operated with an applied voltage of $19.0kV_{pp}$ was the most feasible configuration that would allow the boundary layer to attain the desired controlled shape factor value of 2 (as defined in the system objectives, see Chapter 5).

When the system operated at an applied voltage of $19.0kV_{pp}$ was tested, the resultant boundary layer velocity profiles (Figure 8.8) were observed to be favourable and supportive of the hypothesis from the applied voltage parametric study. As evident in the plots of $\frac{\partial u}{\partial y}$, the inflection introduced immediately downstream of the actuator was seen to attenuate. Additional inflections appear at $x = 283mm$ but again these were observed to attenuate further downstream. Furthermore, immediately downstream of the actuator, the velocity profile was observed to be thinned by the presence of the plasma and this thinning was maintained to a distance of $50mm$ downstream of the actuator. These observations suggested that the low-voltage actuator was able to improve the stability characteristics of the flow, and preserve these over the entire investigation region.

The results for the actuator operated at $19.0kV_{pp}$ suggested good potential for actuators operated at lower applied voltages (henceforth referred to as a *low-voltage* actuator) as LFC devices. The low-voltage actuator was seen to be capable of controlling the boundary layer, augmenting its velocity profile, without destabilising the flow in the manner observed for the case of a comparatively higher applied voltage of $22.2kV_{pp}$. Apparent geometric similarities were observed to exist between the measured, augmented velocity profiles for the low-voltage actuator system, and the velocity contours of the investigation region suggested that the low-voltage actuator was not adversely

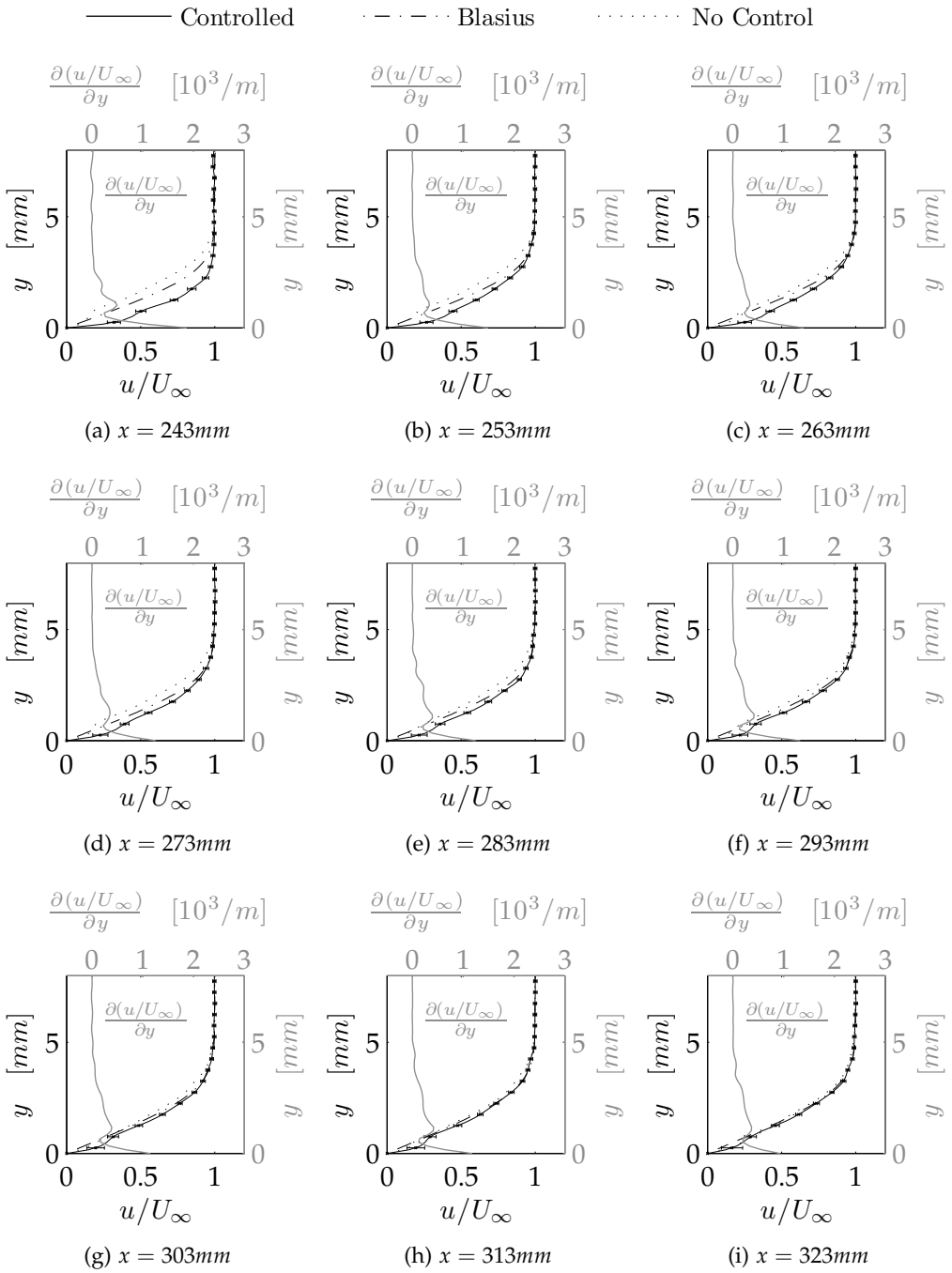

(a) $x = 243mm$ (b) $x = 253mm$ (c) $x = 263mm$

(d) $x = 273mm$ (e) $x = 283mm$ (f) $x = 293mm$

(g) $x = 303mm$ (h) $x = 313mm$ (i) $x = 323mm$

Figure 8.8: Velocity profiles with suction, $V_{app} = 19.0kV_{pp}$, $U_\infty = 5.31^m/_s$, $\frac{Re_x}{x} = 360000^1/_m$. Derivative data for controlled case only. $x = 243mm$ data from parametric study. 'No Control' case from FPR test shown for indicative reference only.

affecting flow stability and creating irregularities in the development of the boundary layer (Figure 8.9).

In contrast to the favourable benefits of the low-voltage actuator, the boundary layer was seen to become severely unstable with an applied voltage of $21.4kV_{pp}$ (Figure 8.10). Immediately downstream of the actuator, localised regions of the boundary layer were observed to exceed the velocity of the freestream. The instability arising from this seemingly damped initially, before amplifying at $x = 283mm$ at the location where other instabilities were observed to enter the upper regions of the boundary layer. Some damping of these additional instabilities were observed to occur further downstream, however, this damping was accompanied with an increase in the shear of the fluid at the wall. In addition, at $x = 313mm$ the instabilities were observed to locally retard the boundary layer, with localised regions experiencing velocities less than the values for the corresponding base flow. Rather than suggesting that the flow was behaving stably, the most-downstream velocity profile measurements indicated the onset of an increasingly turbulent boundary layer structure, and this observation was supported by the observed rapid thickening of the boundary layer downstream of $x = 293mm$ (Figure 8.11).

The response of the boundary layer to an applied voltage of $21.4kV_{pp}$ (henceforth referred to as a *high-voltage*) actuator was seen to be more chaotic

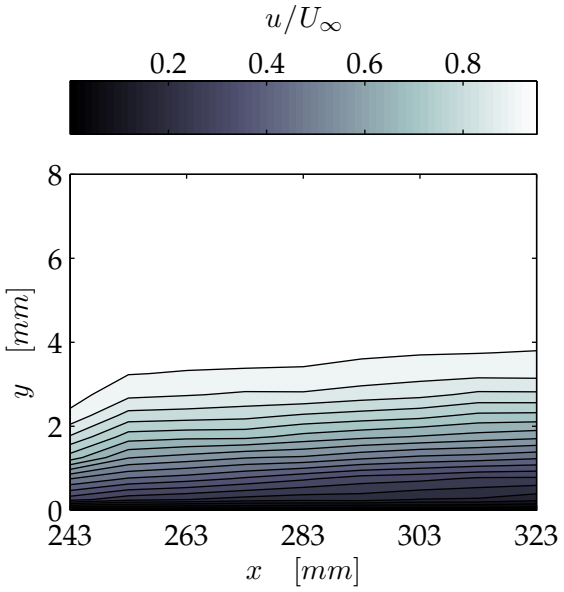

Figure 8.9: Velocity contours with suction, $V_{app} = 19.0kV_{pp}$, $U_\infty = 5.31^{m}/_{s}$, $\frac{Re_x}{x} = 360000^{1}/_{m}$.

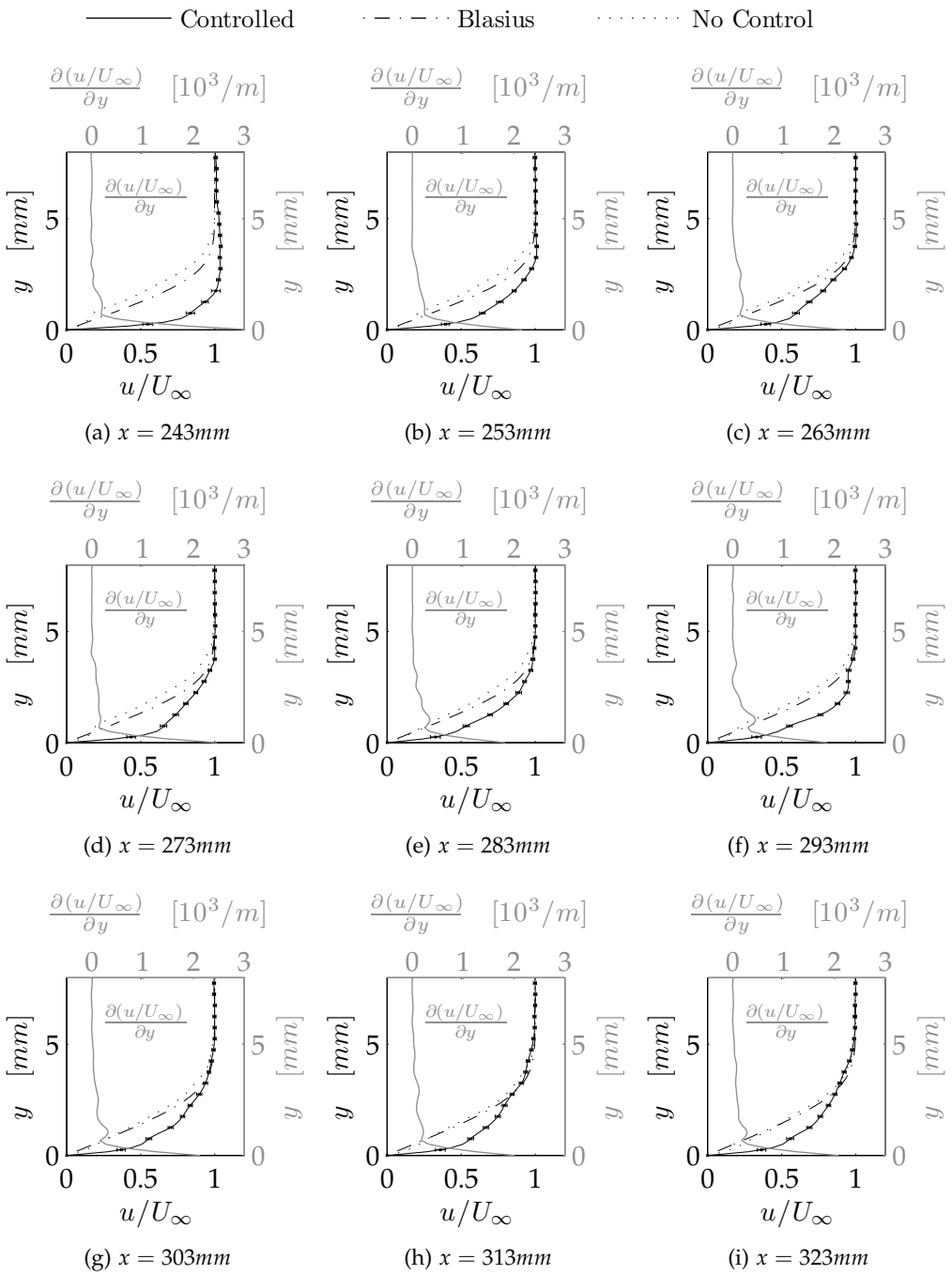

(a) $x = 243mm$ (b) $x = 253mm$ (c) $x = 263mm$

(d) $x = 273mm$ (e) $x = 283mm$ (f) $x = 293mm$

(g) $x = 303mm$ (h) $x = 313mm$ (i) $x = 323mm$

Figure 8.10: Velocity profiles with suction. $V_{app} = 21.4kV_{pp}$, $U_\infty = 5.60^m/_s$, $\frac{Re_x}{x} = 370000^1/_m$. Derivative data for controlled case only. $x = 243mm$ data from parametric study. 'No Control' case from FPR test shown for indicative reference only.

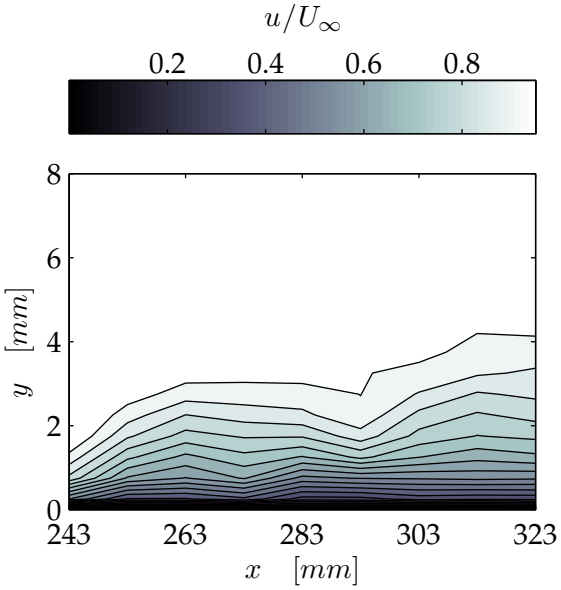

Figure 8.11: Velocity contours with suction, $V_{app} = 21.4kV_{pp}$, $U_\infty = 5.60^{m}/_{s}$, $\frac{Re_x}{x} = 370000^{1}/_{m}$.

and spatially varying than that observed for an applied voltage of $22.2kV_{pp}$. Thus, as predicted by the parametric study, there appears to be a most adverse applied voltage that leads to dramatic destabilisation of the flow, and this voltage is comparatively high.

Further support for the use of low-voltage actuators for LFC is garnered by studying the spatial evolutions of the displacement thickness (Figure 8.12) and shape factor of the flow (Figure 8.13). The use of low-voltage actuators reduced the displacement thickness over the entire mapped area, and until $x = 293mm$ the thinning was more dramatic than that experienced by the flow when it was only exposed to the mild suction (Figure 8.12a). More important however was that the spatial thickening of the boundary layer with the combined plasma and suction was monotonic, and differed dramatically to the fluctuations in displacement thickness observed for the high-voltage device. Even though the boundary layer attained its lowest displacement thickness values with the high-voltage actuator, the fluctuations in the measured values suggested destabilisation of the flow occurred. Such a fluctuation was also seen in the case with just the mild suction effect, and this indicated that the low-voltage plasma actuator used in conjunction with the mild suction was able to control the boundary layer without destabilising the flow.

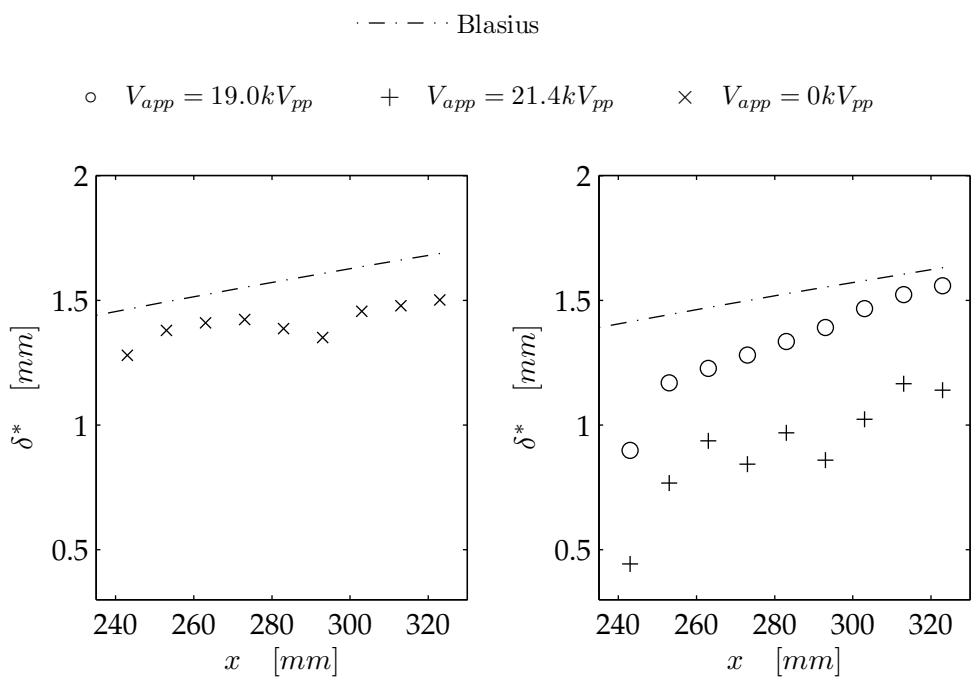

(a) Without plasma

(b) With plasma

Figure 8.12: Evolution of displacement thickness for configurations with mild suction.

Investigation of the evolution of the shape factor again supports the use of low-voltage actuators for a LFC system. Use of the high voltage actuator was seen to cause a rapid drop in the value of the shape factor towards 1.6, which was consistent with destabilisation of the flow. Conversely, use of the low-voltage device caused the shape factor of the flow to attain a value of approximately 2 (the desired value) for roughly $40mm$ downstream of the device. Further downstream the values began to increase, but they did so monotonically and without exceeding the value for Blasius flow. Until $x = 303mm$ the shape factor values were less than or equivalent to the values with just suction (Figure 8.13). From these observations it was concluded that the combined low voltage DBD and suction system can be used to augment the behaviour of the boundary layer in a way to improve the stability of the flow, and that this low-voltage system is the best performing of the configurations used in conjunction with suction.

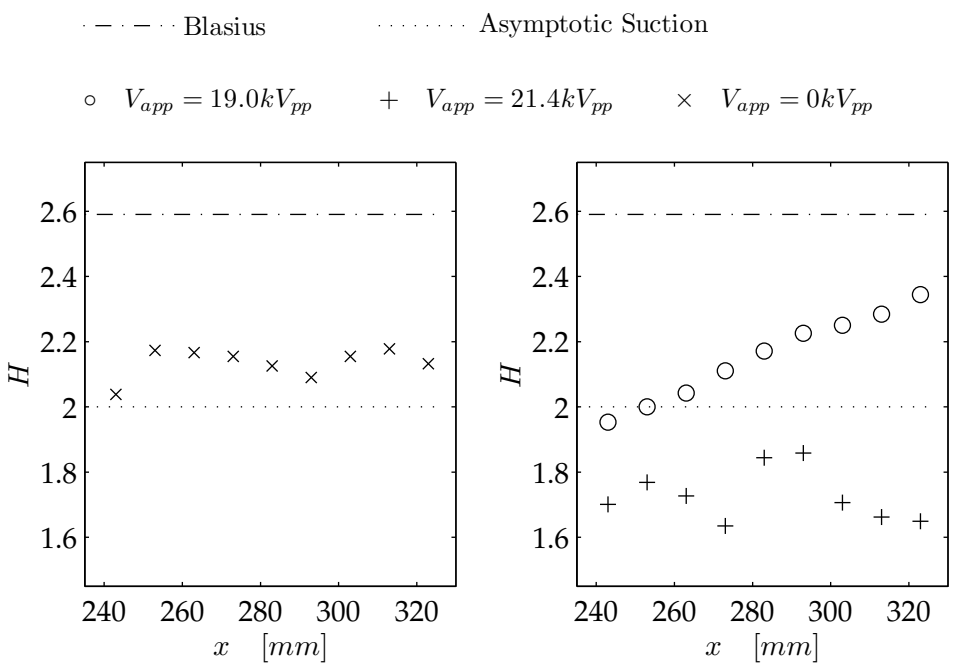

(a) Without plasma

(b) With plasma

Figure 8.13: Evolution of shape factor for configurations with mild suction.

8.3.2 Plasma control without suction

The response of the boundary layer to just the plasma actuator, without the additional suction effect, was also studied in order to obtain further results and insights into the capabilities of the orthogonal actuator system. Although the results of the preliminary experimental investigations suggested that such an arrangement created greater instability in the flow, it was deemed to be of interest to investigate whether similar destabilisation of the flow would occur with the low-voltage actuator.

The use of the low-voltage actuator was found to again dramatically thin the boundary layer and create fuller velocity profiles, similar to the case with suction. However, it did this whilst introducing a slight destabilisation of the flow (Figure 8.14). At $x = 243mm$ an inflection in the velocity profile was seen, in conjunction with a drop in the boundary layer thickness at this point (Figure 8.15), and this instability was observed to grow downstream, as seen in the growth of the maxima/minima of the $\frac{\partial u}{\partial y}$ plot. Although the growth was not dramatic, it is likely that the flow was marginally stable to the instability in the investigation region, and that ultimately the instability would have grown further downstream, beyond the area investigated. Hence,

since the instability was not damped, it would be unwise to claim that the low-voltage actuator without suction improved the stability of the flow.

Consistent with the observations for the LFC systems with suction, use of the high-voltage actuator in the absence of suction was seen to destabilise the boundary layer. An inflection in the velocity profile was observed at $x = 243mm$, and this instability was seen to amplify downstream whilst other instabilities were observed to enter the boundary layer (Figure 8.16). Some damping of these additional instabilities were observed to occur further downstream, however, this damping was accompanied with an increase in the shear of the fluid. Along with oscillatory thinning and thickening of the boundary layer was obvious downstream of the actuator (Figure 8.17), these observations indicated destabilisation of the flow.

The evolution of the displacement thickness for the two cases without suction again supported the use of low-voltage actuators. Both applied voltages drastically thinned the boundary layer, but the boundary layer exposed to the high-voltage actuator experienced significant oscillations in the displacement thickness, indicative of flow destabilisation (Figure 8.18). The evolution of the displacement thickness for the low-voltage case was not monotonic, with a slight decrease occurring at $x = 273mm$. This point was noticeable on the contour plot for this case (Figure 8.15) where there was a sharp drop in the thickness of the layer. As previously discussed it is believed that this sudden reduction in thickness was due to the observed instability in the boundary layer introduced by the plasma device that was not damped. Therefore, whilst the low voltage actuator did not destabilise the flow to the same extent as the high-voltage device, it would be unwise to use such an actuator without a slight suction effect.

The evolution of the shape factor of the boundary layer (Figure 8.19) supported the conclusions from the analysis of the displacement thickness evolution. For the high-voltage actuator, the shape factor dropped off suddenly and remained low, at around 1.6, suggestive of the onset of transitional flow. The low-voltage actuator was seen to initially reduce the shape factor below 2, but then it recovered and remained close to 2 for the entire region under investigation. However, the instability that was present and apparently undamped could not be ignored, and consequently, in this case, the seemingly good shape factor values attained with the use of the low-voltage actuator did not indicate improvements in the stability of the flow.

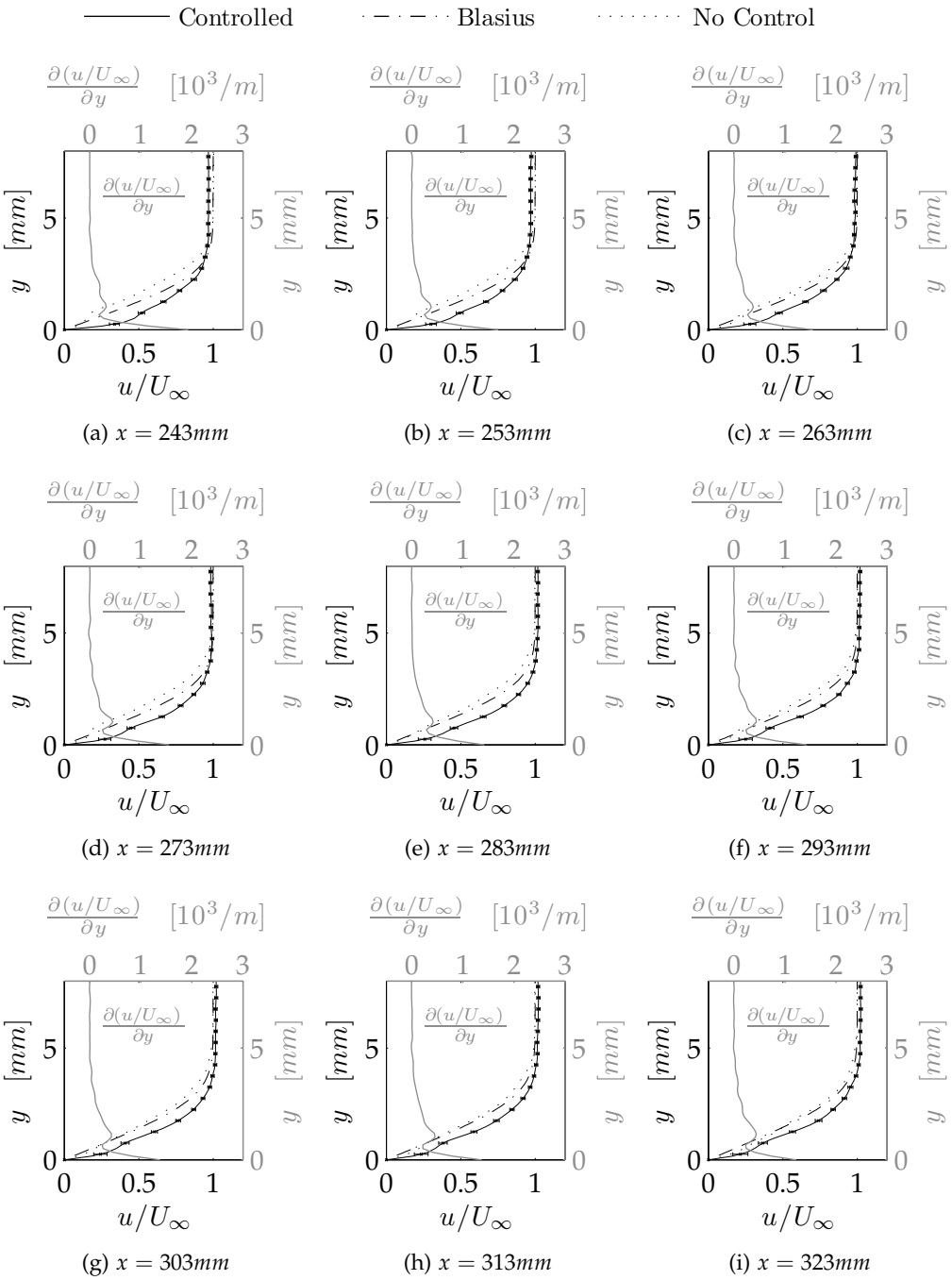

(a) $x = 243mm$ (b) $x = 253mm$ (c) $x = 263mm$

(d) $x = 273mm$ (e) $x = 283mm$ (f) $x = 293mm$

(g) $x = 303mm$ (h) $x = 313mm$ (i) $x = 323mm$

Figure 8.14: Velocity profiles without suction, $V_{app} = 19.0kV_{pp}$, $U_\infty = 5.50^m/_s$, $\frac{Re_x}{x} = 360000^1/_m$. Derivative data for controlled case only. 'No Control' data from FPR test shown for indicative reference only.

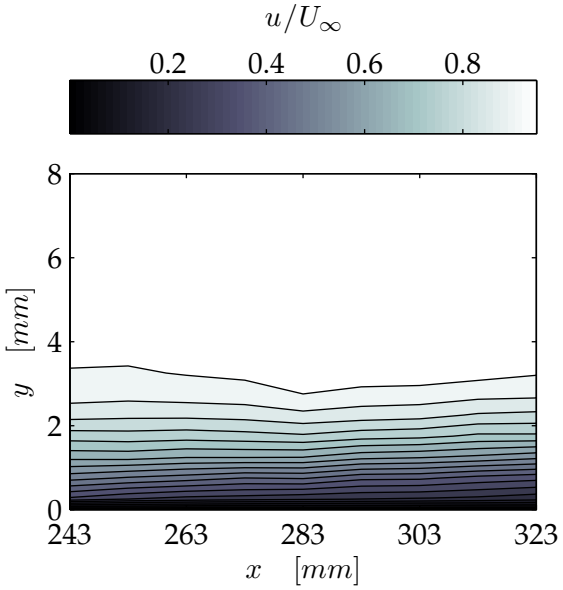

Figure 8.15: Velocity contours without suction, $V_{app} = 19.0kV_{pp}$, $U_\infty = 5.50^{m}/_{s}$, $\frac{Re_x}{x} = 360000^{1}/_{m}$.

8.4 Summary & conclusions

In an attempt to achieve improvements to hydrodynamic stability using orthogonal actuators, a parametric investigation was undertaken looking at the response of the boundary layer, at the most immediate downstream location from the actuator, to variations in the applied voltage of the actuator. The velocity profile of the boundary layer was measured at $x = 243mm$ for various applied voltages as operated in conjunction with a mild suction effect. Using the criteria of keeping the shape factor close to 2, it was identified that an applied voltage of $19.0kV_{pp}$ (a *low-voltage* actuator) produced a velocity profile augmentation that would most favourably improve the stability of the flow, and do so in a way that could not be achieved by mild suction alone. This observation was supported by a Linear Stability Analysis performed on a idealised flow exhibiting characteristics of a flow augmented by this system. The results of the LSA showed that if such flow control can be maintained throughout the layer, then the critical Reynolds number can potentially be improved by teo orders of magnitude. Conversely, a voltage of $21.4kV_{pp}$ (a *high-voltage* actuator) was identified as the most adverse applied voltage and the value that would produce the most detriment to the stability of the flow.

The results of the investigations that followed the parametric study sup-

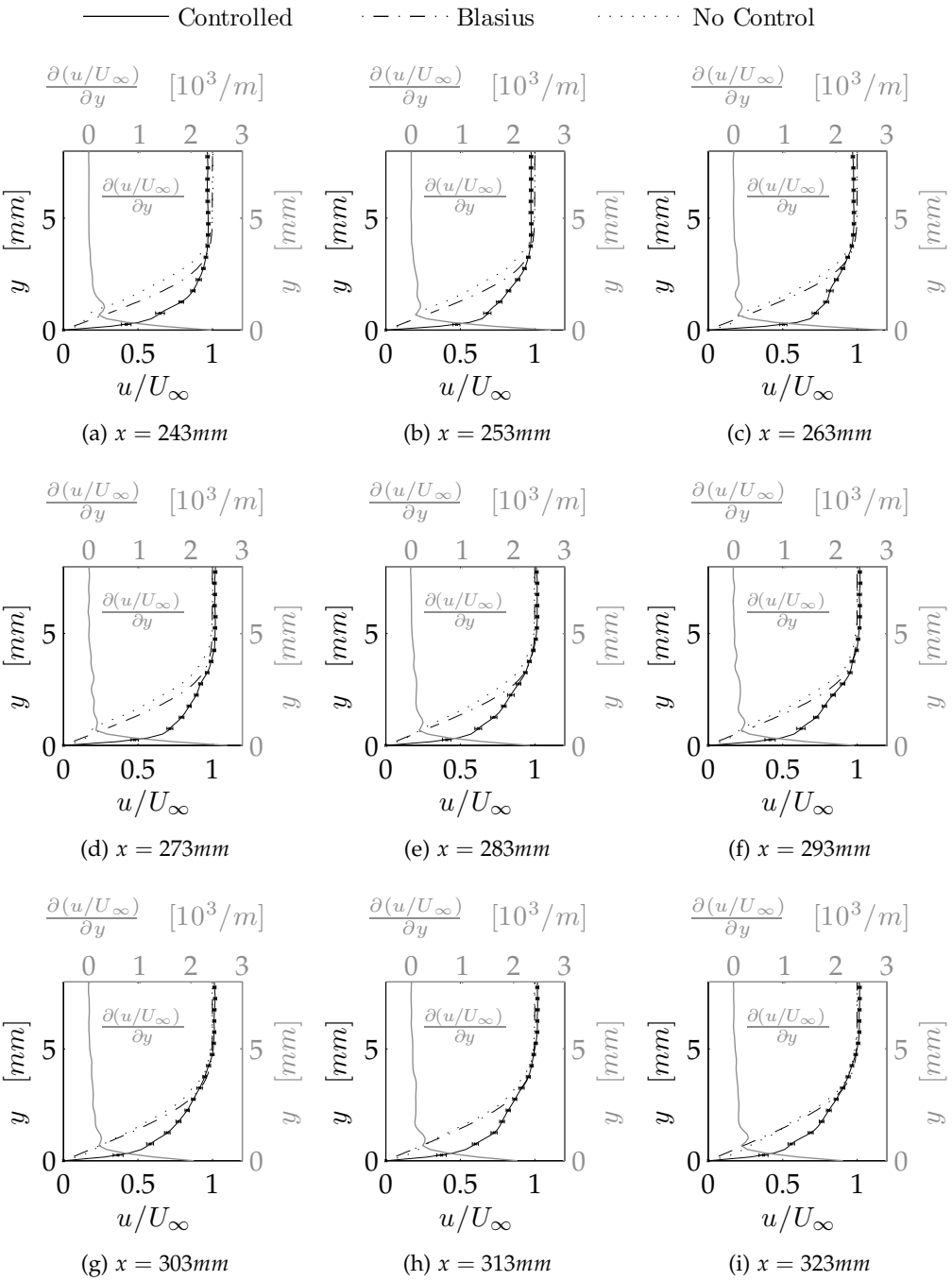

(a) $x = 243mm$ (b) $x = 253mm$ (c) $x = 263mm$

(d) $x = 273mm$ (e) $x = 283mm$ (f) $x = 293mm$

(g) $x = 303mm$ (h) $x = 313mm$ (i) $x = 323mm$

Figure 8.16: Velocity profiles without suction, $V_{app} = 21.4kV_{pp}$, $U_\infty = 5.51^m/_s$, $\frac{Re_x}{x} = 370000^1/_m$. Derivative data for controlled case only. 'No Control' case from FPR test shown for indicative reference only.

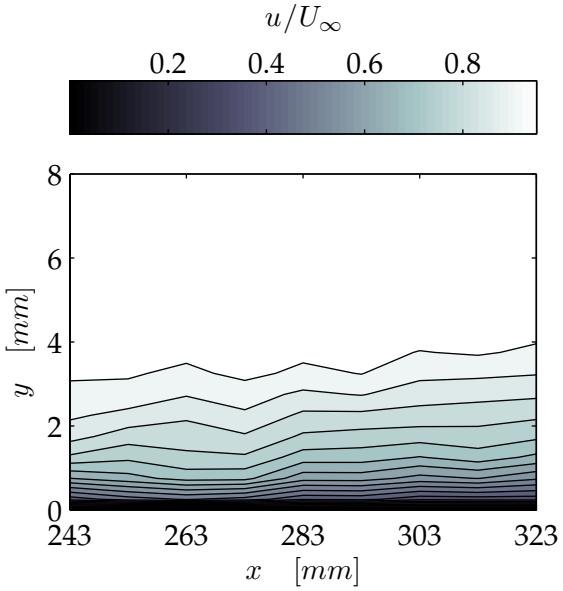

Figure 8.17: Velocity contours without suction, $V_{app} = 21.4kV_{pp}$, $U_\infty = 5.51^m/_s$, $\frac{Re_x}{x} = 3700001/_m$.

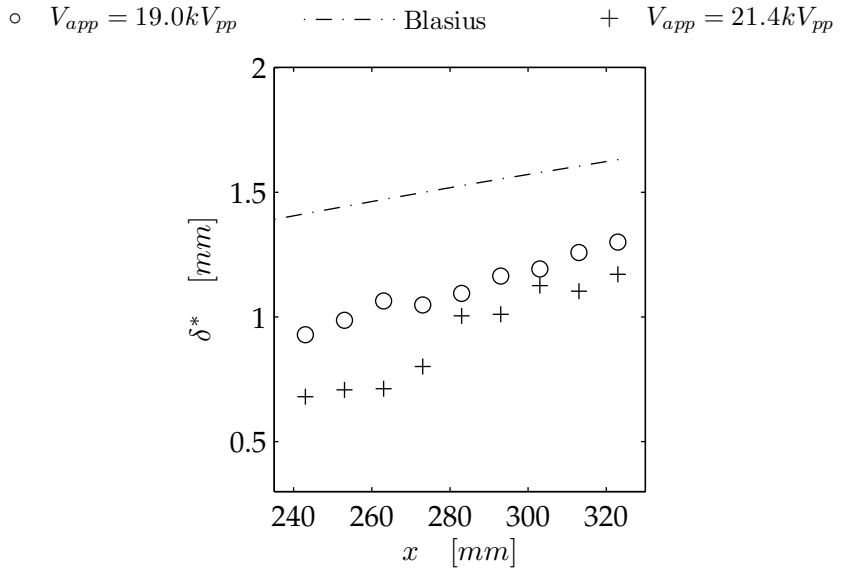

Figure 8.18: Evolution of displacement thickness for configurations without suction.

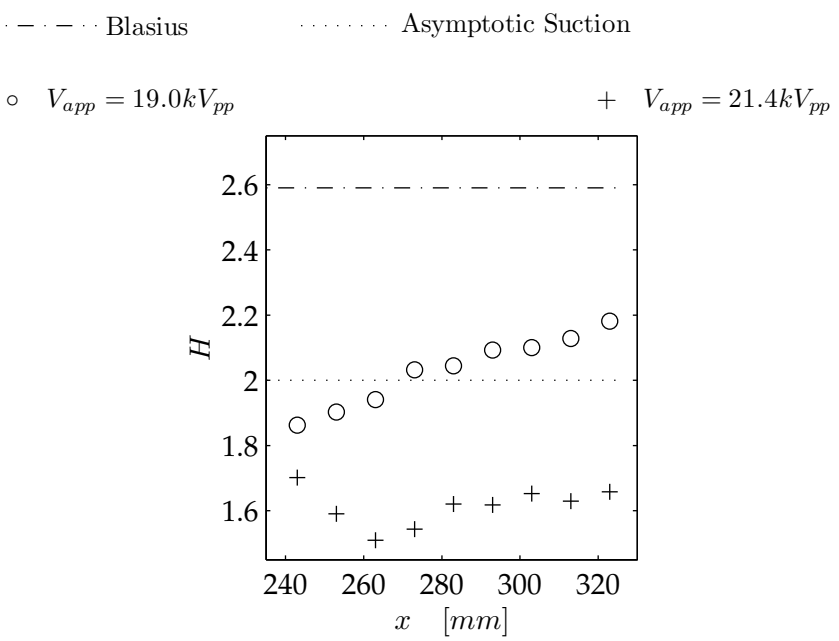

Figure 8.19: Evolution of shape factor for configurations without suction.

ported the resulting hypothesis from the parametric investigations. Without the mild suction effect, the flow was seen to become destabilised, and additionally the high-voltage actuator used in conjunction with the suction effect was seen to adversely affect the stability of the boundary layer. Conversely, the low-voltage device was seen to provide improvements to the flow stability, compelling the boundary layer to attain a lower shape factor over the entire region investigated, without destabilising the flow. Furthermore, the shape factor of the flow attained a value close to 2 for a distance of $50mm$ downstream of the actuator; boundary layer control that could not be achieved with the mild suction alone. Hence the investigation successfully demonstrated a LFC system using orthogonal actuators that performed as required.

Having identified that the low-voltage actuator, in conjunction with the mild suction effect, was able to reduce the shape factor of the flow to the desired value for approximately $50mm$, the subsequent challenge is to maintain the value further downstream. A dramatic drop in shape factor was observed to occur immediately downstream of an actuator, suggesting that subsequent downstream actuators may provide a means by which the reduced shape factor can be maintained. The subsequent investigation focusing on the use of multiple actuators for this purpose is discussed in the next chapter.

9 Attempting to Maintain the Stability Improvements

The response of the flat plate boundary layer to a single orthogonal actuator was initially investigated during this research project and it was found that the stability of the flow is dependent on the applied voltage of the actuator. By using a low voltage actuator, in conjunction with a mild suction effect, the resultant Laminar Flow Control system was found to reduce the shape factor without destabilising the flow for a significant distance downstream of the plasma region. This reduction in shape factor was accompanied by a thinning of the displacement thickness of the flow, but this effect dissipated downstream of the device, with a monotonic increase in both the displacement thickness and shape factor occurring. Trying to maintain the stability improvements was the unsolved challenge resulting from the previous investigations, and in this chapter the results at an attempt to increase the extent of the LFC are presented.

The results of the previous investigations highlighted that significant reductions in both shape factor and displacement thickness occur immediately downstream of the actuator. Hence, by incorporating a second, subsequent, and identical actuator downstream of the first, it was hypothesised that the stability improvements could be maintained. The experimental investigation formulated to test this hypothesis involved placing a second actuator $40mm$ downstream of the first. This distance corresponded with the region where the shape factor value for the case of the low voltage actuator with suction had significantly diverged away from the desired controlled value of 2. The actuators were manufactured from two pieces of acrylic and the design was based on the dimensions of the device used in the single actuator investigations (see Chapter 6, Figure 6.9). Hence the electrodes for each actuator were placed in the same relative positions as used in the single actuator investigations, and the same method of connecting the plasma generator to the electrodes was also used. The only two differences in the design of the

actuators pertained to the total lengths of the devices. The total chordwise lengths of the devices were $60mm$ (reduced from $120mm$) and the lengths of the internal actuator components were also reduced from $60mm$ to $35mm$, in accordance with the actuator positioning requirements of the investigation (Figure 9.1). As was the case for the single actuator, a $5mm$ gap was placed between the trailing edge of the flat plate and the leading edge of the first actuator, as well as between the two actuators so as to allow the actuators enough free space to produce a useful plasma discharge.

To provide a significant database of results, which could be used to support the conclusions of the previous single actuator studies, the double actuator configuration was tested with and without the mild suction effect for applied voltages of $19.0kV_{pp}$ (the most favourable, low voltage) and $21.4kV_{pp}$ (the most adverse, high voltage). Again, measurements were made from $x = 243mm$ to $x = 323mm$ in accordance with the procedures discussed in Section 6.6, with the exception that measurements between $x = 263mm$ and $x = 303mm$ could not be obtained due to the formation of the second plasma region.

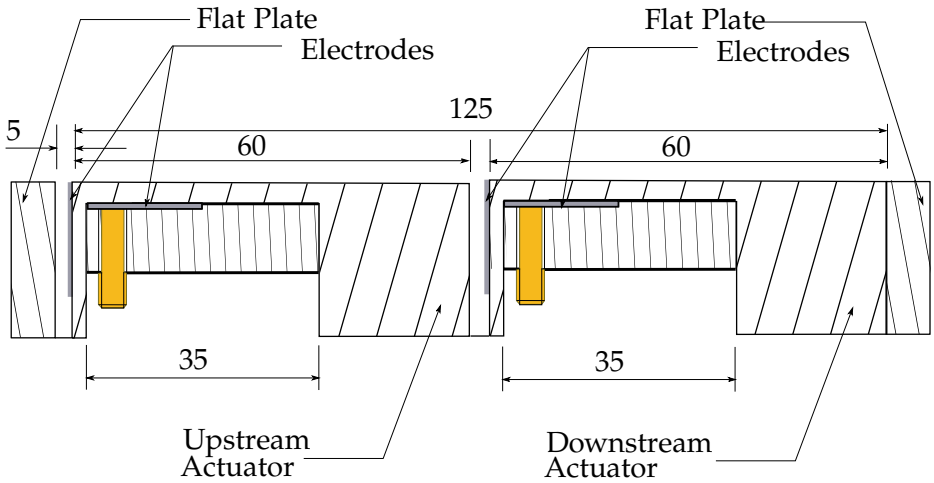

Figure 9.1: Schematic representation of arrangement of double actuators showing critical dimensions (in mm) differing to those of the single actuator.

9.1 Flow response to double actuator operation

9.1.1 Plasma control in conjunction with mild suction

The response of the boundary layer to just the mild suction effect created by the two slots was measured first as a reference against which to gauge the effect of the DBD plasma. The suction was observed to significantly augment and thin the boundary layer, without the introduction of any noticeable instabilities in the measured velocity profiles which significantly amplified downstream of the actuators (Figure 9.2). The velocity contour plots reflected these observations, with a significantly thinned layer maintaining its laminar characteristics throughout the investigation region being seen (Figure 9.3).

The most obvious observation for the results involving the low voltage actuators with suction was the introduction of a significant inflection point in the most upstream velocity profile (Figure 9.4a). This instability however, was seen to attenuate quickly and was not significantly noticeable beyond $x = 263mm$ (Figure 9.4). Downstream of the second actuator, another inflection was noticeable, but again, this was found to attenuate rapidly downstream. Thus, the low voltage actuators were seen to successfully augment the layer without destabilising it. In addition the augmentation was stronger in the downstream regions than had been previously observed with the use of only a single actuator (see Chapter 8), with increased thinning, even more dramatic than that observed with just the double suction slot (Figure 9.5).

The response of the boundary layer to the high voltage actuators again provided support for the use of low voltage devices. In the velocity profile measurements (Figure 9.6), the upstream plasma actuator was seen to introduce an inflection, which amplified downstream. Similarly, downstream of the second actuator, significant amplification of velocity profile inflections was observed. Thus, these observations suggested that the high voltage actuators were more effective at destabilising the flow.

Further support for the use of low voltage actuators was gleaned from the velocity contours for the high voltage system (Figure 9.7). The velocity contour measurements reflected these previously mentioned conclusions, with more irregular growth in the boundary layer throughout the investigation region being observed.

The evolution of the displacement thickness showed that of the three different configurations tested, the systems operated with just the mild suction force and the low voltage actuators had the seemingly most beneficial effect (Figure 9.8). The value of the displacement thickness was approximately constant for both systems ($0.85mm$ and $0.92mm$ respectively) over the entire

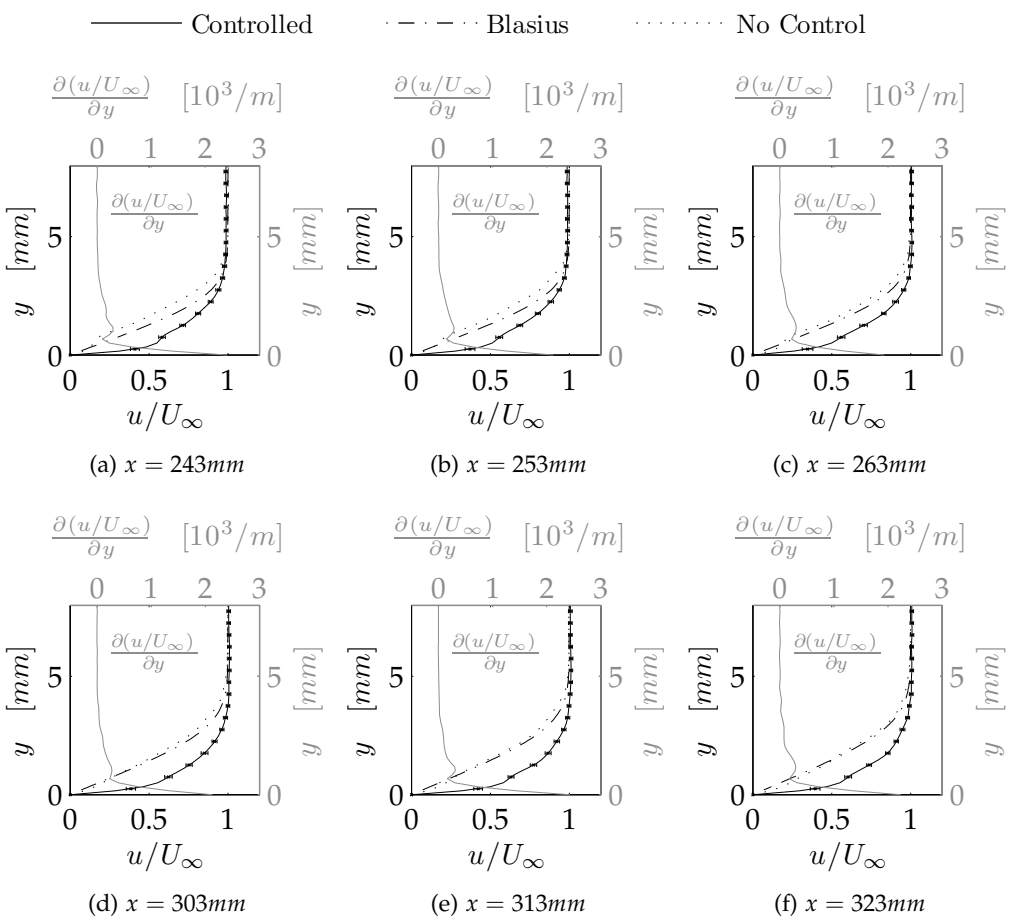

(a) $x = 243mm$ (b) $x = 253mm$ (c) $x = 263mm$

(d) $x = 303mm$ (e) $x = 313mm$ (f) $x = 323mm$

Figure 9.2: Velocity contours for the boundary layer exposed to the mild suction only, $U_\infty = 5.39^m/_s$, $\frac{Re_x}{x} = 360000^1/_m$. Derivative data for controlled case only. 'No Control' case from FPR test shown for indicative reference only.

length of the investigation. Conversely, the use of the high voltage actuators created large oscillations in the values of the displacement thickness, which according to Howe (1981) was indicative of disturbed flow.

The evolution of the shape factor for the configurations tested again supported the notion that high voltage actuators adversely affect the stability of a laminar boundary layer flow (Figure 9.9). The use of the high voltage actuators caused the boundary layer to attain an average shape factor value of approximately 1.6 throughout the entire investigation region, suggesting that the flow had become turbulent.

Interestingly, the evolution of the shape factor for the low voltage case, as well as the suction only case, showed that these two configurations caused

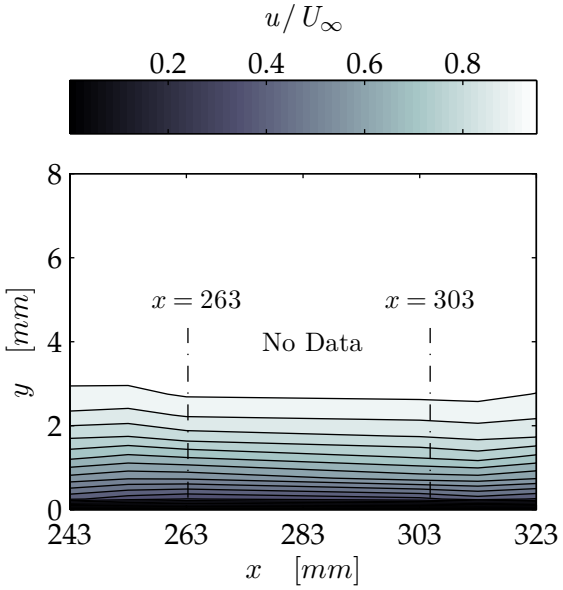

Figure 9.3: Velocity contours for the boundary layer exposed to the mild suction only, $U_\infty = 5.39^{m}/_{s}$, $\frac{Re_x}{x} = 360000^{1}/_{m}$. Data linearly interpolated between $x = 263mm$ and $x = 303mm$.

the shape factor to drop below that of the desired value of 2. However, throughout the investigation regions, the fact that the shape factor for both cases did not drop below 1.6 as well as the lack of amplification of inflections in the downstream velocity measurements, meant that stable laminar flow was probably being preserved (Grundmann and Tropea 2007b, Ogata and Fujita 2009). The system with the low voltage actuators achieved a mean shape factor value of 1.78 compared with 1.72 for the suction-only system, which was closer to the desired value of 2. However, the similarities in these shape factor values, as well as the displacement thickness values, suggested that the low voltage actuator system was having little additional influence over the effect of the mild suction force alone. Hence, in the tested configuration, it was somewhat superfluous to use the combined double-low-voltage actuator/suction system.

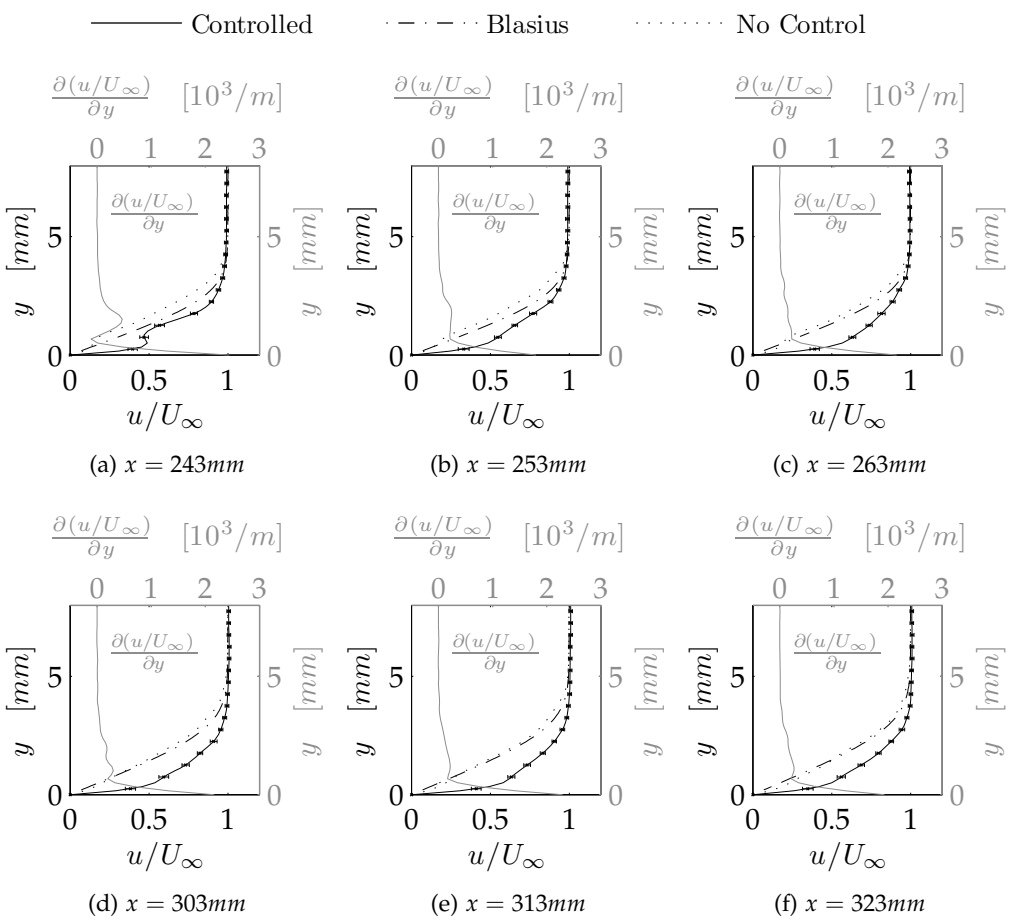

(a) $x = 243mm$ (b) $x = 253mm$ (c) $x = 263mm$

(d) $x = 303mm$ (e) $x = 313mm$ (f) $x = 323mm$

Figure 9.4: Velocity profiles with suction, $V_{app} = 19.0kV_{pp}$, $U_\infty = 5.38^m/_s$, $\frac{Re_x}{x} = 360000^1/_m$. Derivative data for controlled case only. 'No Control' case from FPR test shown for indicative reference only.

9.1.2 Plasma control without suction

Consistent with the results for the single orthogonal actuator, the use of two orthogonal actuators without the mild suction effect was seen to destabilise the flow. The use of two low voltage actuators was seen to introduce an inflection into the velocity profile immediately downstream of the upstream actuator, and inflections were still present and becoming amplified in the flow at the most downstream measurement location, $x = 323mm$ (Figure 9.10), thereby satisfying the general criterion for instability. The destabilisation of the boundary layer caused by the plasma was also seen in the velocity contours (Figure 9.11) where irregularities in the growth of the boundary layer thickness were noticeable.

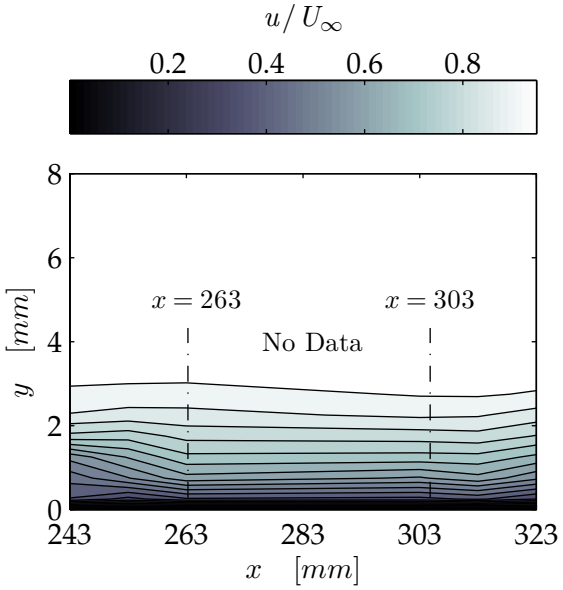

Figure 9.5: Velocity contours with suction, $V_{app} = 19.0kV_{pp}$, $U_\infty = 5.38^{m}/_{s}$, $\frac{Re_x}{x} = 360000^{1}/_{m}$. Data linearly interpolated between $x = 263mm$ and $x = 303mm$.

The high voltage actuator system similarly destabilised the flow, with inflections being observed to grow downstream of the second actuator (Figure 9.12). Interestingly, the inflections downstream of the upstream actuator were observed to experience some initial damping, and hence the second actuator seemingly improved the flow between the two regions of plasma. This effect was also observed slightly in the low voltage case, but the attenuation of the inflections in this region was not achieved to the same degree as with the high voltage devices. However, as was the case with the low voltage devices, the high voltage actuators were unable to maintain the attenuation over the whole investigation region, and instabilities were seen to infiltrate the layer in the regions downstream of the second actuator. Hence the high voltage system was again seen to have an adverse effect on flow stability, and the effect was observed to be greater than that produced by the low voltage system

The velocity contours for the high voltage actuator system show similar traits to those for the low voltage system (Figure 9.13). Hence, no extra conclusions were able to be drawn from study of the velocity contours for the high voltage case.

The evolution of the displacement thickness of the boundary layer was

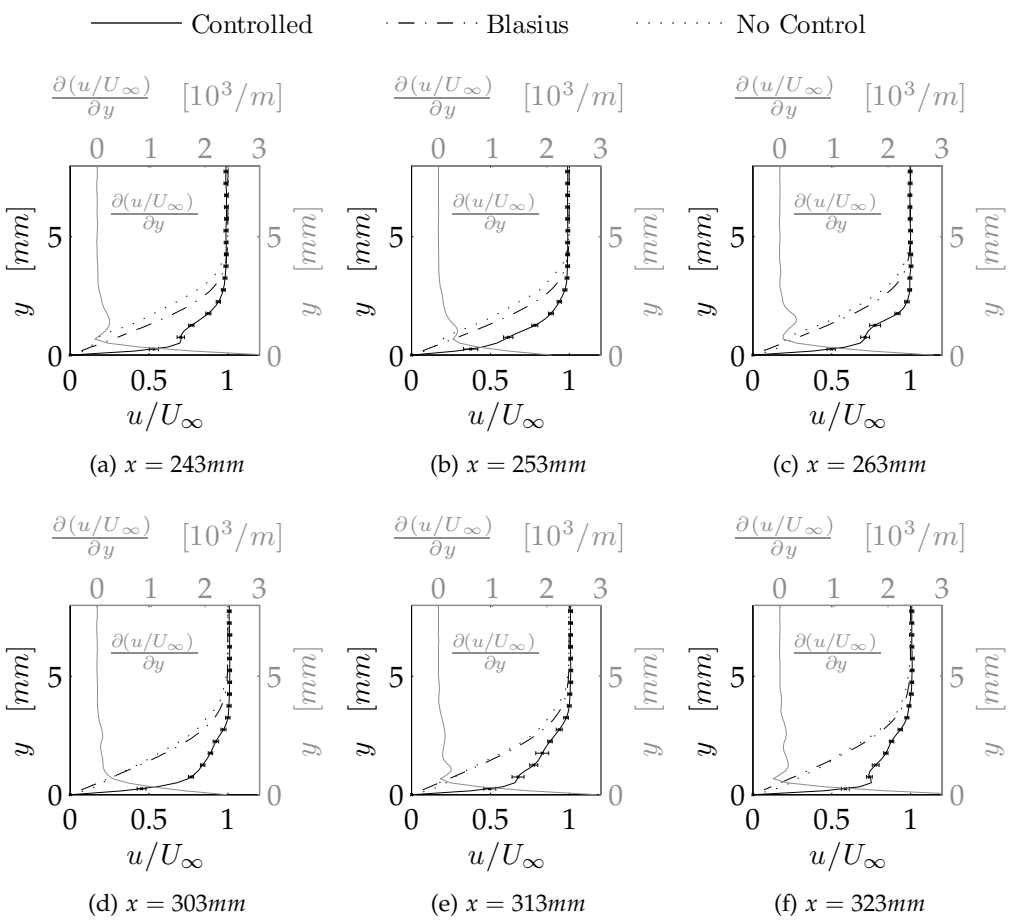

(a) $x = 243mm$ (b) $x = 253mm$ (c) $x = 263mm$

(d) $x = 303mm$ (e) $x = 313mm$ (f) $x = 323mm$

Figure 9.6: Velocity profiles with suction, $V_{app} = 21.4kV_{pp}$, $U_\infty = 5.36^m/_s$, $\frac{Re_x}{x} = 360000^1/_m$. Derivative data for controlled case only. 'No Control' case from FPR test shown for indicative reference only.

found to be almost identical for both the low voltage and high voltage double actuator configurations without suction (Figure 9.14). The displacement thickness was seen to increase until $x = 263mm$, before experiencing a sharp reduction through the actuators, such that at the most downstream location the displacement thickness was lower than the value at $x = 263mm$. The values were similar to those measured for the case with mild suction, and given the fact that the velocity profiles exhibited undamped inflections throughout the measurement region, the fluctuations in the displacement thickness values for both cases were suggestive of flow destabilisation.

The evolution of the shape factor values for the cases without mild suction (Figure 9.15) differed slightly to the results with suction. Both the high and

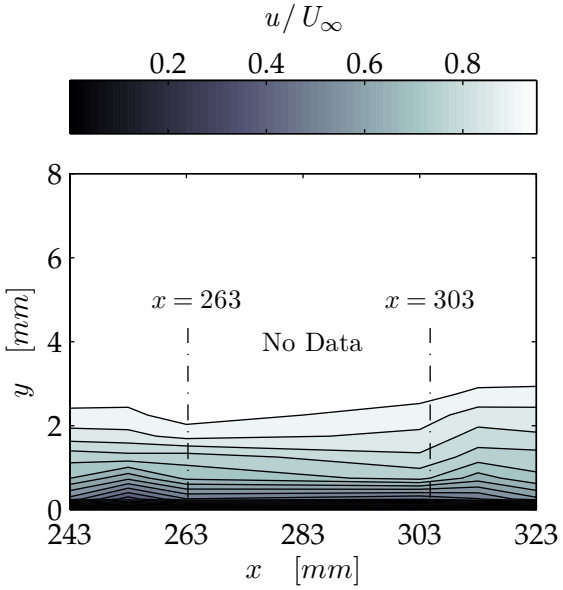

Figure 9.7: Velocity contours with suction, $V_{app} = 21.4kV_{pp}$, $U_\infty = 5.36^{m}/_{s}$, $\frac{Re_x}{x} = 360000^{1}/_{m}$. Data linearly interpolated between $x = 263mm$ and $x = 303mm$.

low voltage actuators exhibited very similar evolutionary graphs, and unlike the case with suction, the shape factor evolutions in the upstream regions were seen to increase towards the desired value of 2. This observation was attributed to the noted damping of instabilities in the upstream velocity profile measurements for both configurations. However, the sharp drop in the shape factor values beyond $x = 263mm$ for both systems was suggestive of flow destabilisation, and was supported by the observed inflections in the velocity profiles for both systems.

9.2 Summary & conclusions

The experimental investigation detailed in this chapter was formulated so as to attempt to maintain the favourable flow augmentation observed for the single orthogonal actuators operated in conjunction with mild suction (see Chapter 8). The investigations looked at the response of the boundary layer to two orthogonal actuators placed in series with one another, and for completeness, the response of the layer was also measured for the actuators operating with and without the suction effect and at the low and high applied voltages used in the previous experimental investigations.

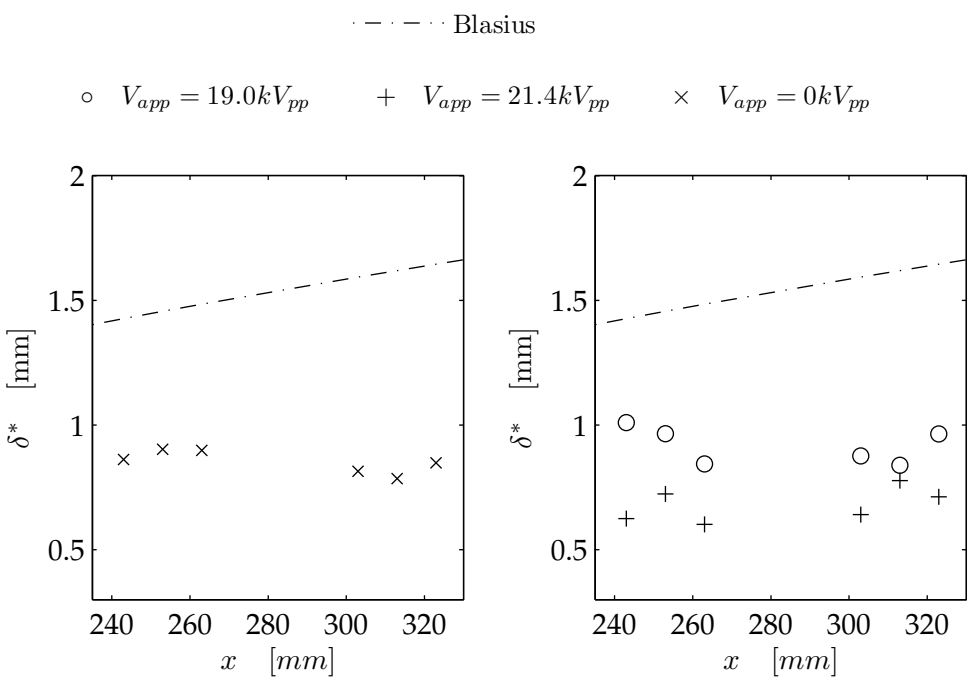

(a) Without plasma

(b) With plasma

Figure 9.8: Evolution of displacement thickness for double actuator configurations with mild suction.

The low voltage actuators, in conjunction with the mild suction effect, were seen to favourably augment the flow, with instabilities becoming effectively damped downstream of the actuators and the shape factor being reduced to a stable, laminar value. However, the effect of this combined double actuator/suction system differed only slightly from the suction-only system, meaning that in the current configuration, the use of the plasma was somewhat superfluous. Hence it can be concluded from the results of the research that a single low voltage actuator operated in conjunction with a mild suction effect is more effective as a LFC system than a single mild suction slot, but a combined double low voltage actuator/suction system is no better than a simpler and less energy-consuming double mild suction slot system.

With the exception of the low voltage system with mild suction, all other plasma configurations tested introduced inflections in the measured velocity profiles that remained present in the flow and became amplified at the most downstream measurement locations. These results agreed with the conclusions derived from the single actuator investigations, namely that high

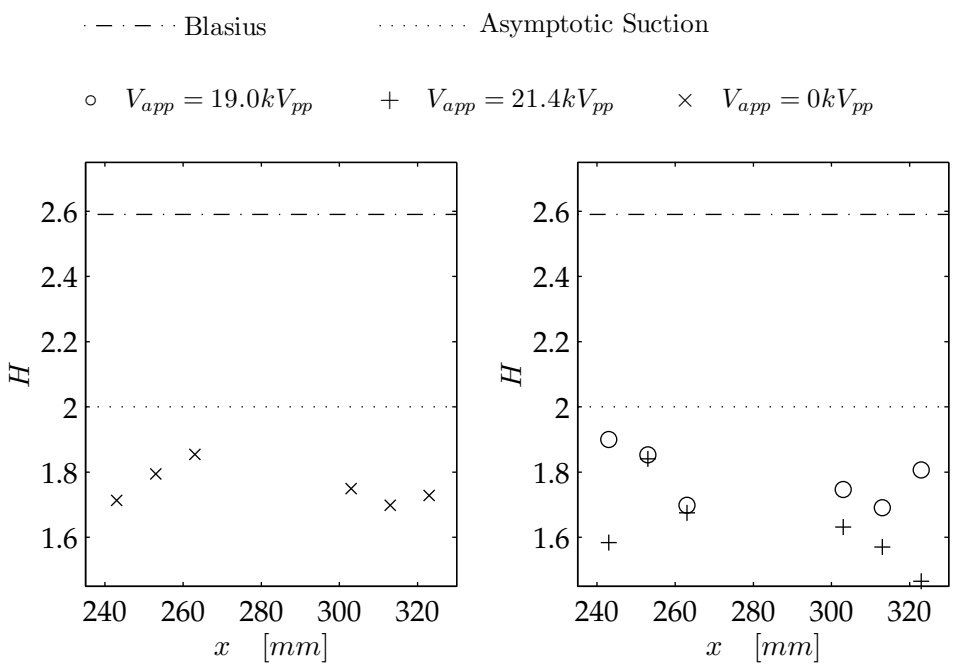

(a) Without plasma (b) With plasma

Figure 9.9: Evolution of shape factor for double actuator configurations with mild suction.

voltage actuators and ones which are sealed (i.e. not operated in conjunction with a mild suction effect) adversely affect the stability of the flow.

Even though favourable flow augmentation was not maintained without the use of the mild suction force, there was another interesting observation observed in the results. In the region between the two sealed actuators, the instabilities introduced by the upstream actuator were seen to be slightly damped by the presence of the downstream actuator. This is an interesting and unexpected result, which suggests that the presence of a downstream sealed actuator (i.e. one operated in the absence of the mild suction effect) is effective at damping large instabilities that are introduced into the flow upstream, (which in this investigation were introduced by the upstream actuator). Although downstream of the second actuator, the flow became unsteady again, it is feasible to suggest that the use of additional, downstream sealed actuators could be effective at eliminating large instabilities that may enter a flow. In addition, these additional actuators may allow for a system that can achieve LFC even more effective than the double suction slot system, (which was found to be the most effective system tested in this research). Limitations in the current experimental set up prevented this hypothesis

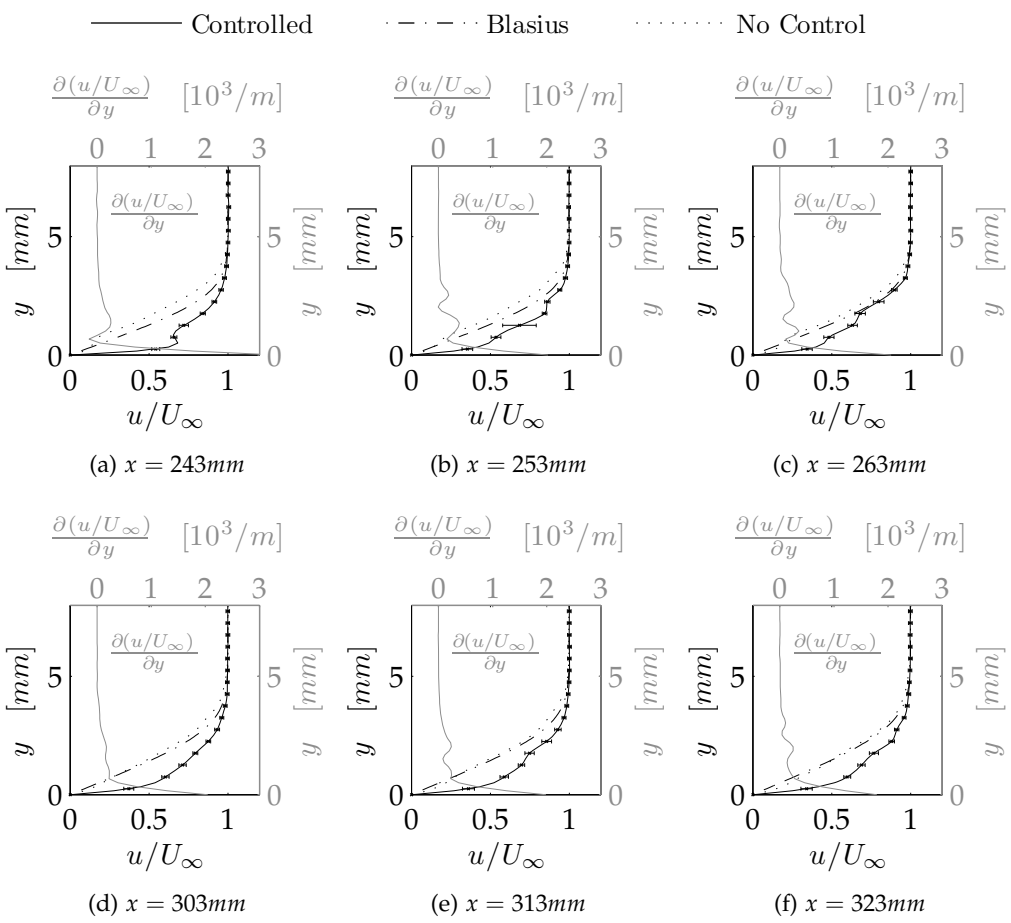

(a) $x = 243mm$ (b) $x = 253mm$ (c) $x = 263mm$

(d) $x = 303mm$ (e) $x = 313mm$ (f) $x = 323mm$

Figure 9.10: Velocity profiles without suction, $V_{app} = 19.0kV_{pp}$, $U_\infty = 5.43^m/_s$, $\frac{Re_x}{x} = 360000^1/_m$. Derivative data for controlled case only. 'No Control' case from FPR test shown for indicative reference only.

from being investigated and it is consequently recommended as a necessary future work. Further details of this suggested work and other proposed future investigations are discussed in the next chapter.

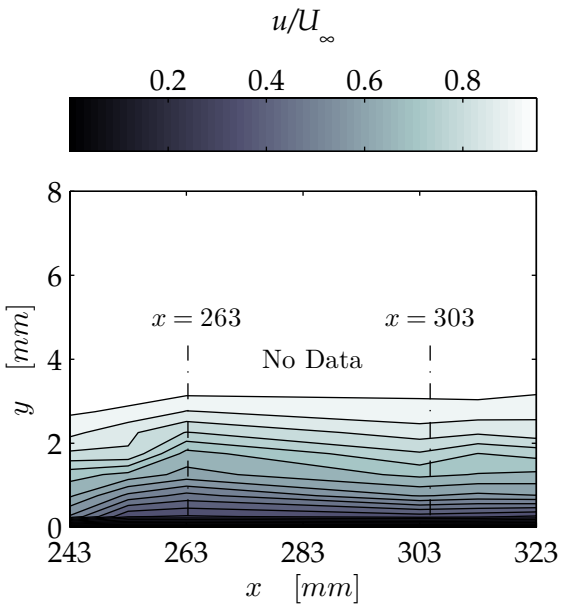

Figure 9.11: Velocity contours without suction, $V_{app} = 19.0kV_{pp}$, $U_\infty = 5.43^m/_s$, $\frac{Re_x}{x} = 360000^1/_m$. Data linearly interpolated between $x = 263mm$ and $x = 303mm$.

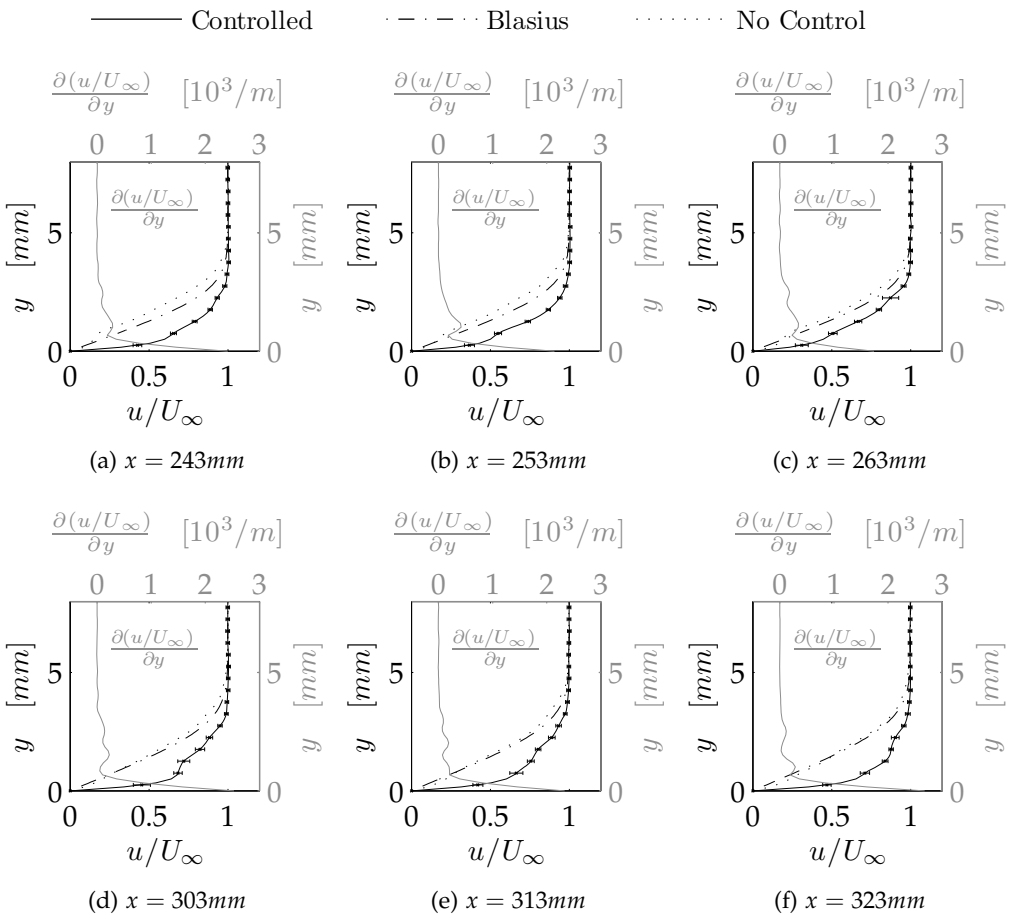

(a) $x = 243mm$ (b) $x = 253mm$ (c) $x = 263mm$

(d) $x = 303mm$ (e) $x = 313mm$ (f) $x = 323mm$

Figure 9.12: Velocity profiles without suction, $V_{app} = 21.4kV_{pp}$, $U_\infty = 5.42^m/_s$, $\frac{Re_x}{x} = 360000^1/_m$. Derivative data for controlled case only. 'No Control' case from FPR test shown for indicative reference only.

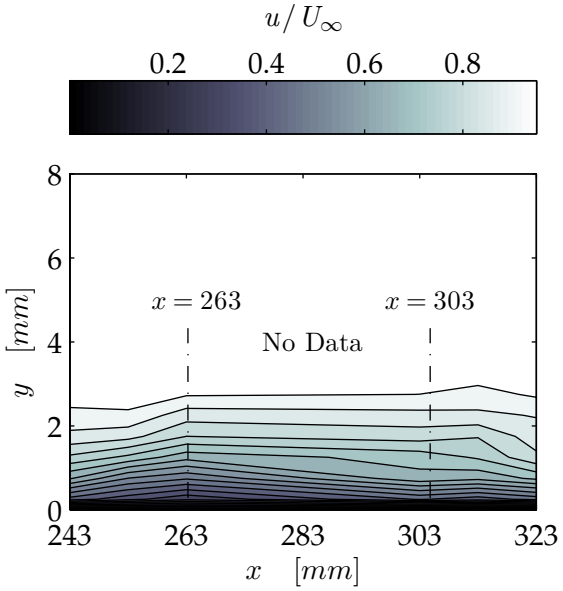

Figure 9.13: Velocity contours without suction, $V_{app} = 21.4kV_{pp}$, $U_\infty = 5.42^{m}/_{s}$, $\frac{Re_x}{x} = 360000^{1}/_{m}$. Data linearly interpolated between $x = 263mm$ and $x = 303mm$.

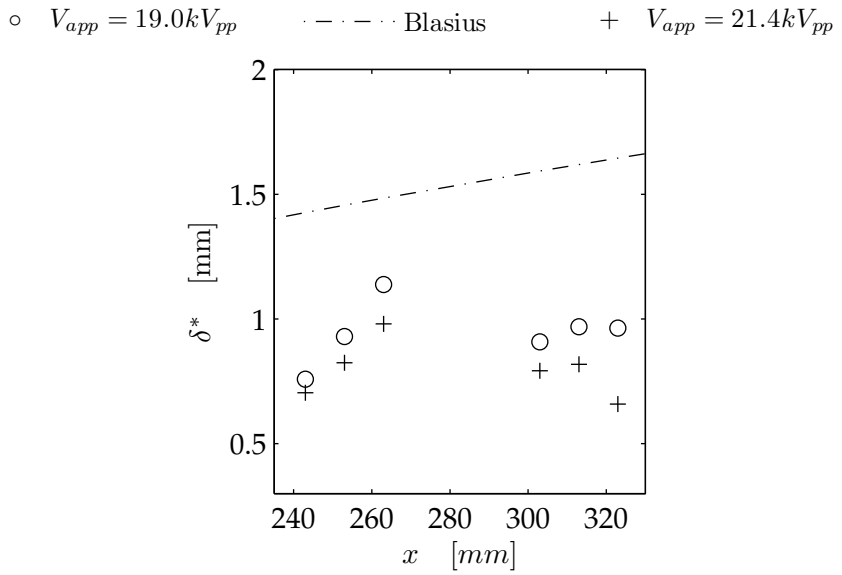

Figure 9.14: Evolution of displacement thickness for double actuator configurations without suction.

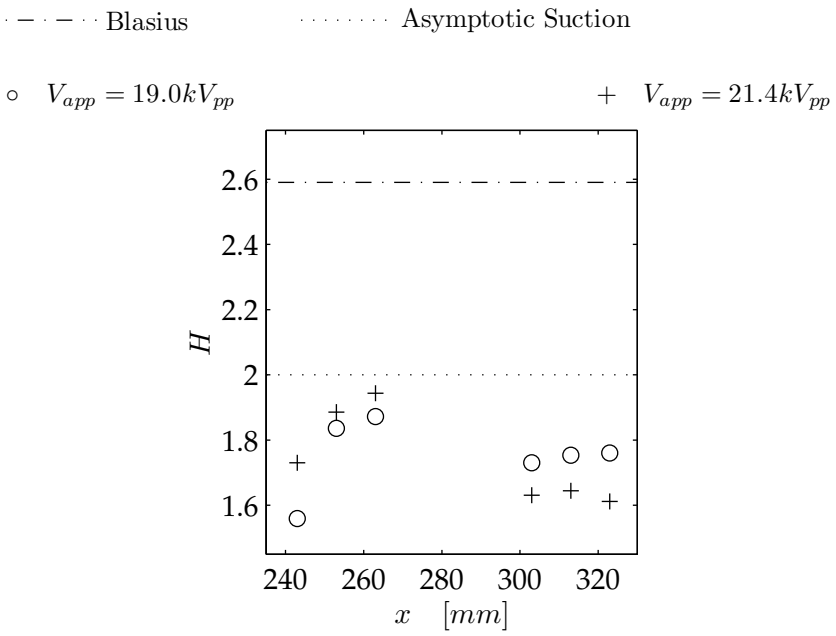

Figure 9.15: Evolution of shape factor for double actuator configurations without suction.

10 Conclusions & Future Work

The development of a Laminar Flow Control system employing Dielectric Barrier Discharge plasma actuators is a complex and challenging task and the mysteries of how to tackle the problem are only just beginning to come to light. The aim of this research was to contribute to the knowledge of the field by assessing changes to the hydrodynamic stability of a laminar boundary layer brought about by the use of a novel DBD-based LFC system. The research has included both theoretical and experimental work, focusing on the design and performance assessment of the novel actuator designs that constitute the plasma LFC system. This chapter summarises the major conclusions, outcomes and achievements of the research.

The complexities of DBD-based LFC systems are such that on completion of this research, areas of significant future work have become evident. For this reason, the second section of this chapter highlights these areas, as identified by the author, and discusses how they will complement and further the research presented in this thesis.

10.1 Conclusions

The focus of this research was the development of Laminar Flow Control technology utilising Dielectric Barrier Discharge plasma. The research assessed the effectiveness of such technology by studying the augmentation of the velocity profile of the most fundamental of boundary layer flows, one formed over a flat plate in a Zero Pressure Gradient, brought about by novel DBD actuators operated in a variety of configurations.

To address the significant lack of information pertaining to successful DBD-based LFC technology, the research commenced by first identifying novel actuator designs possessing the potential to improve the stability of a laminar layer. In addition, a further objective of this initial work was to find a way to control the characteristics of the induced wall jet developed by the plasma, including the position and magnitude of the maximum velocity

of the jet. By recognising that the height to which the exposed electrode sits proud above the surface of an actuator (y_{exp}) would have an affect on the developed region of plasma, it was postulated that variation of this height would lead to an augmentation in the volume of developed plasma and hence allow for control over the characteristics of the induced jet. The parametric study undertaken to investigate this hypothesis resulted in the development and use of novel actuators with electrodes placed perpendicular to one another. Not only were these orthogonal actuators found to be capable of producing the wall jetting effect associated with conventional DBD devices, they were found to do so by producing fuller induced velocity profiles, with shallower velocity gradients at the wall, and hence less fluid shear. Moreover, the jetting profile, magnitude and position of the maximum jetting velocity was found to be affected by the electrode exposure height, providing the electrode lay flush with or beneath the surface (i.e. $y_{exp} \leq 0mm$). This result subsequently highlighted a mechanism through which the DBD-based LFC could be tuned and it is for this reason, in conjunction with the more voluminous jetting characteristics already discussed, that the LFC system subsequently developed and tested as part of this research utilised these novel orthogonal actuators.

Linear Stability Theory was utilised throughout the research to identify benchmark objectives for the DBD-based LFC system to which the real actuators were to be tuned. This methodology was employed to hasten development time and eliminate the need to perform time-consuming *trial and error* experimentation as used by other researchers. Linear Stability Analyses were performed on a number of idealised boundary layer flows obtained from curve fitting analytical functions to published DBD-augmented boundary layer data, as well as from boundary layer theory. The LSAs were conducted using the Orr-Sommerfeld Equation solver developed as part of this research, which itself was a major outcome of the work because of the capability it provides for future works stemming from this research.

The outcome of the LSAs was that the developed DBD-based LFC system was to attempt to augment the boundary layer so as it would attain characteristics of a Blasius boundary layer exposed to uniform wall suction. Such an LFC system would potentially give the boundary layer a limit of stability almost two orders of magnitude greater than the base flow, without the need for a complex and energy-consuming suction system.

A Flat Plate Rig was developed for the purpose of testing the novel DBD-based LFC system developed during this research. Through the use of movable wall panels, it was possible to achieve a near-zero pressure gradient (ranging between $-0.50^{Pa}/_{m}$ and $0.02^{Pa}/_{m}$) over the FPR, which

subsequently allowed the development of a boundary layer approximating a Blasius layer. Into this boundary layer, orthogonal actuators were positioned and the response of the layer around the critical Reynolds Number of the flow ($80000 < Re_x < 120000$) was measured.

In order to develop a volume of plasma from the orthogonal actuators that could augment the boundary layer flows studied, a small reservoir of air was required upstream of the exposed electrode. Due to the design of the FPR, the subsequent gap in the rig that this reservoir represented allowed the performance of the orthogonal actuators to be studied with and without a mild suction effect. This effect was measured to be approximately $4Pa$, and a single suction slot by itself was found not to be sufficiently strong to augment the flow so as to attain the characteristics of a boundary layer with uniform wall suction.

Initial results of the DBD-based LFC system showed that the system had adverse affects on the stability of the boundary layer. The first system trialled utilised a single actuator, and this was found to destabilise the flow whether or not the suction effect was present. However, of the two scenarios tested, the destabilisation of the flow in the absence of the mild suction effect was found to be more severe.

To address the initial adverse control affects achieved with the DBD-based LFC system, tuning of the actuators was undertaken. Having recognised, from the literature, that the variation of the operating voltage of an actuator affects the characteristics of the induced jet, it was decided to vary the applied voltage of the original actuator and thus tune the system. Using this tuning technique it was found that a single actuator operated with an applied voltage of $19.0kV_{pp}$ (a *low-voltage* actuator), in conjunction with the mild suction effect, could control the boundary layer in a way that mimicked uniform wall suction for a short distance ($50mm$) downstream of the device. Without the need to vary the exposed electrode exposure height, which would have been more labour intensive, this result was a significant outcome, providing support for the use of orthogonal actuators. This result showed that an orthogonal actuator operated in this configuration could enhance the mild suction effect and provide improved LFC over the single suction slot.

In addition to identifying an actuator configuration that could provide favourable improvements to the stability of a laminar boundary layer, an actuator operated with an applied voltage of $21.4kV_{pp}$ (a *high-voltage* actuator) was found to produce the most adverse effect. This confirmed a hypothesis resulting from the literature review, that lower voltage actuators would be more beneficial for LFC than higher voltage devices.

To maintain the stability effects for a greater downstream distance, it

was proposed that subsequent downstream actuators would be needed. Consequently a study was undertaken using two DBD devices placed in series. These DBD actuators were based on the design used for the single actuator experiments, but were only half the total length. Systems with both high and low voltage actuators, with and without the mild suction effect, were tested. With the exception of the low voltage system operated in conjunction with the mild suction effect, all double-actuator configurations tested were found to adversely affect the stability of the flow. Whilst the combined low-voltage actuator/suction system was seen to favourably augment the flow, the effect of this combined double-actuator/suction system differed only slightly from the suction-only system, meaning that in the configuration tested, the use of the plasma was somewhat superfluous. Hence it was concluded that a single low-voltage actuator operated in conjunction with a mild suction effect is more effective as a LFC system than a single mild suction slot, but a combined double-actuator/suction system operated at a low voltage (like that tested during this research) is no better than a simpler and less energy-consuming double mild-suction slot system.

The research discussed in this thesis was undertaken with the intention of contributing to the field of DBD-based LFC flow control. The development of successful systems requires significant knowledge on which to base designs and to date few results have been published on the performance of DBD-based LFC system. Hence the results presented here provide additional material from which knowledge can be drawn, including novel actuators and tuning techniques to be used in the development of such LFC technology. The research has shown that low-voltage, orthogonal actuators can be used to enhance mild suction effects in a stable fashion, allowing the effectiveness of a single mild-suction-slot-based LFC system to be enhanced. Although it was found that two of these plasma actuators in the configuration tested become somewhat superfluous when used with two mild-suction slots, through future work it is anticipated that the use of additional actuators, correctly tuned using the techniques discussed, will allow for a system that can achieve LFC even more effectively than a double-suction slot system. Hence, the additional and valuable insights this research has provided to the field of DBD-based LFC has meant that the original intentions of the work have been fulfilled.

10.2 Suggested future work

The results of this research represent only the beginning of the development of DBD-based LFC systems, particularly those incorporating orthogonal actuators. Consequently a significant amount of potential work exists as a result of the conclusions of this research.

The completed research was the first to utilise orthogonal actuators for producing DBD plasma. The direct consequence of this is that there is limited published information regarding the effects of varying different geometric and electrical parameters on orthogonal actuator performance, as compared to what is available for conventional, parallel-type devices. To assist in understanding the jetting characteristics of orthogonal actuators further, it is therefore suggested that parametric studies be undertaken to investigate the jetting characteristics of these actuators. From these investigations it is anticipated that additional ways to augment the jetting characteristics of the actuators will be identified. This would consequently provide additional mechanisms (in addition to varying exposed electrode height and applied voltage) through which a DBD-based LFC system can be tuned so as to achieve the desired flow augmentation.

The DBD-based LFC system studied in this project was tuned according to desired flow characteristics obtained from assumed velocity data and Linear Stability Theory (see Chapter 5). The velocity data was obtained from published results and boundary layer theory as no direct experimental results for an orthogonal-actuator-based LFC system were available. With the measurements obtained from this research it is now possible to calculate the stability limits able to be attained using the plasma-based LFC systems studied here. This task is no small undertaking however, and will require a significant amount of effort. Nevertheless, the outcome of the analyses would provide more refined estimates of the expected effects on stability arising from the plasma, as well as details of the expected disturbance growth rates. Both of these groups of information would subsequently provide significant detail from which to properly assess the potential of orthogonal-actuator-based LFC systems

The LFC system tuning performed in this work was done by varying the applied voltage of the actuators. Since the jetting characteristics of the orthogonal actuators were observed to be dependent on the exposed electrode exposure height in addition to the applied voltage, it would be of significant benefit to investigate the tuning potential of the LFC system through variation of y_{exp}.

The experimental investigations completed during this research were

done around the critical Reynolds Number of a Blasius flow. As mentioned throughout the thesis, this position represents the limit of stability of the flow and not necessarily the point of transition of the boundary layer. Therefore future experiments should focus on identifying the actual point of transition in the flow and assessing the change in that position arising from the use of the orthogonal actuators. This point could then be correlated with the predictions from the future Linear Stability Analyses, and hence allow for verification of the accuracy and outcomes of these future numerical works.

Given the large distances over which transition may occur in Blasius flow, it might be necessary to promote transition in the future experiments. This could be achieved by exposing the layer to an adverse pressure gradient, so as to encourage the amplification of transition-inducing instabilities. Alternatively, the freestream flow speed could be increased so as to hasten the development of the boundary layer and its transition from laminar to turbulence. Investigating the performance of the system at different flow speeds would also be very beneficial, since the thickness of the layer would change, and it would be of interest to know how the tune of the LFC system would need to be modified so as to cope with this.

In identifying the point of transition, measurement of the disturbance growth rates between the base flow and control flow would provide significant details to verify the stability analyses with. In addition, this information could also be used in conjunction with a modified form of the developed OSE solver to predict the location of transition resulting form the plasma control using the e^n methodology as discussed in Chapter 2. Obtaining this data would require the use of anemometry equipment with a high frequency response, ideally hot-wire anemometry. As discussed in Chapter 6, hot-wire anemometry faces many challenges when implementing it in the vicinity of a plasma-augmented flow. Hence a significant amount of work would be required in developing the experimental apparatus to acquire this data, and this is suggested as a subject for future work. Although this would require much effort to implement, doing so would provide a better estimate of the expected performance of future DBD-based LFC systems.

In the experiments involving two DBD actuators (Chapter 9) it was noticed that the second actuator seemingly improved the behaviour of the flow downstream of the first device. This suggests that the actuators operated in the absence of suction can stabilise disturbed flow upstream of itself, and this result should be experimentally studied in greater detail. As postulated in Chapter 9, it is feasible to suggest that the use of additional actuators that have undergone appropriate tuning would allow for the development of a LFC even more effective than the systems studied in this research.

Studying the effectiveness of the DBD-based system in three dimensions is also an important future task that should be conducted as the technology is developed. As discussed in Section 6.6.4, the extent of the spanwise variation in the boundary layer, as brought about by the DBD-based system with mild suction, is uncertain. The impact, favourable or adverse, must also be ascertained.

As further work is undertaken to delay boundary layer transition, it is anticipated that the actuators will have to operate in increasingly disturbed fluid, attenuating increasing numbers of instabilities of different wavelengths and frequencies. It is therefore recommended that some work be performed looking at the effect of DBD actuators, particularly orthogonal devices, on controlling transitioning and/or turbulent flow. Some preliminary work has already been undertaken in regards to the operation of orthogonal actuators in a low Reynolds Number turbulent boundary layer. The results are presented in Appendix A, and in summery the results suggest that the orthogonal actuators are incapable of augmenting a low Reynolds Number turbulent boundary layer. However these results are preliminary, with little work done to re-tune the actuators to suit the turbulent flow. Hence future work is recommended in this area.

To be able to undertake these future investigations, it is pertinent to make a comment on the viability of the developed experimental rig for providing the conditions for such studies to be made. Throughout this work, the FPR was set up so that investigations around the region of the Critical Reynolds Number for Blasius flow could be made. These observations occurred within the first 25% of the length of the rig. Investigations for different flow speeds and Reynolds Numbers, as recommended, could be easily accommodated for by the FPR by rearranging the removable panels of the rig. The movable walls of the FPR would also be capable of providing the desired pressure gradients if a non-zero distribution was sought. Constraints in the design of the rig enclosure may cause some measurement *black spots* where standard anemometry probes may not be able to be reach. However, this issue could be easily solved through probe redesign, without the need to modify the rig. Hence, the FPR as designed will be capable of handling future investigations with minimal need to redesign.

The future works that have been recommended can be summarised into two groups. The first of these pertains to numerical analyses. Using the experimental results from this research, including the evolution of the velocity within the controlled boundary layers, stability analyses should be conducted so that better estimates of expected stability limits for DBD-augmented flows can be ascertained. In addition, the analyses should focus on estimating

the growth rates of disturbances within the controlled boundary layers. Concurrently, the second category of future work, experimental investigations, should be undertaken. Further experiments should be done utilising single and multiple orthogonal actuators. These investigations should measure the evolution of the velocity profile within the layer, the growth rate of disturbances, as well as the location of transition, so as to provide validation of the numerical analyses as well as experimental evidence of the capability of DBD-based LFC systems. The undertaking of both categories of work would provide the best direction forward for developing a tuned DBD LFC system that provides effective flow control, which may ultimately help address the energy and operating cost concerns of the global aviation industry.

Acknowledgement & Disclaimer

Research undertaken for this thesis has been assisted with a grant from the Smith Fund (**www.smithfund.org.au**). The support is acknowledged and greatly appreciated.

The Smith Fund by providing for this project does not verify the accuracy of any findings or any representation contained in it. Any reliance in any written report or information provided to you should be based solely on your own assessment and conclusions.

The Smith Fund does not accept any responsibility or liability from any persons, company or entity that may have relied on any written report or representations contained in this report if that person, company or entity suffers any loss (financial or otherwise) as a result.

THE SIR ROSS & SIR KEITH SMITH FUND

A Measured Responses of Tripped Layers to the Orthogonal Actuators

The orthogonal actuators developed as a result of this research were found to be highly effective at augmenting the laminar boundary layer studied in the experimental investigations (Chapter 7, 8, & 9). The significant boundary layer thinning and shape factor reduction resulting from the orthogonal actuators suggested that the actuators might be capable of augmenting a low Reynolds number turbulent boundary layer also, reducing its thickness and possibly the skin friction associated with it. Consequently a preliminary experiment was devised in which the boundary layer was tripped into turbulence and its response to a single orthogonal actuator measured.

The preliminary investigation was performed using the same methodologies and procedures employed for the laminar boundary layer studies. The response was measured for cases with and without the mild suction effect, for the configurations involving the low-voltage actuator ($V_{app} = 19.0kV_{pp}$) and the high-voltage device ($V_{app} = 21.4kV_{pp}$). The measurements obtained from this preliminary investigation are presented in this appendix.

A.1 Experimental set up

To achieve a low Reynolds number turbulent boundary layer flow, a trip wire was used. According to Braslow et al. (1966), with the use of an appropriately sized trip wire, boundary layer transition will move forward of its natural location. In subsonic flows, the transition location moves upstream so as to be very close to the trip wire itself (Braslow et al. 1966). This meant that by selecting an appropriate diameter trip wire, the orthogonal actuator could be operated in a low Reynolds number turbulent boundary layer.

Sizing of the trip wire was based on the work of Braslow et al. (1966) and

involved defining a Reynolds number based on k, the diameter of the trip wire (Equation A.1). In the formulation of this new Reynolds number, u_k and v_k correspond to the local values of the fluid velocity and kinematic viscosity respectively, at a position on top of the wire (Figure A.1).

$$Re_k = \frac{u_k k}{\nu_k} \tag{A.1}$$

For the purpose of sizing the trip wire, u_k was estimated from the Blasius boundary layer solution, whilst the kinematic viscosity was assumed to be equal to the freestream value. Ultimate validation of the suitability of these assumptions was to be made by analysing the resultant boundary layer formed in response to the trip wire.

As previously mentioned, the downstream edge of the actuator was placed at a chordwise Reynolds number (Re_x) equal to 80000. To make sure that the flow would be attached to the wall and turbulent in the direct vicinity of the plasma actuator, it was decided to place the trip wire a distance of at least 10 wire diameters upstream of the plasma region. The intention was to place the wire at $x = 163mm$, corresponding with $Re_x \approx 60000$. According to Braslow et al. (1966), a trip wire placed at $Re_x \approx 60000$ should achieve a value of approximately 1000 for Re_k. After solving for the wire diameter it was found that a trip wire positioned at this location needed to be approximately $3mm$ in diameter. This value was suitable, as the trip location was greater than 10 diameters upstream of the actuator. In addition, at this trip position,

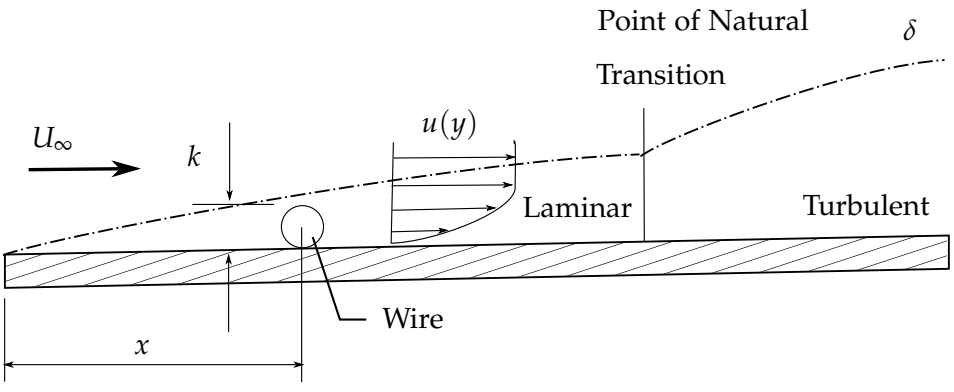

Figure A.1: Definition of parameters for sizing of trip wire (adapted from Braslow et al. 1966).

the thickness of the layer is approximately $3.5mm$, meaning that the wire would be fully contained within the dimensions of the layer. However, it should be noted that this is not a strict requirement to promote transition, and transition can still occur when the trip wire is greater than the thickness of the layer (Braslow et al. 1966).

When installed, the trip wire was found to be most effective at promoting transition in the boundary layer, as is evident by the measured velocity profiles for the flow (Figure A.2). These profiles were obtained in the manner described in Section 6.6.2, with the exception that the near-wall measurements were made at $y = 0.1mm$ instead of $y = 0mm$, due to greater ease in identifying this position for the experimental set up without the plasma actuators. At $x = 253mm$, the boundary layer shows approximate agreement to the power law fit discussed by Cebeci and Cousteix (1999) (Equation A.2), and this agreement increasingly improves downstream, such that the NRMSD between the curve fit and the measurements is 3.5% at $x = 323mm$. At $x = 243mm$, the agreement between the fit and the results is found to be poorer, with an NRMSD value of 16%. However the thickness and behaviour of the velocity profile at this location is noted as being far from laminar. Indeed, by looking at the velocity contours for the flow (Figure A.3), the turbulent nature of the flow at $x = 243mm$ and beyond can be clearly seen. Thus the experimental set up, and assumptions used to develop it described in this appendix were deemed suitable for conducting preliminary investigations into the effect of the orthogonal actuators for augmenting a low Reynolds number, turbulent boundary layer.

$$\left(\frac{u}{u_e}\right) = \left(\frac{y}{\delta}\right)^{1/7} \tag{A.2}$$

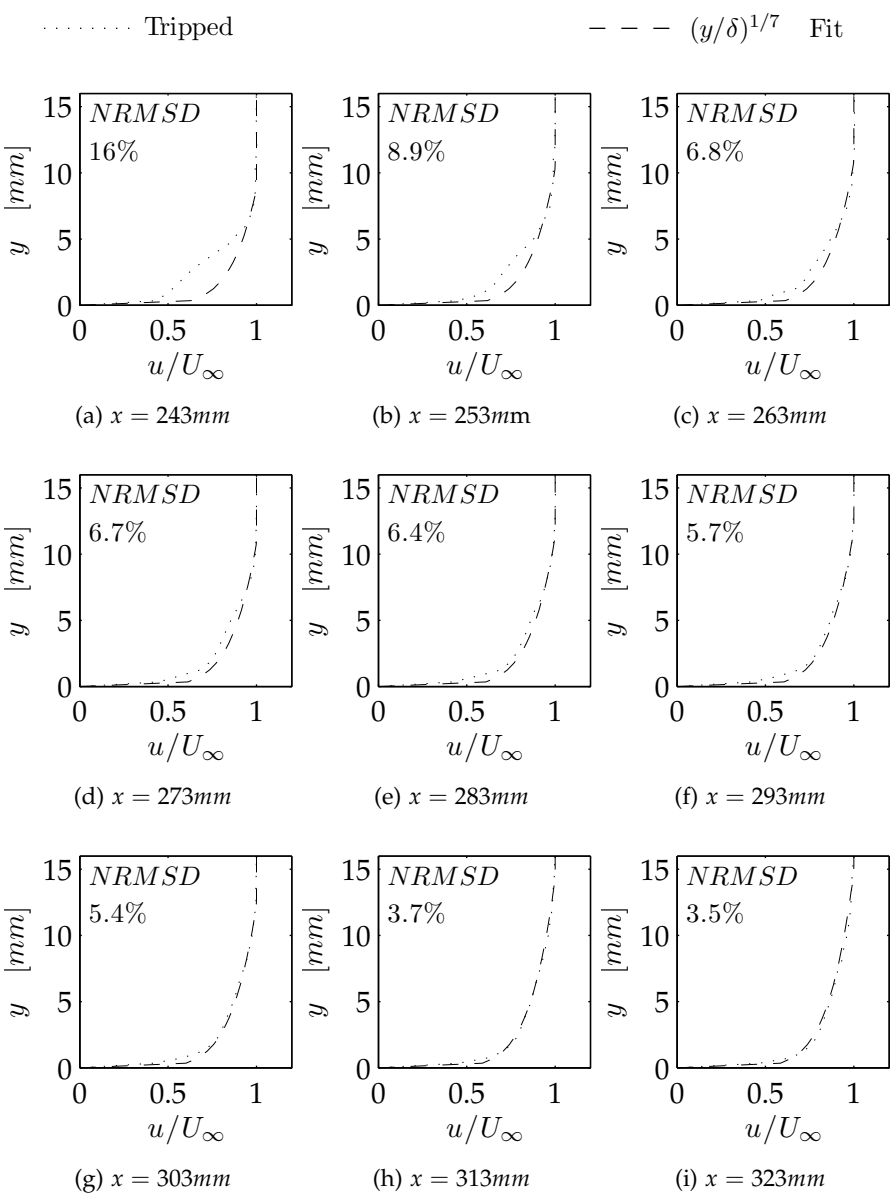

(a) $x = 243mm$ (b) $x = 253m$m (c) $x = 263mm$

(d) $x = 273mm$ (e) $x = 283mm$ (f) $x = 293mm$

(g) $x = 303mm$ (h) $x = 313mm$ (i) $x = 323mm$

Figure A.2: Velocity profile measurements of the tripped boundary layer in the investigation region, $U_\infty = 5.56^m/_s$, $\frac{Re_x}{x} = 370000^1/_m$. Smoothed cubic splines shown only.

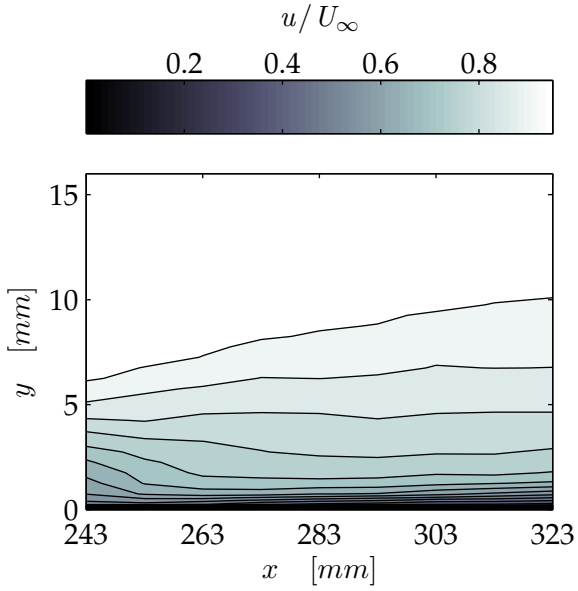

Figure A.3: Velocity contours of the tripped boundary layer in the investigation region, $U_\infty = 5.56^{m}/_{s}$, $\frac{Re_x}{x} = 370000^{1}/_{m}$.

A.2 Low *Re* turbulent layer response to a single orthogonal actuator

The low Reynolds number turbulent boundary layer was observed to be highly unresponsive to all of the actuator configurations tested. In addition, the velocity profile augmentation from the LFC system was found to be essentially independent to the voltage of the actuator and the mild suction effect. The velocity profile measurements for the low and high-voltage actuator operated in conjunction with the suction effect can be seen in Figure A.4 & A.5 respectively. No significant difference between the two sets of results is found, and neither configuration is seen to augment the velocity profiles at any location in a favourable fashion. Only at $x = 243mm$ is the velocity profile augmented by the presence of the plasma (for both voltages), but the augmentation, if anything, appears to encourage the development of turbulent flow (in both cases).

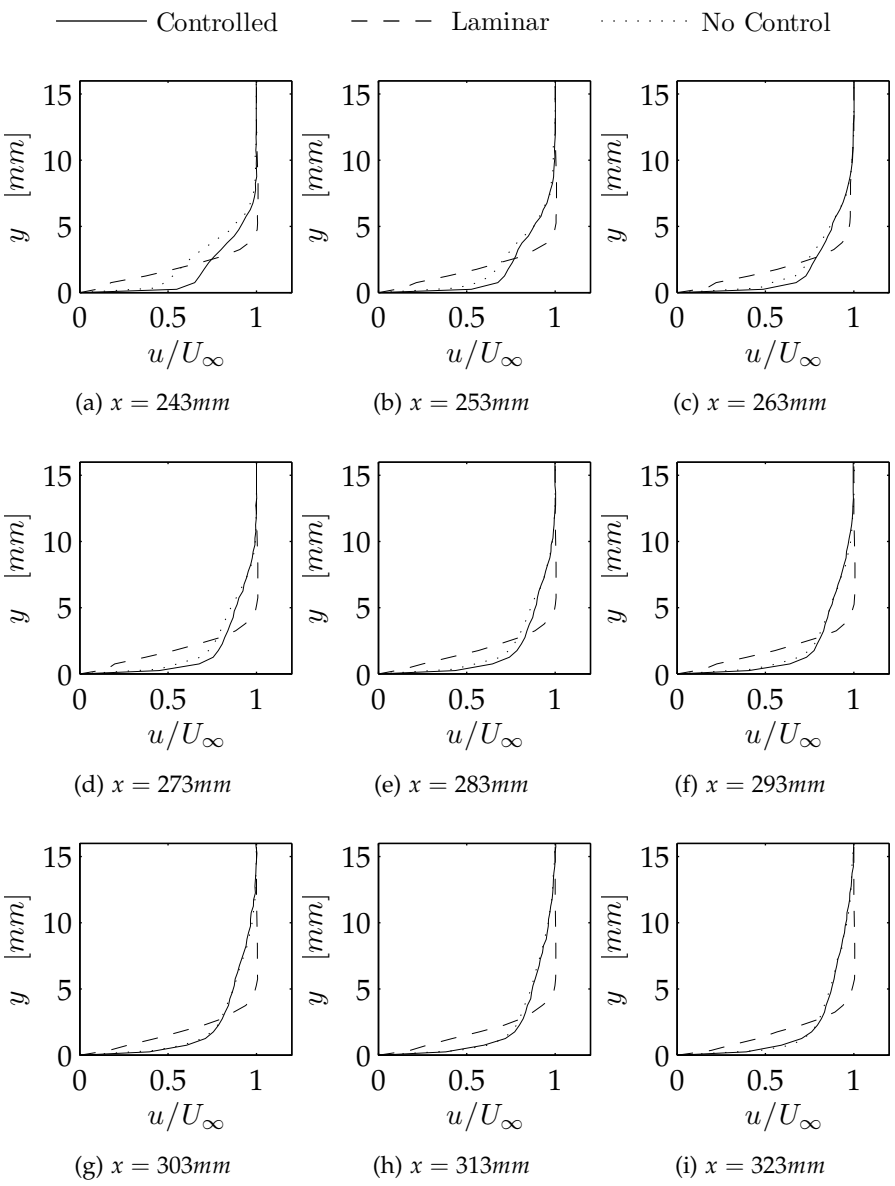

(a) $x = 243mm$ (b) $x = 253mm$ (c) $x = 263mm$

(d) $x = 273mm$ (e) $x = 283mm$ (f) $x = 293mm$

(g) $x = 303mm$ (h) $x = 313mm$ (i) $x = 323mm$

Figure A.4: Velocity profiles with suction, $V_{app} = 19.0kV_{pp}$, $U_\infty = 5.29^{m}/_{s}$, $\frac{Re_x}{x} = 360000^{1}/_{m}$. Smoothed cubic splines shown only.

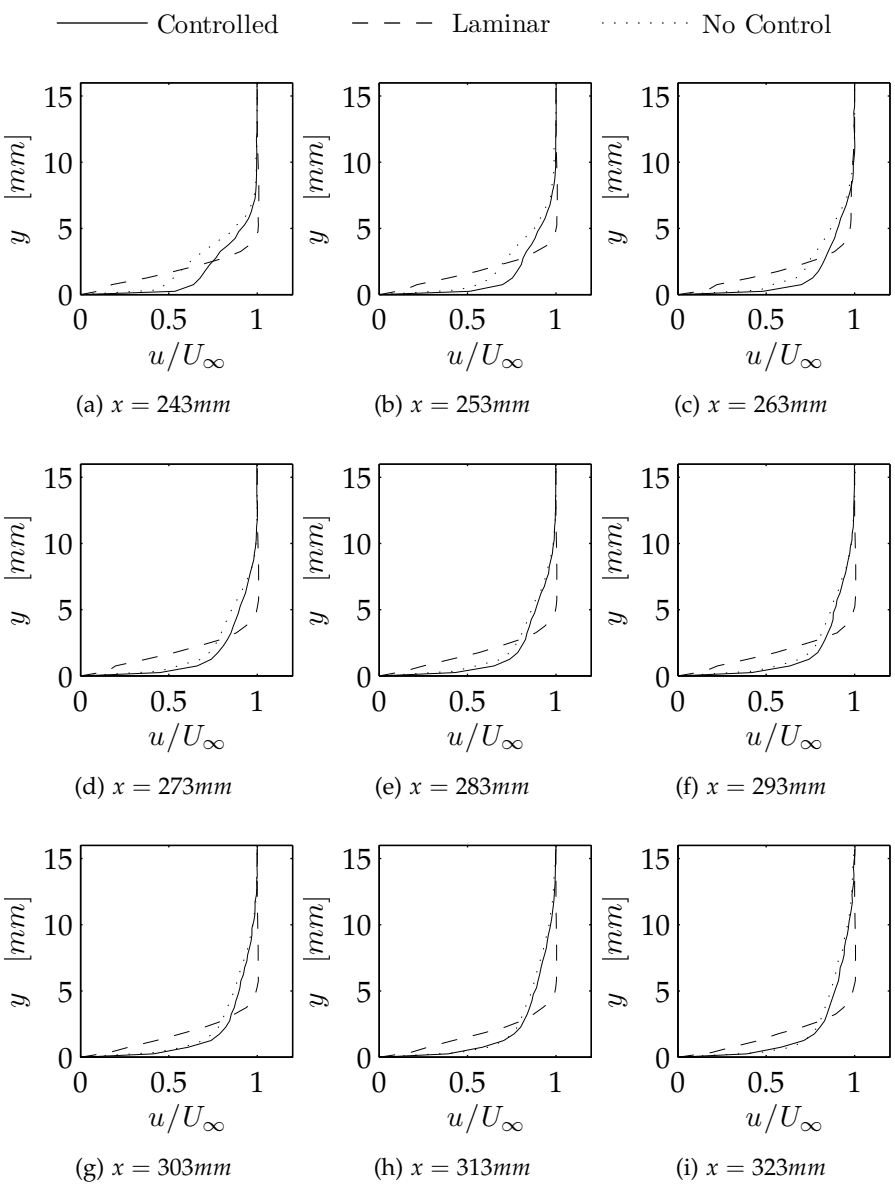

(a) $x = 243mm$ (b) $x = 253mm$ (c) $x = 263mm$

(d) $x = 273mm$ (e) $x = 283mm$ (f) $x = 293mm$

(g) $x = 303mm$ (h) $x = 313mm$ (i) $x = 323mm$

Figure A.5: Velocity profiles with suction, $V_{app} = 21.4kV_{pp}$, $U_\infty = 5.29^{m}/_{s}$, $\frac{Re_x}{x} = 360000^{1}/_{m}$. Smoothed cubic splines shown only.

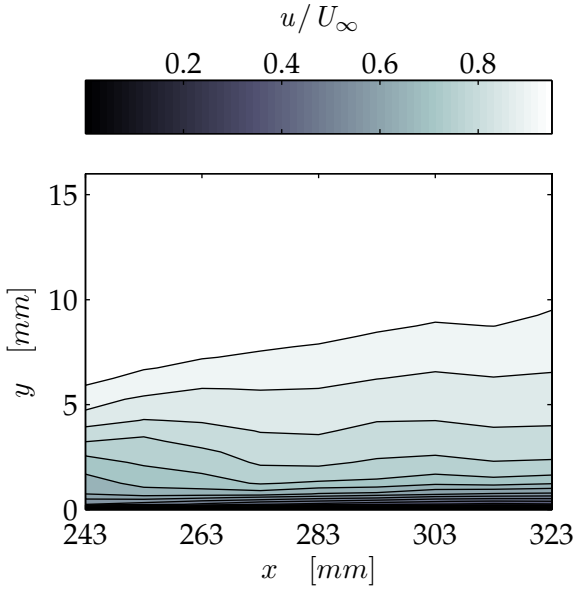

Figure A.6: Velocity profiles with suction, $V_{app} = 19.0kV_{pp}$, $U_\infty = 5.29^{m}/_{s}$, $\frac{Re_x}{x} = 360000^{1}/_{m}$.

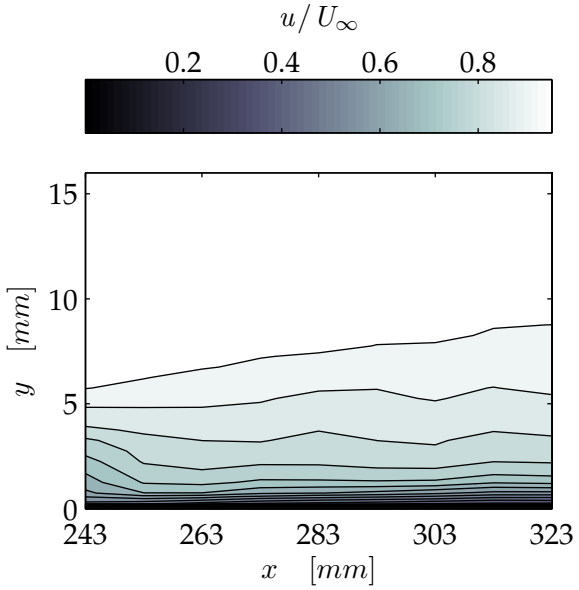

Figure A.7: Velocity contours with suction, $V_{app} = 21.4kV_{pp}$, $U_\infty = 5.29^{m}/_{s}$, $\frac{Re_x}{x} = 360000^{1}/_{m}$.

The velocity contours for both cases with suction support the observations gleaned from the measurements of the velocity profiles (Figure A.6 & A.7). In the contours, neither configuration is seen to affect the behaviour of the boundary layer, and no improved laminar characteristics are noticeable in either case.

The velocity measurements for the cases without suction were found to be very similar to those with suction (Figure A.8 & A.9). Again little to no change is noticed at the downstream measurement locations and only at $x = 243mm$ is any augmentation discernible (for both cases). Like the cases with the mild suction effect, the observed augmentation at $x = 243mm$ suggests, if anything, that the plasma is encouraging the development of turbulent flow in the boundary layer.

The little influence on the flow provided by the plasma actuators without suction is again seen in the velocity contours for the augmented flows. The results for both the low-voltage case (Figure A.10) and the high-voltage case (Figure A.11), produce similar velocity contours, and both differ little from those for the configurations tested with suction (Figure A.6 & A.7).

Studying the evolution of the shape factor for the cases with plasma supports the conclusions obtained from the velocity measurements (Figure A.12). The shape factor evolution is seen to be independent of the presence of the mild suction effect, and moreover the shape factor values with plasma are found to be extremely low, beneath 1.5 for all measurement locations, and actuator configurations. Interestingly, the shape factor values for the cases with plasma are lower than those for the cases without plasma until $x = 303mm$. Again this suggests that the orthogonal actuators were, if anything, encouraging the development of turbulence in the low Reynolds number turbulent boundary layer and hence were providing no benefit to reducing the thickness and developed skin friction of the layer.

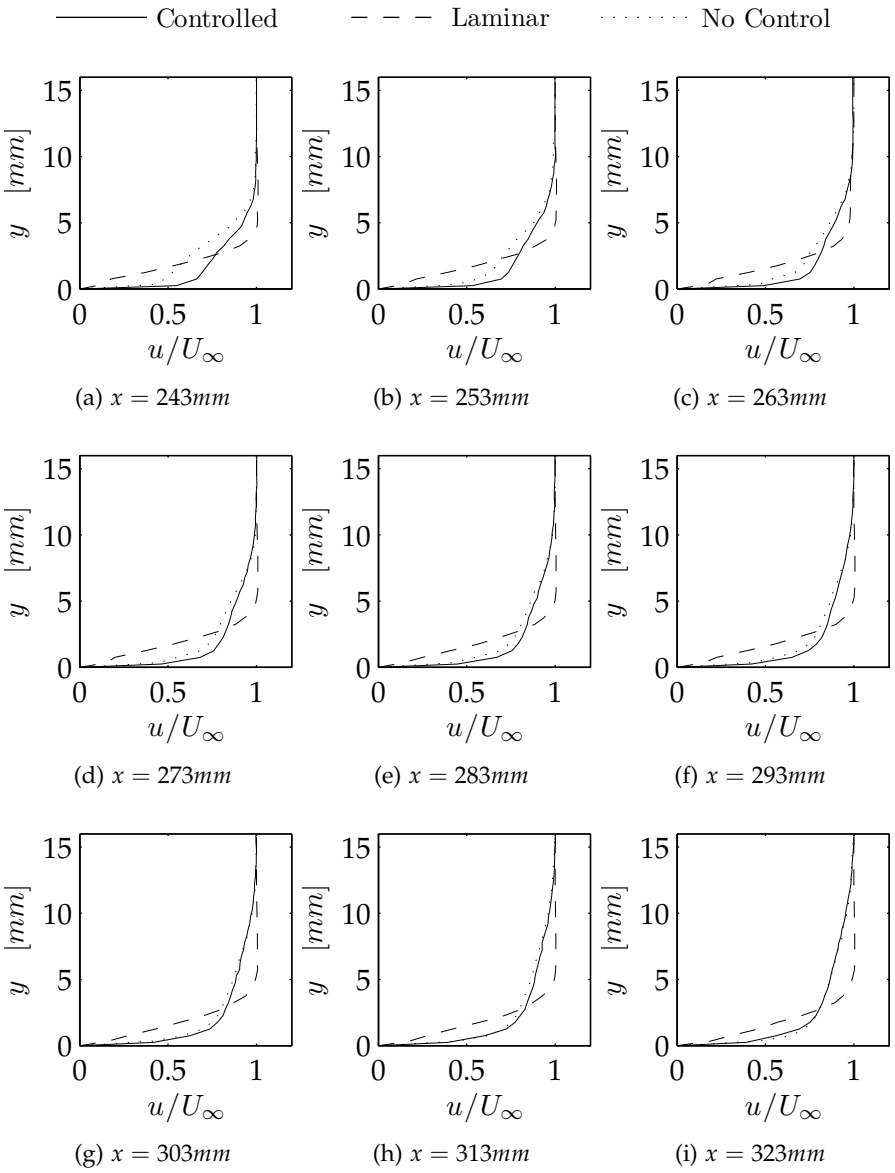

(a) $x = 243mm$ (b) $x = 253mm$ (c) $x = 263mm$

(d) $x = 273mm$ (e) $x = 283mm$ (f) $x = 293mm$

(g) $x = 303mm$ (h) $x = 313mm$ (i) $x = 323mm$

Figure A.8: Velocity profiles without suction, $V_{app} = 19.0kV_{pp}$, $U_\infty = 5.36^m/_s$, $\frac{Re_x}{x} = 360000^1/_m$. Smoothed cubic splines shown only.

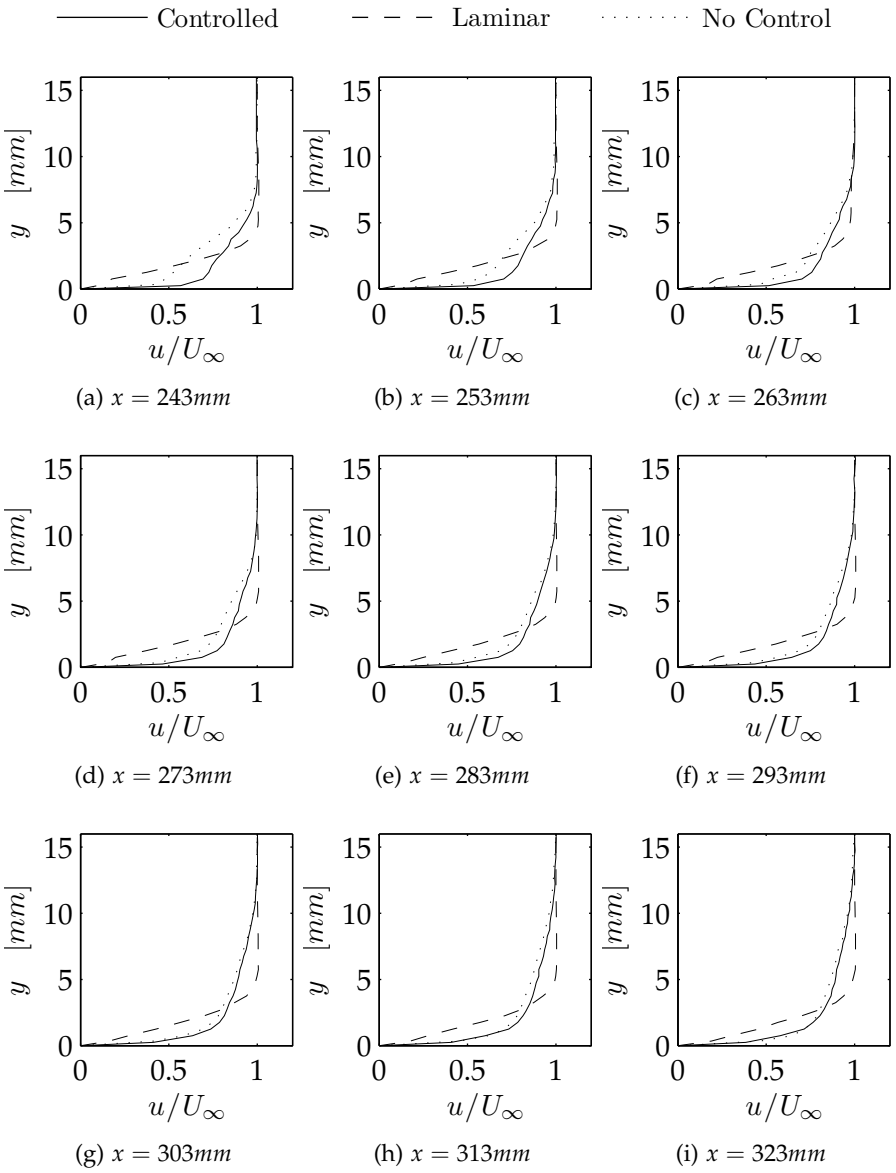

(a) $x = 243mm$ (b) $x = 253mm$ (c) $x = 263mm$

(d) $x = 273mm$ (e) $x = 283mm$ (f) $x = 293mm$

(g) $x = 303mm$ (h) $x = 313mm$ (i) $x = 323mm$

Figure A.9: Velocity profiles without suction, $V_{app} = 21.4kV_{pp}$, $U_\infty = 5.36^m/_s$, $\frac{Re_x}{x} = 360000^1/_m$. Smoothed cubic splines shown only.

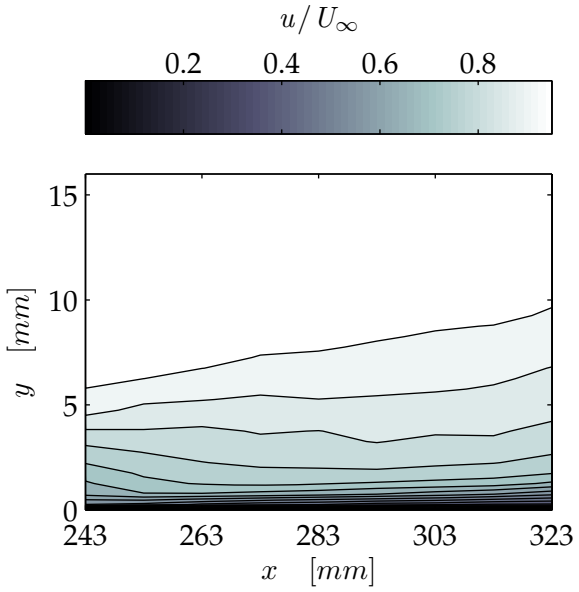

Figure A.10: Velocity contours without suction, $V_{app} = 19.0kV_{pp}$, $U_\infty = 5.36^{m}/_{s}$, $\frac{Re_x}{x} = 360000^{1}/_{m}$.

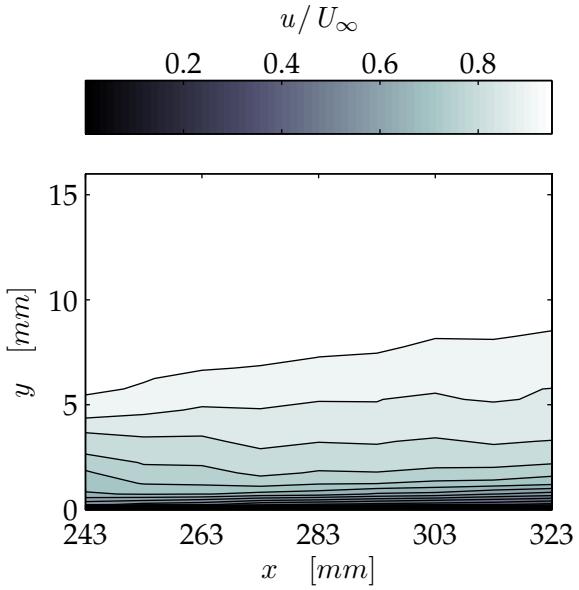

Figure A.11: Velocity contours without suction, $V_{app} = 21.4kV_{pp}$, $U_\infty = 5.36^{m}/_{s}$.

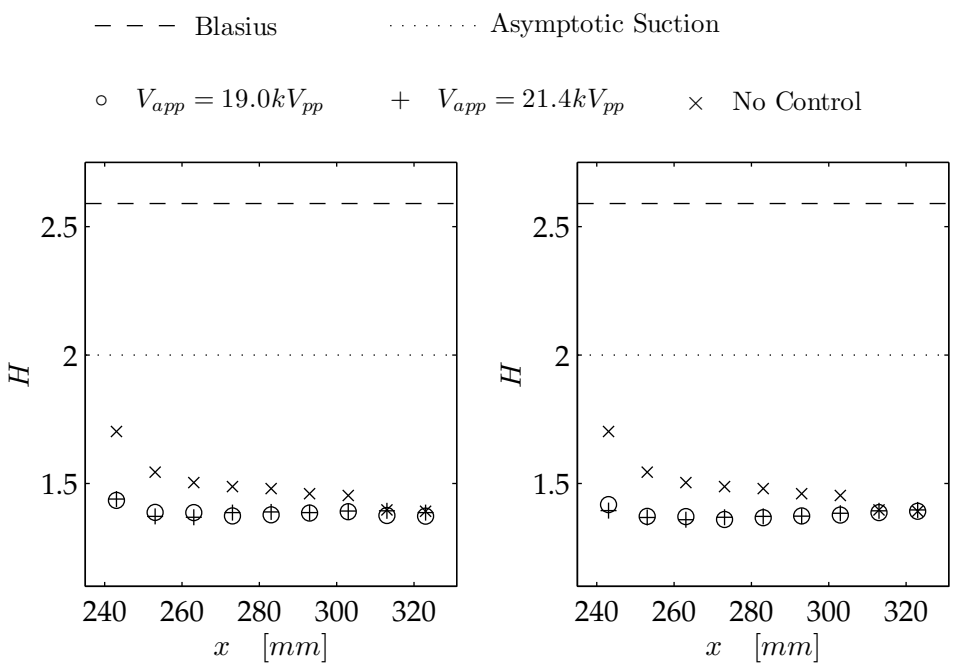

(a) With suction

(b) Without suction

Figure A.12: Evolution of shape factor for the tripped boundary layer.

A.3 Summary & conclusions

Through the use of a trip wire, a low Reynolds number turbulent boundary layer was created inside the Flat Plate Rig. The trip was sized and implemented successfully such that low Reynolds number turbulent flow was created in the region of influence of the orthogonal actuators.

The results of the preliminary investigation into the use of the orthogonal actuators to reduce the thickness and skin friction of low Reynolds number turbulent boundary layers showed that the plasma actuators had little influence over the flow. If anything, the actuators were observed to encourage the development of turbulence in the boundary layer for both cases with and without suction. Hence, it can be concluded that the orthogonal actuators tested in this investigation do not have the ability to influence a low Reynolds number turbulent boundary layer in a way so as to reduce skin friction drag. Consequently, it is suggested that any flow control that the actuators are used for will need to be implemented prior to the boundary layer undergoing transition.

References

Abe, T., S. Sato, and N. Kimura (2007). "A Parametric Experimental Study for Momentum Transfer by Plasma Actuator". In: *45th AIAA Aerospace Sciences Meeting and Exhibit*. 2007-0187. Reno, NV (cit. on pp. 31, 41, 44).

Balcer, B. E., M. E. Franke, and R. B. Rivir (2006). "Effects of Plasma Induced Velocity On Boundary Layer Flow". In: *44th AIAA Aerospace Sciences Meeting and Exhibit*. Reno, NV (cit. on p. 37).

Baughn, J. W., C. O. Porter, B. L. Peterson, T. E. McLaughlin, C. L. Enloe, G. I. Font, and C. Baird (2006). "Momentum Transfer for an Aerodynamic Plasma Actuator with an Imposed Boundary Layer". In: *44th AIAA Aerospace Sciences Meeting and Exhibit*. 2006-168. Reno, NV (cit. on pp. 32, 35, 36, 42, 43).

Baumann, M., D. Sturzebecher, and W. Nitsche (2000). "Active Control of TS-Instabilities on an Unswept Wing". In: *Laminar-Turbulent Transition: Proceedings of the IUTAM Symposium 1999, Sedona, USA*. Springer Verlag, pp. 155–160 (cit. on p. 26).

Bertin, J. L. (2002). *Aerodynamics for Engineers*. USA: Pearson Education (cit. on pp. 1, 2, 14).

Bradshaw, P., T. Cebeci, and J. H. Whitelaw (1981). *Engineering Calculation Methods for Turbulent Flow*. Great Britain: Academic Press Inc. (cit. on pp. 56, 59).

Brandt, L., P. Schlatter, and D. S. Henningson (2004). "Transition in Boundary Layers Subject to Free-stream Turbulence". In: *Journal of Fluid Mechanics* Vol. 517, pp. 167–198 (cit. on pp. 111, 112).

Braslow, A. L., R. M. Hicks, and R. V. Harris jr. (1966). *Use Of Grit-Type Boundary-Layer-Transition Trips On Wind-Tunnel Models*. Tech. rep. NASA (cit. on pp. 205–207).

Bruun, H. H. (1995). *Hot wire anemometry : principles and signal analysis*. Great Britain: Oxford University Press (cit. on pp. 120, 131).

Bussmann, K. and H. Münz (1942). "Die Stabilität der laminaren Reibungsschicht mit Absaugung". In: *Jb. dt. Luftfahrtforschung* Vol. 1, pp. 36–39 (cit. on p. 25).

Cebeci, T. (1999). *An Engineering Approach to the Calculation of Aerodynamic Flows*. Germany: Horizons Publishing Inc. (cit. on pp. 54, 68, 75, 78).

Cebeci, T. and J. G. Cousteix (1999). *Modeling and Computation of Boundary-Layer Flows*. Germany: Horizons Publishing Inc. (cit. on pp. 11–15, 18, 22, 54, 55, 59, 60, 65, 68, 74, 76–78, 80, 81, 103, 207).

Chang, P. K. (1976). *Control of Flow Separation*. USA: Hemisphere Publishing Corporation (cit. on p. 155).

Cho, Y. C., B. Jayaraman, F. Viana, R. Haftka, and W. Shyy (2008). "Surrogate Modeling for Characteriszing the Performance of Dielectric Barrier Discharge Plasma Actuator". In: *46th AIAA Aerospace Sciences Meeting and Exhibit*. 2008-1381. Reno, NV (cit. on pp. 31, 41, 44).

Chue, S. H. (1975). "Pressure Probes for Fluid Measurements". In: *Progress in Aerospace Science* Vol. 16, No. 2, pp. 147–223 (cit. on p. 129).

Corke, T. C., E. J. Jumper, M. L. Post, D. Orlov, and T. E. McLaughlin (2002). "Application of Weakly-ionized Plasmas as Wing Flow-control Devices". In: *40th AIAA Aerospace Sciences Meeting and Exhibit*. 2002-350. Reno, NV (cit. on pp. 32, 33).

Corke, T. C., C. L. Enloe, and S. P. Wilkinson (2010). "Dielectric Barrier Discharge Plasma Actuator for Flow Control". In: *Annual Review of Fluid Mechanics* Vol. 42, pp. 505–529 (cit. on pp. 29–32, 41, 44, 47, 132).

Cousteix, J. and G. Pailhas (1979). *Etude Exploratoire d'un Processus de Transition Laminaire-Turbulent au Voisinage du Décollement d'une Couche Limite Laminaire*. Tech. rep. 1979-3. Aérosp. (cit. on p. 23).

Danabasoglu, D. and S. Biringen (1990). "A Chebyshev Matrix Method For The Spatial Modes Of The Orr-Sommerfeld Equations". In: *International Journal for Numerical Methods in Fluids* Vol. 11, No. 7, pp. 1033–1037 (cit. on p. 54).

Drazin, P. G. (2002). *Introduction to Hydrodynamic Stability*. United Kingdom: Cambridge University Press (cit. on pp. 14, 18, 21, 68, 76, 77, 103).

Duchmann, A., A. Reeh, R. Quadros, J. Kriegseis, and C. Tropea (2010). "Linear Stability Analysis for Manipulated Boundary-Layer Flows using Plasma Actuators". In: *Seventh IUTAM Symposium on Laminar-Turbulent Transition: IUTAM Bookseries* Vol. 18, No. 2, pp. 153–158 (cit. on pp. 39, 40).

East, L. F. (1966). "Aerodynamically Induced Resonance in Rectangual Cavities". In: *Journal of Sound and Vibration* Vol. 3, No. 3, pp. 277–287 (cit. on p. 141).

Enloe, C. L., T. E. McLaughlin, R. Van Dyken, K. D. Kachner, E. J. Jumper, and T. C. Corke (2003). "Mechanisms and Responses of a Single Dielectric Barrier Plasma". In: *41st Aerospace Sciences Meeting and Exhibit*. 2003-1021. Reno, NV (cit. on pp. 86, 118).

Enloe, C. L., T. E. McLaughlin, R. Van Dyken, K. D. Kachner, E. J. Jumper, T. C. Corke, M. Post, and O. Haddad (2004a). "Mechanisms and Responses of a Single Dielectric Barrier Discharge Plasma Actuator: Geometric Effects". In: *AIAA Journal* Vol. 42, No. 3, pp. 595–604 (cit. on pp. 44, 86, 118).

Enloe, C. L., T. E. McLaughlin, R. D. Van Dyken, K. D. Kachner, E. J. Jumper, and T. C. Corke (2004b). "Mechanisms and Responses of a Single Dielectric Barrier Plasma Actuator: Plasma Morphology". In: *AIAA Journal* Vol. 42, No. 3, pp. 589–594 (cit. on pp. 31, 86, 89, 118).

Enloe, C. L., T. E. McLaughlin, and D. Orlov (2009). "Plasma-induced force and self-induced drag in the dielectric barrier discharge aerodynamic plasma actuator". In: *47th AIAA Aerospace Sciences Meeting and Exhibit*. 2009-1622. Orlando, FL (cit. on p. 32).

Falkenstein, Z. and J. Coogan (1997). "Microdischarge behaviour in the silent discharge of nitrogen-oxygen and water-air mixtures". In: *Journal of Physics D: Applied Physics* Vol. 30, No. 5, pp. 817–825 (cit. on pp. 31, 32).

Fischer, M. C., A. S. Wright Jr., and R. D. Wagner (1983). *A Flight Test of Laminar Flow control Leading-Edge Systems*. Tech. rep. TM-85712. NASA (cit. on p. 27).

Fjørtoft, R. (1950). "Application of Integral Theorems in Deriving Criteria of Stability for Laminar Flows and for the Baroclinic Circular Vortex". In: *Geofys. Publ.* Vol. 17, pp. 1–52 (cit. on p. 21).

Font, G. I. (2004). "Boundary Layer Control with Atmospheric Plasma Discharges". In: *40th AIAA/ASME/SAE/ASEE Joint Propulsion Conference and Exhibit*. 2004-3574. Fort Lauderdale, FL (cit. on pp. 31, 32).

Font, G. I. and W. L. Morgan (2005). "Plasma discharges in atmospheric pressure oxygen for boundary layer separation control". In: *35th AIAA Fluid Dynamics Conference and Exhibit*. Toronto, Canada (cit. on p. 32).

Forte, M., J. Jolibois, J. Pons, E. Moreau, G. Touchard, and M. Cazalens (2006). "Optimization of a Dielectric Barrier Discharge Actuator by Stationary and Non-stationary Measurements of the induced Flow Velocity: Application to Airflow Control". In: *3rd AIAA Flow control Conference*. 2006-2863. San Francisco, CA (cit. on p. 32).

— (2007). "Optimization of a Dielectric Barrier Discharge Actuator by Stationary and Non-stationary Measurements of the induced Flow Velocity: Application to Airflow Control". In: *Experimental Fluids* Vol. 43, No. 6, pp. 917–928 (cit. on pp. 31, 41, 42, 44, 47, 86, 90, 92).

Freymuth, P. (1977). "Frequency response and electronic testing for constant-temperature hot-wire anemometers". In: *Journal of Physics E: Scientific Instruments* Vol. 10, No. 7, pp. 705–71 (cit. on p. 122).

Gaitonde, D., M. Visbal, and S. Roy (2006). "A Coupled Approah for Plasma-based Flow Control Simulations of Wing Sections". In: *44th AIAA Aerospace Sciences Meeting and Exhibit*. 2006-1205. Reno, NV (cit. on p. 33).

Gibson, B. A., R. M. Kelso, and M. Arjomandi (2009a). "Investigation of the Effect of Electrode Arrangement on Plasma Actuator Performance". In: *47th AIAA Aerospace Sciences Meeting and Exhibit*. 2009-1003. Orlando, FL (cit. on pp. iv, 84, 118, 156).

— (2009b). "Plasma Actuator Influence on Laminar Boundary Layer Flow". In: *2009 Asia-Pacific International Symposium on Aerospace Technology*. Nagaragawa, GIFU, Japan (cit. on pp. iv, 29).

— (2012). "The Response of a Laminar Flat Plate Boundary Layer to an Orthogonally Arranged Dielectric Barrier Actuator". In: *Journal of Physics D: Applied Physics* Vol. 45, No. 2, pp. 25202–25213 (cit. on pp. v, 145).

Glauert, M. B. (1956). "The Wall Jet". In: *Journal of Fluid Mechanics* Vol. 1, No. 6, pp. 625–643 (cit. on p. 31).

Grundmann, S. and C. Tropea (2007a). "Active Cancellation of Artificially Introduced Tollmien-Schlichting Waves Using Plasma Actuators". In: *Experiments in Fluids* Vol. 44, No. 5, pp. 795–806 (cit. on pp. 27, 39, 40, 50, 110, 112, 113, 153, 155, 160).

— (2007b). "Experimental Transition Delay Using Glow-discharge Plasma Actuators". In: *Experimental Fluids* Vol. 42, No. 4, pp. 653–657 (cit. on pp. 15, 27, 37–40, 50, 110, 112, 113, 119, 120, 153, 155, 183).

— (2009). "Experimental damping of boundary-layer oscillations using DBD plasma actuators". In: *International Journal of Heat and Fluid Flow* Vol. 30, No. 3, pp. 394–402 (cit. on pp. 27, 40, 50, 110, 112, 113, 142, 153, 155, 160).

Hefner, J. N. and F. E. Sabo (1987). *Research in Natural Laminar-Flow COntrol*. Tech. rep. CP-2487. NASA (cit. on p. 27).

Hoskinson, A. R., N. Hershkowitz, and D. E. Ashpis (2008). "Force Measurements of Single and Double Barrier DBD Plasma Actuators in Quiescent Air". In: *Journal of Physics D: Applied Physics* Vol. 41, No. 24, pp. 245209–245217 (cit. on p. 44).

Hoskinson A. R., a. H. N. (2009a). "2-D Simulations of Single and Double DBD Plasma Actuators with Finite Electrode Thicknesses". In: *47th AIAA Aerospace Sciences Meeting and Exhibit*. 2009-484. Orlando, FL (cit. on p. 44).

— (2009b). "Comparisons of Force Measurement Methods for DBD Plasma Actuators in Quiscent Air". In: *47th AIAA Aerospace Sciences Meeting and Exhibit*. 2009-485. Orlando, FL (cit. on p. 44).

Howe, M. S. (1981). "On the unsteady wake-induced lift on a slotted airfoil, part II: The influence of displacement thickness fluctuations". In: *Journal of Sound and Vibration* Vol. 74, No. 3, pp. 311–322 (cit. on pp. 14, 182).

Huang, J. (2005). "Separation Control over Low Pressure Turbine Blades using Plasma Actuators". PhD thesis. University of Notre Dame (cit. on p. 119).

Hultgren, L. S. and D. E. Ashpis (2003). *Demonstration of Separation Delay with Glow-Discharge Plasma Actuators*. Tech. rep. TMŮ2003-212204. NASA (cit. on p. 119).

Humphrey J. A. C., a. T. A. M. K. and J. H. Whitelaw (1977). "Laminar Fow in a Square Duct of Strong Curvature". In: *Journal of Fluid Mechanics* Vol. 83, No. 3, pp. 509–527 (cit. on p. 142).

Ingen, J. L. van (1956). "A Suggested Semi-empirical Method for the Calculation of the Boundary Layer Transition Region". In: *2nd European Aeronautical Congress*. 37. Scheveningen (cit. on p. 21).

Jacob, J., R. Rivir, C. Carter, and J. Estevadeordal (2004). "Boundary Layer Flow Control Using AC Discharge Plasma Actuators". In: *AIAA 2nd Flow Control Meeting*. 2004-2128. Portland, OR (cit. on p. 34).

Johnson, G. A. and S. J. Scott (2001). "Plasma-aerodynamic Boundary Layer Interaction Studies". In: *32nd AIAA Plasmadynamics and Lasers Conference and 4th Weakly Ionized Gases Workshop*. 2001-3052. Anaheim, CA (cit. on pp. 36, 37, 119, 155).

Jordinson, R. (1970). "The flat plate boundary layer. Part 1. Numerical integration of the Orr-Sommerfeld equation". In: *Journal of Fluid Mechanics* Vol. 43, No. 4, pp. 801–811 (cit. on p. 54).

Joslin, R. D. (1998). "Aircraft Laminar Flow Control". In: *Annual Review of Fluid Mechanics* Vol. 30, No. 1, pp. 1–29 (cit. on pp. 10, 26, 27, 29, 40, 141).

Keller, H. B. (1978). "Numerical Methods In Boundary Layer Theory". In: *Annual review of Fluid Mechanics* Vol. 10, pp. 417–433 (cit. on p. 55).

Kogelschatz, U., B. Eliasson, and W. Egli (1997). "Dielectric-Barrier Discharges. Principle and Applications". In: *Journal of Physics IV (France)* Vol. 7, No. C4, pp. 47–66 (cit. on pp. 31, 89).

Kriegseis, J., T. Dehler, M. Pawlik, and C. Tropea (2009). "Pattern-Identification Study of the Flow in Proximity of a Plasma Actuator". In: *47th AIAA Aerospace Sciences Meeting and Exhibit*. 2009-1001. Orlando, FL (cit. on pp. 38, 50, 116).

Li, Y. and M. Gaster (2006). "Active Control of Boundary-layer Instabilities". In: *Journal of Fluid Mechanics* Vol. 550, pp. 185–205 (cit. on p. 26).

Liepmann, H. W. (1945). *Investigation of Boundary Layer Transition on Concave Walls*. Tech. rep. ACR-4J28. NACA (cit. on p. 21).

Liepmann, H. W. and D. M. Nosenchuck (1982). "Active Control of Laminar-Turbulent Transition". In: *Journal of Fluid Mechanics* Vol. 118, pp. 201–204 (cit. on p. 26).

Liepmann, H. W., G. L. Brown, and D. M. Nosenchuck (1982). "Control of Laminar-instability Waves using a New Technique". In: *Journal of Fluid Mechanics* Vol. 118, pp. 187–200 (cit. on p. 26).

Lissaman, P. B. S. (1983). "Low-Reynolds-Number Airfoils". In: *Annual Review of Fluid Mechanics* Vol. 15, pp. 223–239 (cit. on p. 24).

Mack, L. M. (1977). *Transition and Laminar Instability*. Tech. rep. Jet Propulsion Laboratory (cit. on p. 21).

MacMillan, F. A. (1954). "Viscous Effects on Pitot Tubes at Low Speeds". In: *Journal of the Royal Aeronautical Society* Vol. 58, No. 8, pp. 837–839 (cit. on p. 125).

— (1957). *Experiments on Pitot-Tubes in shear flow*. Tech. rep. Aeronautical Research Council (cit. on pp. 125, 126).

Maddalon, D. V. and A. L. Braslow (1990). *Simulated Airline Service Flight Tests of Laminar Flow Control With Perforated Surface Suction Systems*. Tech. rep. TP-2966. NASA (cit. on p. 27).

Magnier, P., V. Boucinha, B. Dong, R. Weber, A. Leroy-Chesneau, and D. Hong (2009). "Experimental Study of the Flow Induced by a Sinusoidal Dielectric BArrier Discharge Actuator and Its Effects on a Flat Plate Natural Boundary Layer". In: *Journal of Fluids Engineering* Vol. 131, No. 1, pp. 203–213 (cit. on pp. 36, 37).

McKeon, B. J., J. Li, W. Jiang, J. F. Morrison, and A. J. Smits (2003). "Pitot probe corrections in fully developed turbulent pipe flow". In: *Measurement Science and Technology* Vol. 14, No. 8, pp. 1449–1458 (cit. on pp. 125–127).

Mello, H. C. d. M., F. M. Catalano, and L. F. de Souza (2007). "Numerical Study of Synthetic Jet Actuator Effects in Boundary Layers". In: *Journal of the Brazilian Society of Mechanical Sciences and Engineering* Vol. 24, No. 1, pp. 34–41 (cit. on pp. 30, 37).

Milling, R. W. (1981). "Tollmien-Schlichting Wave Cancellation". In: *Physics of Fluids* Vol. 24, No. 5, pp. 979–981 (cit. on p. 26).

Morkovin, M. V. (1988). *Recent Insights Into Instability And Transition To Turbulence In Open-Flow Systems*. Tech. rep. NASA (cit. on p. 16).

Munska, M. D. and T. E. McLaughlin (2006). "Circular Cylinder Flow Control Using Plasma Actuators". In: *43rd AIAA Aerospace Sciences Meeting and Exhibit*. 2005-141 2005-141 2005-141 2005-141 2005-141 2005-141 2005-141. Reno, NV (cit. on p. 33).

Narasimha, R. and S. N. Prasad (1994). "Leading Edge Shape for Flat Plate Boundary Layer Studies". In: *Experiments in Fluids* Vol. 17, No. 5, pp. 358–360 (cit. on pp. 112, 113).

Newcamp, J. M. (2005). "Effects of Boundary Layer Flow Control Using Plasma Actuator Discharges". PhD thesis. Department of Air Force Air University (cit. on pp. 34, 35, 37, 96–100).

Ogata, S. and T. Fujita (2009). "Effect of a Surfactant Additives on Generation and Development of Laminar Boundary Layer on a Flat Plate". In: *Journal of Fluid Science TEchnology* Vol. 4, No. 3, pp. 558–566 (cit. on pp. 15, 183).

Operating Manual for TSI IFA-100 Constant-Temperature Anemometer (2000). TSI Inc. MN USA (cit. on pp. 121, 122).

Opfer, H. (2002). "Active Cancellation of 3D Tollmien-Schlichting Waves in the Presence of Sound and Vibrations". PhD thesis. Georg-August-Universität-Göttingen (cit. on p. 26).

Orlov, D. M. (2006). "Modelling and simulation of single dielectric barrier discharge plasma actuator effects". PhD thesis. Univeristy of Notre Dame (cit. on pp. 32, 41, 44, 46–48, 84, 117).

Orlov, D. M., T. C. Corke, and M. P. Patel (2006). "Electric circuit model for aerodynamic plasma actuator". In: *44th AIAA Aerospace Sciences Meeting and Exhibit*. Reno, NV (cit. on pp. 32, 44, 46–48, 84).

Patel, V. C. (1965). "Calibration of the Preston tube and limitations on its use in pressure gradients". In: *Journal of Fluid Mechanics* Vol. 23, No. 1, pp. 185–208 (cit. on p. 125).

Penner, J. E. (1999). *Aviation and the Global Atmosphere*. Intergovenrnmental Panel on Climate Change. URL: `http://www.grida.no/climate/ipcc/aviation/index.htm` (cit. on p. 1).

Pentelow, L. and D. Scott (2010). "The Implications of Climate Change Mitigation Policy and Oil Price Volatility for Tourism Arrivals to the Caribbean". In: *Tourism and Hospitality Planning & Development* Vol. 7, No. 3, pp. 301–315 (cit. on p. 1).

Perry, A. E. (1982). *Hot-wire Anemometry*. Northern Ireland: Oxford University Press (cit. on p. 120).

Porter, C. O., T. E. McLaughlin, C. L. Enloe, G. I Font, and J. W. Baughn (2007). "Boundary Layer Control Using a DBD Plasma Actuator". In: *45th AIAA Aerospace Sciences Meeting and Exhibit*. 2007-786. Reno, NV (cit. on pp. 36, 37, 155).

Post, M. L. and T. C. Corke (2003). "Separation Control on High Angle of Attack Airfoil Using Plasma Actuators". In: *41st AIAA Aerospace Sciences Meeting and Exhibit*. 2003-1024. Reno, NV (cit. on pp. 33, 37).

Quadros, R. (2009). "Numerical Optimization of Boundary-Layer Control using Dielectric Barrier Discharge Plasma Actuators". PhD thesis. Technische Universität Darmstadt (cit. on pp. 39, 40).

Quadros, R. S., S. Grundmann, C. Tropea, and a. G. R. Albrecht T. (2009). "Numerical investigation of the boundary-layer stabilization using plasma actuators". In: *Journal of Flow, Turbulence and Combustion* Vol. Speial Issue ETMM7, Accepted (cit. on p. 39).

Rayleigh, J. W. S. (1880). "On the stability, or instability, of certain fluid motions". In: *Proceedings of the London Mathematical Society* Vol. 11, pp. 57–70 (cit. on p. 21).

Reeh, A. D. (2008). "Development and Implementation of a Method for Linear Stability Analysis in Natural and Manipulated Boundary-Layer Flows". PhD thesis. Technische Universität Darmstadt (cit. on pp. 54, 103).

Renneaux, J. (2004). "Overview on Drag Reduction Technologies for Civil Transport Aircraft". In: *2004 ECCOMAS*. Jyväskylä, Finland (cit. on p. 1).

Rizzetta, D. P. and M. R. Visbal (2011). "Numerical Investigation of Plasma-Based Control for Low-Reynolds-Number Airfoil Flows". In: *AIAA Journal* Vol. 49, No. 2, pp. 411–425 (cit. on p. 33).

Roth, J. R. (2001). *Industrial Plasma Engineering; Volume 2 - Applications to Non-thermal Plasma Processing*. USA: Institute of Physics Publishing (cit. on p. 31).

Roth, J. R. and X. Dai (2006). "Optimization of the Aerodynamic Plasma Actuator as an Electrohydrodynamic (EHD) Electrical Device". In: *44th AIAA Aerospace Sciences Meeting and Exhibit*. 2006-1203. Reno, NV (cit. on pp. 29, 31, 41–45).

Roth, J. R., D. Sherman, and S. P. Wilkinson (1998). "Boundary layer flow control with one atmosphere uniform glow discharge surface plasma". In: *36th AIAA Aerospace Sciences Meeting and Exhibit*. Reno, NV (cit. on p. 29).

Roth, J. R., D. M. Sherman, and S. P. Wilkinson (2000). "Electrohydrodynamic Flow Control with a Glow-Discharge Surface Plasma". In: *AIAA Journal* Vol. 38, No. 7, pp. 1166–1172 (cit. on pp. 33, 34, 40).

Santhanakrishan, A. and J. D. Jacob (2006). "On Plasma Synthetic Jet Actuators". In: *44th AIAA Aerospace Sciences Meeting and Exhibit*. Reno, NV (cit. on p. 30).

— (2007). "Flow control with plasma synthetic jet actuators". In: *Journal of Physics D: Applied Physics* Vol. 40, No. 3, pp. 637–651 (cit. on p. 30).

Saric, W. S., H. L. Reed, and E. J. Kerschen (2002). "Boundary-Layer Receptivity To Freestream Disturbances". In: *Annual Review of Fluid Mechanics* Vol. 34, pp. 291–319 (cit. on pp. 15–17).

Schlichting, H. (1933). *Zur Entstehung der Turbulenz bei der Plattenstromung*. Germany: Nachr. Ges. Wiss. Gottingen (cit. on pp. 14, 16, 20, 26, 68).
— (1955). *Boundary Layer Theory*. Great Britain: Pergamon Press Ltd. (cit. on pp. 3, 11, 12, 15, 16, 18, 20, 23–25, 68, 76–78, 103, 162).
Schrauf, G. H. and K. H. Horstmann (2004). "Simplified Hybrid Laminar Flow Control". In: *European Congress on Computational Methods in Applied Sciences and Engineering*. Jyväskylä, Finland (cit. on p. 27).
Schubauer, G. B. and H. K. Skramstad (1950). *Laminar-Boundary-Layer Oscillationsand Transition on a Flat Plate*. Tech. rep. 909. National Advisory Committee on Aeronautics (cit. on pp. 16, 65, 110, 112).
Scott, D., D. Amelung, S. Becken, J. Ceron, G. Dubois, S. Gossling, P. Peeters, and M. C. Simpson (2008). "Climate change and tourism: Responding to global challenges". In: *Madrid: United Nations World Tourism Organization; Paris: United Nations Environment Program; Geneva: World Meteorological Organization* (cit. on p. 1).
Selig, M. S., J. F. Donovan, and D. B. Fraser (1989). *Airfoils at Low Speeds*. USA: SoarTech Publications (cit. on p. 24).
Shyy, W., B. Jayaraman, and A. Anderson (2002). "Modelling of Glow Discharge-Induced Fluid Dynamics". In: *Journal of Applied Physics* Vol. 92, No. 11, pp. 6434–6443 (cit. on pp. 44–47, 84).
Smith, A. M. O. and N. Gamberoni (1956). *Transition, Pressure Gradient, and Stability Theory*. Tech. rep. ES 26388. Douglas Aircraft Company (cit. on p. 21).
Sotiropoulos, F. and V. C. Patel (1992). *Flow in Curved Ducts of Varying Cross-section*. Tech. rep. Iowa Institute of Hydraulic Research (cit. on p. 142).
Sturzebecher, D. and W. Nitsche (2002). "Active Control of Tollmien-Schlichting Instabilities by Multi-channel Sensor Actuator Systems". In: *New Results in Numerical and Experimental Fluid Mechanics: Contributions to the 12th STAB-Symposium, Stuttgart, Germany 2000*. Ed. by Rist U., W. S. and Heinemann, H. J. Vol. 77. Springer Verlag, pp. 375–382 (cit. on p. 26).
— (2003a). "Active Cancellation of Tollmien-Schlichting Instabilities on a Wing using Multi-channel Sensor Actuator Systems". In: *International Journal of Heat and Fluid Flow* Vol. 24, pp. 572–583 (cit. on p. 26).
— (2003b). "Active Control of Boundary-layer Instabilities on an Unswept Wing". In: *Recent Results in Laminar-Turbulent Transition*. Ed. by Wagner S., K. M. and Rist, U. Vol. 86. Notes on Numerical Fluid Mechanics and Multidisciplinary Design. Springer-Verlag, pp. 189–202 (cit. on p. 26).
Tavoularis, S. and M. Szymczak (1989). "Displacement effects of square-ended Pitot tubes in shear flows". In: *Experiments in Fluids* Vol. 7, No. 1, pp. 33–37 (cit. on p. 125).

Thomas, A. (1983). "The Control of Boundary-layer Transition using a Wave-superposition Prinicple". In: *Journal of Fluid Mechanics* Vol. 137, pp. 233–250 (cit. on pp. 26, 113, 114).

Thomas, A. S. W. (1985). *Aircraft drag reduction technology*. Tech. rep. 723. AGARD (cit. on pp. 10, 16).

Thomas, F. O., T. C. Corke, M. Iqbal, A. Kozlov, and D. Schatzman (2009). "Optimization of Dielectric Barrier Discharge Plasma Actuators for Active Aerodynamic Flow Control". In: *AIAA Journal* Vol. 47, No. 9, pp. 2169–2178 (cit. on pp. 32, 41).

Tollmien, W. (1929). *Uber die Enstehung der Turbulenz*. Tech. rep. Nachr. Ges. Wiss. Gottingen, Math.-phys. Klasse, 21-44 (cit. on pp. 16, 26, 54, 68).

Van Dyken, R., T. E. McLaughlin, and C. L. Enloe (2004). "Parametric Investigations of a Single Dielectric Barrier Plasma Actuator". In: *42nd AIAA Aerospace Sciences Meeting and Exhibit*. 2004-0846. Reno, NV (cit. on pp. 31, 41, 44, 86, 118).

Wang, Y. X. and M. Gaster (2005). "Effect of Surface Steps on Boundary Layer Transition". In: *Experiments in Fluids* Vol. 39, No. 4, pp. 679–686 (cit. on pp. 110, 112, 140–142).

Watmuff, J. (2006). "Effects of Weak Freestream Nonuniformity on Boundary Layer Transition". In: *Journal of Fluids Engineering* Vol. 128, No. 2, pp. 247–257 (cit. on pp. 110, 112).

Wazzen, A. R., C. Gazley Jr., and A. M. O. Smith (1981). "H-Rx Method for Predicting Transition". In: *AIAA Journal* Vol. 19, No. 6, pp. 810–812 (cit. on p. 22).

Wehrmann, O. (1965). "Tollmien-Schlichting Waves under the Influence of a Flexible Wall". In: *Physics of Fluids* Vol. 8, pp. 1389–1390 (cit. on p. 26).

White, F. M. (1974). *Viscous Fluid Flow*. USA: McGraw Hill (cit. on pp. 11, 14, 15, 76, 77).

Wilkinson, S. P. (2003). "Investigation of an Oscillating Surface Plasma for Turbulent Drag Reduction". In: *41st Aerospace Sciences Meeting & Exhibit*. 2003-1023. Reno, NV (cit. on p. 119).

Zagarola, M. V. and A. J. Smits (1998). "Mean-flow scaling of turbulent pipe flow". In: *Journal of Fluid Mechanics* Vol. 373, No. 1, pp. 33–79 (cit. on p. 127).